NASA Contract Report 159222

NASA-CR-159222
19800016612

Analytical Study of Interior Noise Control by Fuselage Design Techniques on High-Speed, Propeller-Driven Aircraft

J. D. Revell, F. J. Balena and L.R. Koval

LOCKHEED-CALIFORNIA COMPANY
BURBANK CALIFORNIA

CONTRACT NASI-15427
April 1980

NASA
National Aeronautics and
Space Administration

Langley Research Center
Hampton, Virginia 23665
AC 804 827-3966

NASA Contract Report 159222

Analytical Study of Interior Noise Control by Fuselage Design Techniques on High-Speed, Propeller-Driven Aircraft

J. D. Revell, F. J. Balena and L.R. Koval

LOCKHEED-CALIFORNIA COMPANY
BURBANK CALIFORNIA

CONTRACT NASI-15427
July 1978

NASA
National Aeronautics and
Space Administration

Langley Research Center
Hampton, Virginia 23665
AC 804 827-3966

TABLE OF CONTENTS

TABLE OF CONTENTS (Continued)

LIST OF FIGURES

LIST OF FIGURES (Continued)

LIST OF FIGURES (Continued)

LIST OF FIGURES (Continued)

LIST OF FIGURES (Continued)

LIST OF FIGURES (Continued)

LIST OF TABLES

LIST OF TABLES (Continued)

ANALYTICAL STUDY OF INTERIOR NOISE CONTROL BY FUSELAGE DESIGN TECHNIQUES ON HIGH-SPEED, PROPELLER-DRIVEN AIRCRAFT

J. D. Revell and F. J. Balena
Lockheed-California Company, Burbank, California

L. R. Koval, Consultant
Rolla, Missouri

SUMMARY

This summary follows the arrangement of the report.

Method of Analysis (Section 1)

Objective - The objective of this study is to determine the minimum weight of fuselage sidewall configurations which would provide an interior noise level of 80 dBA for high-speed, propeller-driven aircraft at cruise conditions. Estimates of the mass penalties associated with these configurations are needed to support system studies of fuel-efficient advanced turboprop-powered aircraft such as those based on the Hamilton Standard prop-fan concept.

Approach - A structural-dynamics based analytical method is employed to compute the transmission loss of the outer wall structure. This method is based on theory developed by Professor L. R. Koval and a modification of the well-known method of Cockburn and Jolly supported by further work at Lockheed. Appendixes A through F describe the method of analysis employed.

To evaluate the mass penalties for noise control, three aircraft preliminary designs were studied, each with a different fuselage diameter. The largest is a 4-engine, wide-body aircraft. This is the design evolved by Lockheed in the RECAT study of 1977. The other two aircraft represent a narrow-body transport and a small business aircraft. All three aircraft were defined by the Lockheed Advanced Design Department per current design practice. Thus, the noise-reduction designs are modifications of realistic baseline aircraft.

Two kinds of noise-reduction designs are investigated:

- "Add-On" Noise-Reduction Designs in which modifications of the baseline fuselage structural design are not permitted - the application of non-load-supporting material to provide added damping and mass is permitted.

- "Advanced" Noise-Reduction Designs in which modifications of the baseline fuselage structural design are permitted

The advanced aluminum and advanced composite designs have higher stiffness and higher mass outer-wall structures than their respective baselines. Structural mass is increased in the process of achieving higher stiffness and the added structural mass is considered as part of the acoustic treatment mass penalty. Thus, the same baseline reference is used for both the add-on and advanced noise-reduction designs. The composite baseline aircraft structures have the same stiffness as their aluminum counterparts, but surface densities are about thirty percent less.

The exterior noise environments employed are those estimated for an 8-bladed propfan-powered aircraft at 9144 m (30 000 ft) and at a flight Mach number of 0.8. These estimates are based on Hamilton Standard performance and noise design charts which estimate the characteristics of a fully developed propfan.

Structural Configuration (Section 2)

In this section, details of the outer wall structure are described for the baseline and stiffened aluminum and the baseline and stiffened composite structures. The baseline structures are used unchanged for the add-on design studies. Although composite structures represent advanced materials technology, the baseline composite structure which is used for the add-on design studies is not referred to as advanced. The aluminum and composite design studies are thus consistent in that their baseline structures are used for the add-on design studies and stiffened structures are used for the advanced studies.

Acoustical Treatment Mass Penalties for the Recommended Noise-Reduction Designs (Section 3)

In this section, axial distributions of the required total wall surface density are shown for each of the three aircraft. Above the floor, the total wall surface density is assumed to be constant in the circumferential direction. The penalty surface density values, increments above the trimmed baseline, are then integrated over the entire treatment area to obtain the total acoustical treatment mass penalty. Acoustical treatment mass penalty in this context refers to mass added to outer wall structures as well as the interior trim. The treatment weight penalties are expressed in kilograms (pounds) and as percentages of the takeoff gross weight (TOGW) of the trimmed baseline aircraft defined in this study.

The add-on noise reduction (NR) penalties for the aluminum aircraft range from 2.3% of TOGW for the wide-body, to 1.7% for the business aircraft. The wide-body aircraft has the same TOGW as was defined in the RECAT study of 1977. The baseline composite aircraft have outer-wall surface densities which are 30% less than their aluminum counterparts, but have the same outer-wall stiffness. Add-on noise-reduction penalties for the composite aircraft range from 2.5% of TOGW for the wide-body to 1.8% for the small business aircraft. The baseline composite aircraft TOGWs are assumed to be the same as for the aluminum aircraft of the same type, even though their outer wall surface densities are not the same. It is noted that an aircraft designed with maximum use of composites would require a smaller TOGW for the same payload vs range capacity; however, data for the required resizing of the study aircraft is not available.

The advanced aluminum structures provide reductions in the noise-control penalties when compared to the add-on noise control configurations. The noise-reduction penalties for all three advanced aluminum aircraft are approximately 1.5% of TOGW relative to their respective baseline values. It is noted that the weight increases associated with the advanced structures are included in the calculated noise-control penalties. The advanced composite noise-reduction designs also used part of the penalty mass to provide higher stiffness outer walls than the baseline composite structures. When an advanced composite structure is combined with the correct trim-panel mass for optimum double wall design, the total weight penalties are 1.0% TOGW for the wide-body, 1.4% for the narrow-body and 0.74% for the business aircraft.

The results presented above have implications for the further development of high-speed turboprop aircraft. The add-on acoustic treatment mass penalties are about the same as those which were previously estimated in system studies for fuel-efficient, turboprop-powered aircraft in 1977 (i.e., the RECAT study of Reference 1). The advanced design treatment penalties are significantly lower than the add-on penalties due to a more efficient use of penalty mass. These results are lower than the 2.5% of TOGW penalty estimated during the earlier RECAT study and thus support its estimated economic benefits. The 1977 RECAT study estimated the following advantages for propfan versus turbofan aircraft,

- 17 percent lower block fuel consumption
- 7 percent lower DOC.

The present study is the first attempt to calculate the treatment penalties necessary to achieve an interior noise level of 80 dBA using a sophisticated structural dynamics approach.

INTRODUCTION

The growing worldwide concern for the shortage of petroleum and the attendant rapid price increase have stimulated increased effort to reduce aircraft fuel consumption, which now constitutes over 40 percent of the

direct operating costs of an aircraft. One promising approach to more efficient aircraft propulsion is a new turboprop engine based on the known high efficiency of propellers and modern propeller design methods. The new concept includes an all-new propeller with 8 to 10 highly swept blades and is referred to as a propfan. The propfan has been estimated to be 20% more efficient than comparable, advanced-technology turbofan engines (reference 1), when cruising at 0.80 Mach number at 9144 m (30 000 ft) altitude at stage lengths of 1500 miles.

Passenger surveys conducted by commercial airlines (reference 2) show that a quiet interior is important and that current jet aircraft interior noise levels are a desirable goal. Propfan propellers produce intense acoustic pressure levels at the blade passage frequency and its low-order harmonics. Most of the total power output from a propeller is concentrated in a few relatively low-frequency components. However, jet aircraft fuselage sidewalls are designed to attenuate broadband boundary layer excitation, and special attention is needed to ensure that the propfan sidewall will adequately attenuate propeller noise.

The system studies in references 1 and 3 used preliminary design estimates of the acoustical treatment requirements and provided similar results. Reference 1 used simple double-wall mass law theory and assessed a weight penalty of 2368 kg (5200 lb) or 2.4% of the takeoff gross weight (TOGW) of a 98 641 kg (217 466 lb) wide-body aircraft designed to carry 200 passengers for 2778 km (1500 n.mi). The methodology was suspected of being too optimistic with regard to the required surface density of the treatment mass; however, a conservatively large treatment area was used for nine noise-control segments centered about the propeller disc plane of the inboard engine.

As shown in reference 1, a substantial mass penalty is required in order to achieve an 80 dBA interior noise goal. However, the propfan-powered aircraft still retained a significant net advantage, relative to a turbofan, of about 17% in block fuel consumption and 7% in direct operating cost (DOC). The approximate nature of the initial RECAT system studies required a more sophisticated analysis of propfan aircraft interior noise and the mass penalty required to obtain a level of 80 dBA. This program and a companion study reported in reference 4 were initiated to provide a more detailed and in-depth analysis of propfan interior noise and to recommend suitable noise-reduction designs. The approach used for this program considered two different approaches; (1) "add-on" noise-reduction designs and (2) "advanced" noise-reduction designs. For the add-on designs, it is assumed that the addition of acoustical treatment materials does not result in significant increases in structural stiffness or load-carrying capability. In the advanced noise-reduction designs, it is assumed that the outer-shell structure could be stiffened significantly if that were beneficial. Add-on and advanced noise-reduction design studies were conducted on both aluminum and composite wide-body, narrow-body and business aircraft.

This study was supported by Professor Leslie R. Koval, of Rolla, Missouri, in a consulting capacity.

LIST OF SYMBOLS

English Symbols		Units
a	cylindrical shell or fuselage radius; also frame spacing (Appendix E only)	m (ft)
A	area	m^2 (ft^2)
A_{ij}	coefficients of shell impedance equations (Appendix C)	N/m^3 lb/ft^3)
A_m	coefficient of the Fourier expansion of scattered external acoustic pressure	N/m^2 (psf)
b	acoustic propagation constant for fiberglass blanket; stringer spacing (Appendix E only)	m^{-1} (ft^{-1})
B_m	coefficient of the Fourier expansion of the radially inward transmitted sound pressure wave in the interior of a cylindrical shell	N/m^2 (psf)
B	number of propeller blades	
c	acoustic wave propagation speed	m/sec (ft/sec)
d	spacing between inner wall (trim panel) and outer wall of fuselage shell; also fiberglass blanket thickness	m (in)
D	$Eh^3/12(1-\nu^2)$ plate modulus of fuselage skin also diameter (of fuselage, propeller, etc.)	N-m (lb-m)
e	base of Naperian logarithm, 2.71828	
E	Young's modulus of elasticity	N/m^2 (psi)
$\overline{E}$	ratio of stiffness, EI, of outer wall to baseline stiffness value (Appendices H and I)	
f	frequency of sound wave	Hz

English Symbols		Units
F	general functional dependence	
g	acceleration of gravity	m/sec^2 (ft/sec^2)
G	shear modulus of elasticity	N/m^2 (psi)
h	skin or cylindrical shell thickness	m (in)
$H_m^{(1)} = J_m + jY_m$,	Hankel function of the first kind of order, m	
$H_m^{(2)} = J_m - jY_m$,	Hankel function of the second kind of order, m	
i	index	
I	moment of inertia of skin or stiffener	m^4 (in^4)
j	$= \sqrt{-1}$ imaginary number	
J	torsional moment of inertia of stiffener	m^4 (in^4)
J_m	Bessel function of the first kind of order, m	
k	wave number	m^{-1} (ft^{-1})
K	volume coefficient of elasticity of air (Appendix E)	N/m^2 (psf)
l	length in general sense	m (ft)
L, L_f	length of fuselage	m (ft)
L_{ij}	linear differential operators for shell theory (Appendix C)	N/m^3 (lb ft^{-3})
ℓ_y	stringer spacing (Appendices H and I)	m (ft)
ℓ_x	frame spacing (Appendices H and I)	m (ft)
L_t	length of acoustical treatment	m (ft)

English Symbols		Units
m	number of circumferential half wave lengths of vibrating shell	
m	number of axial half wave lengths (in Appendix D only)	
m	mass or surface density (Appendixes C and E only); σ is used elsewhere	kg/m^2 (psf)
M	Mach number of flow	
n	number of axial half wave lengths of vibrating shell	
n	number of half wave lengths in the circumferential direction (Appendix D only)	
NR	noise reduction	dB
P	fluid static pressure	N/m^2 (psf)
$P_{(ax, cir)}$	(axial circumferential) skin load per unit length due to cabin pressure differential	N/n (lb/in)
P_i	amplitude of incident external acoustic pressure wave	N/m^2 (psf)
Q^a	acoustical cross sectional absorption coefficient (Koval theory)	
r	radial coordinate	m (ft)
r	non-dimensional acoustic resistance	
R_l	acoustic resistance per unit depth	$N\ sec/m^4$ ($lb\ sec/ft^4$)
t	time	sec
TL	transmission loss	dB
u, v, w	axial, circumferential, and radial shell displacements	m (in)

English Symbols		Units
V_T	tangential or blade tip speed	m/sec (ft/sec)
W	weight of aircraft treatment mass	kg (lb)
(U_m, V_m, W_m)	Fourier components of shell displacement	m (in)
x, r, ϕ	cylindrical coordinates	m (ft)
y	= aϕ circumferential arc length	m (ft)
Y	blanket porosity	
Y_m	Bessel function of the second kind of order, m	
Z	acoustical impedance	$\frac{N\ Sec}{m^3}$ (psf) (ft/sec)

Greek Letters		Units
α	acoustical absorption coefficient	
γ	fluid specific heat ratio	
Δ	determinant in shell impedance expressed in Appendix C	N^3/m^9 (lb^3/ft^9)
Δp	differential pressure across cabin wall	N/m^2 (psf)
Δy	propeller tip to fuselage wall clearance	m (ft)
ϵ_m	= 1; m = 0 = 2; m $\geq$ 1	
η	damping loss factor	
θ	angle of the incident wave vector relative to surface	rad (deg)
θ	angle of the incident wave vector relative to the direction normal to the surface (Appendix E only)	rad (deg)

Greek Letters		Units
λ	wave length	m (ft)
ν	Poisson's ratio	
ρ	bulk density of fluid, shell, etc.	$\frac{kg}{m^3}$ (lb/ft^3)
σ	surface density of side wall elements,	$\frac{kg}{m^2}$ (psf)
τ	acoustic transmission coefficient	
ϕ	circumferential or azimuth cylindrical coordinate, also refracted angle of incidence within porous blanket (Appendix E)	rad (deg)
χ	non-dimensional acoustical reactance	
Ω	rotational frequency of blade	rad/sec
	$B\Omega$ blade passage frequency	rad/sec

Superscripts and Subscripts

1	pertains to properties of external flow or outer wall
2	pertains to trim panels and to fluid properties inside cabin; also 1, 2, 3 ... n refers to locations within multilayer noise control treatment (Appendix E only)
a	acoustical or atmospheric
B or BLKT	refers to blanket properties
BL	Base line value
c	Refers to impedance of the contents of the shell (internal fluid and "add-on" layers)
C	coincidence frequency

Superscripts and Subscripts

e	external (sound wave, impedance, etc.)
f	pertains to fuselage
i	pertains to an axial segment of the acoustical treatment
i	refers to incident sound wave
I	refers to incident sound wave
L	longitudinal (elastic wave speed, C_L)
m	circumferential wave number index (except Appendix D); axial wave number index (Appendix D only)
n	circumferential wave number index (Appendix D only); also the number of add-on treatment layers (Appendix E only)
p	panel properties
R	ring frequency
r	pertains to radial components (of wave number, displacement, etc.)
t	refers to acoustical treatment; also to propeller blade tip (speed, etc.)
tr	trace property (wave length, etc. Appendix A)
T	refers to transmitted sound waves (Appendix E)
x	axial component (of wave numbers, etc.) frame spacing (Appendixes H and I)
ϕ, y	tangential component, stringer spacing Appendixes H and I
z	component normal to wall
$(\overline{\ })$	eg $\overline{E}$, $\overline{\ell x}$, $\overline{\ell y}$ ratio of outer wall structural quantity to its baseline value (Appendixes H and I)

1. INTERIOR NOISE PREDICTION METHOD

This section is a brief synopsis of the various assumptions and analytical techniques which are explained more fully in Appendix A, and supported by Appendixes C, D, E, and F.

1.1 Objective

The objective of this study is to determine efficient fuselage sidewall noise-control designs which would achieve an interior noise level of 80 dBA for high-speed, propeller-driven aircraft cruising at 0.8 Mach number and at an altitude of 9144 m (30 000 ft). Also, estimates of the required penalty mass increments for these noise-control designs are needed to support aircraft system design studies for potentially fuel-efficient advanced turboprop-powered aircraft. Two system design studies are documented in references 1 and 3.

The above-mentioned study results are desired for three aircraft which are characterized by different fuselage diameters. Results are desired for add-on noise-reduction designs wherein the strength and stiffness of the basic outer-wall structure is unaltered, and also for advanced noise-reduction design, where the outer wall structure stiffness may be altered.

1.2 Approach

The analytical method employed in this study is based on the structural dynamics of cylindrical shells and upon the use of the best available mathematical models for the performance of noise-control devices in the form of acoustical impedance.

1.3 Aircraft Configuration

To facilitate the study, three aircraft are defined at a preliminary design level of refinement. They are described as a wide-body, a narrow-body, and a small business aircraft. Their design and configuration characteristics are specified by the various tables and figures appearing in Appendix A. The wide-body aircraft selected for this study is the 200-passenger, 2798-km (1500-n.mi.), propfan airplane developed during the Lockheed RECAT study of reference 1. This design, which incorporates four wing-mounted turbo-shaft engines (P&WA STS 476) and the 8-bladed Hamilton Standard propfan, was optimized during the RECAT study for minimum fuel usage for the design mission. The narrow-body and business aircraft are representative of previous Lockheed preliminary designs of turbofan-powered airplanes applicable to the short-haul market. Each design was sized for minimum fuel usage and incorporates propfan propulsion. Preliminary values for required engine power, propfan diameter, and gross weight

have been established as shown in table 1. The aircraft gross weights do not reflect any additional acoustical treatment weight required to maintain acceptable interior noise levels with the propfan.

For each aircraft, an axial exterior noise signature is defined based upon propfan data from Hamilton Standard (reference 5). The axial distribution of the exterior overall sound pressure level (OASPL) is specified in Appendix A. The circumferential distribution is assumed to be a Fourier-Bessel expansion of an incident plane wave as defined by Smith in reference 6. For the 2-engine narrow-body and small business aircraft, a nominal propeller-tip-to-fuselage clearance of 0.8 diameter is selected as recommended by Hamilton Standard in reference 5. For the design conditions described by figures and tables in Appendix A, a peak external OASPL of 134 dB is estimated. The propeller-tip-to-fuselage clearance for the 4-engine wide-body aircraft are selected at 1.2 diameters for the inboard engine and 2.3 diameters for the outboard engine. As shown graphically in Appendix A, the peak noise level is reduced by 2 dB based upon increments relative to the peak noise level for a tip clearance of 0.8 diameters.

The transmission loss (TL) predictions for the outer wall structures used in this study are based on Koval's theory for sound transmission into a cylindrical shell (reference 7). In Koval's mathematical model, the TL of the shell depends strongly upon the angle of incidence of the sound waves as they impinge upon the shell at a known angle with respect to the axis of the fuselage.

Data in Appendix A describes the variation of angle of incidence with distance from the propeller disc plane. For the convenience of parametric studies, the fuselage in the region around the propeller disc plane is subdivided into seven segments which are described in Appendix A. For each segment, nominal uniform levels of external OASPL are assumed. Also, the effects of variation of the angle of incidence along each segment are averaged. The peak noise region is Segment 4, and results of the effects of changing various fuselage sidewall design parameters upon the interior noise of Segment 4 are shown in Appendixes G and H.

1.4 Propeller Noise Harmonic Spectra

In addition to defining the distributions of external OASPL it is necessary to define the spectral distributions of sound pressure level of the tones which occur at multiples of the blade-passage frequency (BPF). Three different distributions are shown in Appendix A.

- The first distribution is the current estimate for the propfan from reference 5
- The second distribution postulates a 3-dB-per-harmonic decrease of the tone SPL

TABLE 1. - AIRCRAFT DESIGN AND MISSION CHARACTERISTICS

		Wide-body	Narrow-body	Small Aircraft
Range	km (n.mi)	2,778 (1,500)	1,852 (1,000)	5,741 (3,100)
No. Pax		200	100	16
Cruise Speed		0.8M	0.8M	0.8M
Initial Cruise Altitude	m (ft)	9,144 (30,000)	9,144 (30,000)	9,144 (30,000)
Field Length	m (ft)	2,134 (7,000)	1,524 (5,000)	1,524 (5,000)
Fuselage Diameter	m (ft)	6.12 (19.8)	3.91 (12.8)	2.24 (7.3)
Fuselage Length	m (ft)	47.5 (155.8)	30.0 (98.58)	17.6 (57.67)
Seat Pitch	m (ft)	.864 (2.8)	.864 (2.8)	.864 (3.2)
Seating Arrangement		8 – Abreast	6 – Abreast	2 – Abreast
TOGW	Kgm (lb_m)	98,641 (217,466)	40,823 (90,000)	14,515 (32,000)
Propulsion		STS 476	STS 476	STS 476
Propfan Diameter	m (ft)	3.84 (12.6)	3.78 (12.4)	2.19 (7.2)
Number of Blades		8	8	8
Tip Speed	(m/s (ft/s)	244 (800)	244 (800)	244 (800)
Power Loading	kW/m^2 (hp/ft^2)	293 (37.1)	242 (30.6)	224 (28.3)
No. Engines		4	2	2
Cruise Thrust	N/engine (lb/engine)	14,813 (3,330)	13,345 (3,000)	4,182 (940)
Blade Passage Frequency	(Hz)	162	164	283
Propeller Efficiency		0.837	0.852	0.854
$\frac{\text{Sea Level Static Thrust}}{\text{Takeoff Gross Weight}}$		0.26	0.27	0.27
Maximum Power kW (hp) at SLS	(SLS)/engine)	6,609 (8,863)	4,549 (6,100)	1,566 (2,100)
Sea Level Static Thrust	N/engine (lb/engine)	62,876 (14,135)	55,249 (12,420)	19,216 (4,320)

- The third distribution assumes 10 equal tones each 10 dB lower than the OASPL.

Most of the study results shown pertain to the first spectrum since it was considered the most realistic and it usually required larger acoustic treatment weights to meet the 80-dBA interior noise goal.

1.5 Procedure for Calculating Noise Reduction

The interior of the cabin is assumed to be a semireverberant environment with an average diffuse absorption coefficient postulated for all of the interior surfaces. Appendix A contains a curve of absorption coefficient versus frequency, and the simple equation relating noise reduction to the sidewall transmission coefficient and the absorption coefficient. The absorption coefficient schedule assumed in this study is considered to be nearly minimum values for a commercial transport aircraft.

1.6 Procedure for Calculating Transmission Loss (TL)

Appendix A describes the means by which the transmission loss of the treated fuselage is calculated by a synthesis of Koval's shell TL theory (reference 7) and the methods of Cockburn and Jolly (reference 8), Beranek and Work (reference 9) and others (references 10 to 14) for computing the incremental TL due to various sidewall add-on acoustical impedance elements.

Koval's shell theory (reference 7) includes inflight effects of external flow and cabin pressurization and is an extension of the approach of P. W. Smith (reference 6). A mathematical outline of Koval's theory is given in Appendix C, and Appendix D contains a critique of the present use of reference 7 for semimonocoque structures, especially the assumption wherein the stiffeners are "smeared" into the skin of an equivalent orthotropic but monocoque shell.

In Appendix D it is shown, based upon more recent work of Koval (references 15 and 16) that the smeared stiffener approximation gives a reasonable approximation to discrete stiffener results at excitation frequencies below the ring frequency which is relevant to propfan noise. Experimental data given in Appendix F show that the present methodology may be somewhat conservative at low frequencies for angles near normal incidence.

The analytical method for evaluating the performance of add-on noise-control impedance elements is described in Appendix E. This method is supported by test data for flat multilayer panels as shown in Appendix F. The use of flat panel data is considered a good approximation for this study, since the relevant acoustic wave lengths are large compared to the double-wall depth and the panel dimensions.

1.7 Damping Loss Factor Assumptions

For the baseline structure a damping loss factor of 6% is assumed throughout this study. Whenever a viscoelastic damping treatment is added to the outer-wall structure, it is assumed that the damping loss can be increased according to the schedule shown in Appendix G in connection with add-on noise-reduction results. For example, when the outer-wall surface density attains 19.5 kg/m^2 (4 psf), the loss factor is assumed to be 14%. The damping schedule assumed in this study is considered reasonable based upon unpublished Lockheed studies using the methods of references 17 and 18.

2. STRUCTURAL CONFIGURATION

2.1 Baseline Aluminum Structures

Aluminum baseline structures are defined for each of the three aircraft sizes on the basis of strength design considerations. The constructions are of a conventional semimonocoque type. Appendix B contains tables of all of the section property data needed for detailed design, weight analysis, and construction.

In order to calculate treatment mass penalties, it is necessary to know the baseline (zero penalty) surface densities for each aircraft. Table 2 shows the baseline surface density data which have been derived from the data in Appendix B.

2.2 Baseline Composite Orthogrid Structure

Appendix B shows sketches and dimensions of the composite strength-designed orthogrid structures designed for this study. These turn out to have essentially the same outer-wall stiffness as their aluminum counterparts; however, the outer-wall surface densities were smaller by factors ranging from 32 to 41% for the three aircraft. As a simplifying and somewhat conservative assumption, it was decided to use the same section properties and Young's modulus values as are used for the aluminum structure, but the density of the composite structure is assumed to be 70% of the aluminum density. These assumptions yield as baseline surface densities the values shown in table 3. These surface densities are the proper zero penalty reference values for a truly all-composite fuselage.

2.3 Definitions of Noise Reduction Concepts

The noise reduction approaches considered in this study include acoustical treatments that could conceivably be added on to currently existing fuselage structures (add-on), and those that would involve completely new fuselage designs (advanced).

TABLE 2. - BASELINE SURFACE DENSITY DATA FOR STRENGTH-DESIGNED ALUMINUM AIRCRAFT

Component	Wide-body		Narrow-body		Business Aircraft	
	kg/m^2	(psf)	kg/m^2	(psf)	kg/m^2	(psf)
Outer Wall	9.18	(1.88)	6.25	(1.28)	4.68	(0.96)
Fiberglas Blanket	0.73	(0.15)	0.73	(0.15)	0.49	(0.10)
Baseline Trim Panel	1.61	(0.33)	1.61	(0.33)	1.61	(0.33)
Total Wall	11.52	(2.36)	10.69	(1.76)	6.78	(1.39)

TABLE 3. - BASELINE SURFACE DENSITY DATA FOR AN ALL-COMPOSITE STRENGTH-DESIGNED ORTHOGRID STRUCTURE

Component	Wide-body		Narrow-body		Business Aircraft	
	kg/m^2	(psf)	kg/m^2	(psf)	kg/m^2	(psf)
Outer Wall	6.39	(1.31)	4.35	(0.89)	3.27	(0.67)
Fiberglas Blanket	0.73	(0.15)	0.73	(0.15)	0.49	(0.10)
Baseline Trim Panel	1.61	(0.33)	1.61	(0.33)	1.61)	(0.33)
Total Wall	8.73	(1.79)	6.69	(1.37)	5.37	(1.10)

2.3.1 Add-on noise-reduction design concept.- In add-on treatments, it is assumed that the surface density and structural damping of the outer wall can be increased, but not the stiffness. Increases in outer wall stiffness are examined in the advanced concepts study but could be implemented in an add-on fashion if that were feasible. Thus, the "limp-wall" approach proposed in the RECAT study (reference 1), which essentially involved the use of only mass and damping to increase TL, is an add-on approach. Appendix G, describes the add-on elements and the side wall design.

2.3.2 Advanced noise-reduction concepts.- Advanced noise-control methods explore the potential benefits not only of mass optimization and damping but also of significant increases in stiffness. The advanced configurations considered in this study are designated as advanced aluminum and advanced composite concepts. Both designs have increased outer-wall stiffness and increased outer-wall mass compared to their respective baselines. Structural

weight is increased in the process of increasing stiffness, and the added structural weight is considered as part of the acoustic treatment mass penalty. Thus, the same baseline reference is used for both the add-on and advanced noise-reduction designs. Although the composite baseline aircraft structures have the same stiffness level and TOGW as their aluminum counterparts, their surface densities are 30% less.

2.4 Effects of Add-On Elements in Advanced Noise-Reduction Concepts

For each combination of outer-wall mass and stiffness which is associated with the various advanced noise-reduction designs, it is necessary to select the trim-panel mass required to achieve the desired interior noise goal. Efficiency comparisons can then be made on the basis of finding the least total wall surface density which will provide an interior noise level of 80 dBA. Appendixes G and H contain such results for add-on and advanced designs.

3. ACOUSTICAL TREATMENT MASS PENALTIES OF RECOMMENDED NOISE-REDUCTION DESIGNS

3.1 Aluminum Add-On Noise Reduction Designs

Appendix I tabulates add-on design characteristics for the three aircraft, and figures 1, 2 and 3 show the axial distribution of total wall surface density to achieve an interior noise level of 80 dBA for the 4-engine wide-body, 2-engine narrow-body, and small business aircraft, respectively. These mass distribution results are derived from parametric optimization studies of the effects of varying outer wall and trim-panel mass in a double-wall configuration as described in Appendix G. The exterior noise signatures described in Appendix A were initially used to select the outer-wall and trim-panel surface densities required to obtain an interior noise level of 80 dBA. This was felt to be an overly conservative approach, which results in an excessive penalty mass. An alternate approach is presented here wherein the local exterior noise level is used to select the local surface density required to achieve 80 dBA. Thus, the total wall surface density is continuously varied to account for the local exterior noise level variation in lieu of a constant surface density for an entire segment. This is accomplished using the previously derived parametric studies of Appendix G. The change in external OASPL (the difference between the assumed segment design levels and the directivity curves of Appendix A) can be used to select a new double wall configuration since the parametric study results in Appendix G are plotted versus change in interior noise level at constant exterior OASPL. These results are equivalent to plotting required surface density versus external OASPL at constant interior noise level. Therefore, a local decrease of external OASPL permits a decrease of surface density comparable to allowing the interior noise to increase by the same amount.

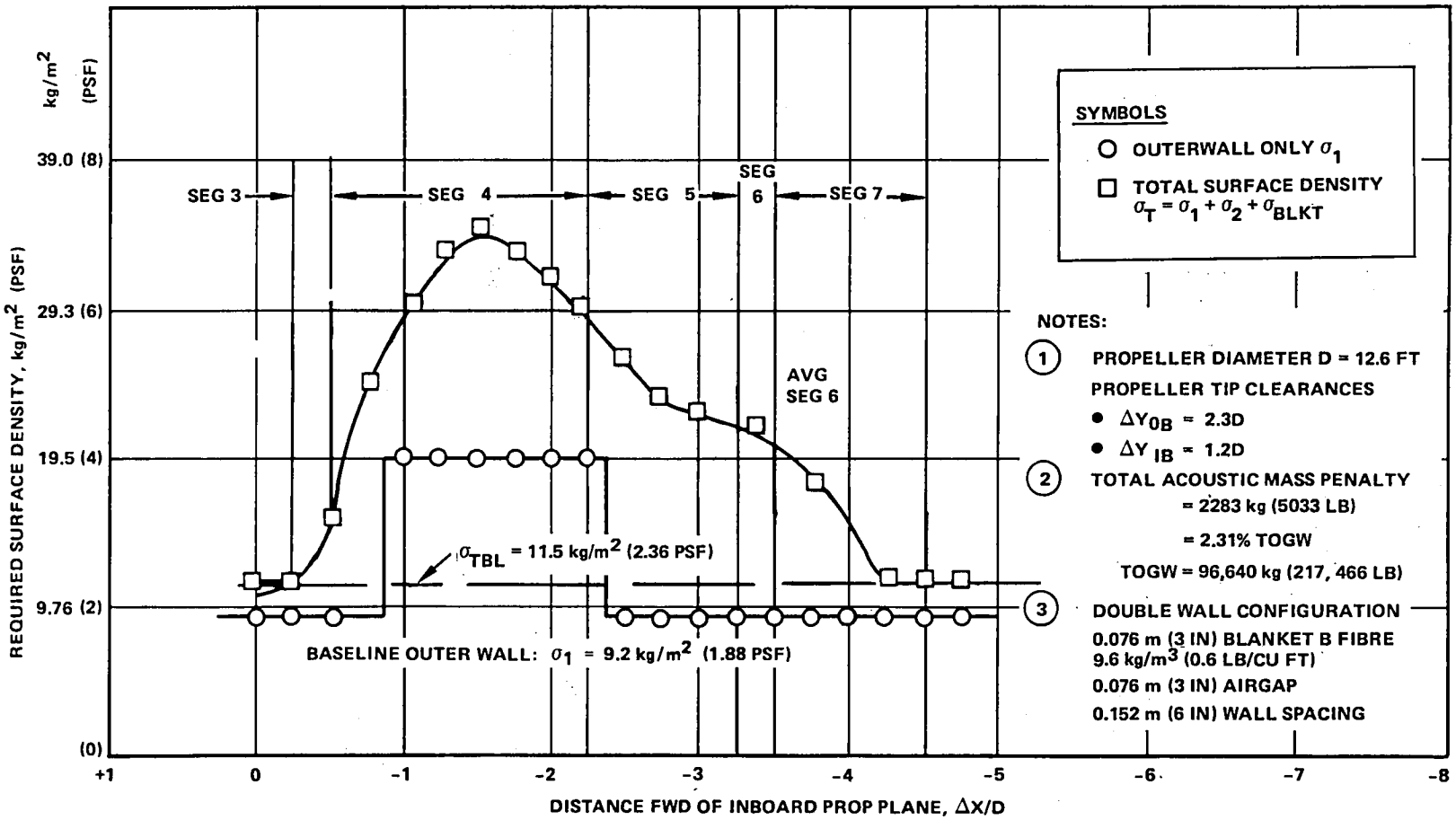

Figure 1. - Required fuselage surface density distribution; 4-engine wide-body add-on design.

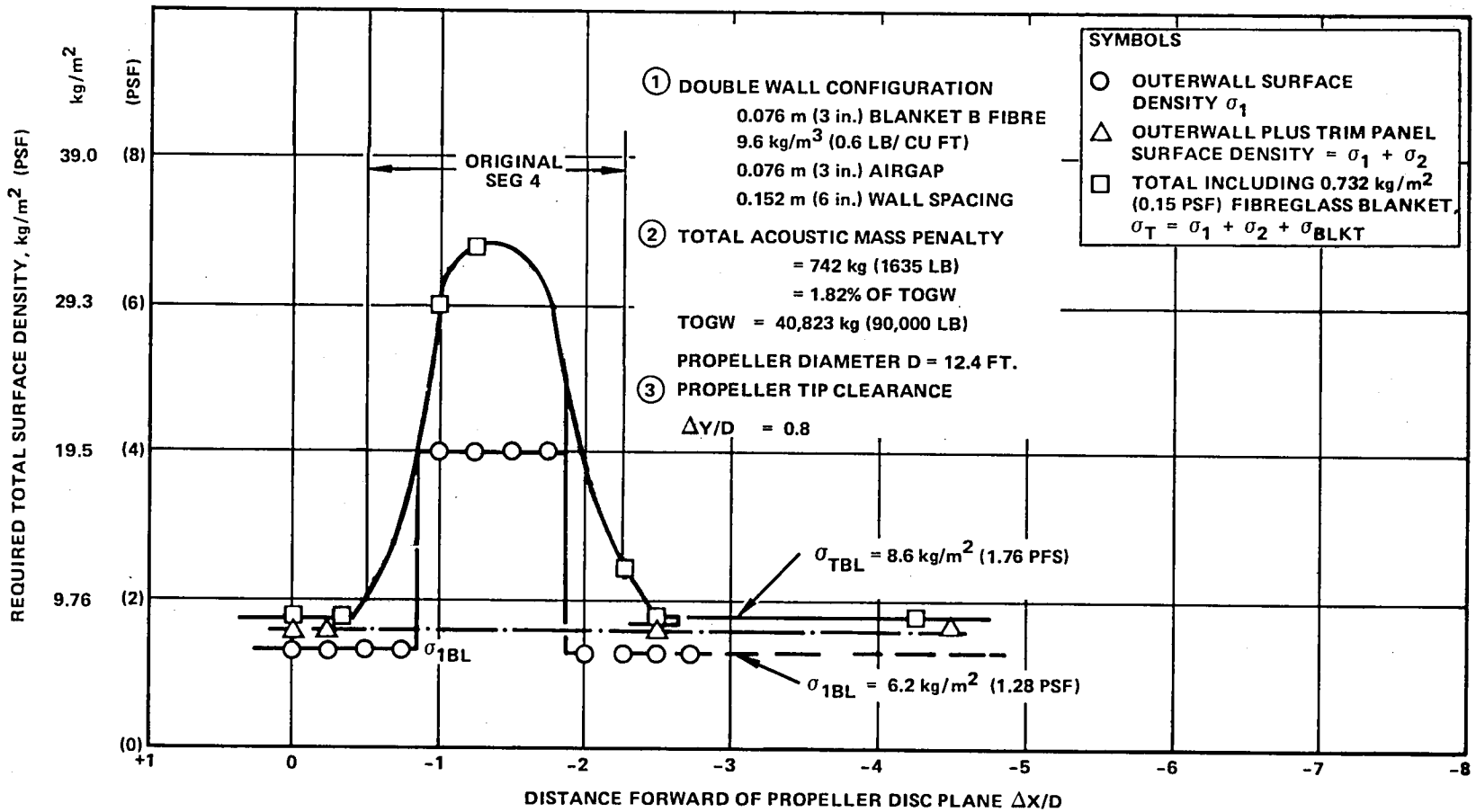

Figure 2. - Required fuselage surface density distribution; 2-engine narrow-body add-on design.

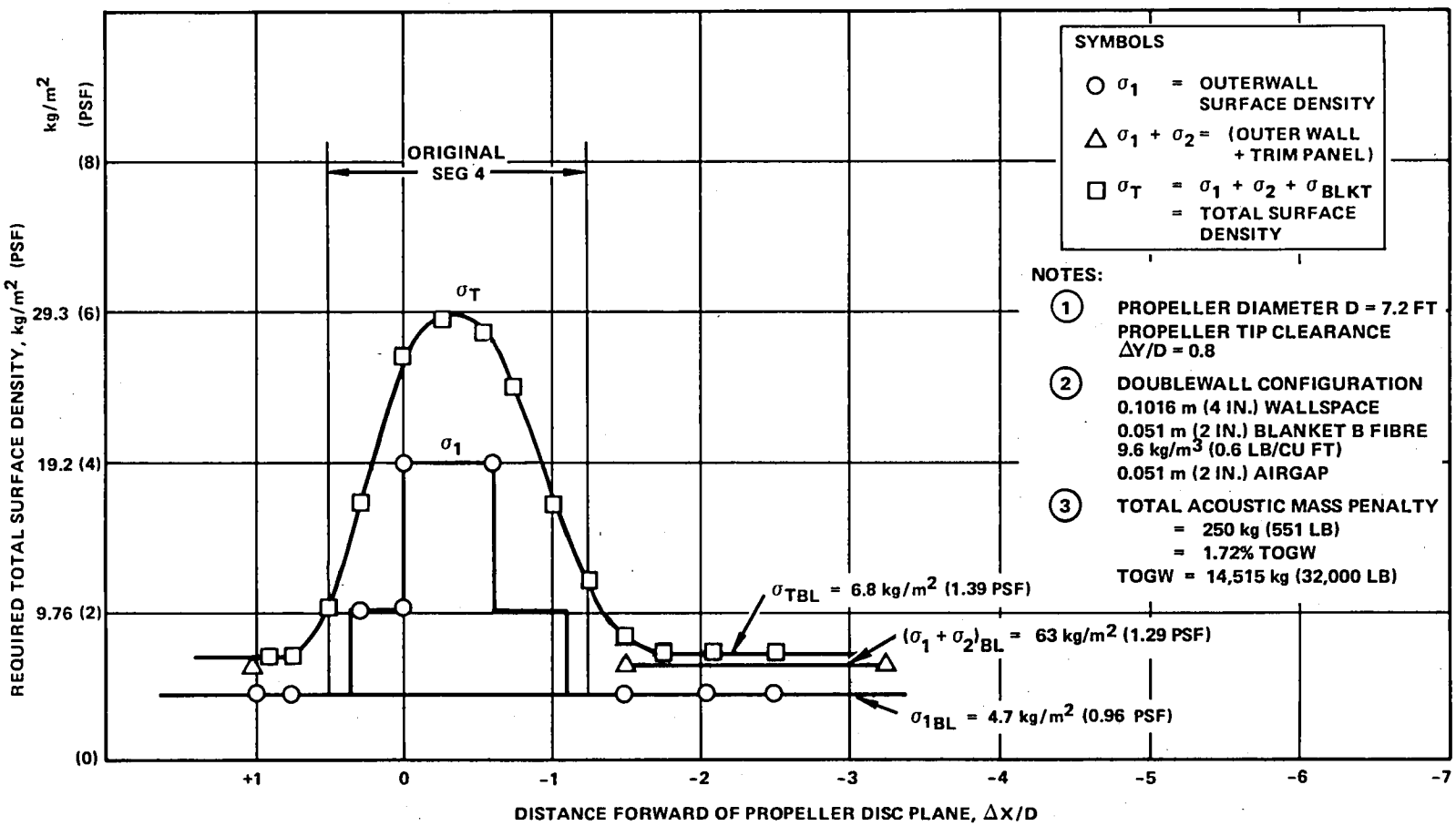

Figure 3. - Required fuselage surface density distribution; 2-engine business aircraft; add-on design.

Figure 1 shows the effect of the extended external noise signature associated with the 4-engine, wide-body aircraft configuration. Notice that the optimum outer-wall surface density if 19.5 kg/m^2 (4 psf) within Segment 4 as is discussed in Appendix G. In the lower noise regions, it is better to retain the baseline outer-wall mass value and use the treatment penalty mass in the form of increased trim panel mass. These results generally reflect the fact that the best performance is achieved in an add-on, double-wall design when both the trim panel and outer-wall mass are equal. Thus the higher external noise levels of segment 4 cannot be as efficiently attenuated by a simple add-on approach as is done in the other segments.

A comparison between the 4-engine aircraft results of figure 1 and those for the 2-engine aircraft in figures 2 and 3 demonstrates the beneficial effects of reduced propeller tip clearances. Reduced tip clearances result in external noise signatures with more limited axial extent and shallower grazing angles of incidence at locations away from the propeller disc plane (see Appendix A). No attempt was made to optimize the tip clearance for the 2-engine aircraft, although some improvements were made for the 4-engine aircraft.

Table 4 shows a summary of the acoustical treatment penalty mass requirements for conventional aluminum aircraft. These penalties include treatment of 60% of the sidewall circumference (the fraction above the floor). This assumption is less conservative than was used in reference 1, where full circumferential treatment was assumed; however, the current assumptions are considered justifiable by virtue of a better prediction methodology. The wide-body weight penalty is 2283 kg (5033 lb) which is remarkably close to the value 2368 kg (5220 lb) given on p 2-2 of reference 1. The present study resulted in higher surface density values of 35 kg/m^2 (7.2 psf) in the peak noise region combined with a smaller treatment area compared to the results of reference 1. In reference 1, lower peak surface density values of about 22 kg/m^2 (4.5 psf) combined with a conservatively larger treatment area to give a nearly equal penalty. The treatment penalties shown in table 4 range from 1.7% to 2.5% of the gross weights of the aircraft involved.

The results of table 4 are considered encouraging in that the acoustical treatment penalty requirements for cabin noise control are comparable to or less than the values estimated in the RECAT study, reference 1. Therefore, the estimated 17% net savings in fuel consumption, shown in reference 1 for the propfan-powered aircraft, relative to comparable turbofan-powered aircraft still appears to be valid. This conclusion is based upon the present assessment of add-on noise-control technology and it is one of the major conclusions of the present study.

3.2 Composite Add-On Noise-Reduction Designs

This outer-wall structural concept is a potential candidate if designers select an all-composite fuselage on the basis of nonacoustical considerations.

TABLE 4. - SUMMARY OF ADD-ON ACOUSTIC TREATMENT MASS PENALTIES

I. ADD-ON NOISE CONTROL DESIGNS

- OUTER WALL STIFFNESS = BASELINE VALUE
- OPTIMUM OUTER WALL MASS
- FLIGHT CONDITIONS – 9144 m (30,000 ft), M = 0.8, V_t = 244 m/s (800 ft/sec), 8 BLADES
- 60% OF SIDEWALL PERIMETER TREATED (ABOVE FLOOR ONLY)

ALUMINUM AIRCRAFT

TYPE NO. ENG.	TAKEOFF GROSS WEIGHT TOGW kg (lb)	FUSELAGE DIAMETER m (ft)	PROP DIAMETER m (ft)	BASELINE OUTER WALL SURFACE DENSITY kg/m^2 (PSF)	BLADE PASSAGE FREQUENCY Hz	MASS PENALTY kg lb	% TOGW
WB/4	98 461 (217 466)	6.10 (20.00)	3.84 (12.6)	9.17 (1.88)	162	2 283 (5 033)	2.31
NB/2	40 823 (90 000)	3.90 (12.80)	3.78 (12.4)	6.25 (1.28)	164	742 (1.635)	1.82
SBA/2	14 515 (32 000)	2.23 (7.33)	2.19 (7.2)	4.68 (0.96)	283	250 (551)	1.72

An all composite aircraft designed for the same mission requirements would be considerably lighter in weight and have resized powerplants. Complete redesigns of the composite aircraft are considered beyond the scope of this study; therefore, the composite aircraft are assumed to have the same TOGW as their aluminum counterparts. The outer-wall stiffness of the three different-sized aircraft are essentially unchanged from their aluminum counterparts; however, the baseline outer-wall surface densities are approximately 70% of the baseline surface densities of the corresponding aluminum aircraft. The results are important because they indicate what may result in regard to noise reduction penalties if acoustical design requirements are not incorporated initially into the structural design. The available noise reduction tools are, in this case, restricted to outer-wall mass and damping treatments, trim panel mass variations, and other interior nonstructural modifications.

The mass penalty results are summarized in table 5. They are higher than the aluminum add-on penalties shown in table 4 by amounts ranging from 0.16% TOGW for the wide-body to 0.11% TOGW for the small business aircraft. The mass penalty increases are 7% for the wide-body, 16% for the narrow-body and 7% for the small business aircraft. These slight increases are due to the fact that the total surface density in the peak region is about the same as for the aluminum add-on designs shown in figures 1, 2 and 3, but the baseline surface densities for the composite aircraft are 30% lower than for the aluminum aircraft.

TABLE 5. - ACOUSTICAL TREATMENT MASS PENALTIES FOR ADD-ON COMPOSITE STRUCTURAL DESIGNS

Aircraft No. Engines	Takeoff Gross Weight kg (lb)	Fuselage Diameter m (ft)	Propeller Diameter m (ft)	σ_1 Baseline Outerwall Surface Density kg/m^2 (psf)	Blade Passage Frequency Hz	Mass Penalty	% TOGW
WB/4	98,641 (217,466)	6.1 (19.8)	3.84 (12.6)	6.39 (1.31)	162	2441 (5,381)	2.47
NB/2	40,823 (90,000)	3.9 (12.8)	3.78 (12.4)	4.34 (0.89)	164	860 (1,895)	2.11
SBA/2	14,515 (32,000)	2.23 (7.33)	2.19 (7.2)	3.27 (0.67)	283	266 (586)	1.83

NOTES:

(1) Baseline outer wall stiffness is same as that of the aluminum baseline structure.

(2) Baseline outer wall surface density is 70 percent of aluminum baseline surface density.

(3) Outer wall surface density increased in Segment 4 only to 19.5 kg/m^2 (4 psf) for 80 dBA requirement.

(4) Remainder of noise control penalty mass represents increased trim panel surface density.

3.3 High Stiffness Advanced Noise-Reduction Designs

The results discussed here pertain to benefits to be obtained by further increases of outer-wall stiffness, which may be achievable using aluminum, and for a possible all-composite material, orthogrid fuselage design in the future. A preliminary design study determined the section properties required to achieve higher-stiffness, outer-wall structures for each aircraft size for both aluminum and graphite/epoxy structures. The weight increases associated with increases in outer-wall stiffness were calculated and these relationships are shown in figures 4 and 5. In each case, the baseline outer-wall stiffnesses are equal for the aluminum and composite aircraft; however, the baseline surface densities vary for the 3 different aircraft sizes according to table 2 for aluminum aircraft and table 3 for the all-composite aircraft. The baseline section properties are described in Appendix B for aluminum, and the composite properties are the same except the outer wall bulk density is 70% of the aluminum value.

Figure 6 shows the mass distribution comparisons between the add-on and advanced aluminum noise-reduction designs. These results are obtained by finding the minimum total wall surface density needed to achieve 80 dBA for each segment. Using the sidewall design charts in Appendixes G and H, the minimum wall surface density is selected on the basis of outer-wall mass, stiffness, loss factor, and trim panel mass. These results demonstrate the synergistic benefit of combining optimum double-wall performance in conjunction with stiffening the outer wall under realistic conditions. Appendixes B and I contains a more complete description of these designs.

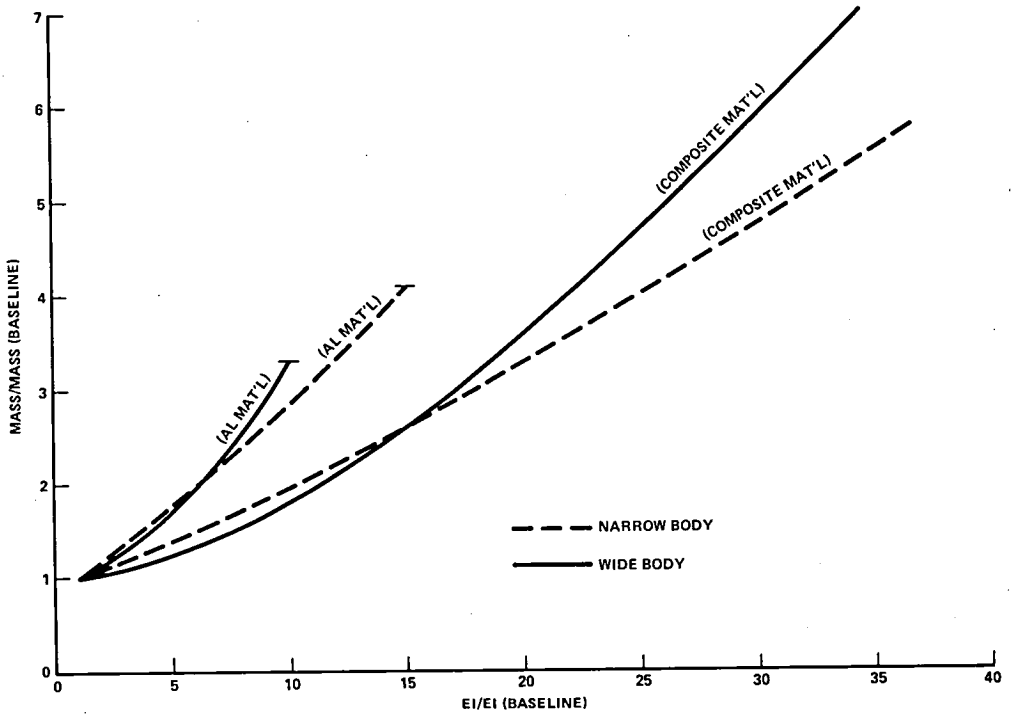

Figure 4. - Fuselage outerwall mass required vs stiffness level for wide-body and narrow-body advanced noise-reduction designs.

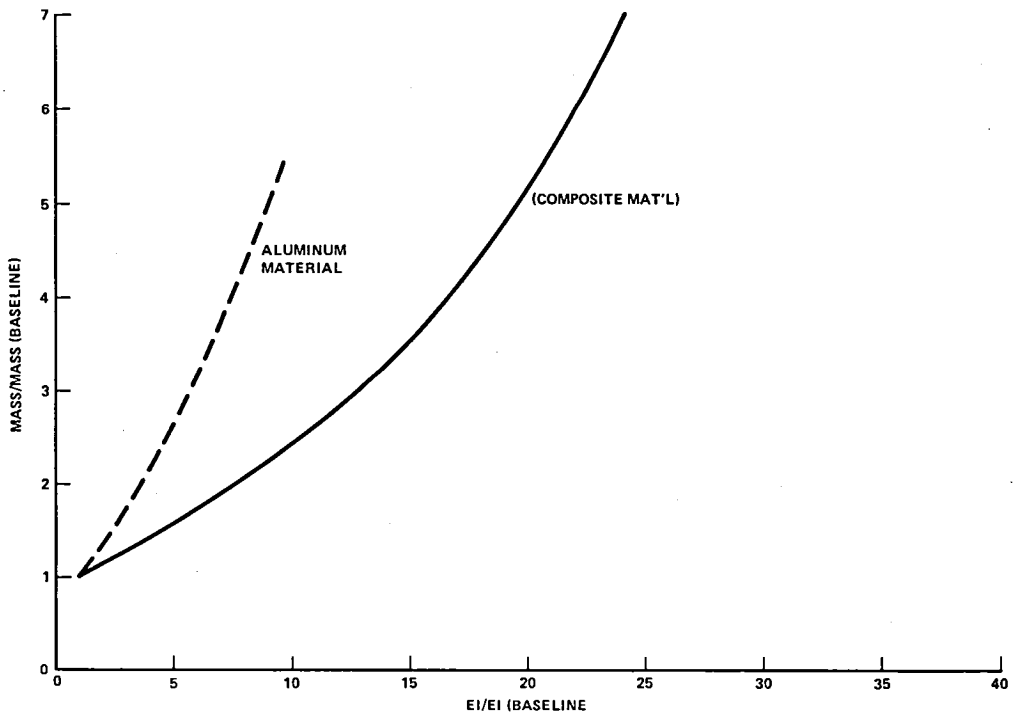

Figure 5. - Fuselage outerwall mass required vs stiffness level for business aircraft advanced noise-reduction designs.

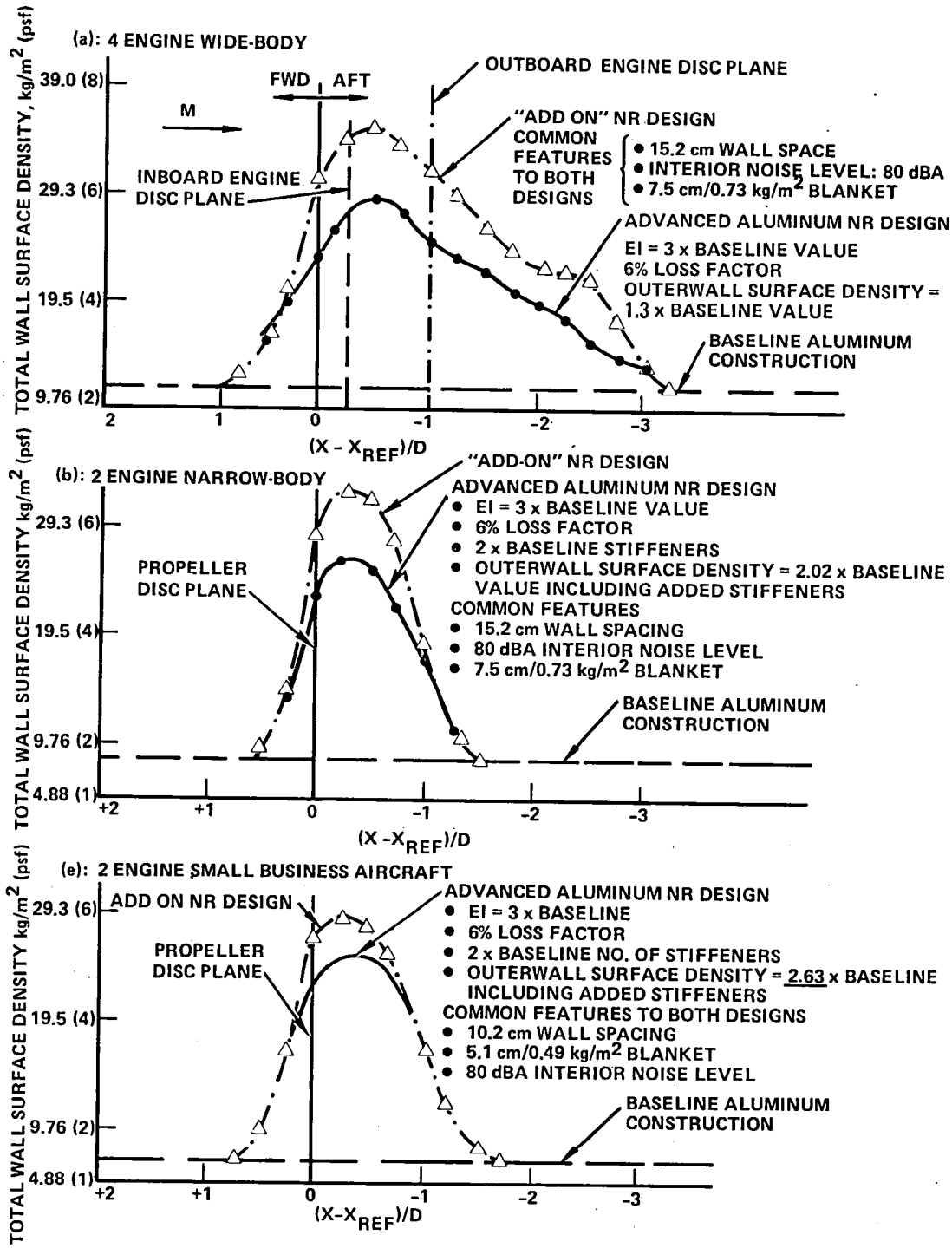

Figure 6. - Comparison of required surface density distributions advanced noise-reduction design vs add-on noise-reduction design.

Table 6 summarizes the integrated acoustical treatment mass penalties for the various aircraft sizes and for various advanced noise-reduction concepts. It is seen that the use of all-composite fuselages would further reduce the penalties to about 1% of TOGW for the 4-engine, wide-body aircraft and 1.4% for the 2-engine, narrow-body aircraft. It is possible that the choice of a different propeller tip clearance for the 2-engine narrow-body aircraft could bring the results in closer agreement with the wide-body as regards the benefits of the advanced design.

Parametric studies of outer-wall stiffness effects for advanced noise-reduction designs are given in Appendix H. Appendixes B and I contain descrip-descriptions of the advanced noise-reduction designs. It is generally found that when the outer-wall stiffness is increased in the range of five to tenfold, efficient noise control is achieved with small amounts of trim panel mass.

The results of table 6 are considered encouraging in that the advanced noise-reduction designs indicate significant mass penalty reductions relative to the add-on results even for aluminum aircraft.

4. DESCRIPTION OF FUSELAGE SIDEWALL DESIGNS

4.1 Baseline Designs and Maximum Noise Reduction Designs

Appendix B contains descriptions of eighteen different fuselage sidewall construction designs evolved in this study. These designs include six baseline (strength-designed or nonacoustical) designs and twelve high noise reduction designs calculated to provide an interior noise level of 80 dBA or less in the region of peak exterior noise near the propeller disc plane. The various designs can be classified into six categories for each

TABLE 6. - SUMMARY OF MASS PENALTY DATA

AC / TOGW	Wide-body A/C 9864 kg (217 466 lb)			Narrow-body A/C 40 823 kg (90 000 lb)			Business A/C 14 515 kg (32 000 lb)		
Concept	kg	(lb)	W_{TR} % TOGW	kg	(lb)	% TOGW	kg	(lb)	% TOGW
(1) Add-on Aluminum	2283	5033	2.31	741	1635	1.82	250	551	1.72
(2) Advanced Aluminum	1523	3358	1.54	616	1357	1.51	225	445	1.55
(3) Add-on Composites	2441	5381	2.47	660	1895	2.11	266	586	1.83
(4) Advanced Composites	1009	2225	1.02	573	1264	1.40	107	237	0.740

of the three aircraft sizes (wide-body, narrow-body and small business aircraft) as follows:

1. Baseline aluminum designs

2. Baseline composite material designs

3. Add-on aluminum noise reduction designs

4. Add-on composite noise reduction designs

5. Advanced aluminum noise reduction designs

6. Advanced composite noise reduction designs

Appendix B presents details of the sidewall construction using generalized dimensions, and provides the numerical values of the dimensions for each of the side wall designs described above. Also given are dimensional data for the skin and stiffeners for each of the designs, and the section properties of the stiffeners.

4.2 Definition of Fuselage Side Wall "Smeared" Stiffness

Average or smeared stiffness is defined as the stiffness per unit length of the combined section which includes a stiffener and piece of skin whose width is equal to the spacing between stiffeners (see Appendix B). These single element section properties are used to calculate the properties of the combined skin and stiffener sections. Bending moments of inertia are calculated about the neutral axis of the combined section and these data are used to calculate the relative stiffness ratios. The mass increases associated with increased outer-wall stiffness are consistent with the mass-versus-stiffness ratio plots presented in figures 4 and 5. The composite advanced noise-reduction designs use high modulus material only for the flanges of the frames and stringers whereas the modulus of the webs and skin remain at the baseline values. The inner flange modulus is increased as much as 2.5 times the baseline value by the addition of high modulus, uniaxial fibers to the inner flange.

Stiffener torsional constants were not changed from the baseline values when the advanced aluminum and advanced composite aircraft were analyzed. The actual values did change -- occasionally higher or lower than the baseline values. This occurred because the detail design of the advanced aircraft was not finalized when the noise-reduction calculations were performed. This is not considered significant since within the framework of Koval's smeared stiffener analysis, the torsion constant has only a minor effect on the shell impedance.

4.3 Axial Variations of Sidewall Design Characteristics

The fuselage side wall construction details described above represent two extremes 1) the baseline design, having a zero penalty mass, and 2) the maximum noise-reduction design. For fuselage locations which are close to the propeller plane but not exactly at the peak external noise location, a lesser amount of side wall modification is required. For the add-on noise-reduction designs, figures 1 through 3 indicate the axial distributions of

- Total sidewall surface density
- Total outer-wall surface density

Appendix I gives the axial distribution of noise control parameters for each of the six add-on designs, three aluminum and three composite outer-wall structures, including

- Total side-wall density
- Total outer-wall surface density
- Surface density of outer-wall viscoelastic damping treatment added
- Thickness of the viscoelastic damping layer
- Damping loss factor
- Trim panel surface density

Appendix I describes the axial variation of the noise control parameters for each of the six advanced noise-reduction designs, including

- Relative stiffness level of the outer wall compared to the baseline stiffness
- Relative stiffener spacing compared to the baseline structure
- Total outer-wall surface density including the effects of stiffener spacing changes
- Trim panel surface density
- Total side-wall surface density

APPENDIX A
METHODOLOGY AND ASSUMPTIONS

A1. EXTERIOR NOISE SIGNATURES AND AIRCRAFT DESIGN DESCRIPTION

The fuselage wall in the vicinity of the propeller disc plane was divided into five segments of varying length as shown in figures 7 and 8 and table 7. Segment lengths and exterior noise levels were selected to represent the estimated noise signatures derived from the Hamilton Standard data of reference 5. Seven segments were originally selected but the propeller noise levels at segments 1 and 2 (forward of the propeller disc plane) were low enough to be ignored. For the 2-engine aircraft, the normalized propeller tip clearance $\Delta y/D$ is 0.8, and the propeller disc plane is the reference location $\Delta x/D = 0$. The segment OASPL's selected for the 2-engine aircraft are very conservative as shown in figure 7 except for segment 4, where the 134 dB peak exterior noise level is the selected segment design level. The directivity data derived from reference 5 for the 4-engine, wide-body aircraft are shown in figure 8. Normalized propeller tip clearances ($\Delta y/D$) of 1.2 and 2.3 were used for the inboard and outboard propellers, respectively. As the engines move outboard on the wing they also move aft and the axial locations of the inboard and outboard propeller disc planes are $-0.27\ \Delta x/D$ and $-1.01\ \Delta x/D$. The segment design levels are shown in figure 8, where the peak noise level of 132 dB is selected for segment 4. This is lower than the peak level for the 2-engine aircraft because the inboard engine is further outboard; however, the exterior noise signature is shown to be more extensive in the axial direction due to the outboard engine contribution. The segment boundaries and exterior noise levels are listed in table 7.

Interior noise calculations are performed for each segment as though it represented the entire fuselage. The segment exterior noise level and range of angle of incidence are considered typical and the fuselage is designed to achieve an interior noise level of 80 dBA. Segment noise reduction is a function of angle of incidence and is obtained by an antilogarithmic summation and average of the noise reduction calculated at several specific angles of incidence within the segment. For the peak noise region of segment 4, the range of incidence angle is quite large, and fifteen equally spaced angles of incidence are used to obtain segment noise reduction. The range of incidence angles within each segment is given in table 7, and incidence angle is given as a function of axial position in figure 9. Koval's theory (reference 7) predicts that the low-frequency sound waves are attenuated less as the angle of incidence approaches normal incidence. Thus, there are optimum propeller tip clearances which minimize the combined effect of the more intense inboard propeller noise signature and the greater axial extent of the outboard propeller's directivity. The optimum propeller tip clearance is a $\Delta y/d$ of 1.2 for the inboard engine of the 4-engine, wide-body aircraft. A trade-off study between intensity and directivity is also possible for the 2-engine aircraft; however, schedule time did not permit tip clearance optimization studies for the 2-engine aircraft.

TABLE 7. - FUSELAGE SEGMENT PROPERTIES

Propeller Tip Clear. $\left(\frac{\Delta y}{D}\right)_{IB}$	Propeller Tip Clear. $\left(\frac{\Delta y}{D}\right)_{OB}$	Segment No.	Position $\frac{(X - X_{IB})}{D}$	Location	Average ΔOASPL For Segment* dB	Local Graze Angle of Incident Sound Wave From: Inboard Prop Rad	Inboard Prop (Deg)	Outboard Prop Rad	Outboard Prop (Deg)
A. Two-Engine Aircraft									
0.8	N/A	3	1.42	Forward Edge, Seg. 3	-10	2.63	(151)	N/A	
			0.47	Aft Edge, Seg. 3		2.10	(120)		
		4	0.47	Forward Edge, Seg. 4	0	2.10	(120)		
			0	Inboard Engine Propeller Disc Plane		1.57	(90)		
			-1.23	Aft Edge, Seg. 4		0.58	(33)		
		5	-1.23	Forward Edge, Seg. 5	-10	0.58	(33)		
			-2.18	Aft Edge, Seg. 5		0.35	(20.2)		
		6	-2.18	Forward Edge, Seg. 6	-20	0.35	(20.2)		
			-2.48	Aft Edge, Seg. 6		0.31	(17.8)		
		7	-2.48	Forward Edge, Seg. 7	-30	0.31	(17.8)		
			-2.78	Aft Edge, Seg. 7		0.28	(16.1)		
B. Four-Engine Wide-Body Aircraft									
1.2	2.3	3	1.42	Forward Edge, Seg. 3	-10	2.44	(140)	2.12	(127)
			0.47	Aft Edge, Seg. 3					
		4	0.47	Forward Edge, Seg. 4	- 2	1.94	(111)	1.77	(102)
			-0.27	Inboard Disc Plane		1.39	(77)	1.45	(83)
			-1.012	Outboard Disc Plane		0.87	(49.9)	1.16	(66.2)
			-1.23	Aft Edge, Seg. 4		0.77	(44.3)	1.08	(61.9)
		5	-1.23	Forward Edge, Seg. 5	- 7	0.77	(44.3)	1.08	(61.9)
			-2.18	Aft Edge, Seg. 5		0.50	(28.8)	0.81	(46.5)
		6	-2.18	Forward Edge, Seg. 6	-12	0.50	(28.8)	0.81	(46.5)
			-2.48	Aft Edge, Seg. 6		0.45	(25.8)	0.75	(42.8)
		7	-2.48	Forward Edge, Seg. 7	-15	0.45	(25.8)	0.75	(42.8)
			-2.78	Aft Edge, Seg. 7		0.41	(23.3)	0.69	(39.6)

NOTE:*

(1)ΔOASPL = OASPL - 134 db

(2) Segments 1 and 2 forward of those described in this table are found not to require acoustic treatment and therefore are omitted from this report.

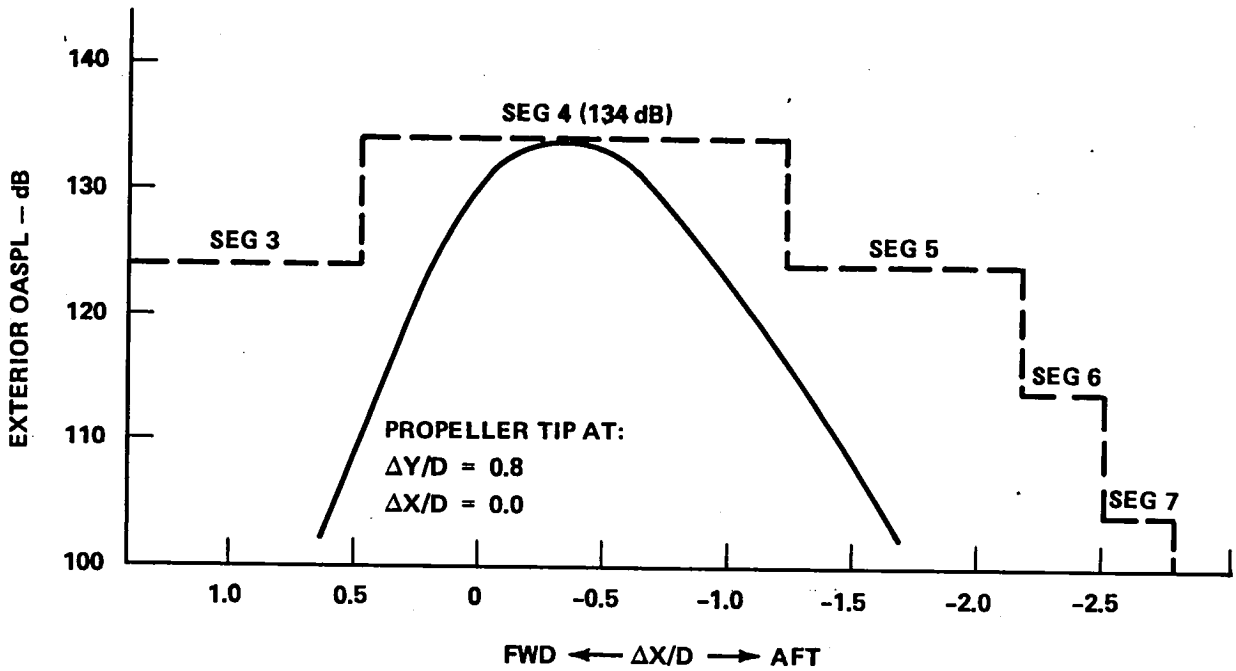

Figure 7. - 2-Engine aircraft exterior noise signature and treatment segments.

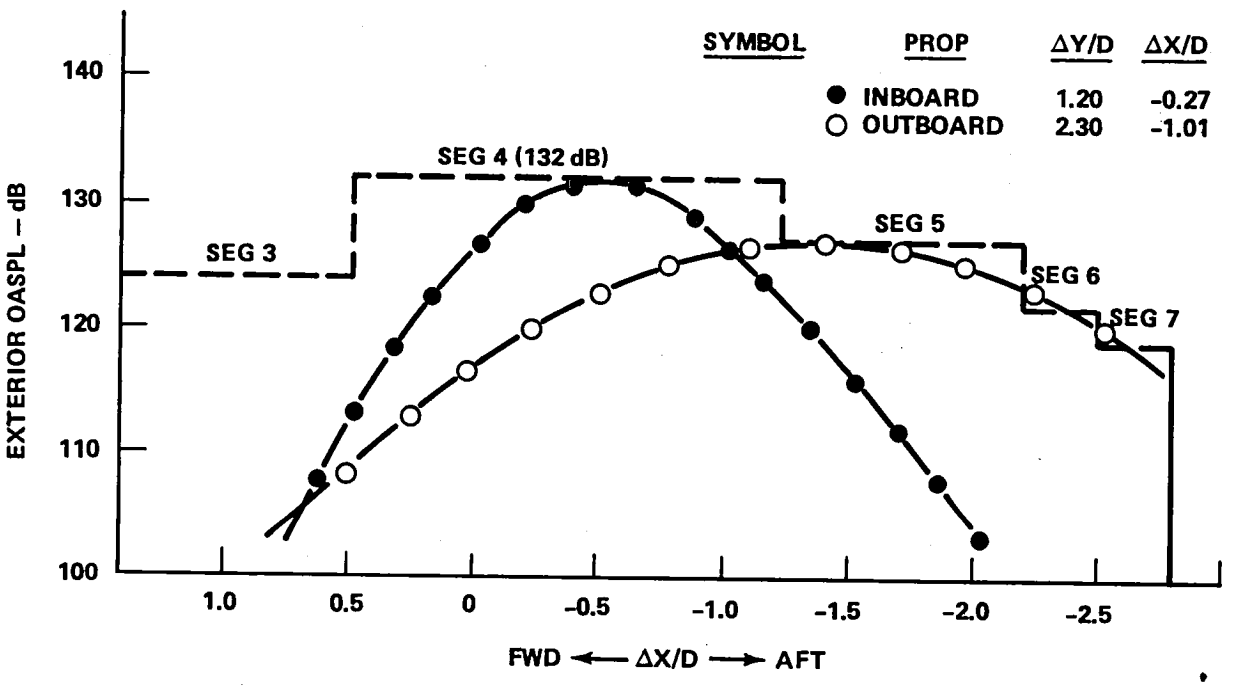

Figure 8. - 4-Engine wide-body aircraft exterior noise signature and treatment segments.

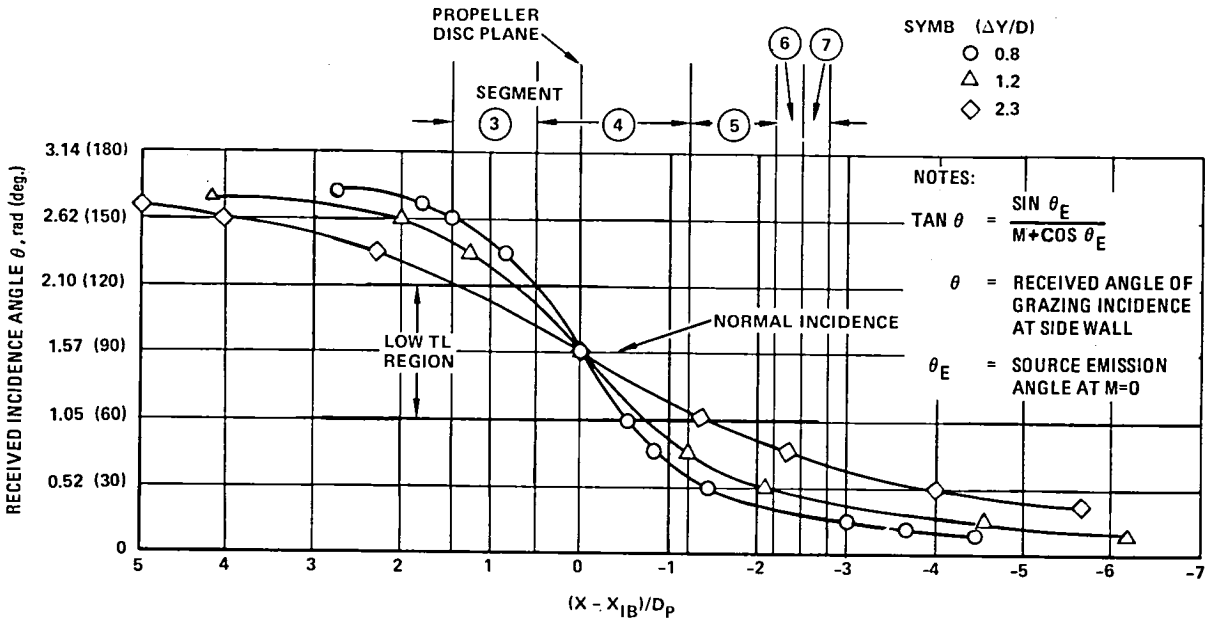

Figure 9. - Angle of incidence versus axial position.

It is noted that the segment noise levels discussed above are, in general, much higher than those provided by Hamilton Standard, and would lead to an excessively conservative amount of acoustical treatment. The segment levels were employed in order to simplify the analysis in deriving the wall surface density versus interior noise-level relationships discussed in Appendix G. In the final analysis, the required surface density was adjusted downward to account for the noise-level differential between the segment levels and the continually varying levels provided by Hamilton Standard. This approach is described in Section 3.1.

Table 1 itemizes the design characteristics of the three aircraft selected for this study. Figures 10, 11 and 12 show the general arrangements of the wide-body, narrow-body, and business aircraft, respectively. The wide-body aircraft design used in this study is the same one derived in the RECAT study of reference 1. This similarity allows a direct comparison of the acoustical treatment penalties of the current study with the preliminary design estimates of reference 1. The other two aircraft used for this study are possible commercial aircraft candidates using narrow-body and small business aircraft diameters. The number and sizing of propellers is related to each aircraft mission. The business aircraft is a long-range version of the Lockheed JetStar and has a propeller loading design value SHP/D^2 = 223 kW/m^2 (28.3 HP/Sq ft), only

CHARACTERISTICS	WING		HORIZ	VERT
	BASIC	TOTAL		
AREA (m^2)	185	209	26.4	24.2
ASPECT RATIO (%)	10		5	1.6
SPAN (m)	43.2		11.5	6.2
ROOT CHORD (m)	6.6	7.8	3.5	6.0
TIP CHORD (m)	2.0		1.1	1.8
MAC (m)	4.7		2.5	4.3
TAPER RATIO	0.3		0.3	0.3
SWEEP (rad)	0.44		0.44	0.56
T/C ROOT (%)		14 ①	10	10
T/C TIP (%)	11		8	8

① AT BL 3.0 m

POWER PLANT: PRATT & WHITNEY STS 476
REMATCHED TURBOSHAFT ENGINE
SLS THRUST 62 872N (6609 kW)

3.84 m HAMILTON
STANDARD PROPELLER

- 4 PROPFANS
- 200 PAX
- MACH 0.8
- 2 778 km

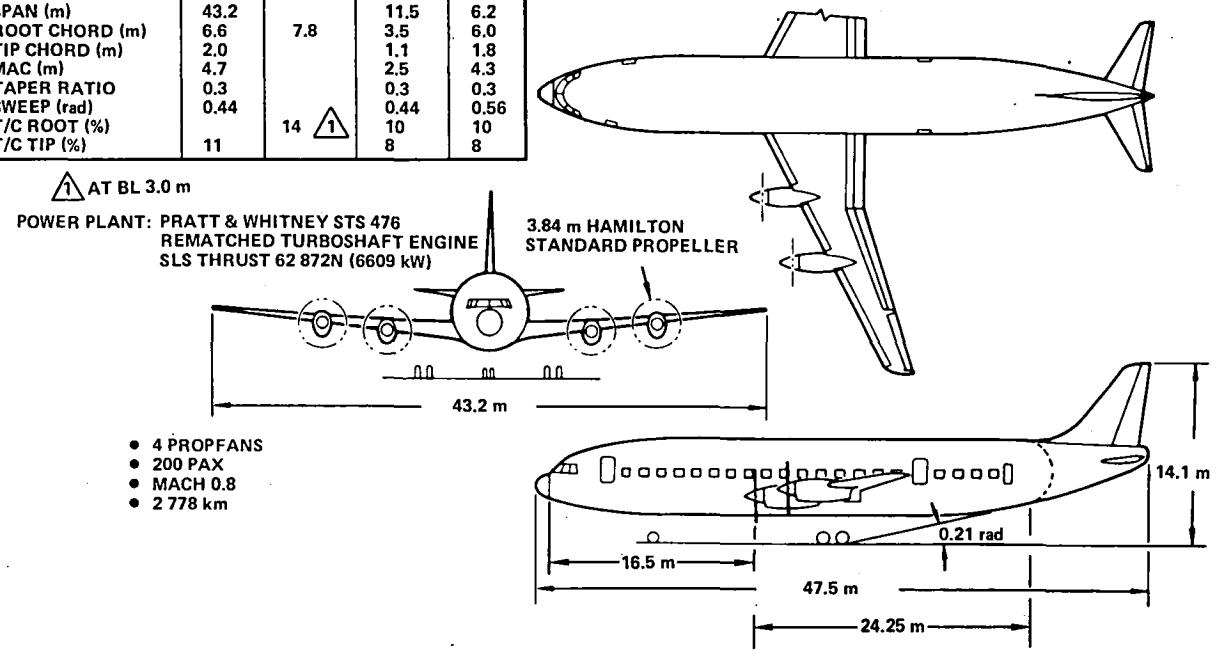

Figure 10. - General arrangement - wide body.

TAKE-OFF GROSS WEIGHT – 41 730 kg
POWER PLANT (2)
PRATT & WHITNEY STS 476
SCALED TO 4549 kw
STANDARD SEATING 20% – 80% MIX;
4 – 6 ABREAST

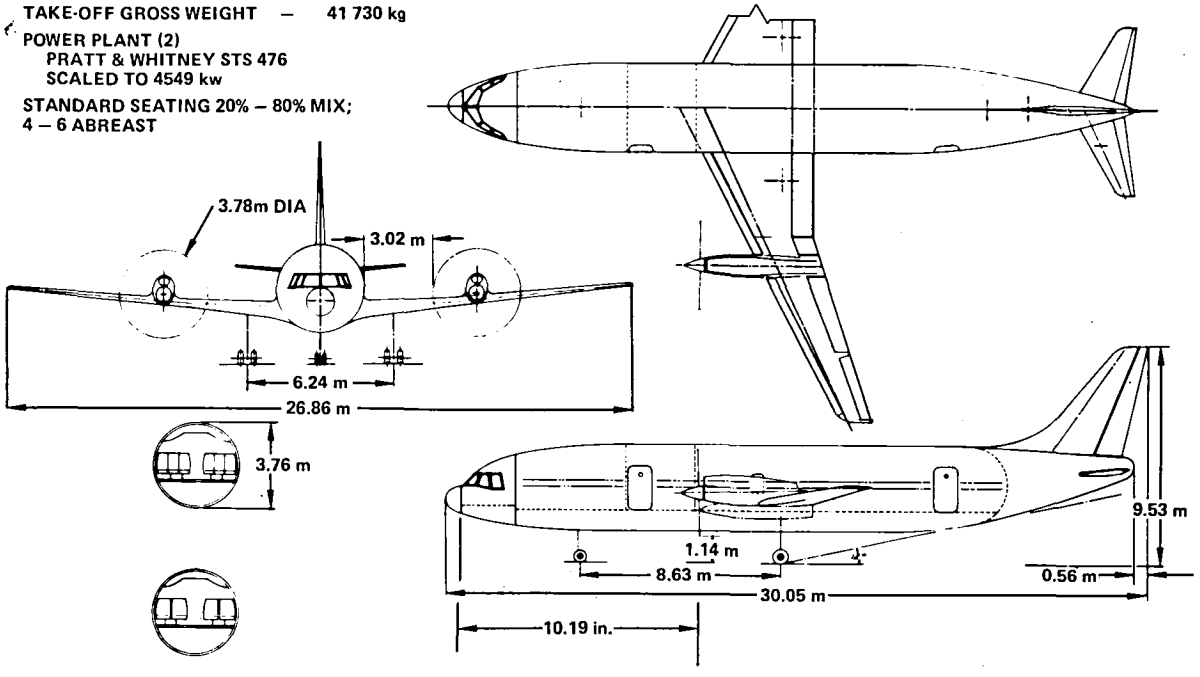

Figure 11. - General arrangement - narrow-body.

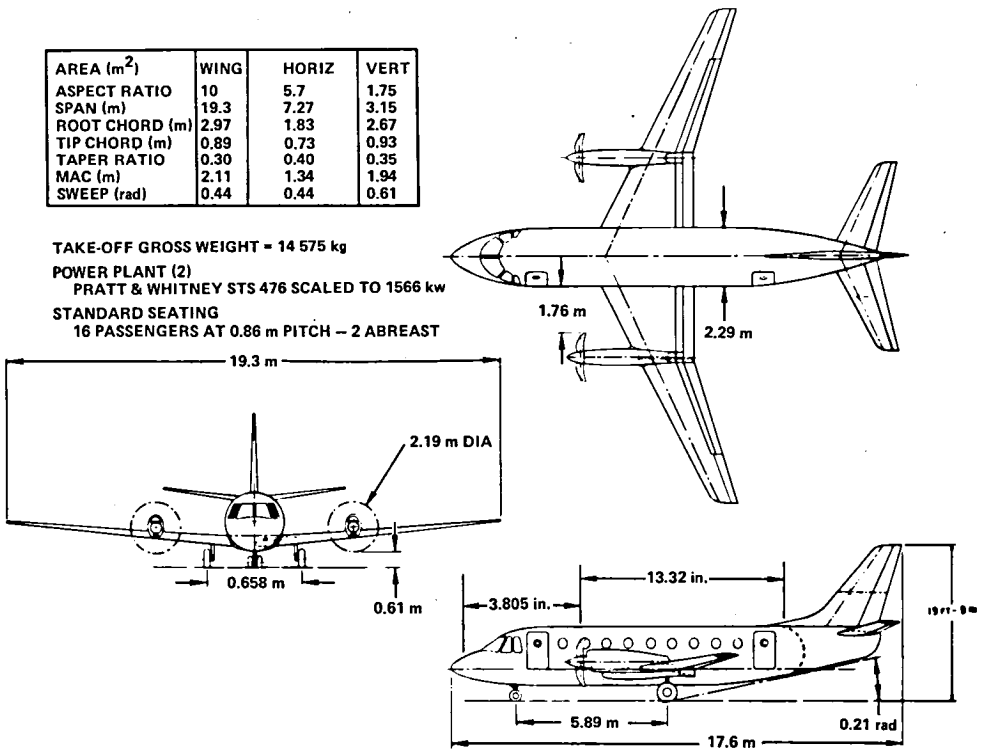

Figure 12. - General arrangement - business aircraft.

slightly lower than that for the narrow-body aircraft. Both of these aircraft have propfan diameters which are nearly equal to their fuselage diameters. A higher propeller power loading, 293 kW/m^2 (37.1 HP/sq ft) is used for the 4-engine wide-body whose propfan diameter is only 60% of its fuselage diameter. It should be noted that the required propeller diameter is proportional to the square root of the required thrust or aircraft TOGW, and if the wide-body had only two engines, then its propfan diameter would be nearly equal to its fuselage diameter.

A2. PROPELLER HARMONIC DISTRIBUTIONS ASSUMED FOR EXTERNAL ACOUSTIC PRESSURE DISTRIBUTION

Figure 13 displays the three kinds of propeller noise harmonic spectrum assumptions employed by this study. They include:

- Spectrum 1 - the estimated spectrum for the propfan according to reference 3.5
- Spectrum 2 - a 3-dB-per harmonic decreasing spectrum
- Spectrum 3 - a flat spectrum of 10 tones including the blade passage fundamental tone.

each 10 dB lower than the OASPL (p14)

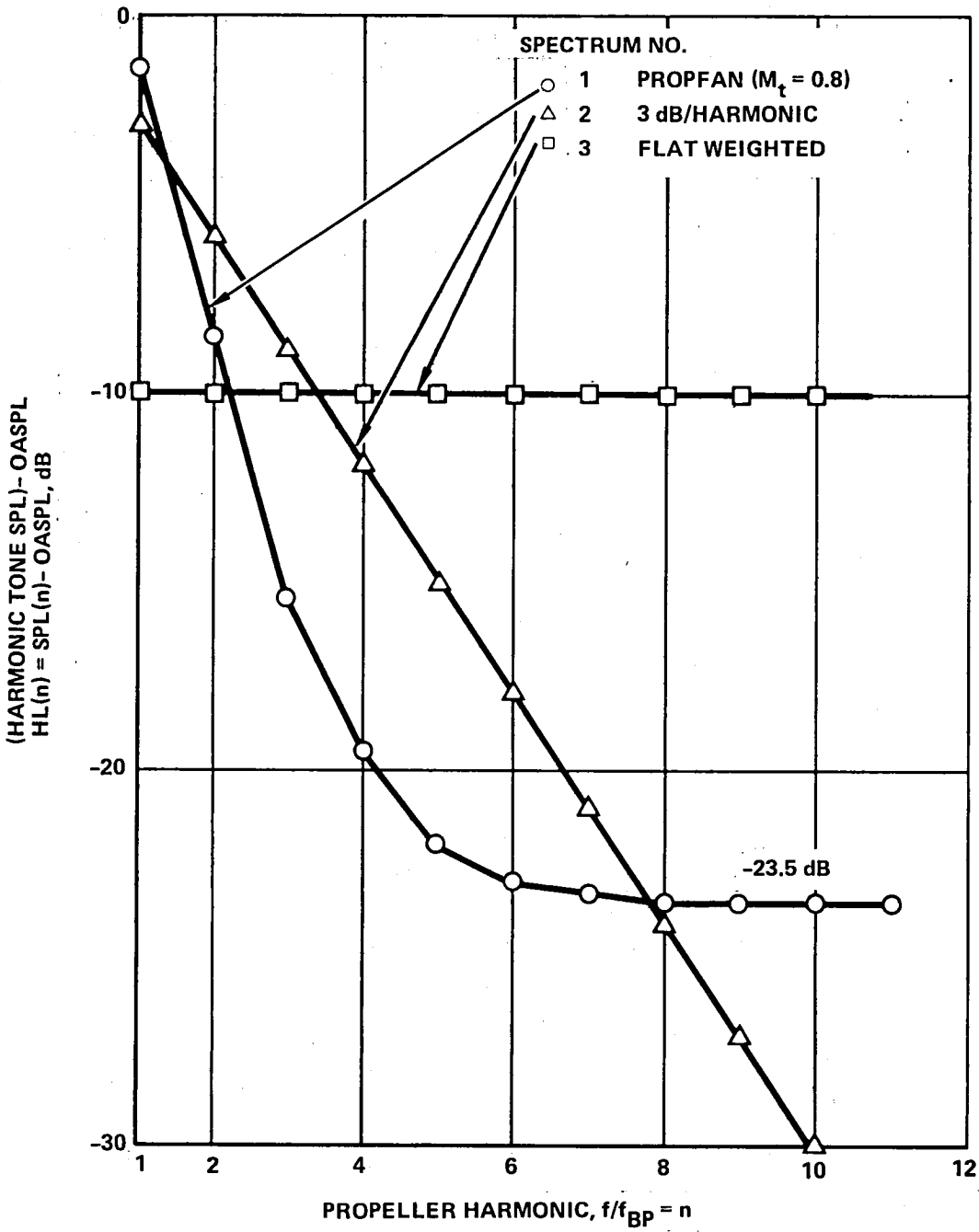

Figure 13. - Relative tone SPL versus harmonic number for the three propeller harmonic spectra employed in study.

The harmonics are all expressed as tone SPL increments relative to the local external OASPL. The first spectrum is currently considered most realistic. The third spectrum is typical of earlier high-speed propeller noise predictions, and the second spectrum represents an intermediate case.

Because the interior noise objective of the study is expressed in dBA, figure 14 is included for the convenience of the reader, with the frequencies of the first three tones indicated for each of the three study aircraft. Figure 15 shows the A-weighted external free-field sound pressure resulting from spectrum 1 for each of the three study aircraft. The results show the cumulative A-weighted sum as more propeller harmonics are included. Figure 14 shows that because of the high blade-passage frequencies associated with multibladed propfans, their external noise signatures have a relatively higher A-weighted SPL than do conventional propellers for a given OASPL level. On the other hand, many add-on noise-control elements perform better at high frequencies, so that the net effect of increased blade passage frequency upon the interior noise for a highly treated cabin wall is not immediately obvious. The preliminary double wall mass law predictions of reference 1 showed that the higher blade-passage frequency was beneficial to that concept of noise control.

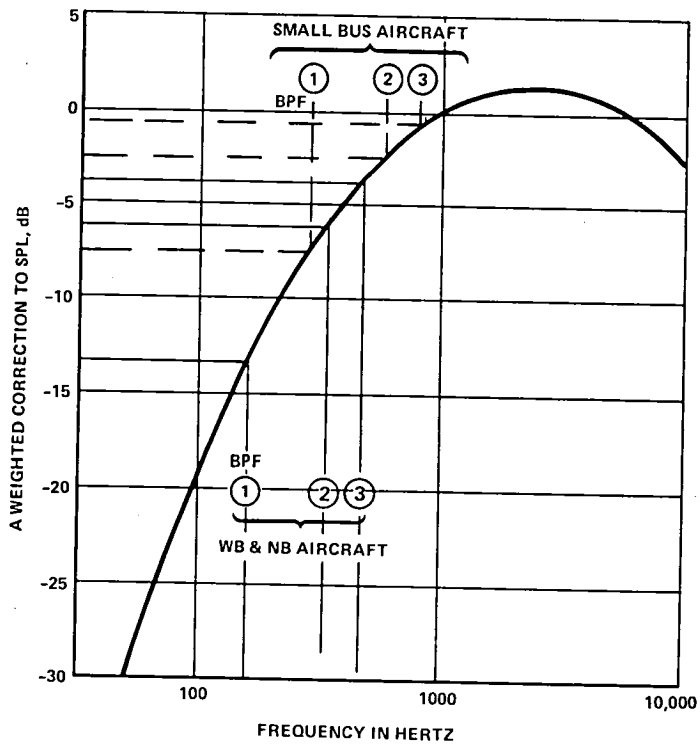

Figure 14. - A-weighting correction versus frequency.

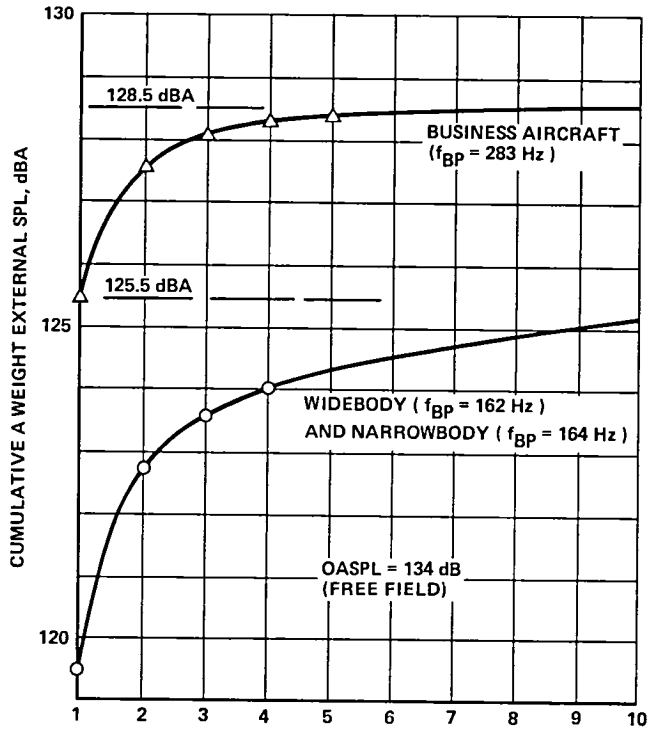

Figure 15. - Cumulative A-weighted external sound pressure versus number of propeller harmonics included, Spectrum 1.

A3. CALCULATION OF TREATED CYLINDER NOISE REDUCTION; INTERIOR ACOUSTICAL ABSORPTION

Figure 16 describes the approximate relationship between noise reduction and transmission loss which is used in this study and the assumed schedule of diffuse absorption coefficients achievable in the cabin versus frequency. As the average absorption coefficient increases, the difference between noise reduction (NR) and transmission loss (TL) decreases. If the average absorption coefficient were equal to 1.0, and τ is small, then NR would be equal to TL. By simply equating the acoustic energy flux through the cabin wall to the energy absorbed throughout the cabin interior, it can be shown that the noise reduction, NR, is given by the following equation which is used throughout this study:

$$NR = 10 \log_{10} \left(\frac{p_{ext}^2}{p_{int}^2} \right) = 10 \log \left(1 + \frac{\alpha}{\tau}\right) \qquad (1)$$

where τ is the sidewall transmission coefficient, and α is the average absorption coefficient of all the interior absorbers when referred to the transmitting surface area of the sidewall.

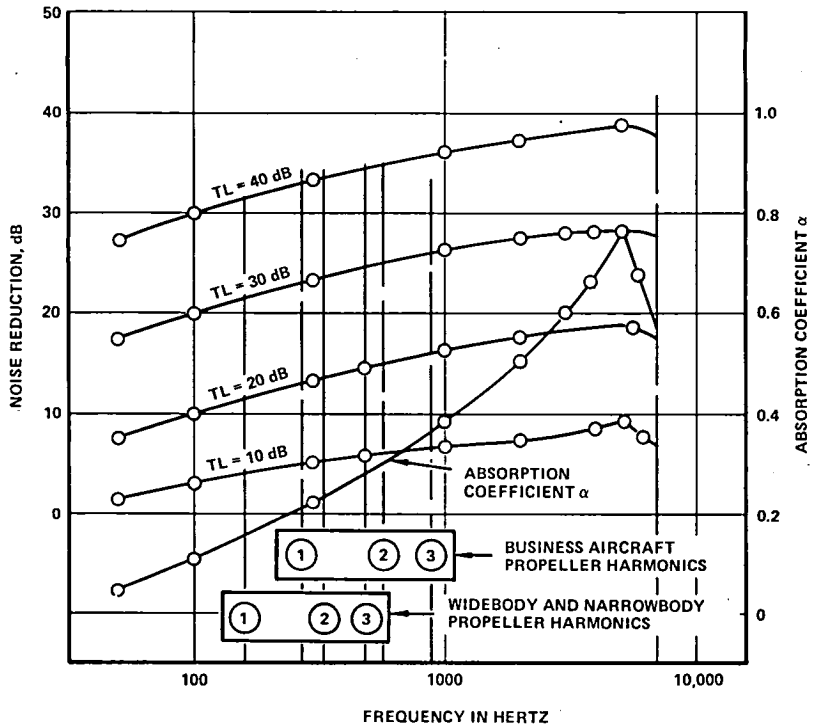

Figure 16. - Effect of absorption on noise reduction.

Equation (1) is subject to two limitations. First, the above relationship is employed in lieu of attempting to delineate the interior cavity acoustical modes, which could be done for a well-defined geometry such as a purely cylindrical cavity. Here a typical commercial aircraft interior is considered to be an extremely complex spatial configuration of acoustical absorbers. The seats are the major contributors to the total amount of interior absorption for a typical commercial aircraft. Equation (1), in effect, transfers all of that absorption to the sidewalls, ignoring the details of the multiple reflections of individually transmitted sound rays.

A second approximate aspect of equation (1) is pertinent to the analysis of baseline aircraft when subjected to a localized high-intensity exterior noise source, such as is the case near the propeller disc plane. In this case, there will exist a strong gradient along the axis of the fuselage of the flux of acoustical energy through the cabin wall. If equation (1) is applied locally, as is done in the current study, then the locally predicted interior noise levels have an axial distribution which mirrors the distribution of the energy flux through the wall using the local values of energy flux and absorption coefficient. A more accurate result would be obtained by writing an ordinary differential equation describing the axial flow of the acoustical energy within the cabin. Solutions of this energy flux

differential equation tend to allow interior acoustical energy to flow towards absorption material located in regions which are not adjacent to the peak noise transmission region. The resulting equilibrium distribution of the interior SPL would tend to display the following features in comparison to results from equation (1):

- Lower SPL values adjacent to the propeller disc plane region. The net noise-reduction values are closer to TL values than is shown in Figure 16.
- Higher local values of SPL in regions further away from the propeller disc region.
- Less severe axial gradients of interior SPL.

The errors due to neglect of the axial flow of accoustical energy flux are expected to be small in the present study for the high-noise-reduction designs since acoustical material is applied in proportion to the local requirements of equation (1). The result of this acoustical treatment procedure will be to produce a nearly uniform energy flux through the cabin wall over the entire length of the cabin, and hence, the axial gradients of interior SPL will be minimal for the treated aircraft.

The assumed distribution of acoustical absorption coefficient versus frequency as shown in figure 16 is taken directly from a computer test case for the method of Cockburn and Jolly (reference 8). Table IV, p 328 of reference 8 gives data which can be used to estimate the effects of certain items such as carpets, etc. Independent calculations indicate that the schedule of absorption used in this study, as shown in figure 16, is conservative and could be improved upon in the project design phase of a new commercial aircraft. The main reason for employing a low schedule of absorption values is to leave the designer some margin for improvement of the interior noise levels, even after the structural design of the aircraft has been frozen through release of drawings and by major financial commitments for tooling.

A4. TREATED CYLINDER TRANSMISSION LOSS - AN OUTLINE OF THE ANALYTICAL PROCEDURE

A4.1 General Outline

The sound transmission losses (STLs) of acoustically treated stiffened cylinders are obtained by combining component losses in a systematic manner. This is a previously unpublished, structural-dynamics-based technique developed at Lockheed, and it provides a significent improvement in prediction methodology when compared to the preliminary design methods which were used in the RECAT study (reference 1). Justification for the method used here is based partly on existing test data presented in Appendix F, and by discussions given in Appendixes A through E.

An acoustically treated stiffened cylinder is analyzed as follows (figures 17, 18 and 19):

1. Calculate the STL of a small flat skin panel bounded by stiffeners per Cockburn and Jolly (reference 8).

2. Calculate the STL of an untreated stiffened cylinder using Koval's (reference 7) smeared stiffness approach - see Appendix C.

3. Calculate the STL of a small flat skin panel with the desired acoustic treatments per Beranek and Work (reference 9) and Cockburn and Jolly (reference 8). Errors detected in reference 8 are noted in Appendix E.

4. The STL of a stiffened but untreated cylinder is then defined as the lower envelope of 1. and 2. above.

5. The STL increment due to the added acoustic treatment was obtained by subtracting 1. from 3. above.

6. Treated cylinder STL was then obtained by adding 4. and 5. above.

The total configuration STL and the interior absorption coefficient data are then used to calculate a noise reduction for each segment of the aircraft fuselage as described previously in Section A3. The exterior noise spectrum for each segment is then reduced by the calculated noise reduction and an interior noise spectrum is obtained. The calculated interior noise at the propeller fundamental and the first nine harmonics are weighted and summed to obtain the A-weighted overall interior noise.

Section A4 describes the propeller harmonic distributions assumed for this study. Transmission loss calculations were performed for the 7 fuselage segments discussed in Section A1 and the interior noise was determined for 3 harmonic distributions of the propeller noise for each segment. For most configurations 6 trim panel surface densities were used; therefore, a single computer run involved 6 trim panel weights times 7 fuselage segments times 3 propeller harmonic distributions for a total of 126 cases.

Appendix C contains a mathematical outline of Koval's methodology (reference 7), which is described qualitatively below. Appendix D contains a critique by Professor Koval of limitations of the theory, especially of the smeared-stiffener concept, in light of his more recent work.

A4.2 Description of Koval's Theory

The following is a brief physical description of Koval's theory of noise transmission into a cylindrical shell under flight conditions.

Figure 20 shows the geometry of the idealization by Koval (reference 7) in which oblique plane acoustic traveling waves are convected parallel to the

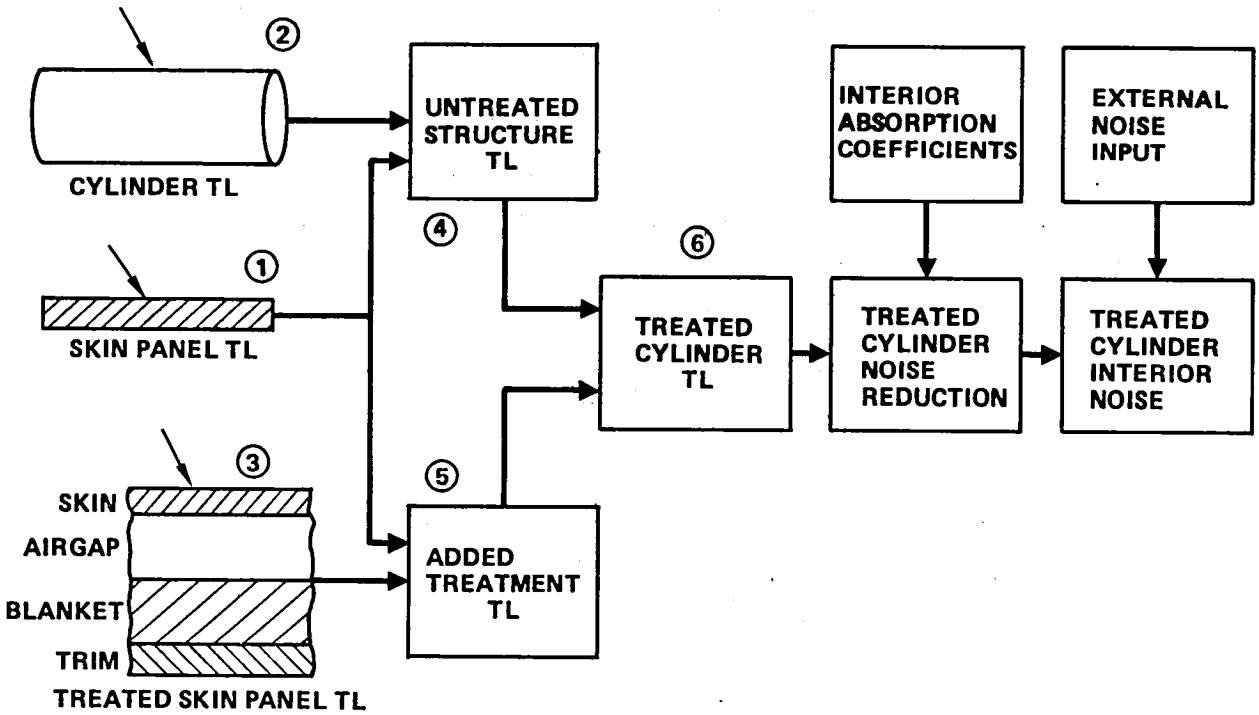

Figure 17. - Method used to calculate treated cylinder noise reduction.

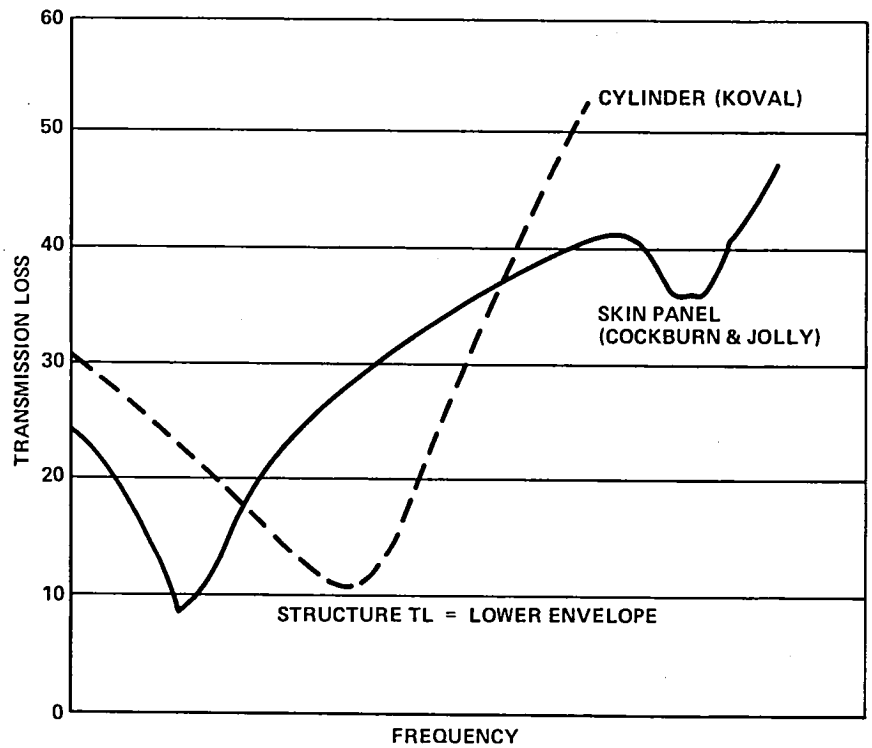

Figure 18. - Transmission loss of an untreated cylinder.

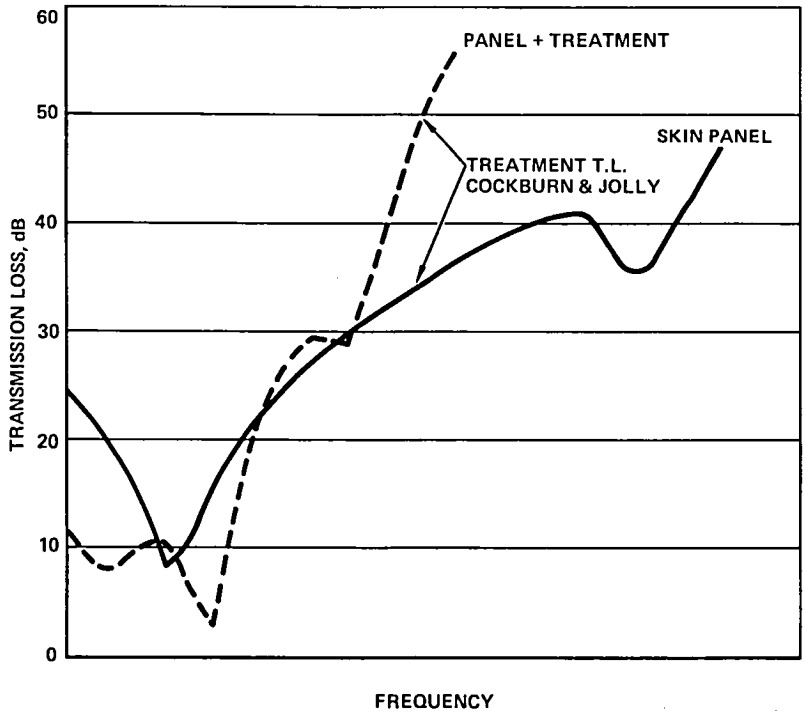

Figure 19. - Incremental transmission loss of add-on acoustical treatments.

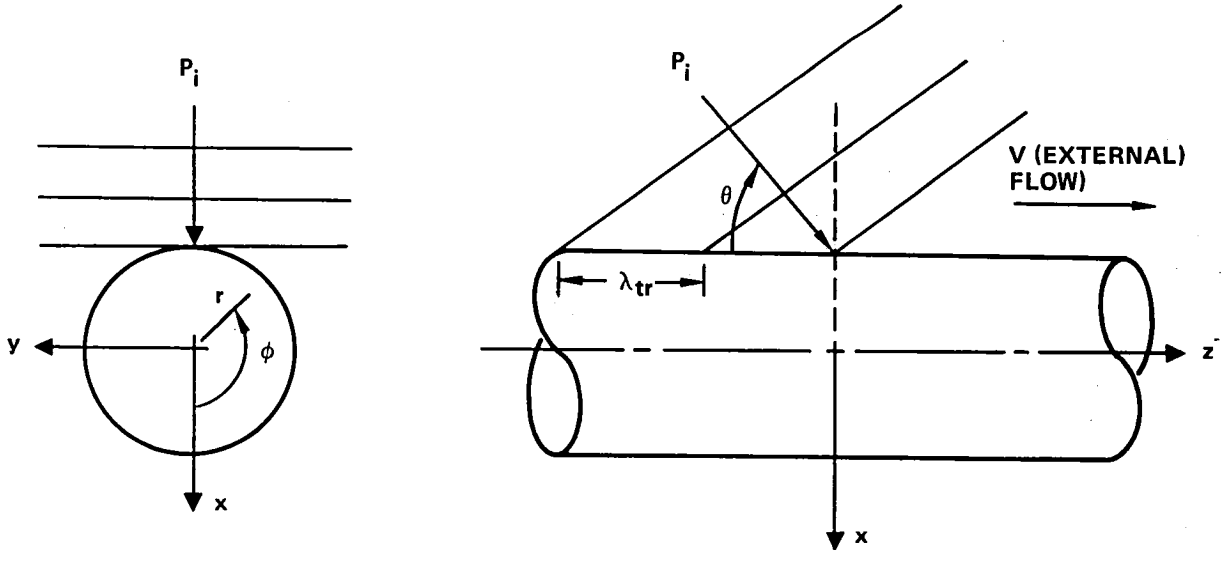

Figure 20. - Geometry of sound waves impinging on cylindrical shell in high-speed flight.

cylinder axis by a high-speed subsonic flow with Mach number, M. The sound waves impinge upon the fuselage at an oblique grazing angle of incidence, θ. The amplitude of the incident pressure wave has a prescribed amplitude, P_i, which is assumed to be known in the current study from the data in figures 7 and 8 and reference 5. The external sound pressure field is governed by the convected wave equation which determines the components of the wave number along the axial and radial directions in terms of the frequency, Mach number, and the acoustic propagation speed, c_1, in the external field.

The presence of the cylinder causes a reflected or scattered wave field to be set up in the external fluid which radiates energy externally. The surface of the shell deforms in accordance to the structural dynamic equations of motion of a cylindrical shell. This causes a sound wave to be transmitted into the interior of the cabin. The interior acoustic field is governed by the ordinary wave equation based upon fluid properties designated with a subscript 2.

In reference 7, Koval assumes that the interior sound field is that associated with a radially inward traveling wave, following the approach of P. W. Smith (reference 6). This assumes that there is some mechanism inside the cabin which can absorb the acoustical energy flux associated with such waves. The present study accounts for the semireverberant increase of interior noise in the manner already described in Section A3.

Koval's theory computes the mechanical impedance of the cylindrical shell and the acoustical termination impedance of the interior fluid based on the radially inward traveling wave field described in terms of Hankel functions of the first kind.

The boundary conditions satisfied in Koval's theory require the following principles:

- Matching of axial wave number components between the applied external acoustic pressure field, the scattered pressure field, the deformation of the shell, and the sound pressure field transmitted to the interior
- Matching of radial displacements of the fluid particle and the shell at the surface of the shell
- Writing of a force balance equation in the radial direction across the outer shell surface using appropriate impedance expressions.

A4.3 Justification for Selection of Koval's Approach

Koval's theory in reference 7 pertains to monocoque shells and in the present application requires smearing of the stiffeners to produce an equivalent orthotropic, monocoque cylindrical shell. Experimental discussion in

Appendix F, and more recent theoretical work by Koval discussed in Appendix D, shows that this is still a reasonably good engineering approximation when used in conjunction with Cockburn and Jolly as in our present theory.

The noteworthy advantages of Koval's theory are as follows:

- It provides a rational structural dynamic theory with which to systematically evaluate many important factors affecting noise control, such as stiffness, panel dimensions, skin thickness, stiffener properties, shell diameter and length, pressurization, damping loss factor, and mass additions to the outer wall of the fuselage. Investigation of such complex effects is beyond the scope of preliminary design studies such as reference 1.

- Koval's use of the impedance approach allows easy generalization for inclusion of add-on noise-control elements by modification of the termination impedance.

- Koval's theory has already been recently generalized without great computational effort to include discrete stiffener effects. Inclusion of floor effects will require more computational effort.

- The theory provides a good representation of the flow field convection of the applied acoustic pressure field, and also of the reflection or scattering of the incident acoustic pressure waves including the effects of the deformation (mobility) of the shell.

- Experience has shown that the computational costs are very reasonable for investigating the effects of a very large number of parameters.

A5. METHOD FOR CALCULATING THE TRANSMISSION LOSS FOR ADDED ACOUSTIC TREATMENTS

A5.1 General Outline

The sound transmission losses (STL) of acoustically treated aircraft structures are obtained by determining the STLs of the untreated cylinder and added treatment separately. This process is described in Section A4, and also in Appendixes C and E. Partial experimental verification for each prediction technique using existing data is given in Appendix F. At present no experimental verification is available for the STL of a fuselage structure with the very heavy acoustical treatments of the kind required to meet the current study goal.

A significant part of the STL of acoustically treated aircraft structures is provided by the material added to the basic structure. The most common additions are in the form of damping tiles or tape, fiberglass blankets,

septa and decorative trim panels. In addition, the effects of the absorption of sound by carpeting, seats, ceiling panels, and passengers is evaluated in the manner described in Section A3.

A5.2 Basis for Treatment Layer Characteristics Prediction Method

Beranek (references 9, 10, and 11) derived the characteristic impedance expression for porous materials and he showed how multilayered treatments could be combined analytically to obtain total configuration impedance expressions. Beranek's method was incorporated into a prediction method by Cockburn and Jolly (reference 8) for aircraft interior noise prediction. The basic approach of the Cockburn and Jolly method was followed and modifications or corrections were applied where appropriate. Appendix E contains the equations as used in this study and also includes the original Cockburn and Jolly equations for reference. Mulholland, Price and Parbrook (reference 12) developed the means whereby the Beranek and Work method of reference 9 could be applied for oblique angles of incidence. When the changes suggested by Mulholland, et al., were applied, the resulting impedance expressions for porous materials and airspaces subjected to obliquely incident sound were in agreement with Beranek's earlier investigation of reference 10. Koval has derived a previously unpublished expression for the STL of a panel subjected to obliquely incident sound with an external airflow. These results are given in Appendix E. His derivation defined the transmission coefficient as the ratio of the transmitted over the incident pressure. Beranek's derivation did not include an external airflow and defined the transmission coefficient as the ratio of the transmitted over the surface pressure instead of the incident pressure.

APPENDIX B
STRUCTURAL CONFIGURATIONS AND SIDEWALL DESIGN DESCRIPTIONS

B1. SIDEWALL CONSTRUCTION DETAILS

Figure 21 describes the aircraft sidewall construction details using generalized dimensions. Table 8 provides the key to Figure 21, giving specific data for 18 different sidewall designs including 6 baseline nonacoustical designs and 12 high noise reduction designs. These designs are in groups of 3, one each for the wide-body, narrow-body and small business aircraft. The designs are classified as follows:

(1) Baseline aluminum designs used in regions of the fuselage not impacted by propeller noise reduction requirements.

(2) Baseline composite material designs used in regions of the fuselage not impacted by propeller noise reduction requirements.

(3) Aluminum aircraft with add-on high-noise reduction designs for the corresponding peak external noise locations.

(4) Composite aircraft with add-on noise reduction designs for the peak external noise locations.

(5) Aluminum aircraft with advanced noise reduction designs for the peak external noise locations.

(6) Composite aircraft with advanced noise reduction designs for the peak external noise locations.

B2. SECTION PROPERTIES AND DIMENSIONAL DATA OF STIFFENERS

Tables 9 through 12 provide the section properties and figures 22 through 34 show the dimensions of the stiffeners used in the 18 sidewall designs described above.

B3. DISCUSSION OF STRUCTURAL DESIGNS

For the wide-body and narrow-body designs, the stiffeners were equal in area and equally spaced. The design of the small business aircraft included frames at 50.8 cm (20 in.) spacing and intercostals at 16.9 cm (6.67 in.) between frames. Since a constant stiffener spacing and equal cross sectional area stiffeners are more convenient for analysis, the small business aircraft frames and intercostals were modified. In one configuration, the mass and stiffness of the intercostals were absorbed by the frame. A second configuration, and the one used for the small business aircraft study, had the

intercostals and frames equal in area with a 16.9 cm (6.67 in) spacing. The averaged or smeared stiffnesses of the small business aircraft configurations were equal to that of the baseline structure. A summary of the baseline structural arrangements and properties of the cylinders, frames, and stringers are given in table 9. The internal and external environments assumed for the analyses are also tabulated.

The design of the composite structure reflects new design concepts and manufacturing techniques developed at Lockheed. Ingenious manufacturing techniques make possible the interlocking of orthogonal stiffeners into a continuous structure referred to as orthogrid. The orthogrid concept, depicted in figure 26, consists of elements arranged parallel and normal to the longitudinal axis with alternating layers of syntactic resin and graphite. A preliminary design of the composite wide-body structure is shown in figure 35. A composite replication of the aluminum structure for all three aircraft results in equally stiff structures with surface density values which are 66, 67, and 65 percent of the aluminum baseline for the wide-body, narrow-body, and business aircraft, respectively. Increased stiffness can be achieved by increasing the section modulus or Young's modulus of the skin and stiffeners. Figures 4 and 5 of Section 3 show the variation of stiffness as a function of outer wall mass for the three study aircraft. Results in Section 3.2 show the noise-control merits of such stiffened outer wall designs when combined with an optimum double wall design.

Appendix H shows results of parametric studies which help to define the optimum outer wall stiffness level both for advanced aluminum and advanced composite structures. Appendix I describes the axial variation on the various sidewall noise reduction design parameters for both the add-on and the advanced noise reduction designs.

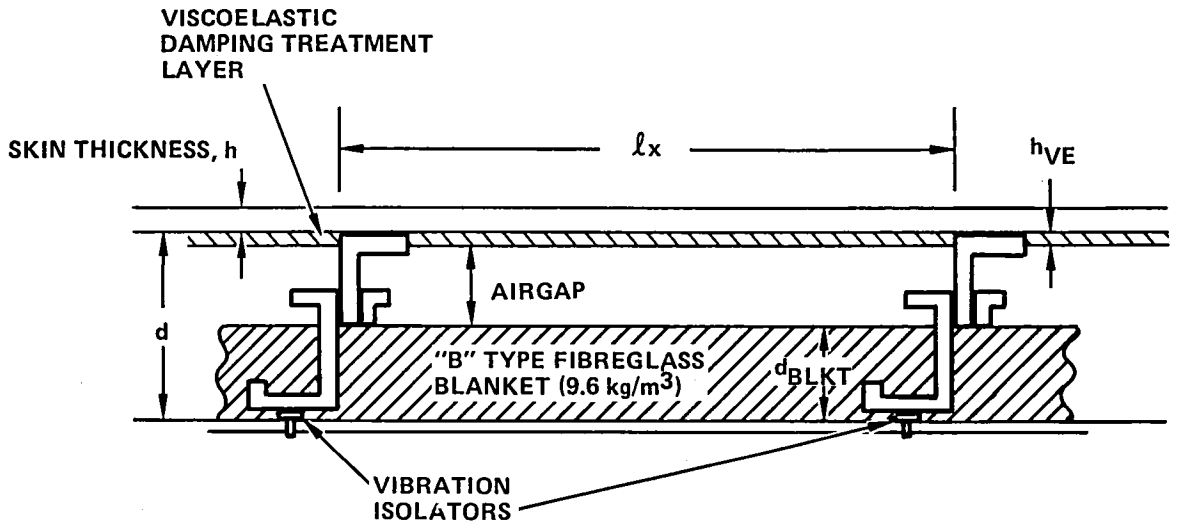

(a) CROSS SECTION OF FRAMES AND SIDEWALL CONSTRUCTIONS

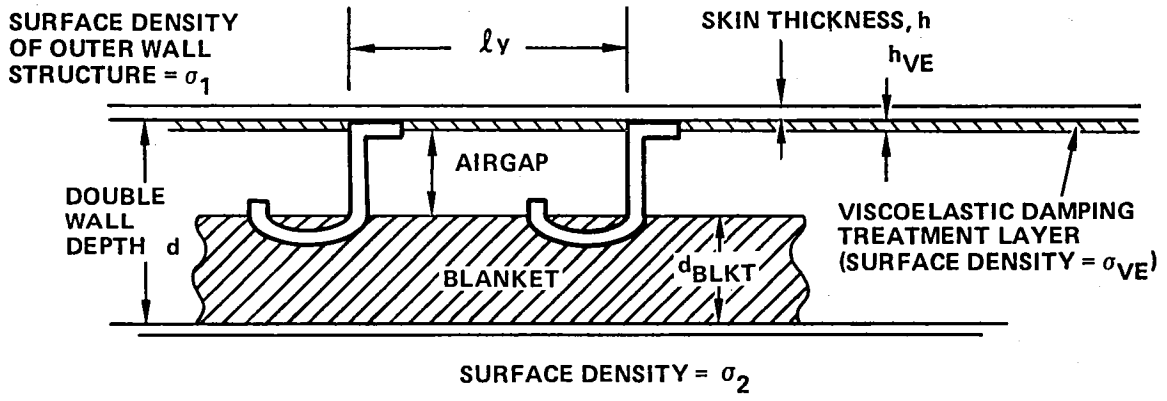

(b) CROSS SECTION OF STRINGERS AND SIDEWALL CONSTRUCTION

NOTE: SEE TABLE 8 FOR DIMENSIONS FOR VARIOUS DESIGNS

Figure 21. - Generalized sidewall construction details for various noise reduction design concepts.

TABLE 8. - KEY TO FUSELAGE SIDEWALL DIMENSIONAL DATA FOR VARIOUS NOISE REDUCTION DESIGNS FOR PEAK NOISE REGION

Design No.	Aircraft Type	Material	Noise Reduction Design Concept	Relative Stiffness Ratio	Frame Spacing	Stringer Spacing	Wall Spacing	Fiberglass Blanket Thickness	Airgap Thickness	Skin Thickness	Viscoelastic Layer Thickness	Surface Density of Outer Wall Structure	Surface Density of Trim Panel	Surface Density of Visoelastic Layer	References to Section Property Data
					Symbols used in Figure 21										
					l_x	l_y	d	d_{Blkt}	d_{AG}	h	h_{VE}	$\sigma_{1_{Struc}}$	σ_2	σ_{VE}	
No.	A/C	Material	Concept	E	CM (In.)	CM (In.)	CM (In.)	CM (In.)	CM (In.)	CM (In.)	CM (In.)	KG Sq M PSF	KG Sq M PSF	KG Sq M PSF	Fig. No. Table No.
1	WB	Aluminum	Baseline	1	50.8 (20)	21.6 (8.5)	15.2 (6)	7.62 (3)	7.62 (3)	0.173 (0.068)	0	9.17 (1.88)	1.61 (0.33)	0	22 9
2	NB	Aluminum	Baseline	1	48.3 (19)	15.2 (6)	15.2 (6)	7.62 (3)	7.62 (3)	0.144 (0.045)	0	6.25 (1.28)	1.61 (0.33)	0	23 9
3	SBA	Aluminum	Baseline	1	16.9 (6.67)	58.4 (23)	10.2 (4)	5.08 (2)	5.08 (3)	0.081 (0.032)	0	4.68 (0.96)	1.61 (0.33)	0	24,25 9
4	WB	Composite	Baseline	1	50.8 (20)	21.6 (8.5)	15.2 (6)	7.62 (3)	7.62 (3)	0.203 (0.080)	0	6.39 (1.31)	1.61 (0.33)	0	26 9
5	NB	Composite	Baseline	1	48.3 (19)	15.2 (6)	15.2 (6)	7.62 (3)	7.62 (3)	0.127 (0.050)	0	4.35 (0.89)	1.61 (0.33)	0	27 9
6	SBA	Composite	Baseline	1	16.9 (6.67)	58.4 (23)	10.2 (4)	5.08 (2)	5.08 (2)	0.102 (0.040	0	3.27 (0.67)	1.61 (0.33)	0	28 9
7	WB	Aluminum	Add-On NR Design	1	50.8 (20)	21.6 (8.5)	15.2 (6)	7.62 (3)	6.88 (2.71)	0.173 (0.068)	0.747 (0.294)	9.17 (1.88)	14.6 (3.0)	10.4 (2.12)	22 9
8	NB	Aluminum	Add-On NR Design	1	48.3 (19)	15.2 (6)	15.2 (6)	7.62 (3)	6.65 (2.62)	0.114 (0.045)	0.960 (0.378)	6.25 (1.28)	13.4 (2.75)	13.3 (2.72)	23 9
9	SBA	Aluminum	Add-On NR Design	1	16.9 (6.67)	58.4 (23)	10.2 (4)	5.08 (2)	6.55 (2.58)	0.081 (0.032)	1.072 (0.422)	4.68 (0.96)	9.03 (1.85)	14.8 (3.04)	24,25 9
10	WB	Aluminum	Advanced NR Design	5	50.8 (20)	21.S (8.5)	15.2 (6)	7.62 (3)	7.62 (3)	0.241 (0.095)	0	15.6 (3.2)	12.2 (2.5)	0	29 11
11	NB	Aluminum	Advanced NR Design	6	24.1 (9.5)	7.62 (3)	15.2 (6)	7.62 (3)	7.62 (3)	0.152 (0.060)	0	12.7 (2.6)	13.2 (2.7)	0	30 11
12	SBA	Aluminum	Advanced NR Design	6	8.46 (3.33)	29.2 (11.5)	10.2 (4)	5.08 (2)	5.08 (2)	0.178 (0.070)	0	12.2 (2.5)	13.2 (2.7)	0	31 11
13	WB	Composite	Advanced NR Design	6	25.4 (10)	10.8 (4.25)	15.2 (6)	7.62 (3)	7.62 (3)	0.216 (0.085)	0	10.4 (2.13)	7.81 (1.6)	0	32 12
14	NB	Composite	Advanced NR Design	10	24.1 (9.5)	7.62 (3)	15.2 (6)	7.62 (3)	7.62 (3)	0.178 (0.070)	0	9.52 (1.95)	14.6 (3.0)	0	33 12
15	SBA	Composite	Advanced NR Design	10	8.46 (3.33)	29.2 (11.5)	10.2 (4)	5.08 (2)	5.08 (2)	0.203 (0.080)	0	8.0 (1.64)	6.83 (1.4)	0	34 12
16	WB	Composite	Add-On NR Design	1	50.8 (20)	21.6 (8.5)	15.2 (6)	7.62 (3)	7.62 (3)	0.203 (0.080)	0.95 (0.374)	6.4 (1.31)	14.6 (3.0)	13.1 (2.69)	26 10
17	NB	Composite	Add-On NR Design	1	48.3 (19)	15.2 (6.0)	15.2 (6)	7.62 (3)	7.62 (3)	0.127 (0.050)	1.10 (0.432)	4.34 (0.89)	12.2 (2.5)	15.2 (3.11)	27 10
18	SBA	Composite	Add-On NR Design	1	16.9 (6.67)	58.4 (23)	10.2 (4)	5.08 (2)	5.08 (3)	0.102 (0.040)	0.82 (0.324)	3.27 (0.67)	11.2 (2.3)	11.4 (2.33)	28 10

Notes: (1) Vascoelastic layer thickness based on a bulk density of 1384 KG/m^3 (86.4 lb/ft^3)

(2) Damping loss factor η = 0.06 for σ_{VE} = 0, and increases linearity to η = 0.2 at σ_{VE} = 20.1 KG/m^2 (4.12 psf)

TABLE 9. - OUTER WALL STRUCTURAL PROPERTIES BASELINE ALUMINUM (STRENGTH DESIGNED STRUCTURE)

Item	Units		Aircraft Type: Wide-Body		Narrow-Body		Business A/C	
	SI	English	SI	English	SI	English	SI	English
CYLINDRICAL SHELL								
Radius	m	(ft)	3.05	(10.0)	1.96	(6.42)	1.14	(3.75)
Length	m	(ft)	35.8	(117.5)	23.0	(75.5)	10.8	(35.5)
Skin Thickness	cm	(in)	.173	(.068)	.114	(.045)	.0813	(.032)
Skin Bulk Density	kg/m^3	(lb/in^3)	2768	(.10)	2768	(.10)	2768	(.10)
Elastic Modulus Skin	GN/m^2	(psi)	68.9	(10^7)	68.9	(10^7)	68.9	(10^7)
Damping LOSS Factor	none	none	.06	.06	.06	.06	.06	.06
Surface Density Skin plus Stiffeners	kg/m^2	(psf)	9.17	(1.88)	6.25	(1.29)	4.68	(.969)
Ratio: (Stiffness)/(Baseline Stiffness)			1.0	1.0	1.0	1.0	1.0	1.0
FRAMES								
Spacing	cm	(in)	50.8	(20)	48.3	(19)	16.9	(6.67)
Depth	cm	(in)	15.2	(6)	15.2	(6)	7.62	(3)
Cross Sectional Area	cm^2	(in^2)	4.27	(.662)	2.48	(.385)	.928	(.144)
Bulk Density	kg/m^3	(lb/in^3)	2768	(.10)	2768	(.10)	2768	(.10)
Elastic Modulus Web and outer flange	GN/m^2	(psi)	68.9	(10^7)	68.9	(10^7)	68.9	(10^7)
Inner flange	GN/m^2	(psi)	68.9	(10^7)	68.9	(10^7)	68.9	(10^7)
Area centroid (re: skin ℄)	cm	(in)	6.49	(2.56)	(6.92)	(2.73)	3.85	(1.52)
2nd Area Moment (re: Skin ℄)	cm^4	(in^4)	297.2	(7.14)	188.6	(4.53)	21.1	(.508)
Torsion Constant	cm^4	(in^4)	.0393	(.000943)	.00668	(.000161)	.00204	(.0000491)
STRINGERS								
Spacing	cm	(in)	21.6	(8.5)	15.2	(6)	58.4	(23)
Depth	cm	(in)	3.43	(1.35)	3.05	(1.2)	6.35	(2.5)
Cross Sectional area	cm^2	(in^2)	1.605	(2.49)	.916	(.145)	2.03	(.315)
Bulk Density	kg/m^3	(lb/in^3)	2768	(.10)	2768	(.10)	2768	(.10)
Elastic Modulus Web and outer flange	GN/m^2	(psi)	68.9	(10^7)	68.9	(10^7)	68.9	(10^7)
Inner flange	GN/m^2	(psi)	68.9	(10^7)	68.9	(10^7)	68.9	(10^7)
Area centroid re: Skin ℄	cm	(in)	1.46	(.576)	1.49	(.587)	2.18	(.857)
2nd Area Moment (re: Skin ℄)	cm^4	(in^4)	6.13	(.147)	3.35	(.0806)	20.6	(.494)
Torsion Constant	cm^4	(in^4)	.0221	(.00053)	(.00725)	(.000174)	.0134	(.000325)
Smeared Stiffness Properties (Skin plus stiffeners, with skin width equal to stiffener spacing)								
FRAMES								
Skin width	cm	(in)	50.8	(20)	48.3	(19)	16.9	(6.67)
2nd Area Moment (re: neutral axis)	cm^4	(in^4)	238.3	(5.72)	151.5	(3.64)	15.61	(.375)
Neutral axis distance to skin ℄	cm	(in)	2.21	(.8708)	2.20	(.868)	1.593	(.627)
Torsion Constant	cm^4	(in^4)	.1265	(.00304)	.0307	(.000738)	.00508	(.0001219)
Total Section Area	cm^2	(in^2)	13.04	(2.022)	8.00	(1.240)	2.30	(.357)
STRINGERS								
2nd Area Moment (re: neutral axis)	cm^4	(in^4)	5.11	(.1228)	2.63	(.0632)	17.69	(.425)
Neutral axis distance to skin ℄	cm	(in)	.526	(.2072)	.579	(.228)	.693	(.273)
Torsion Constant	cm^4	(in^4)	.0592	(.00142)	.01483	(.000356)	.0239	(.000573)
Total Section Area	cm^2	(in^2)	5.34	(.827)	2.68	(.415)	6.78	(1.051)
Skin Width	cm	(in)	(21.6)	(8.5)	15.2	(6)	58.4	(23)

A EXTERIOR FLUID ENVIRONMENT

- Cruise Mach No. = 0.8 at 9144 m (30 000 ft) Altitude
- Absolute Static Pressure of Air = 30.1 kPa (630 psfa)
- Ambient Air Density = .460 kg/m^3 (.0287 lb/ft^3)
- Ambient Speed of Sound = 303.3 m/sec (995 ft/sec)
- Ambient Temperature = 228.8°K (412°R)

B INTERIOR CABIN ENVIRONMENT

- Cabin Pressure Differential = 45.1 kPa (6.54 psi)
- Absolute Static Pressure = 75.3 kPa (1572 psfa)
- Speed of Sound = 344.4 m/sec (1130 ft/sec)
- Air Density = .887 kg/m^3 (.0554 lb/ft^3)
- Air Temperature = 21.8°C (71.6°F)

TABLE 10. - OUTER WALL STRUCTURAL PROPERTIES BASELINE COMPOSITE (STRENGTH-DESIGN) STRUCTURE

Item	Units		Aircraft Type: Wide-Body		Narrow-Body		Business A/C	
	SI	English	SI	English	SI	English	SI	English
CYLINDRICAL SHELL								
Radius	m	(ft)	3.05	(10.0)	1.96	(6.42)	1.14	(3.75)
Length	m	(ft)	35.8	(117.5)	23.0	(75.5)	10.8	(35.5)
Skin Thickness	cm	(in)	.203	(.080)	.127	(.050)	.102	(.04)
Skin Bulk Density	kg/m^3	(lb/in^3)	1605.6	(.058)	1605.6	(.058)	1605.6	(.058)
Elastic Modulus Skin	GN/m^2	(psi)	68.93	(10^7)	68.93	(10^7)	68.93	(10^7)
Damping LOSS Factor	none	none	.06	.06	.06	.06	.06	.06
Surface Density Skin plus Stiffeners	kg/m^2	(psf)	5.90	(1.25)	4.20	(.86)	3.07	(.63)
Ratio: (Stiffness)/(Baseline Stiffness)			1.0	1.0	1.0	1.0	1.0	1.0
FRAMES								
Spacing	cm	(in)	50.8	(20)	48.3	(19)	16.9	(6.67)
Depth	cm	(in)	15.2	(6)	15.2	(6)	7.62	(3)
Cross Sectional Area	cm^2	(in^2)	3.99	(.619)	2.65	(.411)	.941	(.146)
Bulk Density	kg/m^3	(lb/in^3)	1605.6	(.058)	1605.6	(.058)	1605.6	(.058)
Elastic Modulus Web and outer flange	GN/m^2	(psi)	68.9	(10^7)	68.9	(10^7)	68.9	(10^7)
Inner-flange	GN/m^2	(psi)	68.9	(10^7)	68.9	(10^7)	68.9	(10^7)
Area Centroid distance (re: skin ℄)	cm	(in)	6.52	(2.57)	6.97	(2.75)	3.86	(1.52)
2nd Area Moment (re: Skin ℄)	cm^4	(in^4)	291.8	(7.01)	213.9	(5.14)	21.6	(.519)
Torsion Constant	cm^4	(in^4)	.0364	(.000875)	.00986	(.000237)	.00207	(.0000498)
STRINGERS								
Spacing	cm	(in)	21.6	(8.5)	15.2	(6)	58.4	(23)
Depth	cm	(in)	3.30	(1.3)	3.30	(1.3)	(6.35)	(2.5)
Cross Sectional area	cm^2	(in^2)	2.15	(.333)	1.210	(.1875)	(2.07)	(.321)
Bulk Density	kg/m^3	(lb/in^3)	1605.6	(.058)	1605.6	(.058)	1605.6	(.058)
Elastic Modulus Web and outer flange	GN/m^2	(psi)	68.9	(10^7)	68.9	(10^7)	68.9	(10^7)
Inner flange	GN/m^2	(psi)	68.9	(10^7)	68.9	(10^7)	68.9	(10^7)
Area Centroid re: Skin ℄	cm	(in)	1.41	(.554)	1.23	(.483)	2.90	(1.14)
2nd Area Moment (re: Skin ℄)	cm^4	(in^4)	6.69	(.1608)	3.23	(.0777)	29.3	(.703)
Torsion Constant	cm^4	(in^4)	(.1493)	(.00359)	.0203	(.000481)	.0182	(.000438)
SMEARED STIFFNESS PROPERTIES (SKIN PLUS STIFFENER, with Skin width equal to stiffener spacing)								
FRAMES								
Skin width	cm	(in)	50.8	(20)	48.3	(19)	16.9	6.67
2nd Area Moment re: neutral axis	cm^4	(in^4)	244.3	(5.87)	114.8	(4.20)	16.65	(.400)
Neutral axis distance to skin ℄	cm	(in)	1.92	(.757)	2.17	(.854)	1.42	(.558)
Torsion Constant	cm^4	(in^4)	.1786	(.00429)	.0428	(.001029)	.00799	(.000192)
Total Section area	cm^2	(in^2)	14.32	2.219	8.78	(1.361)	2.66	(.413)
STRINGERS								
Skin width	cm	(in)	21.6	(8.5)	15.2	(6)	58.4	(23)
2nd Area Moment re: neutral axis	cm^4	(in^4)	5.28	(.1268)	2.79	(.0670)	24.8	(.595)
Neutral axis distance to skin ℄	cm	(in)	.452	(.178)	.454	(.1788)	.800	(.315)
Torsion Constant	cm^4	(in^4)	.210	(.00504)	.0298	(.0007153)	.0586	(.000929)
Total Section Area	cm^2	(in^2)	6.54	1.013	3.15	(.4875)	8.00	(1.24)

A EXTERIOR FLUID ENVIRONMENT

- Cruise Mach No. = 0.8 at 9144 m (30 000 ft) Altitude
- Absolute Static Pressure of Air = 30.1 kPa (630 psfa)
- Ambient Air Density = .460 kg/m^3 (.0287 lb/ft^3)
- Ambient Speed of Sound = 303.3 m/sec (995 ft/sec)
- Ambient Temperature = 228.8°K (412°R)

B INTERIOR CABIN ENVIRONMENT

- Cabin Pressure Differential = 45.1 kPa (6.54 psi)
- Absolute Statis Pressure = 75.3 kPa (1572 psfa).
- Speed of Sound = 344.4 m/sec (1130 ft/sec)
- Air Density = .887 kg/m^3 (.0554 lb/ft^3)
- Air Temperature = 21.8°C (71.6°F)

TABLE 11. - OUTER WALL STRUCTURAL PROPERTIES FOR ALUMINUM ADVANCED NOISE REDUCTION DESIGNS AT PEAK NOISE LOCATION

Item	Aircraft Type							
	Units		Wide-Body		Narrow-Body		Business A/C	
	SI	English	SI	English	SI	English	SI	English
CYLINDRICAL SHELL								
Radius	m	(ft)	3.05	(10.0)	1.96	(6.42)	1.14	(3.75)
Length	m	(ft)	35.8	(117.5)	23.0	(75.5)	10.8	(35.5)
Skin Thickness	cm	(in)	.241	(.095)	.152	(.060)	.178	(.070)
Skin Bulk Density	kg/m^3	(lb/in^3)	2768	(.10)	2768	(.10)	2768	(.10)
Elastic Modulus Skin	GN/m^2	(psi)	68.9	(10^7)	68.9	(10^7)	68.9	(10^7)
Damping LOSS Factor	none	none	.06	.06	.06	.06	.06	.06
Surface Density Skin plus Stiffeners	kg/m^2	(psf)	15.4	(3.16)	13.0	(2.60)	11.5	(2.36)
Ratio: (Stiffness)/(Baseline Stiffness)			5	5	6	6	6	6
FRAMES								
Spacing	cm	(in)	50.8	(20)	24.1	(9.5)	8.46	(3.33)
Depth	cm	(in)	15.2	(6)	15.2	(6)	10.2	(4)
Cross Sectional Area	cm^2	(in^2)	12.24	(1.897)	5.29	(.82)	1.471	(.228)
Bulk Density	kg/m^3	(lb/in^3)	2768	(.10)	2768	(.10)	2768	(.10)
Elastic Modulus Web and outer flange	GN/m^2	(psi)	68.9	(10^7)	68.9	(10^7)	68.9	(10^7)
Inner flange	GN/m^2	(psi)	68.9	(10^7)	68.9	(10^7)	68.9	(10^7)
Area centriod (re: skin ℄)	cm	(in)	12.51	(4.93)	12.19	(4.80)	6.14	(2.42)
2nd Area Moment (re: Skin ℄)	cm^4	(in^4)	2140	(51.4)	914.8	(22.0)	74.0	(1.779)
Torsion Constant	cm^4	(in^4)	4.80	(.1152)	.249	(.00598)	.00506	(.000122)
STRINGERS								
Spacing	cm	(in)	21.6	(8.5)	7.62	(3)	29.2	(11.5)
Depth	cm	(in)	6.99	(2.75)	6.60	(2.6)	8.64	(3.4)
Cross Sectional area	cm^2	(in^2)	1.626	(.252)	.661	(.1024)	1.903	(.295)
Bulk Density	kg/m^3	(lb/in^3)	2768	(.10)	2768	(.10)	2768	(.10)
Elastic Modulus Web and outer flange	GN/m^2	(psi)	68.9	(10^7)	68.9	(10^7)	68.9	(10^7)
Inner flange	GN/m^2	(psi)	68.9	(10^7)	68.9	(10^7)	68.9	(10^7)
Area centroid re: Skin ℄	cm	(in)	3.62	(1.426)	3.38	(1.33)	4.77	(1.877)
2nd Area Moment (re: Skin ℄)	cm^4	(in^4)	31.9	(.767)	10.81	(.260)	64.4	(1.548)
Torsion Constant	cm^4	(in^4)	.0126	(.000302)	.00145	3.5×10^{-5}	.0102	(.000246)
Smeared Stiffness Properties (Skin Plus Stiffeners, with Skin width-stiffener spacing)								
FRAMES								
• Skin width	cm	(in)	50.8	(20)	24.1	(9.5)	8.46	(3.33)
• 2nd Area Moment (re: neutral axis)	cm^4	(in^4)	1182.1	(28.4)	442.9	(10.64)	45.5	(1.094)
• Neutral axis distance to skin ℄	cm	(in)	6.38	(2.51)	7.19	(2.83)	3.23	(1.271)
• Total Cross Sectional Area	cm^2	(in^2)	2.45	(3.80)	8.97	(1.390)	2.87	(.445)
• Torsion Constant	cm^4	(in^4)	5.03	(.1209)	.277	(.00666)	.0209	(.000503)
STRINGERS								
• Skin width	cm	(in)	21.6	(8.5)	7.62	(3)	29.2	(11.5)
• 2nd Area Moment (re: neutral axis)	cm^4	(in^4)	26.9	(.645)	8.07	(.194)	52.8	1.269
• Neutral axis distance (re: Skin ℄)	cm	(in)	.983	(.387)	1.300	(.512)	1.367	(.538)
• Total Cross Sectional Area	cm^2	(in^2)	6.83	(1.059)	1.832	(.284)	7.10	(1.100)
• Torsion Constant	cm^4	(in^4)	.1137	(.00273)	.0104	(.000251)	.0650	(.001561)

A EXTERIOR FLUID ENVIRONMENT

- Cruise Mach No. = 0.8 at 9144 m (30 000 ft) Altitude
- Absolute Static Pressure of Air = 30.1 kPa (630 psfa)
- Ambient Air Density = .460 kg/m^3 (.0287 lb/ft^3)
- Ambient Speed of Sound = 303.3 m/sec (995 ft/sec)
- Ambient Temperature = 228.8°K (412°R)

B INTERIOR CABIN ENVIRONMENT

- Cabin Pressure Differential = 45.1 kPa (6.54 psi)
- Absolute Static Pressure = 75.3 kPa (1572 psfa)
- Speed of Sound = 344.4 m/sec (1130 ft/sec)
- Air Density = .887 kg/m^3 (.0554 lb/ft^3)
- Air Temperature = 21.8°C (71.6°F)

TABLE 12. - OUTER WALL STRUCTURAL PROPERTIES FOR COMPOSITE ADVANCED NOISE REDUCTION DESIGNS AT PEAK NOISE LOCATION

Item	Units		Aircraft Type: Wide-Body		Narrow-Body		Business A/C	
	SI	English	SI	English	SI	English	SI	English
CYLINDRICAL SHELL								
Radius	m	(ft)	3.05	(10.0)	1.96	(6.42)	1.14	(3.75)
Length	m	(ft)	35.8	(117.5)	23.0	(75.5)	10.8	(35.5)
Skin Thickness	cm	(in)	.216	(.085)	.178	(.07)	.203	(.080)
Skin Bulk Density	kg/m^3	(lb/in^3)	1605.6	(.058)	1605.6	(.058)	1605.6	(.058)
Elastic Modulus Skin	GN/m^2	(psi)	68.9	(10^7)	68.9	(10^7)	68.9	(10^7)
Damping LOSS Factor	none	none	.06	.06	.06	.06	.06	.06
Surface Density Skin plus Stiffeners	kg/m^2	(psf)	10.4	(2.13)	9.22	(1.89)	7.95	(1.63)
Ratio: (Stiffness)/(Baseline Stiffness)			6	6	10	10	10	10
FRAMES								
Spacing	cm	(in)	25.4	(10)	24.1	(9.5)	8.46	(3.33)
Depth	cm	(in)	15.2	(6)	15.2	(6)	10.2	(4)
Cross Sectional Area	cm^2	(in^2)	37.5	(.90)	5.99	(.928)	1.548	(.240)
Bulk Density	kg/m^3	(lb/in^3)	1605.6	(.058)	1605.6	(.058)	1605.6	(.058)
Elastic Modulus Web and outer flange	GN/m^2	(psi)	68.9	(10^7)	68.9	(10^7)	68.9	(10^7)
Inner flange	GN/m^2	(psi)	137.8	(2×10^7)	172.3	(2.5×10^7)	137.8	(2×10^7)
Area centroid (re: skin ℄)	cm	(in)	11.35	(4.47)	11.89	(4.68)	6.67	(2.63)
2nd Area Moment (re: Skin ℄)	cm^4	(in^4)	906.9	(21.8)	1013.5	(24.3)	90.6	(2.18)
Torsion Constant	cm^4	(in^4)	.287	(.00690)	.340	(.00817)	.01068	(.000257)
STRINGERS								
Spacing	cm	(in)	10.8	(4.25)	7.62	(3)	29.2	(11.5)
Depth	cm	(in)	3.81	(1.5)	5.33	(2.1)	7.37	(2.9)
Cross Sectional area	cm^2	(in^2)	2.21	(.342)	1.123	(.174)	3.19	(.495)
Bulk Density	kg/m^3	(lb/in^3)	1605.6	(.058)	1605.6	(.058)	1605.6	(.058)
Elastic Modulus Web and outer flange	GN/m^2	(psi)	68.9	(10^7)	68.9	(10^7)	68.9	(10^7)
Inner flange	GN/m^2	(psi)	137.8	(2×10^7)	137.8	(2×10^7)	137.8	(2×10^7)
Area centroid re: Skin ℄	cm	(in)	2.43	(.956)	2.76	(1.085)	5.42	(2.13)
2nd Area Moment (re: Skin ℄)	cm^4	(in^4)	17.64	(.424)	13.75	(.330)	114.9	(2.76)
Torsion Constant	cm^4	(in^4)	.0425	(.00102)	.00499	(.000112)	.381	(.00916)
Smeared Stiffness Properties (Skin plus Stiffeners with skin width = stiffener spacing)								
*Denotes that the area and the first and second area moments are weighted by the ratio of modulus of elasticity to baseline value								
FRAMES								
• 2nd Area Moment (re: neutral axis)*	cm^4	(in^4)	730.5	(17.55)	201.9	(4.85)	82.5	(1.983)
• Neutral axis distance to Skin ℄*	cm	(in)	7.95	(3.13)	2.09	(.821)	4.34	(1.708)
• Total Cross Sectional Area*	cm^2	(in^2)	14.39	(2.23)	16.52	(2.56)	3.86	(.599)
• Torsion Constant	cm^4	(in^4)	.373	(.00895)	.747	(.01795)	.0344	(.000826)
• Skin Width	cm	(in)	25.4	(10)	24.1	(9.5)	8.46	(3.33)
STRINGERS								
• 2nd Area Moment (re: neutral axis)*	cm^4	(in^4)	16.19	(.389)	14.28	(.343)	125.3	(3.01)
• Neutral axis distance to Skin ℄	cm	(in)	1.69	(.667)	1.77	(.696)	2.91	(1.144)
• Total Cross-Sectional Area*	cm^2	(in^2)	5.363	(.8312)	2.77	(.429)	11.06	(1.715)
• Torsion Constant	cm^4	(in^4)	.0787	(.00189)	.0193	(.00463)	.466	(.01112)
• Skin Width	cm	(in)	10.8	(4.25)	7.62	(3)	29.2	(11.5)

A **EXTERIOR FLUID ENVIRONMENT**

- Cruise Mach No. = 0.8 at 9144 m (30 000 ft) Altitude
- Absolute Static Pressure of Air = 30.1 kPa (630 psfa)
- Ambient Air Density = .460 kg/m^3 (.0287 lb/ft^3)
- Ambient Speed of Sound = 303.3 m/sec (995 ft/sec)
- Ambient Temperature = 228.8°K (412°R)

B **INTERIOR CABIN ENVIRONMENT**

- Cabin Pressure Differential = 45.1 kPa (6.54 psi)
- Absolute Static Pressure = 75.3 kPa (1572 psfa)
- Speed of Sound = 344.4 m/sec (1130 ft/sec)
- Air Density = .887 kg/m^3 (.0554 lb/ft^3)
- Air Temperature = 21.8°C (71.6°F)

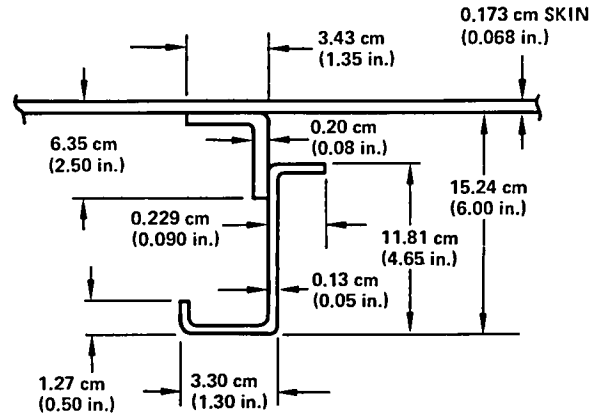

FRAME DETAILS

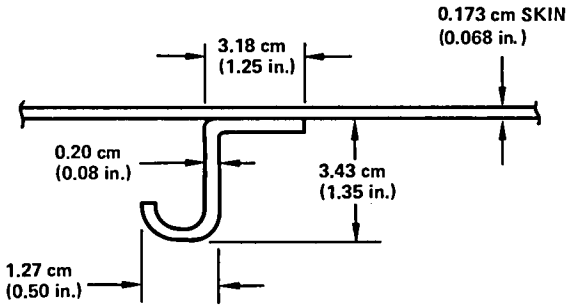

STRINGER DETAILS

Figure 22. - Wide-body aluminum baseline outer wall structure details.

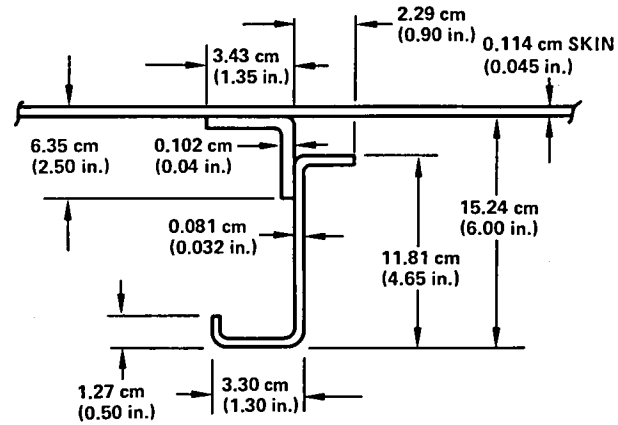

FRAME DETAILS

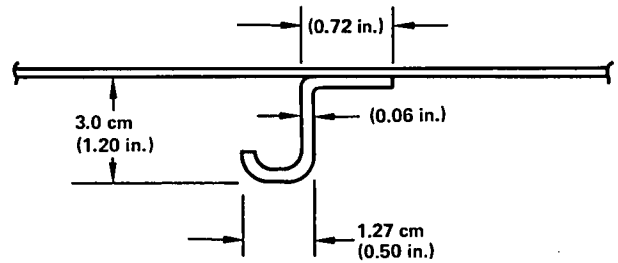

STRINGER DETAILS

Figure 23. - Narrow-body aluminum baseline outer wall structural details.

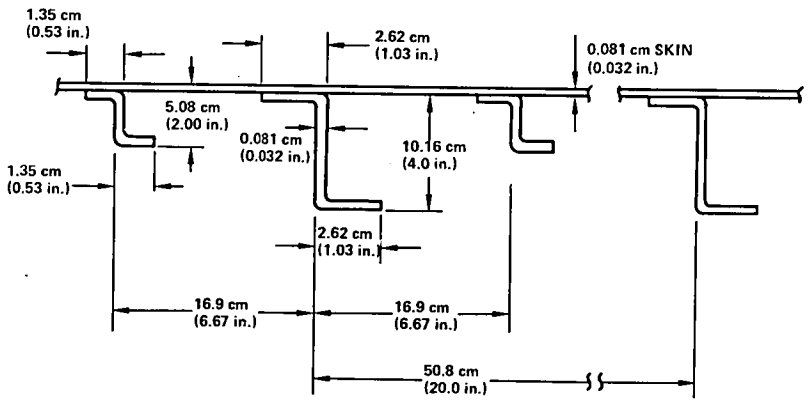

FRAME AND INTERCOSTAL DETAILS

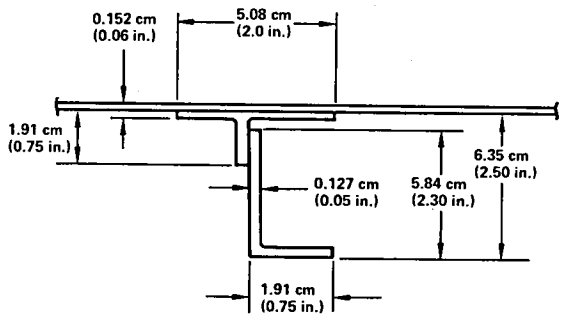

LONGERON DETAILS

Figure 24. - Business aircraft aluminum baseline outer wall structural details.

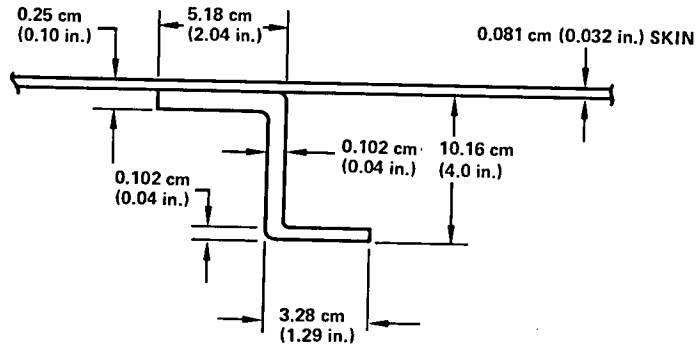

50.8 cm (20 in.) FRAME SPACING (NO INTERCOSTALS)

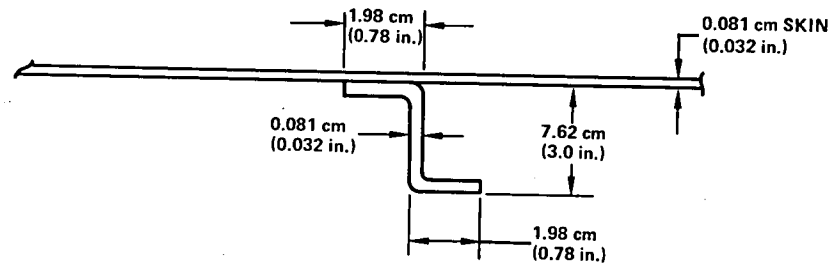

FRAMES AND INTERCOSTALS SET EQUAL
AT 16.9 cm (6.67 in.) SPACING

Figure 25. - Business aircraft alternate frame configurations.

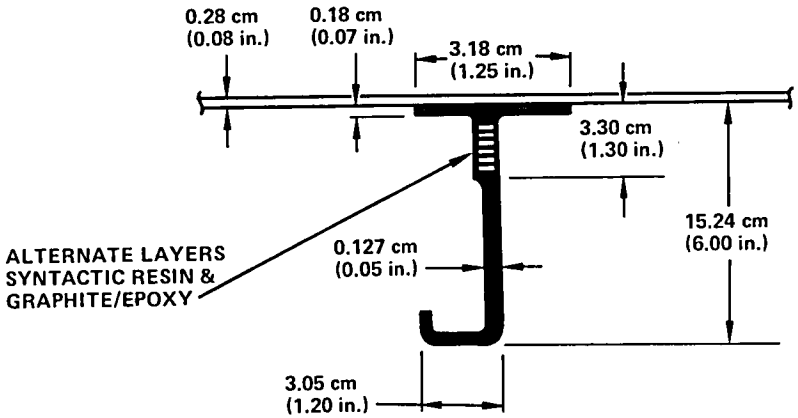

WIDEBODY COMPOSITE SKIN/FRAME CONFIGURATION

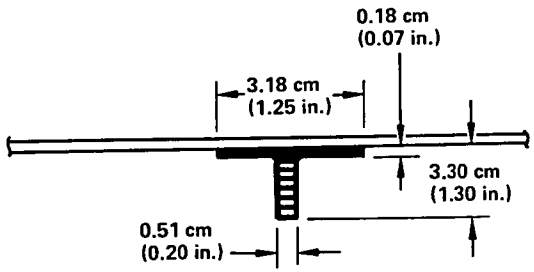

WIDEBODY COMPOSITE SKIN/STRINGER CONSTRUCTION

Figure 26. - Hybrid orthogrid stiffener configurations.

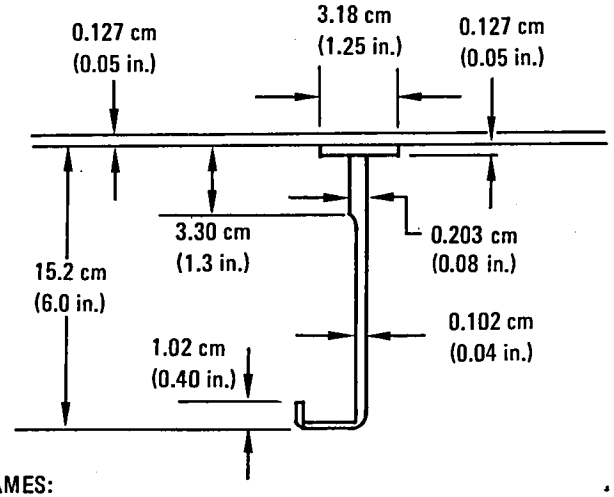

FRAMES:
SPACING = 48.3 cm (19 in.)

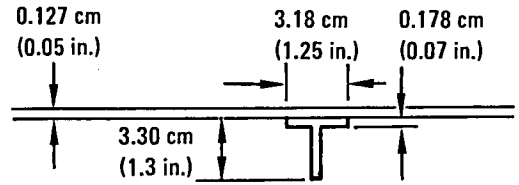

STRINGERS:
SPACING = 15.2 cm (6 in.)
SURFACE DENSITY = 4.2 kg/m^2 (0.86 psf)
MODULUS OF ELASTICITY
E = 68.9 GN/m^2 (10^7 psi)

Figure 27. - Baseline composite narrow-body stiffener configuration.

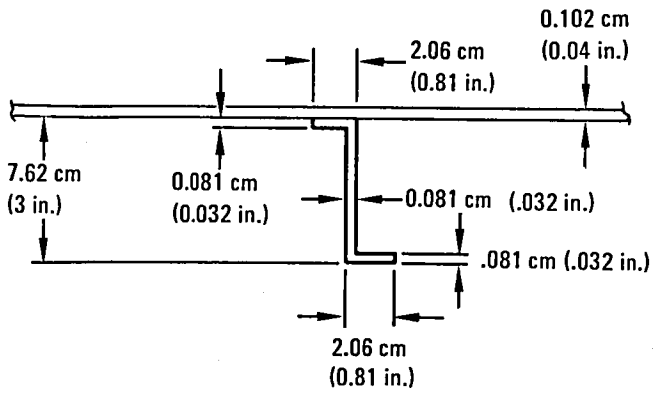

FRAMES:
SPACING = 16.9 cm (6.67 in.)

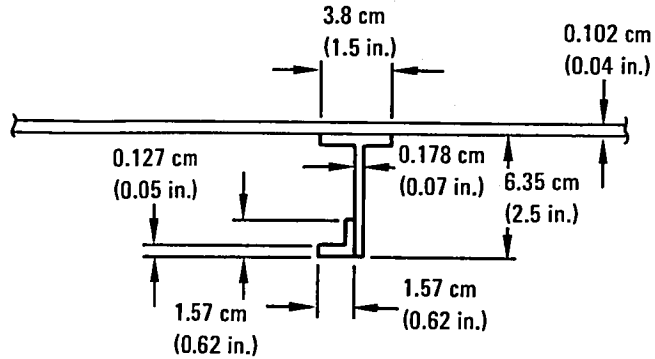

STRINGERS (LONGERONS):
SPACING = 58.4 cm (23 in.)
SURFACE DENSITY = 3.07 kg/m^2 (0.63 psf)
MODULUS OF ELASTICITY
E = 68.9 GN/m^2 (10^7 psi)

Figure 28. - Baseline composite business aircraft stiffener configuration.

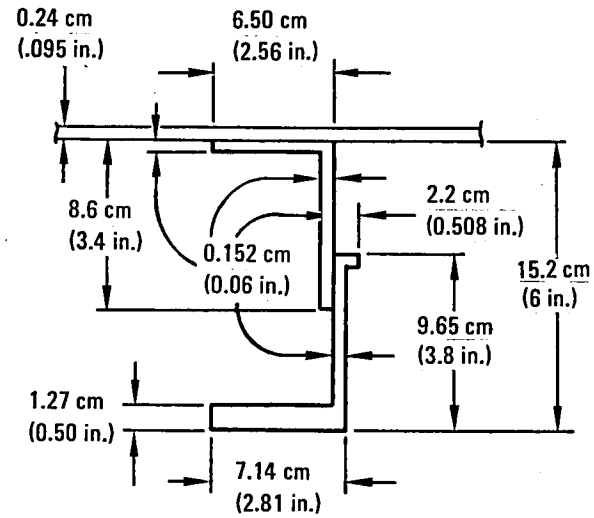

FRAMES:
SPACING = 508 cm (20 in.)
STIFFNESS = 5.0 x BASELINE STIFFNESS

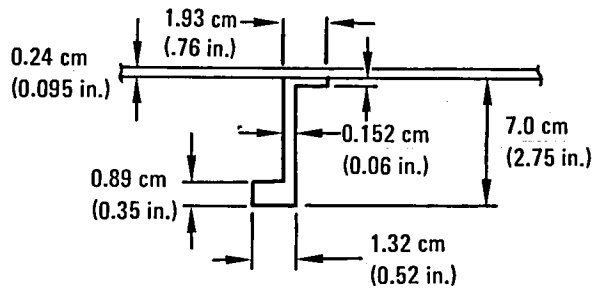

STRINGERS:
SPACING = 21.6 cm (8.5 in.)
STIFFNESS = 5.0 x BASELINE STIFFNESS
SURFACE DENSITY = 15.4 kg/m^2 (3.16 psf)

Figure 29. - Structural details for aluminum wide-body, advanced noise-reduction design.

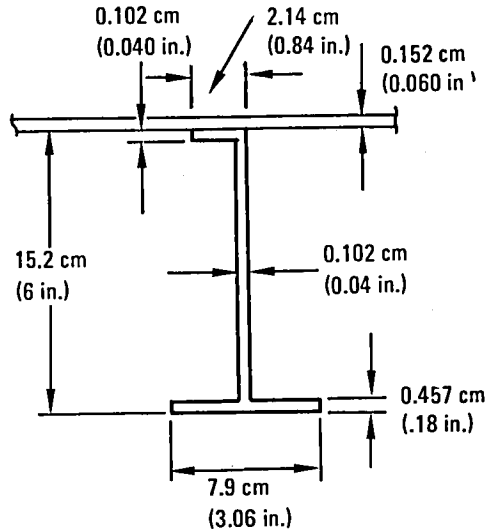

FRAMES:
SPACING = 24.1 cm (9.5 in.)
STIFFNESS = 6.0 x BASELINE STIFFNESS

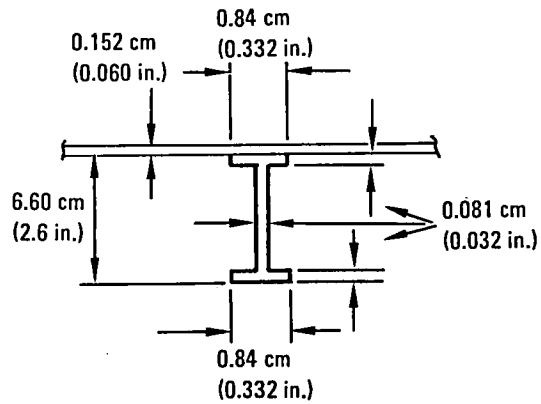

STRINGERS:
SPACING = 7.62 cm (3 in.)
STIFFNESS = 6.0 x BASELINE STIFFNESS
SURFACE DENSITY = 13 kg/m^2 (2.6 psf)

Figure 30. - Structural details for aluminum narrow-body, advanced noise-reduction design.

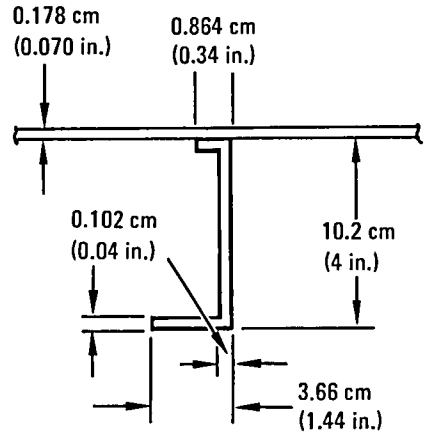

FRAMES:
SPACING = 8.46 cm (333)
STIFFNESS = 6.0 x BASELINE STIFFNESS

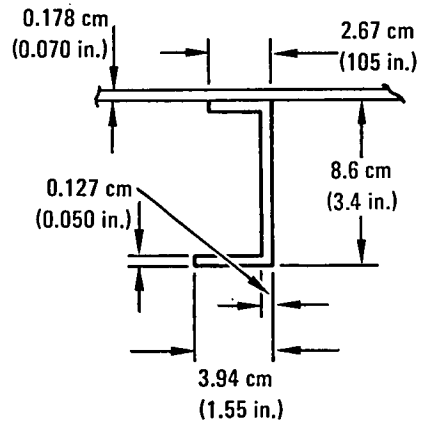

STRINGERS:
SPACING = 29.2 cm (115 in.)
STIFFNESS = 6.0 x BASELINE STIFFNESS
SURFACE DENSITY = 11.5 kg/m^2 (2.36 psf)

Figure 31. - Structural details for aluminum business aircraft, advanced noise-reduction design.

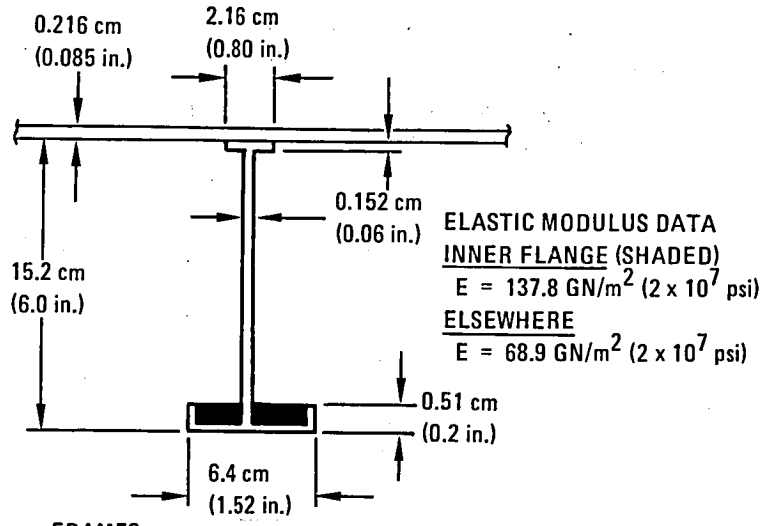

Figure 32. - Structural details for composite wide-body, advanced noise-reduction design.

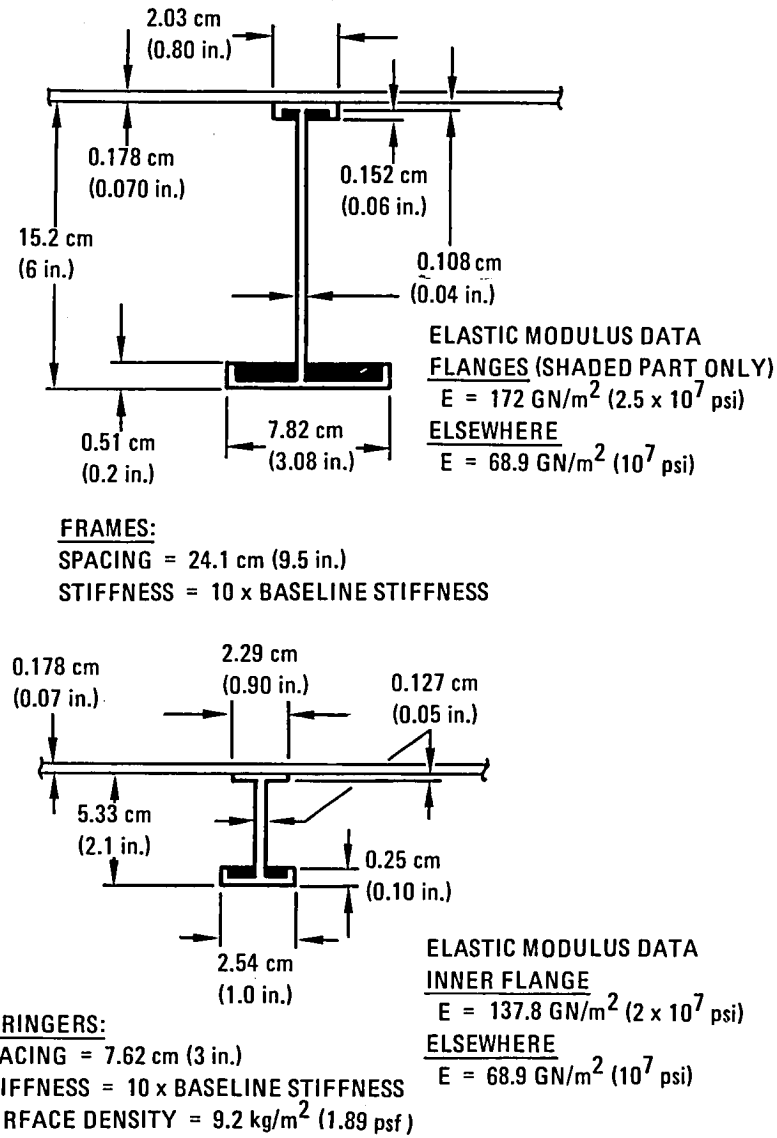

Figure 33. - Structural details for composite narrow-body, advanced noise-reduction design.

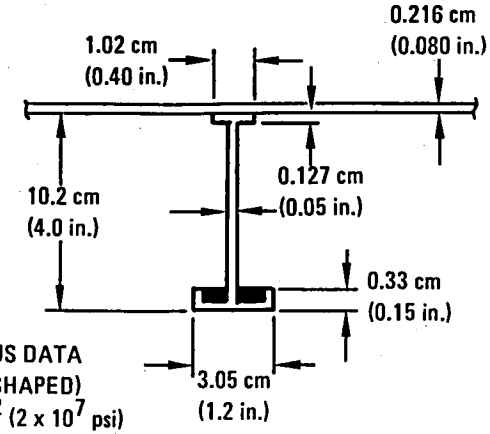

ELASTIC MODULUS DATA
INNER FLANGE (SHAPED)
E = 137.8 GN/m^2 (2 x 10^7 psi)
ELSEWHERE
E = 68.9 GN/m^2 (10^7 psi)

FRAMES: SPACING = 8.46 cm (3.33 in.)
STIFFNESS = 10 x BASELINE STIFFNESS

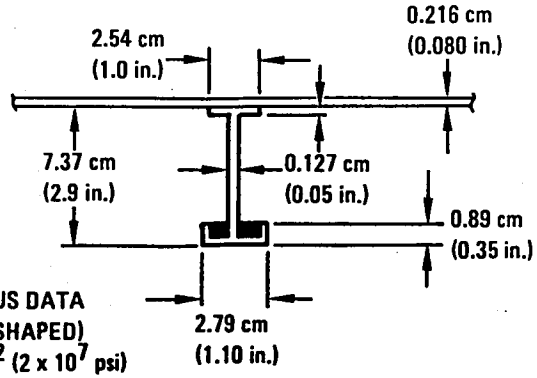

ELASTIC MODULUS DATA
INNER FLANGE (SHAPED)
E = 137.8 GN/m^2 (2 x 10^7 psi)
ELSEWHERE
E = 68.9 GN/m^2 (10^7 psi)

STRINGERS:
SPACING = 29.2 cm (11.5 in.)
STIFFNESS = 10 x BASELINE STIFFNESS
SURFACE DENSITY = 7.95 kg/m^2 (1.63 psf)

Figure 34. - Structural details for composite narrow-body, advanced noise-reduction design.

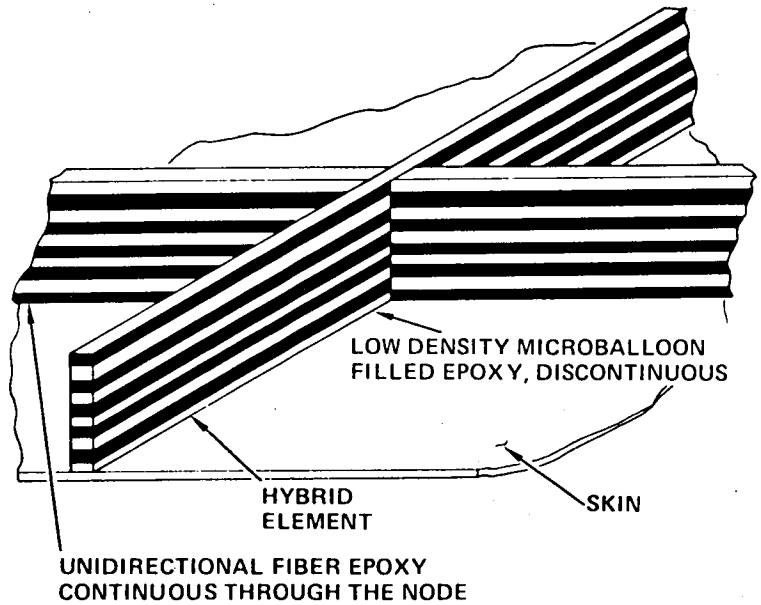

Figure 35. - Composite orthogrid outer wall structure details.

APPENDIX C

ANALYTICAL SUMMARY OF KOVAL'S THEORY OF CYLINDRICAL SHELL NOISE TRANSMISSION

The following is a brief outline of the mathematical analysis of reference 20. The incident plane wave (see figure 20 of Appendix A) is represented by

$$p_i = P_i \exp [j\omega t - j(k_{1x} x + k_{1z} z)] \tag{2}$$

where $k_{1x} = k_1 \sin \theta$, $k_{1z} = k_1 \cos \theta$, and where k_1 is the wave number in the moving external medium given by

$$k_1 = (\omega/c_1)/(1 + M_1 \cos \theta) \tag{3}$$

In this Appendix, the coordinate definitions follow Reference 4, which differs from the remainder of this report. Expressed in cylindrical coordinates, p_i is

$$p_i = P_i \exp [j(\omega t - k_{1z} z)] \sum_{m=o}^{\infty} \varepsilon_m (-j)^m J_m(k_{1r}) \cos m\phi \tag{4}$$

where $k_{1r} = k_{1x}$, $\varepsilon_m = 1$ for $m = 0$, and $\varepsilon_m = 2$ for $m = 1$.

The scattered wave can be written in the form

$$p_s = \exp [j(\omega t - k_{1z} z)] \sum_{m=o}^{\infty} A_m H_m^{(2)} (k_{1r} r) \cos m\phi \tag{5}$$

where $H_m^{(2)}$ is the Hankel function of the second kind of integral order m. The coefficient A_m is yet to be determined.

The shell response can be represented by

$$w = \exp [j(\omega t - k_{1z} z)] \sum_{m=o}^{\infty} W_m \cos m\phi \tag{6}$$

The internal pressure field can be represented by

$$p_2 = \exp\left[j(\omega t - k_{2z} z)\right] \sum_{m=o}^{\infty} B_m H_m^{(1)} (k_{2r} r) \cos m\phi \qquad (7)$$

where $H_m^{(1)}$ is the Hankel function of the first kind and represents, in analogy with the classical definition of transmission loss for a flat panel, a radially inward travelling wave which is assumed to be totally absorbed inside the cabin.

The unknowns in equations (5), (6), and (7) are determined by

- Matching radial fluid particle and transverse shell displacements at the shell surface
- Writing a force balance equation in the radial direction, viz.,

$$\left[p_2 - (p_i + p_s)\right]_{r=a} = \sum_{m=o}^{\infty} (j\omega W_m) Z_m^{sh} \exp\left[j(\omega t - k_{1z} z)\right] , \qquad (8)$$

where Z_m^{sh} is the modal impedance of the shell.

These steps lead to

$$k_{2z} = k_{1z},$$

$$k_{2r} = \left(\frac{\omega}{c_2}\right)\left[1 - \left(\frac{c_2}{c_1}\right)^2 \left(\frac{\cos\theta}{1 + M_1 \cos\theta}\right)^2\right]^{1/2} \qquad (9)$$

and appropriate expressions for A_m, B_m and W_m, given by equations 25, 32 and 33 of reference 19.

Finally, the cylinder transmission loss (TL) can be defined as

$$TL = 10 \log_{10}\left(\frac{\text{Incident Power}}{\text{Absorbed Power}}\right) \qquad (10)$$

$$TL = 10 \log_{10}\left(\frac{p_i^2}{p_2^2}\right)$$

to yield $$TL = 10 \log_{10} Q^a \tag{11}$$

where

$$Q^a = \sum_{m=o}^{\infty} (2\epsilon_m/x_{1r})\ r_m^c\ r_m^s \Big/ \left[\left(r_m + r_m^s\right)^2 + \left(\chi_m + \chi_m^s\right)^2\right] \tag{12}$$

$$r_m = \mathrm{Re}(z_m),\ \chi_m = \mathrm{Im}(z_m),\ x_{1r} = k_{1r}a \tag{13}$$

$$r_m^s = (2/\pi\ x_{1r}) \Big/ \left[(J_m')^2 + (Y_m')^2\right] \tag{14}$$

$$\chi_m^s = -\ (J_m\ J_m' + Y_m\ Y_m') \Big/ \left[(J_m')^2 + (Y_m')^2\right] \tag{15}$$

$$z_m = (Z_m/\rho_1 c_1)\ \sin\theta\ (1 + M_1 \cos\theta) \tag{16}$$

$$r_m^c = \mathrm{Re}(Z_m^c/\rho_1 c_1) \tag{17}$$

In equations (12) through (17), a is the shell radius, $J_m = J_m(k_{1r}a)$ and $Y_m = Y_m(k_{1r}a)$ are Bessel functions, and Z_m is the impedance of the shell and its contents.

$$Z_m = Z_m^{sh} + Z_m^c \tag{18}$$

For a totally absorbing interior with only inward-travelling waves, the impedance of the contents can be shown to be given by

$$Z_m^c = \frac{j\omega\rho_2 H_m^{(1)}(k_{2r}a)}{k_{2r}[H_m^{(1)}(k_{2r}a)]'} = \frac{j\rho_2 c_2 H_m^{(1)}(k_{2r}a)}{\sin\theta_2\ [H_m^{(1)}(k_{2r}a)]'} \tag{19}$$

where

$$\sin\theta_2 = \sqrt{1 - \left(\frac{c_2}{c_1}\right)^2 \frac{\cos^2\theta}{(1 + M\cos\theta)^2}}$$

In equations (14), (15) and (18), primes denote derivatives with respect to the argument.

The shell modal impedance can be obtained from the dynamic equations of motion of the shell

$$\begin{aligned} L_{11}(u) + L_{12}(v) + L_{13}(w) &= m^{sh}\ddot{u} \\ L_{21}(u) + L_{22}(v) + L_{23}(w) &= m^{sh}\ddot{v} \\ L_{31}(u) + L_{32}(v) + L_{33}(w) &= m^{sh}\ddot{w} + p \end{aligned} \tag{20}$$

where L_{ij} are the appropriate differential operators given by equations 5 through 12 in reference 19; u, v, w are shell displacement components; m^{sh} is the shell wall mass per unit area; dots refer to time derivatives; and p is the excitation pressure.

Consistent with equation (6), the three shell displacement components can be written in the form

$$\begin{Bmatrix} u \\ v \\ w \end{Bmatrix} = \sum_{m=o}^{\infty} \begin{Bmatrix} jU_m & \sin m\phi \\ V_m & \cos m\phi \\ W_m & \cos m\phi \end{Bmatrix} \exp\left[j(\omega t - k_{1z} z)\right] \tag{21}$$

When equations 4 and 21 are substituted in equation 20, the resulting simultaneous equations can be solved for radial displacement as a function of excitation pressure. The radial inward-looking modal impedance of the cylindrical shell can then be written in the form

$$Z_m^{sh} = j\, m^{sh}\omega \frac{(\omega_R/\omega)^2\, \Delta}{(1 - \nu^2)\left[A_{12}\, A_{21} - A_{11}\, A_{22}\right]} \tag{22}$$

where ω_R is the monocoque-shell ring frequency and A_{ij} are coefficients that result from substituting the displacements, equation (21), into the shell equations of motion (20). The coefficients A_{ij} and their determinant, Δ, are given in reference 19 for a monocoque cylindrical shell. The effects of stiffeners are smeared by the procedure in reference 20 to yield an equivalent monocoque shell into which the foregoing theory is assumed to apply.

Appendix D provides a critique of the smeared-stiffener theory in light of more recent work.

APPENDIX D

CRITIQUE AND POTENTIAL IMPROVEMENTS

D1. STIFFENED SHELL THEORY

The method used in this study is an amalgamation of two theories. The fuselage transmission loss (TL) is computed from both the cylindrical shell theory of Koval, which emphasizes shell modes, and the method developed by Cockburn and Jolly, which includes panel modes, with the smaller of the two values being used. To this outer-wall TL is added the multilayered wall increment due to fiberglass insulation, trim panel, etc., as computed by a flat-panel model in the Cockburn and Jolly routine. The Koval theory uses a smeared-stiffener model to represent the effects of stringers and ring frames. For the narrow-body fuselage of reference 15, this approach appears to give reasonable results up to the ring frequency when compared to a discrete stiffener analysis. Beyond the ring frequency, it appears to overpredict the TL of the cylinder sidewall.

The discrete-stringer model (reference 16) can be easily incorporated into the present calculations because it involves a Fourier-series expansion in the circumferential coordinate. This would, therefore, be the most logical first improvement to the theory. Since this is the very same expansion employed in the smeared-stiffener theory, no difficulties are foreseen.

The next logical step for improvement is to include a discrete model of the ring frame, although it would be more complex and would involve considerably more computer time. Reference 15 forms the basis of this theory in which a shell of finite length was used (this is an improvement over the smeared-stiffener model which considers the shell to be of infinite length). This length, L, is taken as the length of the shell. The ring-frame modeling then employed a Fourier-series expansion axially as well as circumferentially, so that the shell displacement was taken in the form of a double Fourier series viz.,

$$w(x, y, t) = \sum_{n=1}^{\infty} \sum_{m=1}^{\infty} W_{mn} \cos \frac{ny}{a} \sin \frac{m\pi x}{L} e^{j\omega t} \qquad (23)$$

where a = shell radius.

The coefficient W_{mn} was then calculated from the shell equations (with the effects of discrete ring frames and stringers included) in the form

$$\begin{aligned} L_{11}\ (u) + L_{12}\ (v) + L_{13}\ (w) &= m\ \ddot{u} \\ L_{21}\ (u) + L_{22}\ (v) + L_{23}\ (w) &= m\ \ddot{v} \\ L_{31}\ (u) + L_{32}\ (v) + L_{33}\ (w) &= m\ \ddot{w} + p \end{aligned} \tag{24}$$

where L_{ij} are the appropriate differential operators for the shell where u, v, w are the three shell displacement components, m is the shell mass/area, and p is the applied external pressure. The structural and inertial effects of the rings and stringers are contained in the operators L_{ij}. Details are given in reference 15.

In equation (24), u, v, w and p are expanded in double Fourier series, as in equation (23), and W_{mn} is then computed. The corresponding shell impedance is computed from

$$Z_{mn}^{sh} = \frac{P_{mn}}{j\omega\ W_{mn}} \tag{25}$$

where ω = frequency of the incident acoustic pressure, and P_{mn} is the Fourier coefficient in the expansion of the incidence pressure p.

To make the above formulation fit the scheme employed in the smeared-stiffener model (which involved only a summation of circumferential modes), it would be necessary to remove the axial dependence from the problem. This can be accomplished by defining the shell modal impedance as

$$Z_n^{sh} = \frac{p_{RMS}}{j\omega W_{RMS}} = \frac{1}{j\omega} \sqrt{\frac{\int_o^L (p)^2\ dx}{\int_o^L \left[\sum_{m=1}^{\infty} W_{mn}\ \sin\left(\frac{m\pi x}{L}\right)^2\right] dx}} \tag{26}$$

Substitution for $p = p_o \sin (x_{mj}\, x) \cos (n\phi)\, e^{j\omega t}$ and W_{mn} eventually leads to an expression of the form

$$Z_n^{sh} = \frac{E\,h}{j\omega a^2} \sqrt{\frac{\left[1 - \sin (2\, x_{mz}\, \ell)/(2\, x_{mz}\, \ell)\right]}{\sum_{n=1}^{\infty} \frac{C_m^2}{\Delta^2} \left[A_{11}\, A_{22} - A_{12}\, A_{21}\right]^2}} \qquad (27)$$

where E = shell modulus, h = shell-wall thickness, ℓ = L/a, length, C_m coefficient for Fourier expansion of sin x_{mz} x, A_{ij} = coefficient derived from L_{ij}, Δ = det (A_{ij}), and x_{mz} is a wave number parameter.

The significant thing about equation (27) is that the computation of the shell modal impedance first involves a summation on the axial wave index (m) for each circumferential wave index (n). Since the calculation of TL then requires a summation on (n), the computational effort is considerably larger than for the smeared-stiffener approach.

D2. NUMERICAL COMPARISON OF DISCRETE STIFFENERS VERSUS SMEARED-STIFFENER RESULTS

The question is how do the two approaches (smeared-stiffener versus discrete-stiffener) compare? The results of calculations for a narrow-body jet are illustrated in figures 36 through 39 for angles of incidence θ = 0.52, 0.79, 1.05, 1.31 rad (30, 45, 60, 75 deg), respectively. Inspection of the curves shows that the smeared-stiffener approach overestimates TL above the ring frequency except at 75 deg. But below the ring frequency, the smeared-stiffener theory appears to provide acceptable accuracy, at least for the purpose of preliminary design. It is interesting to observe that the discrete-stiffener model also clearly verifies that relatively small values of transmission loss are obtained near the ring frequency of the shell. This is a result of the nature of the gross cylindrical geometry of the fuselage and does not appear to be particularly sensitive to whether or not the stiffened shell (or fuselage) is modelled by a smeared-stiffener approach or by a discrete-element approach.

Also shown in figure 36 are the small notches in the TL curve for the discrete-stiffener model. These notches are present below the ring frequency in the predominantly stiffness-controlled region of the TL spectrum and tend to slightly decrease the TL from the value predicted by the smeared-stiffener model. These notches may be due to the additional structural resonances that are introduced by the finite length of the shell. Such resonances are not present in the smeared-stiffener theory because the shell length is assumed to be infinite.

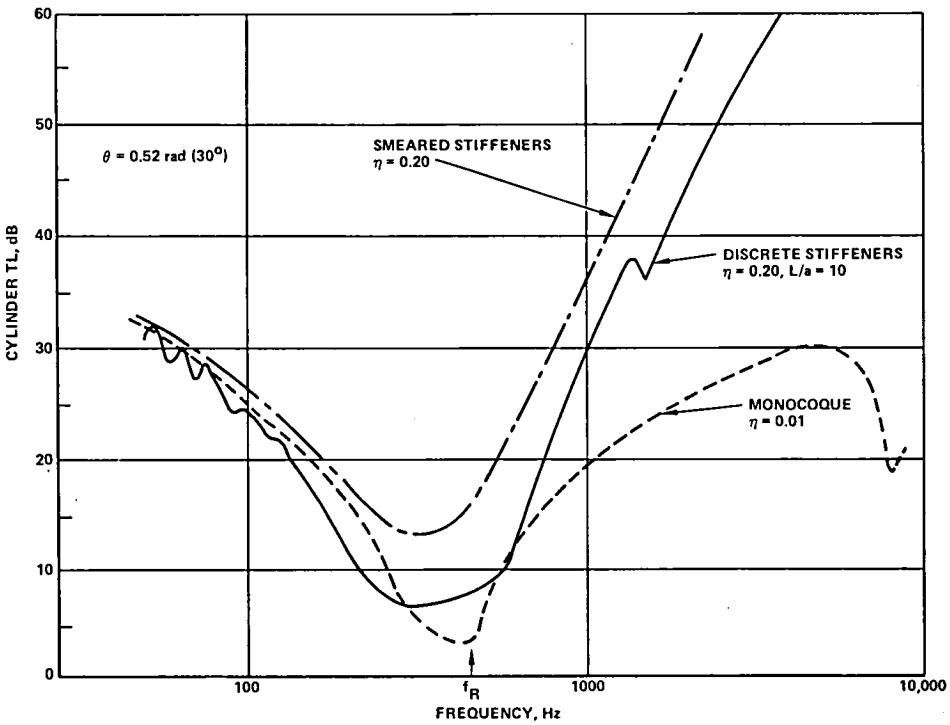

Figure 36. - Cylinder transmission loss at a graze angle of 0.52 rad (30 deg).

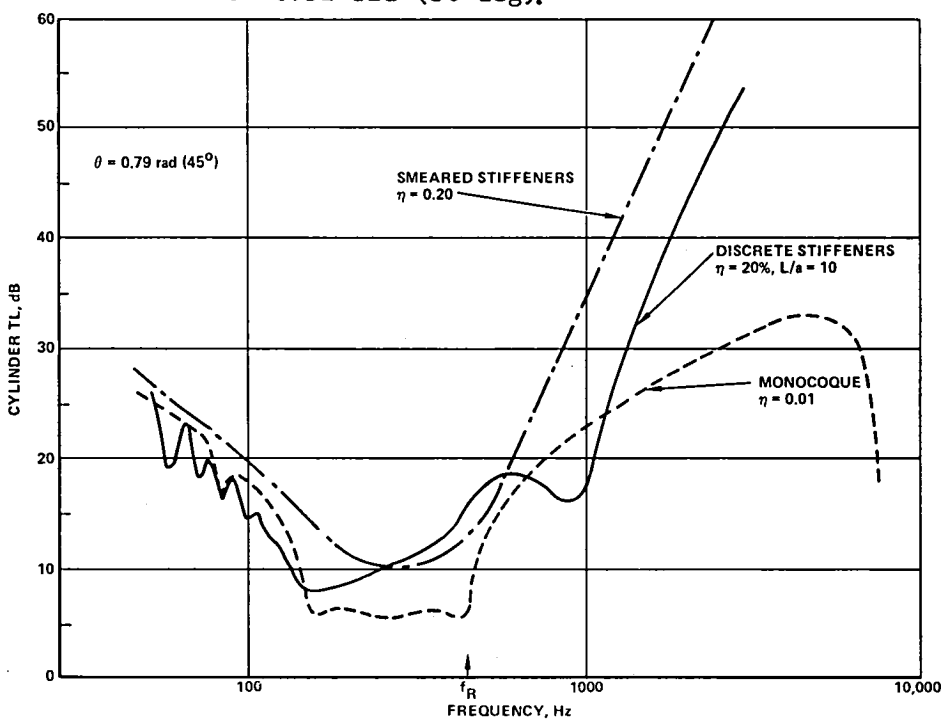

Figure 37. - Cylinder transmission loss at a graze angle of 0.79 rad (45 deg).

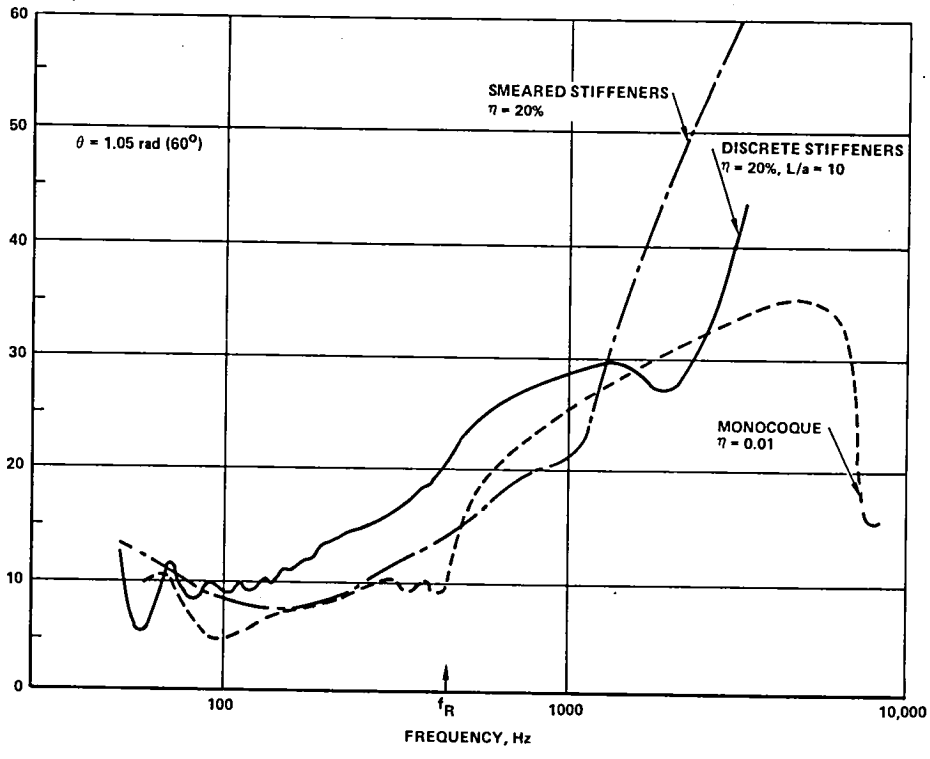

Figure 38. - Cylinder transmission loss at a graze angle of 1.05 rad (60 deg).

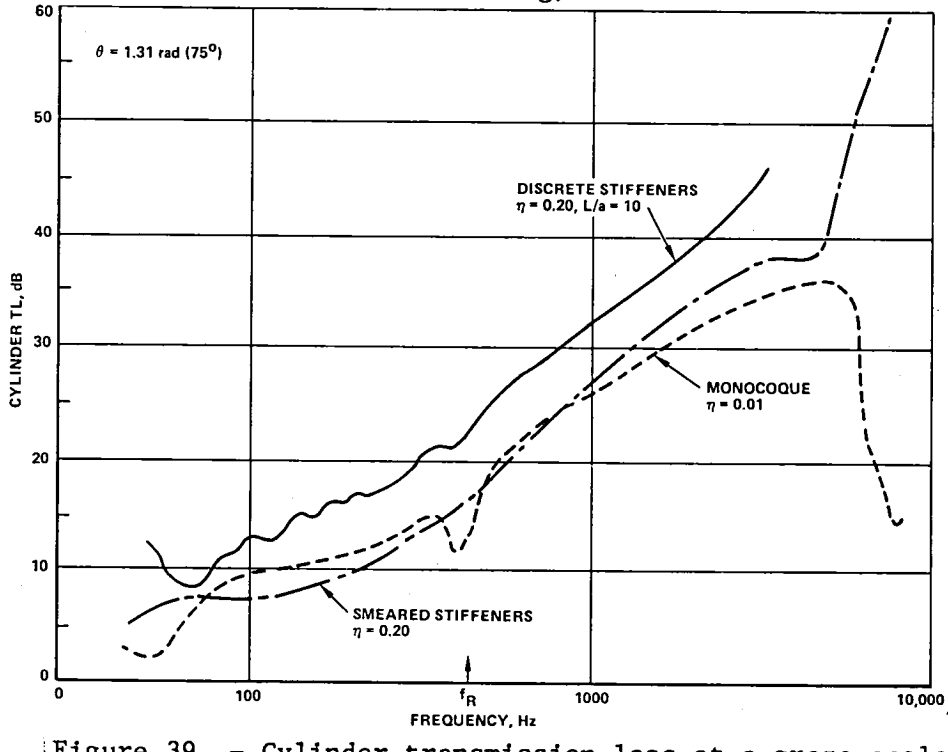

Figure 39. - Cylinder transmission loss at a graze angle of 1.31 rad (75 deg).

D3. EFFECT OF FLOOR

Another feature of a real fuselage that has not been included in the present study is the effect of the floor on the wall vibrations of the fuselage and on the interior noise levels. Such a study for the free vibrations of a monocoque-shell floor system has just appeared in the literature (reference 21). The problem was formulated on a Rayleigh-Ritz basis with Lagrange multipliers used to handle the constraints of matching floor and shell displacements at the appropriate connecting points. Numerical results implied that the floor tended to restrict the shell displacements at the floor connection points. This will probably affect the resulting noise transmission, although to what extent can only be determined by solving the sound transmission problem for cylindrical shell with a floor. This could be done in one of two ways.

The first approach would be the more approximate method in which the effect of the floor is modeled by the in-plane stiffness of the partition. This stiffness would be a longitudinally distributed spring placed at the connecting points of the floor to the cylinder and would be used to restrict the radial deformation of the shell in the same manner as does the floor. The formulation would involve a Fourier-series expansion in the circumferential coordinate. At first, coupling between the various circumferential modes could be ignored, giving a direct calculation of the shell modal impedance for a given circumferential wave number, n. Later, the coupling between circumferential modes could be accounted for. An attempt could be made to fit this problem into the TL calculation scheme now being employed.

A second, more rigorous and more complicated, approach would first solve the coupled shell-floor vibration problem, including the effects of floor mass and floor transverse displacements. It would then compute the noise level within the cabin (upper volume between shell and floor). This would be a rather involved calculation and it would probably be better to compute noise reduction rather than transmission loss. An additional feature would be the noise radiated by the floor.

Once worked out for a monocoque shell, either (or both) of the previous models could be improved by modifying the shell to include the effects of stringers and ring frames.

D4. ADD-ON NOISE REDUCTION MEASURES

TL increments due to the add-on noise reduction treatments have been added to the outer wall TL, computed either from the Koval cylindrical shell theory or the Cockburn and Jolly program (as appropriate). These TL increments are computed using the Cockburn and Jolly flat panel model with multilayer configurations of fiberglass blankets, trim panels, air gaps, and septa.

The use of a flat panel for computing the TL increments is a reasonable approximation based on the fact that the thickness of the layers is very small

compared to the radius of curvature of the fuselage walls, so that the effect of wall curvature on the TL increments is not thought to be significant. The computer program employed for the parametric studies determined the transmission loss of each add-on noise control layer on the basis of plane wave transmission at the proper oblique incidence; therefore, $k_x = k_y = 0$ and $k_{zi} = \omega/c_i$. While not strictly rigorous, the methodology employed is felt to be valid for engineering purposes for the following reasons:

- The lower-order circumferential wave numbers are likely to dominate sound transmission, so that even though equation (28) has a cut-off characteristic for the large-enough n, the error in not including its effect will be small

- The axial wave number used is fixed for all layers

- The analysis of layers containing blankets (one of the principal noise-attenuating elements) is highly empirical, so that the improved accuracy may not have been significant enough to justify the delay in the parametric study that would have been required to implement the refinement.

D5. MISCELLANEOUS ITEMS

D5.1 Axial Variation of Pressure Excitation

The exciting pressure is not uniform along the length of the fuselage since it decreases at locations removed from the propeller disc planes. This is treated by dividing the affected portion of the fuselage into seven segments, and assuming that the OASPL levels in each segment are reduced by an appropriate number of dB. This segmented approach is a reasonable way to treat such a variation, giving a pressure distribution which is conservative. In the calculations, the incidence angle of the noise radiated from the propellers is considered. Koval (reference 7) has shown that this is important.

D5.2 Plane Wave Model in Koval's Theory

For the aircraft designs investigated in the present study, the plane wave model is considered to be a good local approximation to the spherical wave fronts which originally emanated from a small noise source region near the tip of an individual propfan blade. For each aircraft the minimum propeller tip to fuselage clearance is well over one wave length. For the 2-engine aircraft with an 0.8 diameter tip clearance, this distance represents 1.64 wave lengths at the blade passage frequency. For the 4-engine, wide-body aircraft, the inboard propeller clearance of 1.2 diameters represents a distance of 2.45 wave lengths; the outboard propeller with a clearance of 2.3 diameters corresponds to a distance of 4.7 wave lengths. For these conditions the curvature of the spherical wave fronts as they impinge upon the fuselage is likely to have only a small effect upon the scattering of the incoming waves compared to the calculation scheme used in this study.

APPENDIX E
SUMMARY OF EQUATIONS FOR ADD-ON NOISE CONTROL ELEMENTS

The equations used to define the impedances of and pressure ratios across the individual layer types will be described below. In the following discussion, θ denotes the classical incidence angle measured with reference to an axis normal to the surface and positive in the downstream direction.

E1. SKIN PANEL CHARACTERISTICS

For a skin panel subjected to an obliquely incident sound wave with an external airflow, the pressure ratio is obtained from

$$\frac{P_I}{P_T} = 1/2 \left[1 + \frac{Z_p \cos \theta_2}{Z_2} + \frac{\rho_1 C_1 \cos \theta_2}{\cos \theta_1 (1+M \sin \theta_1) Z_2} \right] \tag{28}$$

where

P_I = incident pressure

P_T = transmitted pressure

Z_p = characteristic impedance of skin panel

The characteristic impedance of a flat skin panel bounded by stiffeners and with inplane stresses to simulate pressurization is defined by

$$Z_p = \frac{\omega_o^2}{\omega} m\eta + \frac{\omega^3 D\eta}{C_1^4} \frac{\sin^4 \theta}{(1+M \sin \theta)^4} + j \left[\omega m - \frac{\omega_o^2 m}{\omega} - \frac{\omega_o^3 D}{C_1^4} \frac{\sin^4 \theta}{(1+M \sin \theta)^4} \right] \tag{29}$$

where

ω_o = fundamental frequency of skin panel

$$= \frac{\pi}{(m)^{1/2}} \left[\left(\frac{P_{ax}}{a^2} + \frac{P_{cir}}{b^2} \right) + D\pi^2 \left(\frac{1}{a^2} + \frac{1}{b^2} \right)^2 \right]^{1/2} \tag{30}$$

The corresponding pressure ratio equation from Reference 5 is (EQ 6.4)

$$\frac{P_1}{P_2} = \frac{P_i + P_r}{P_t} = \left[1 + \frac{Z \cos \theta}{Z_2}\right]$$

The differences between the two expressions result from the definition of incident pressure. For this study the incident pressure did not include the reflected pressure, while in Reference 8 the incident pressure was defined as the sum of the incident and reflected pressures. When free-field sound pressure levels are measured or calculated, equation 28 should be used to calculate the pressure ratio across the skin. The characteristic impedance equation from Reference 8 is (EQ 6.5)

$$Z_p = \omega_o m\eta + \frac{\omega^3 D}{C^4} \sin^4 \theta + j\left[\omega m - \frac{\omega_o^2 D}{\omega} - \frac{\omega^3 D}{C^4} \sin^4 \theta\right]$$

The difference in the first term of the equation is probably due to a typographical error in Reference 8, and the denominator of the last term of equation 29 includes a flow effect. The inclusion of the flow effect in equations 28 and 29 was consistent with the flow effect described in Koval's cylindrical shell theory (reference 7).

E2. SEPTA

When an internal layer is either a panel or a septum the following expression is used to determine the pressure ratio across the layer

$$\frac{P_I}{P_T} = 1 + \frac{Z_p \cos \theta_2}{Z_2} \qquad (31)$$

where

Z_p = characteristic impedance of layer

= $j\omega m$ for a septum

= equation 29 (with M = 0) for a panel

Z_2 = termination impedance

Equation 31 is identical with equation 6.4 of reference 8.

E3. AIRSPACES AND POROUS BLANKETS

The pressure ratio across an airspace or a soft porous blanket subjected to an obliquely incident wave is given by

$$\frac{P_I}{P_T} = \frac{\cosh\left[\text{bd cos } \phi + \coth^{-1}\left(\frac{Z_2 \cos\phi}{Z_B}\right)\right]}{\cosh\left[\coth^{-1}\left(\frac{Z_2 \cos\phi}{Z_B}\right)\right]} \tag{32}$$

where

b = complex propagation constant (Reference 8)

$$= j\omega\left[\left(\frac{\bar{\rho}_1 Y}{K}\right)\left(1 - j\frac{\bar{R}_1}{\omega\bar{\rho}_1}\right)\right]^{1/2} \quad \text{for blankets} \tag{33}$$

$$= j\frac{\omega}{C} \text{ for airspaces}$$

Z_2 = termination impedance

Z_B = characteristic impedance of layer

$$= -j\frac{K\,b}{\omega\,Y} \text{ for blankets}$$

$$= \rho C \text{ for airspaces}$$

The corresponding equation from Reference 8 is (EQ 6.11)

$$\frac{P_1}{P_2} = \frac{\cosh\left[\frac{bd}{\cos\phi} + \coth^{-1}\frac{Z_2}{Z_B}\right]}{\cosh\left[\coth^{-1}\frac{Z_2}{Z_B}\right]}$$

The input impedance of panel or septum layers is simply the sum of the layer characteristic impedance and its termination impedance. This simple

relationship does not hold for blankets and airspaces and their input impedance is

$$Z_{IN} = \frac{Z_B}{\cos\phi} \coth\left[bd\cos\phi + \coth^{-1}\left(\frac{Z_2\cos\phi}{Z_B}\right)\right] \qquad (34)$$

This expression is a modification of equations 6.12 and 6.14 of reference 8.

E3. MULTIPLE LAYERED CONFIGURATIONS

The procedure that is used to calculate the pressure ratio across a multilayered configuration will now be described. The pressure ratio across a single layer of a configuration can be calculated if both the characteristic and termination impedances of the layer are known by equations 28, 31 and 32.

The input impedance of each layer is calculated by starting at the innermost layer and working outward to the skin (figure 40). Thus, the input impedance of the trim panel is equal to the sum of its characteristic impedance and its termination impedance

$$Z_{TR} = Z_P \text{ (eq. 29)} + (\rho C)_{Cabin}$$

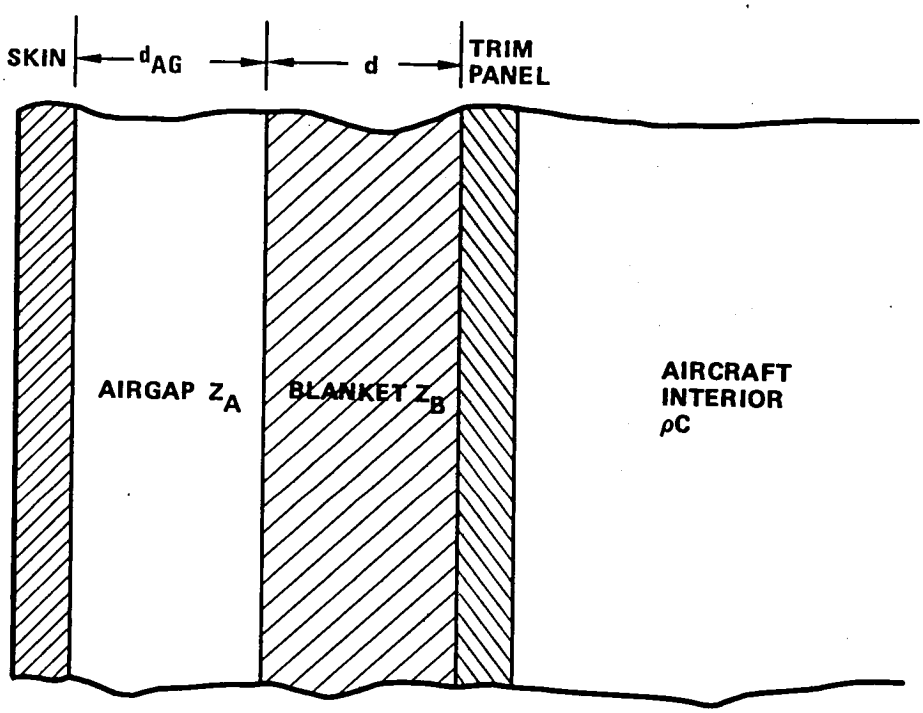

Figure 40. Typical aircraft sidewall configuration

The input impedance of the trim panel is also the termination impedance of the fiberglass blanket and the blanket input impedance is written from equation 34 as

$$Z_{BL} = \frac{Z_B}{\cos\phi} \coth\left[bd\cos\phi + \coth^{-1}\left(\frac{Z_{TR}\cos\phi}{Z_B}\right)\right]$$

The input impedance of the airgap is then

$$Z_{AG} = \frac{Z_A}{\cos\phi} \coth\left[bd\cos\phi + \coth^{-1}\left(\frac{Z_{BL}\cos\phi}{Z_A}\right)\right]$$

Finally, the input impedance of the aircraft skin is defined as

$$Z_{SK} = Z_P \text{ (eq. 29)} + Z_{AG}$$

With the characteristic and termination impedance defined for each layer of the the configuration, the pressure ratio across each layer can now be calculated using equations 28, 31, and 32. The pressure ratio across a multilayered configuration can be expressed in terms of the pressure ratio across the individual layers.

$$\left[\frac{P_I}{P_T}\right]^2 = \left[\frac{P_I}{P_2} \cdot \frac{P_2}{P_3} \cdot \frac{P_3}{P_4} \cdots\cdots \frac{P_n}{P_T}\right]^2 \tag{35}$$

Therefore, the pressure ratio across an entire configuration of η layers is equal to the ratio of the pressure transmitted by the innermost layer to the pressure incident on the outermost layer.

Transmission is calculated from

$$TL = 10 \log\left|\frac{P_I}{P_T}\right|^2 \tag{36}$$

Laboratory verification tests are normally performed most conveniently in a free-field (anechoic) environment or a random incidence environment. The

equations presented earlier are suitable for free-field plane waves at specific angles of incidence. In order to simulate the effect of a random incidence or reverberant environment, the pressure ratio is integrated over a range of incidence angles and averaged (reference 13).

$$\bar{\tau} = \left[\frac{P_T}{P_I}\right]^2 = \frac{2\int_o^{\theta'} \tau(\theta) \sin 2\theta d\theta}{1 - \cos 2\theta'} \tag{37}$$

Where $\bar{\tau}$ is the reverberant field transmission coefficient obtained by averaging $\tau(\theta')$. The angle θ' is the limiting value of the incidence angle θ. A value of 1.48 rad (87.5 deg) was selected for θ' and the integration was approximated using Simpson's rule with a 5-degree step or increment. The denominator $(1 - \cos 2\theta')$ is approximately equal to 2.0 ($\theta' = 1.48$ rad (87.5 deg)) and the above expression for the averaged transmission coefficient is reduced to

$$\bar{\tau} = \int_o^{\theta'} \tau(\theta) \sin 2\theta \, d\theta \tag{38}$$

APPENDIX F

EXPERIMENTAL VERIFICATION OF ANALYSIS METHOD

F1. TEST FACILITIES

Experimental investigations performed at Lockheed with Independent Development funding have provided a limited but supportive data base which is summarized in this appendix. Flat panel sound transmission loss tests and unstiffened cylinder noise reduction tests were performed at the Lockheed-Rye Canyon Acoustics Laboratory. The panel tests were performed with the panel mounted between two reverberant chambers (figure 41). The larger chamber has a volume of 780 m^3 (26 560 ft^3) and the smaller chamber has a volume of approximatelv 227 m^3 (8000 ft^3). Sound pressure levels in the large (source) room were measured using three stationary microphones and sound levels in the receiver room were measured using a single orbiting microphone. An ILG reference sound source was used to determine the characteristics of the receiving room. The unstiffened cylinder noise reduction tests were performed in the large reverberant chamber and in an anechoic chamber. The anechoic chamber had a clear working volume of 5.5 by 5.5 by 4.3 m (18 by 18 by 14 ft) and a design low frequency cut-off of 60 Hz.

F1.1 Panel Transmission Loss Tests

A broadband random noise source was used for the panel sound transmission loss tests. The flat test panel was 2.44 by 2.44 m (8 by 8 ft) with four frames at 50.8 cm (20 in.) spacing and no stringers. A bare or untreated panel sound transmission loss test was performed first (figure 42) and this was followed by a series of tests with added acoustic treatments. Two treatment configurations did not include an inner panel or septum:

- A 7.6-cm (3-in.) wall depth with a 2.5-cm (1-in.) air-gap and a 5.1-cm (2-in.) thick, 19.2-kg/m^3 (1.2-pcf) blanket with mylar wrapping (figure 42).

- A 17.8-cm (7-in.) wall depth with a 7.6-cm (3-in.) air-gap and a 10.2-cm (4-in.) thick, 19.2-kg/m^3 (1.2-lb/ft^3 (pcf) blanket with mylar wrapping (figure 43).

Two treatment configurations included a septum inner wall of 2.4 kg/m^2 (0.5 pounds per square foot (psf)):

- A 7.6-cm (3-in.) wall depth with a 2.5-cm (1-in.) air-gap and a 5-cm (2-in.) thick, 38.4-kg/m^3 (2.4-pcf) blanket with mylar wrapping (figure 44).

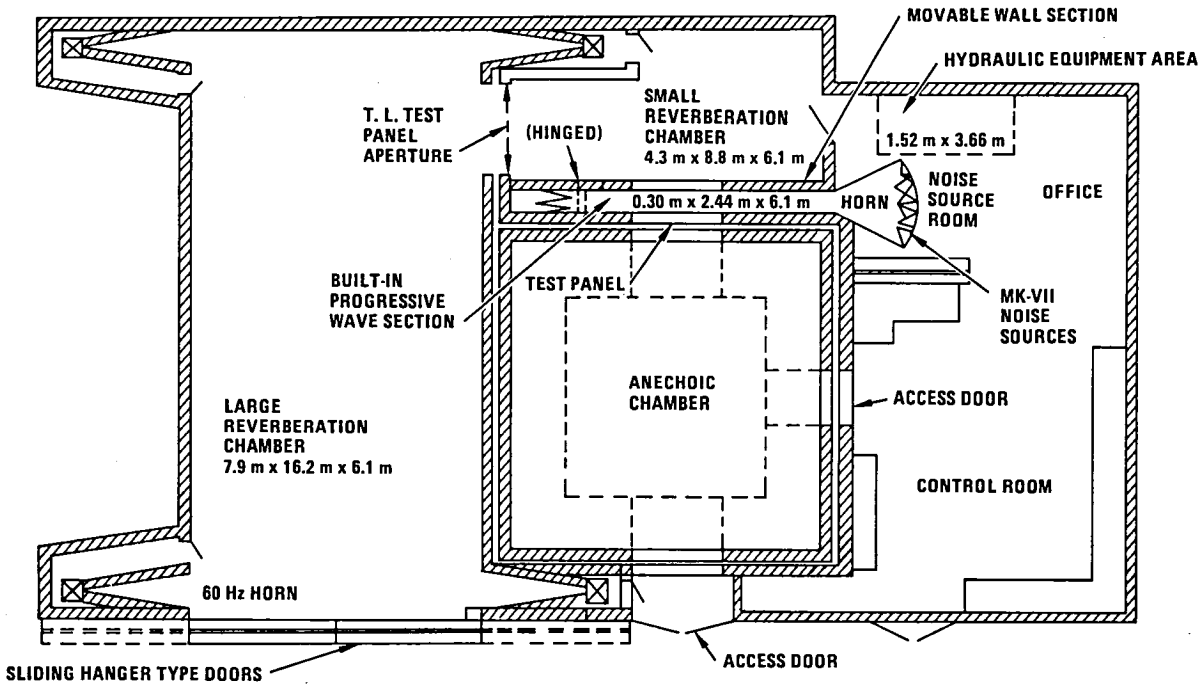

Figure 41. - Schematic of acoustics laboratory.

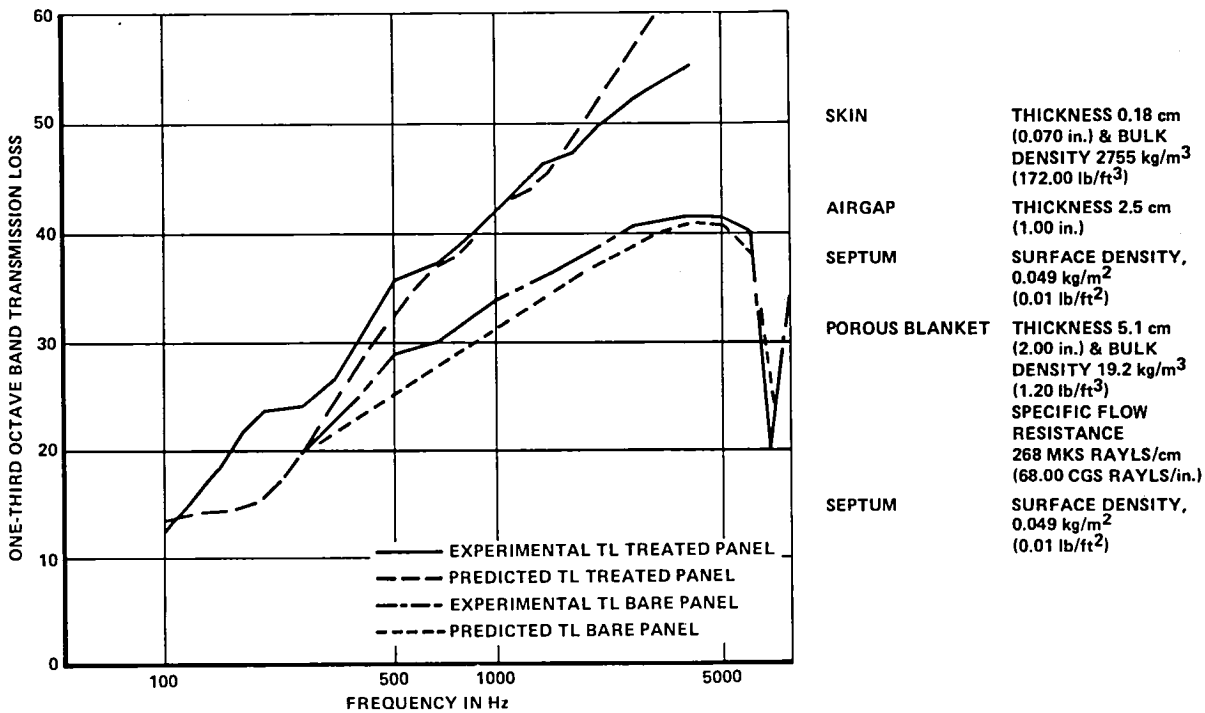

Figure 42. - Panel transmission loss; 7.5 cm (3 in.) wall spacing with a 19.2 kg/m^3 (1.2 pcf) blanket.

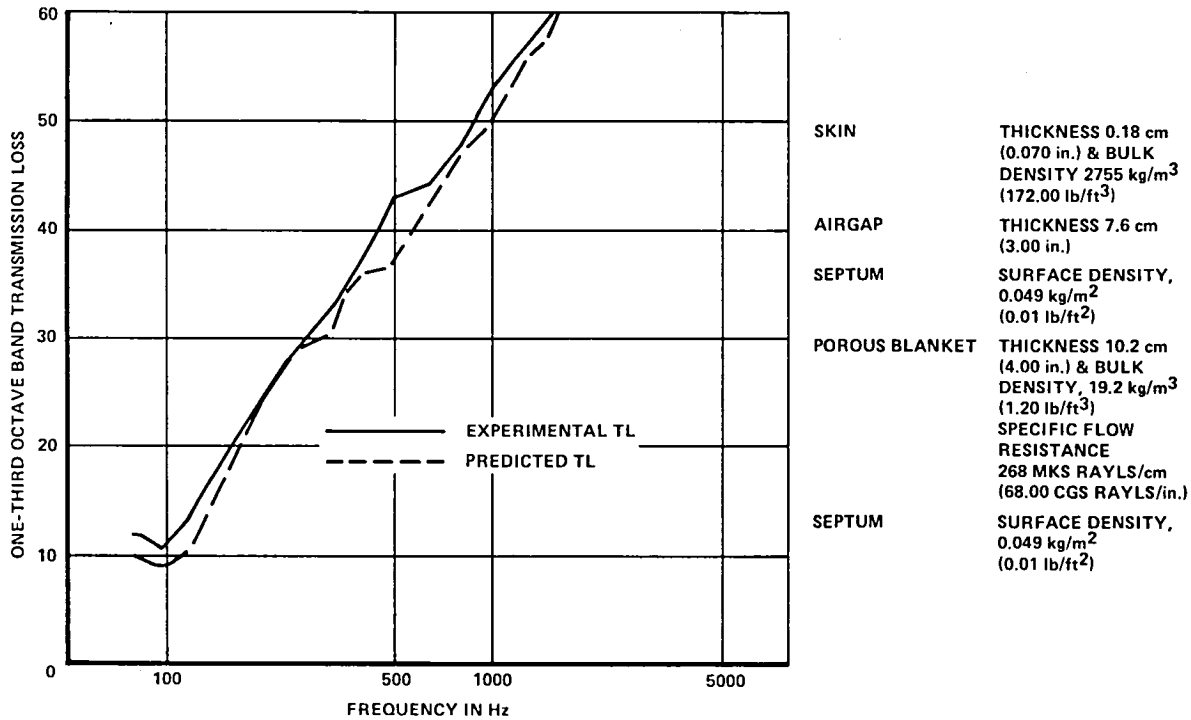

Figure 43. - Panel transmission loss 17.8 cm (7 in.) wall spacing with a 19.2 kg/m^3 (1.2 pcf) blanket.

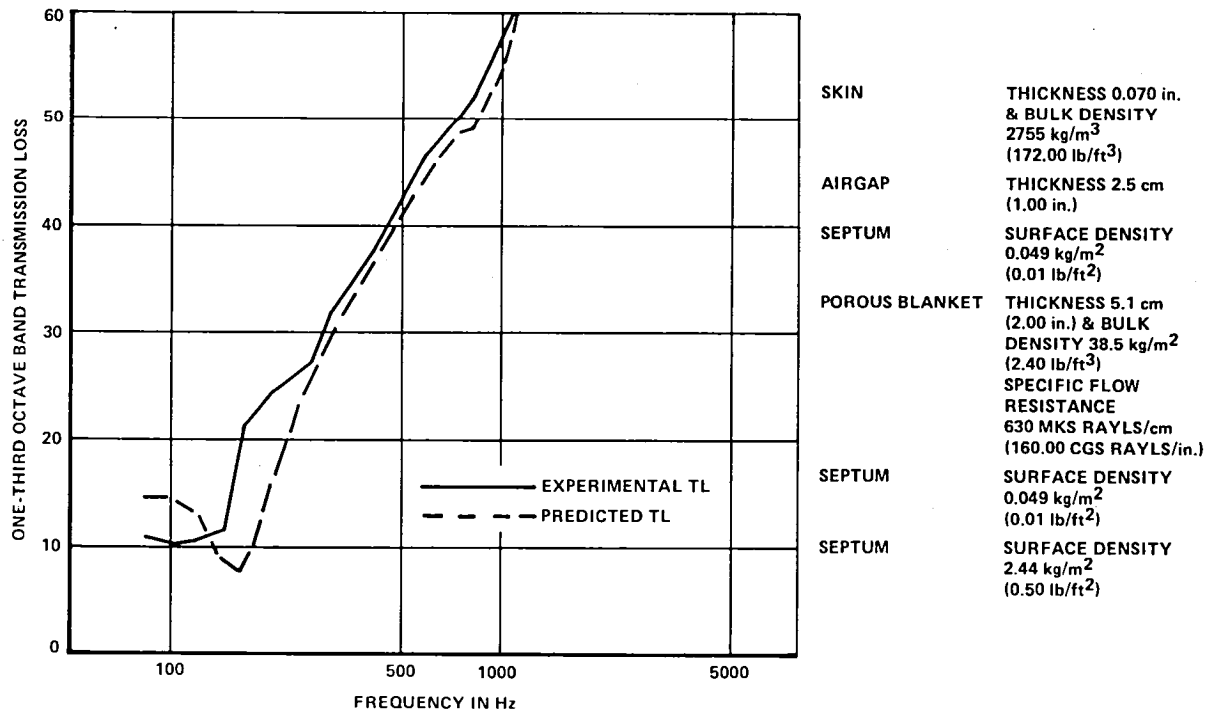

Figure 44. - Panel transmission loss; 7.5 cm (3 in.) wall spacing with a 38.4 kg/m^3 (2.4 pcf) blanket and 2.44 kg/m^2 (0.50 psf) septum.

- A 22.9-cm (9-in.) wall depth with a 7.6-cm (3-in.) air-gap and a 15.2-cm (6-in.) thick, 19.2-kg/m^2 (1.2-pcf) blanket with mylar wrapping (figure 45).

The Beranek/Cockburn and Jolly method that was used predicted the transmission loss of the unstiffened skin panel only and not the loss of the larger multibay stiffened panel. The good agreement between predicted and experimental transmission loss can be seen in figures 42 through 45.

F2. CYLINDER TESTS, UNSTIFFENED

Two series of tests were performed with cylinders: an unstiffened cylinder in an anechoic environment, and a stiffened cylinder in a reverberant environment. The first series of tests was performed in an anechoic chamber where a 50.8-cm (20-in.) diameter, unstiffened cylinder was subjected to one-third octave bands of random noise at specific angles of incidence. Both ends of the cylinder were treated with a 15.2-cm (6-in.) thickness of Scott Foam and lead vinyl, and a 15.2 cm (6-in.) thickness of Scott Foam ran axially the full length of the cylinder. This provided an average absorption coefficient of 64% above 300 Hz. Insertion loss or noise reduction of the cylinder was determined from the results of two separate tests.

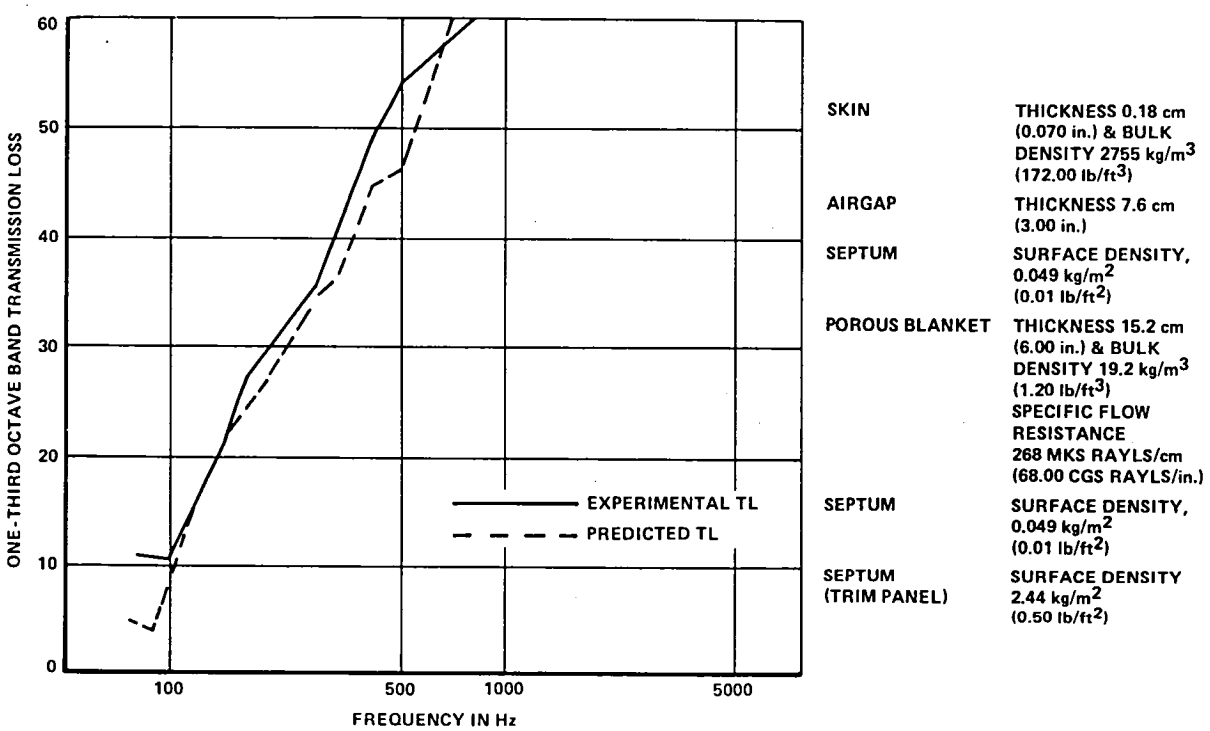

Figure 45. - Panel transmission loss; 22.9 cm (9 in.) wall spacing with a 19.2 kg/m^3 (1.2 pcf) blanket and 2.44 kg/m^2 (0.50 psf) septum.

A loudspeaker source of random noise was used for both tests, and a microphone located close to the source monitored the source levels to ensure that the source output was invariant between tests. A second microphone was located approximately 3.66 m (12 ft) from the source in a free field to measure the source level without the cylinder present. This same microphone was then installed at the center of the test cylinder at the same spatial location with reference to the source. The difference in sound levels measured with and without the cylinder present is the insertion loss or noise reduction associated with the cylinder. The loudspeaker remained stationary for all tests while the cylinder was rotated about an axis which passed through the internal microphone in order to vary angle of incidence (figure 46).

Noise reduction tests were performed at 0.26 rad (15 deg) increments from a graze angle of 0.26 rad (15 deg) to 1.57 rad (90 deg). The results of these free-field tests are shown in figures 47 through 52, along with predicted noise reductions using Koval's method of reference 4. The agreement between theory and experiment is excellent for 0.26, 0.52, 0.79 and 1.0 rad (15, 30, 45 and 60 deg) graze angles; not very good at 1.3 rad (75 deg) and fair at 1.57 rad (90 deg).

F3. STIFFENED CYLINDER TESTS - FLOOR EFFECT

In the second series of tests, a 1.22-m (48-in.) diameter stiffened cylinder was tested in a reverberant or random incidence environment (figure 46). Each end of the cylinder was treated with fiberglass and lead vinyl and an interior absorption coefficient of 16% was estimated for frequencies above 300 Hz. A simulated floor structure was added for one of the tests to determine its effect on noise reduction. Three microphones were installed inside the cylinder and three microphones were used to monitor the levels inside the reverberant test chamber. The experimental noise reductions were obtained from the arithmetic difference between the three exterior and three interior microphones. A comparison of the measured noise reductions for the cylinder with and without a floor structure is shown in figure 53. The effect of the floor is to increase the noise reduction above the ring frequency and to reduce it below the ring frequency. However, the addition did not substantially change the noise reduction characteristics of the cylinder. Noise reductions were then calculated for the stiffened cylinder in a random incidence environment using a Simpsons rule integration of the transmission coefficient. The transmission coefficient was calculated at 0.087 rad (5 deg) increments from 0.044 rad (2.5 deg) to 3.10 rad (177.5 deg) using Koval's theory. Experimental and calculated noise reductions for the stiffened cylinder are compared in figure 54. The compariosn is poor except at the ring frequency; however, the shape of the noise reduction curves are similar. A second analysis of the cylinder noise reduction was performed and the frames were ignored and the cylinder was considered unstiffened. The stiffened cylinder did not have stringers but did have 2.5-cm (1-in.) deep frames spaced 50.8 cm (20 in.) apart. The unstiffened analysis is compared to the stiffened cylinder experimental data in figure 55 and agreement between theory and experiment has improved. Also the experimentally determined noise

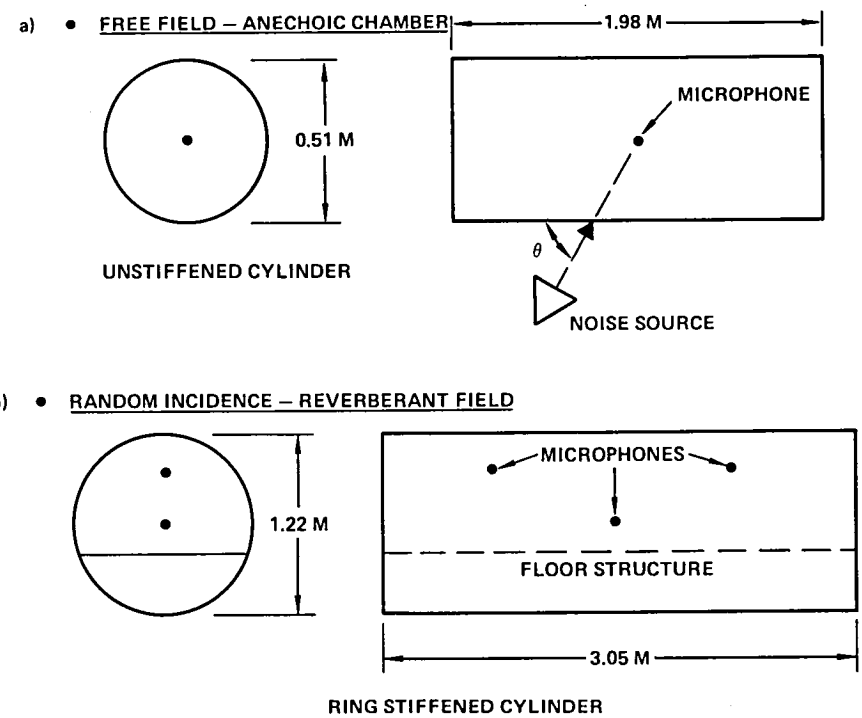

Figure 46. - Cylinder noise-reduction test layouts.

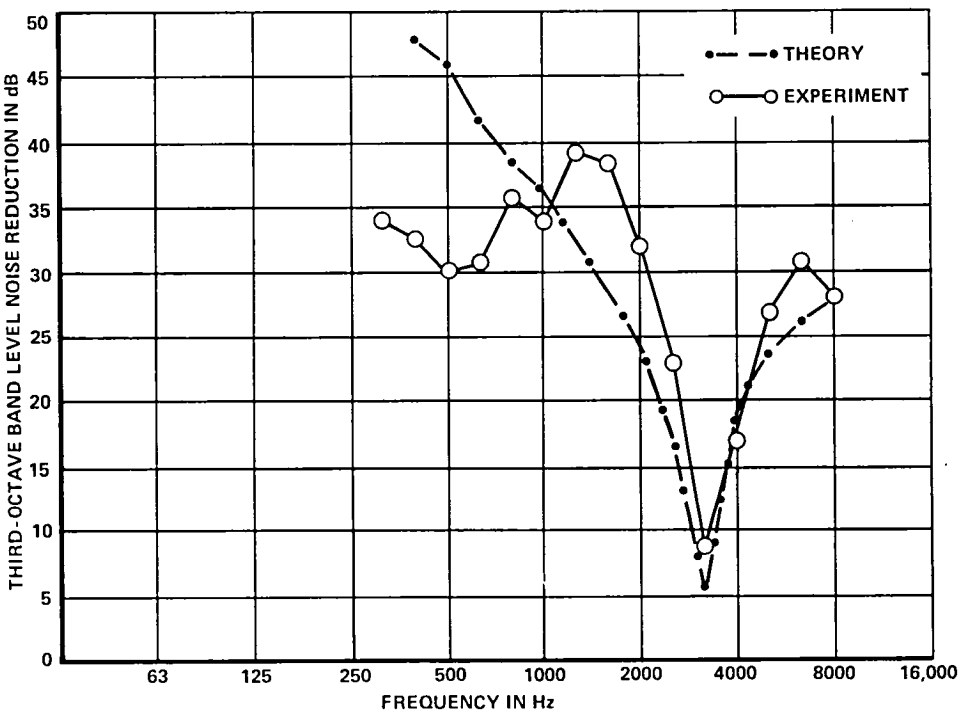

Figure 47. - Noise-reduction test; 50.8 cm (20 in.) cylinder at 0.26 rad (15 deg) graze angle.

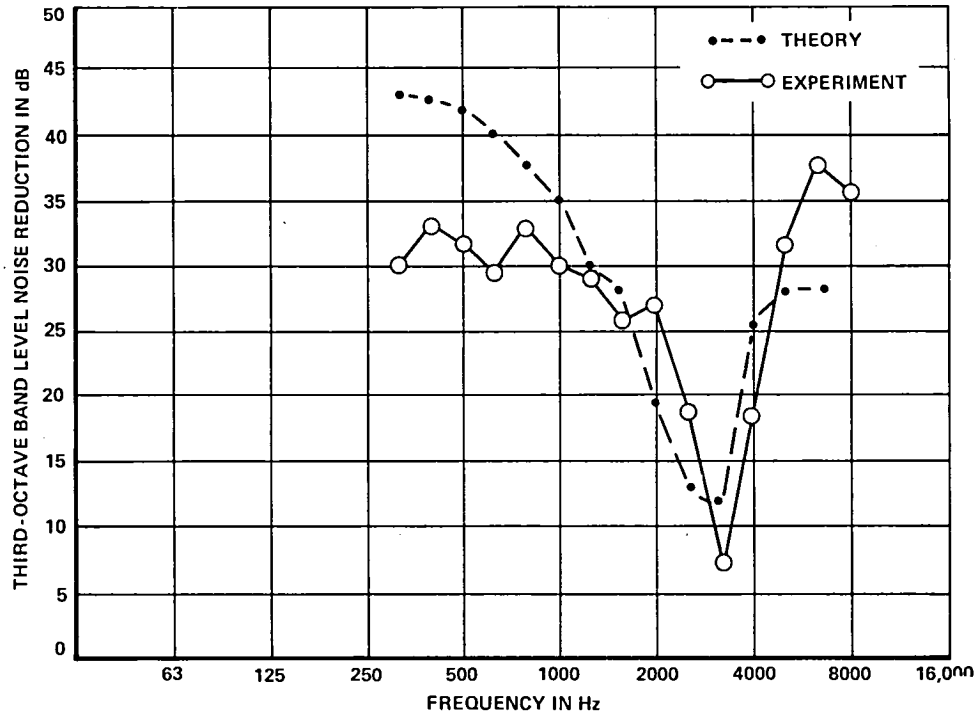

Figure 48. - Noise-reduction test; 50.8 cm (20 in.) cylinder at 0.52 rad (30 deg) graze angle.

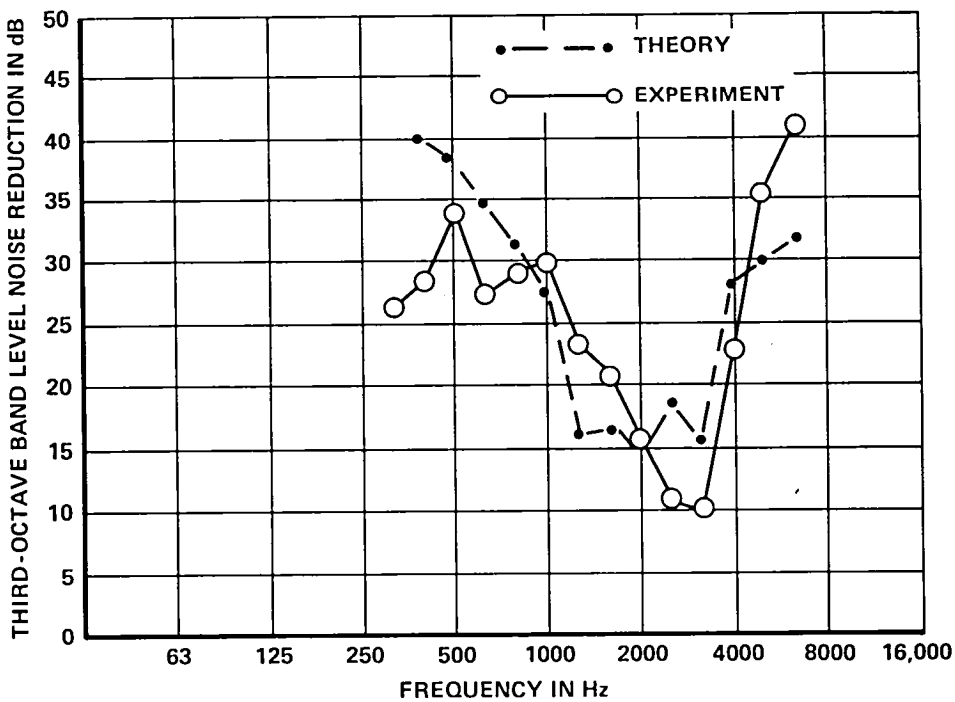

Figure 49. - Noise-reduction test; 50.8 cm (20 in.) cylinder at 0.79 rad (45 deg) graze angle.

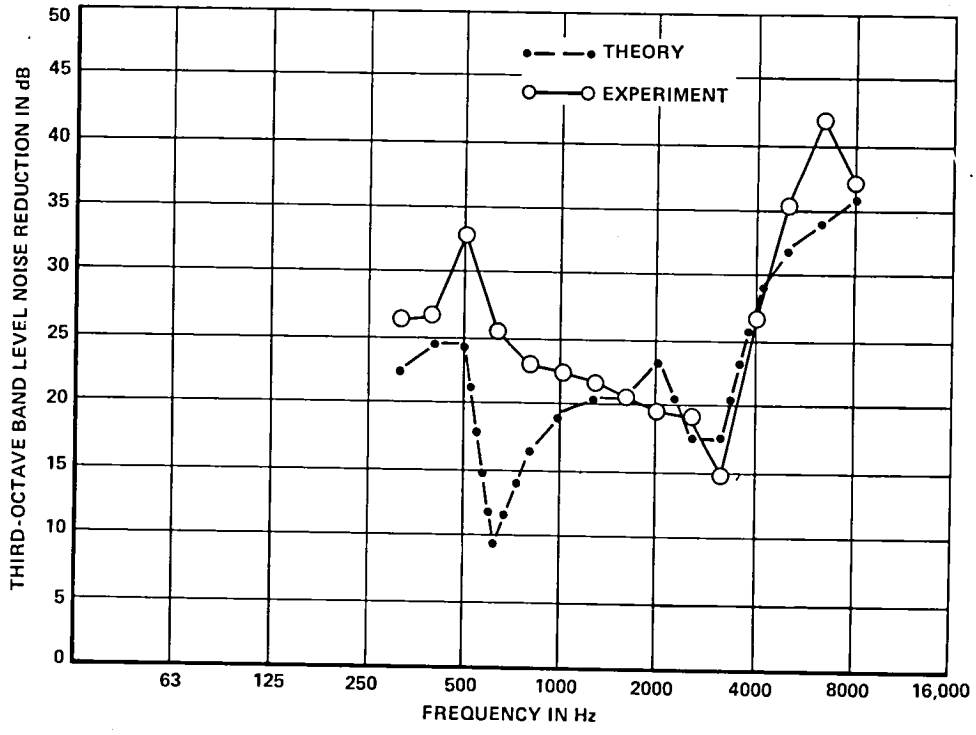

Figure 50. - Noise-reduction test; 50.8 cm (20 in.) cylinder at 1.05 rad (60 deg) graze angle.

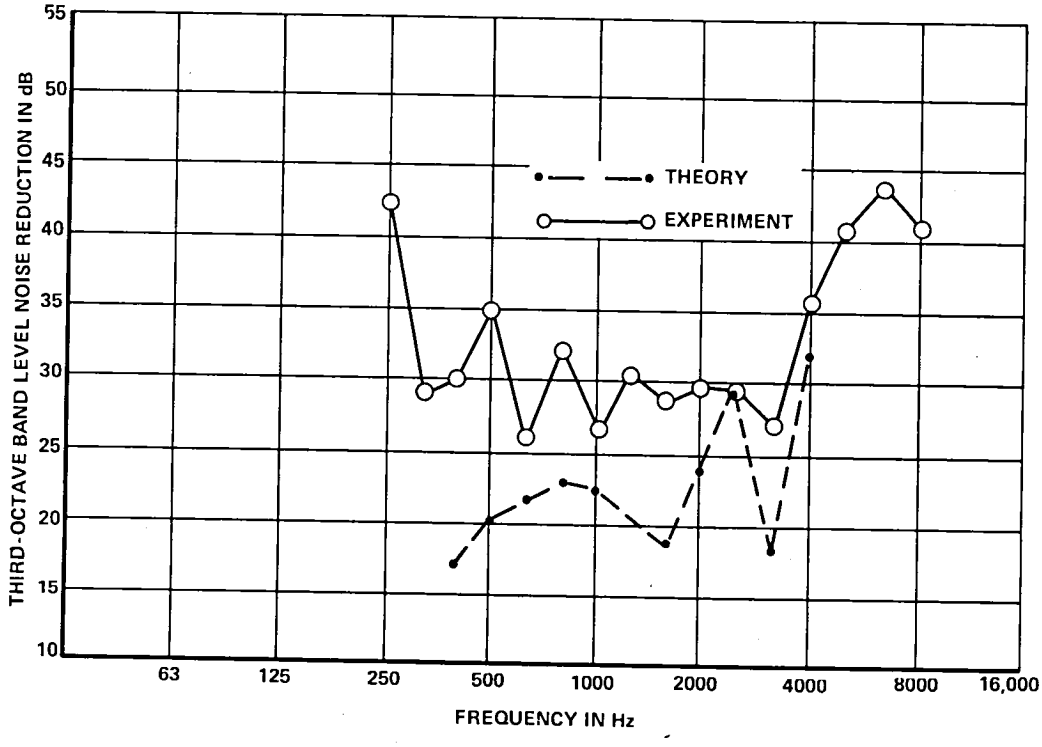

Figure 51. - Noise-reduction test; 50.8 cm (20 in.) cylinder 1.31 rad (75 deg) at 75 deg graze angle

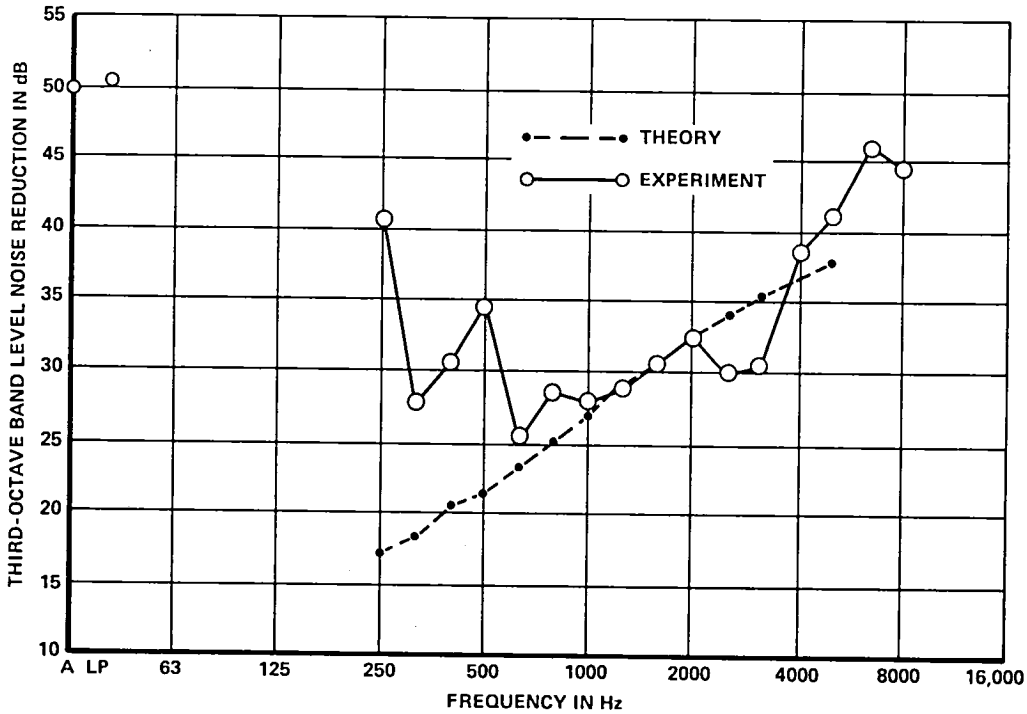

Figure 52. - Noise-reduction test; 50.8 cm (20 in.) cylinder at 1.57 rad (90 deg) graze angle.

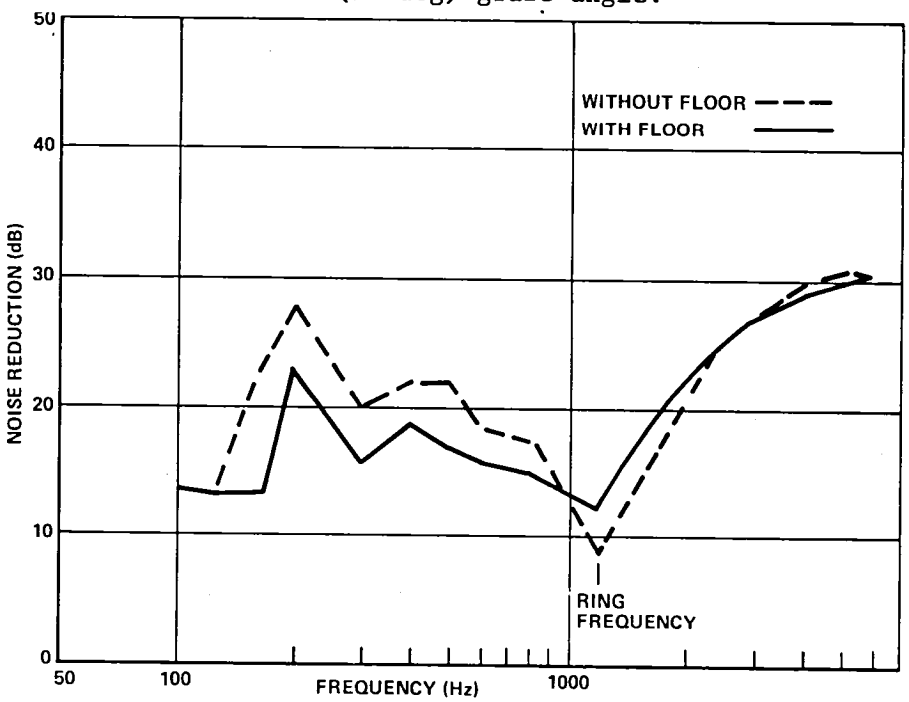

Figure 53. - Measured reverberant field noise-reduction; 1.22 m (4 ft) diameter cylinder; 0.137 cm (0.050 in.) skin, ring stiffened at 45.7 cm (18.0 in.) no stringers.

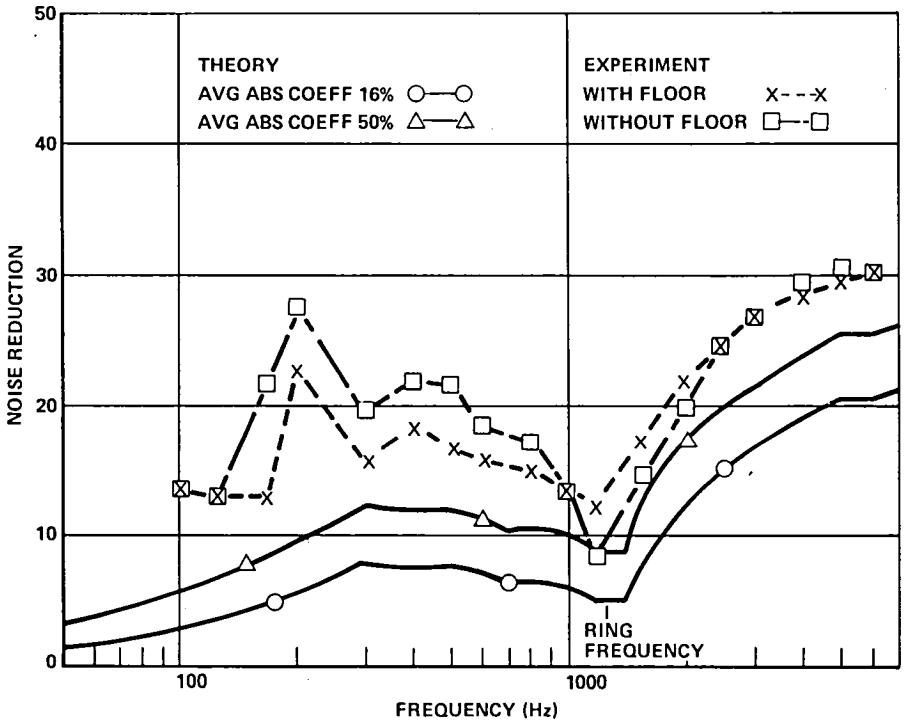

Figure 54. - Theoretical vs experimental treated cylinder noise reduction; 1.22 m (4 ft) diameter cylinder (stiffened) reverberant environment ring spacing 45.7 cm (18.0 in.) no stringer 0.13 cm (0.050 in.) skin thickness.

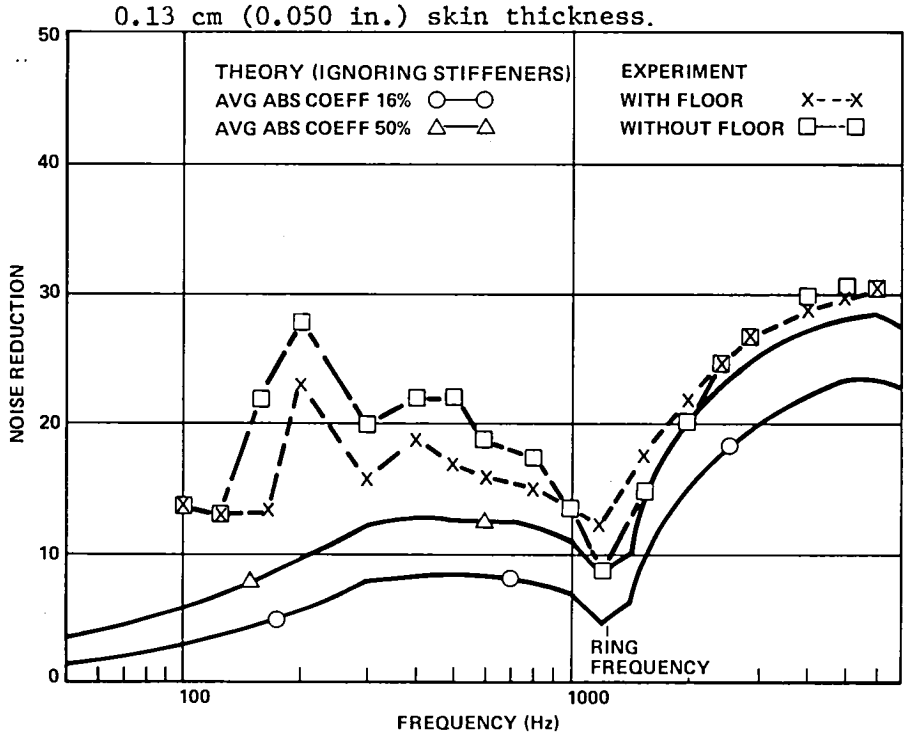

Figure 55. - Theoretical vs experimental treated cylinder noise reduction; 1.22 m (4 ft) diameter cylinder (ignoring stiffeners) reverberant environment.

reductions are several dB higher than the calculated noise reductions when the 16% absorption case is used for comparison. If the 50% absorption case is used for comparison, then the agreement with theory is very good above the ring frequency.

F4. CONCLUSIONS CONCERNING COMPARISONS OF THEORY AGAINST SMALL TEST SPECIMEN DATA

- The data presented in this section demonstrates reasonable agreement between theory employed in this study and test data for small specimens having typical cylindrical shell structural characteristics
- The data substantiates the method for add-on noise control elements for flat-panel configurations, including some which demonstrate very large noise reductions.
- The data for cylinders with and without floors shows that the measured noise reductions are not drastically affected by the presence of the floor.

APPENDIX G
RESULTS OF ADD-ON NOISE REDUCTION PARAMETRIC STUDIES

G1. OUTLINE OF SCOPE OF STUDY

During the course of the study many more calculations were performed in the quest for better noise reductions than are indicated by tables 13 and 14. Only the key results leading to the selected noise-reduction designs are presented here. Secondary effects will be discussed briefly in a later section of this appendix. Table 13 describes parameters investigated under the category of "add-on" noise reduction design. Table 14 summarizes the parameters investigated under the heading of advanced noise-reduction designs.

G2. 4-ENGINE, WIDE-BODY AIRCRAFT RESULTS

G2.1 Baseline Structure and Sidewall Characteristics

The baseline structural properties are shown in Appendix B. The analysis assumes the structure to be of a uniform, axisymmetric semimonocoque construction, with a uniform skin gauge of 0.173 cm (0.068 in.), ring-frame spacing of 50.8 cm (20 in.), stringer spacing of 21.6 cm (8.5 in.) and a fuselage outer shell diameter of 6.12 m (241 in.). The effects of windows are neglected for simplicity. The ring frequency is estimated at 270 Hz based on an elastic wave speed of 5182 m/s (17000 ft/s) for aluminum.

The baseline sidewall construction of the wide-body aircraft is shown in figure 22, Appendix B. The sidewall construction contains a fiberglass blanket for both thermal and acoustical insulation purposes, with an air gap adjacent to the outer skin for the circulation of cooling air. A wall-space depth of 15.2 cm (6 in.) between the outer skin and the interior trim panel was selected, anticipating the benefits of relatively large spacing on the basis of results of the double-wall mass law studies of reference 1; however, some effects of wall spacing are shown in this appendix. The B-type of fiberglass blanket was selected, having a fiber diameter of 3.81×10^{-6} m (150μ in.) and a bulk density of 9.6 kg/m^3 (0.6 lb/ft^3). This selection was based on a number of preliminary studies. Likewise, equal thicknesses of 7.6 cm for the fiberglass blanket and the air gap provide the best noise reduction and were selected based on these preliminary studies. Blanket parameter results are to be discussed elsewhere, since variations of blanket design properties within reason had no large effect on noise reduction.

G2.2 Baseline Aluminum Structural Transmission Loss and Noise Reduction

Figure 56 shows the calculated transmission loss spectrum for the baseline outer wall wide-body structure. Results are shown for several angles of incidence, varying from 0.52 rad (30 deg) to 2.09 rad (120 deg). These

TABLE 13. - MATRIX OF ADD-ON REDUCTION CONFIGURATIONS

NOTES: (A) REPEAT 3 TIMES FOR DIFFERENT EXTERIOR NOISE HARMONICS
(B) OASPL OF EXTERIOR NOISE EQUAL FOR EACH HARMONIC DISTRIBUTION
(C) A SINGLE DESIGN BLADE PASSAGE FREQUENCY FOR EACH AIRCRAFT SIZE

EFFECT STUDIED	NOISE EVALUATIONS TOTAL NO.	FUS. DIAMETER	WALL DEPTH	OUTER WALL STIFFNESS	OUTER WALL DAMPING MASS	INNER WALL MASS	BLANKETS TYPE	BLANKETS DENSITY	BLANKETS THICKNESS	SEPTA NO.	SEPTA MASS
DOUBLEWALL	36	3	2	1	1	2	OPT	OPT	OPT	0	0
DW + SEPTA	36	3	2	1	1	1				1	2
DAMPING	27	3	1	1	3	1				OPT	OPT
STIFFNESS	27	3	1	3	1	1					
	126										

TABLE 14. - MATRIX OF ADVANCED NOISE-CONTROL CONFIGURATIONS

NOTES: (A) REPEAT 3 TIMES FOR DIFFERENT EXTERIOR NOISE HARMONICS
(B) EQUAL EXTERNAL OASPL FOR EACH HARMONIC DISTRIBUTION
(C) A SINGLE VALUE OF DESIGN BLADE PASSAGE FREQUENCY FOR EACH AIRCRAFT SIZE

EFFECT STUDIED	NOISE EVALUATIONS TOTAL NO.	FUS. DIAMETER	WALL DEPTH	OUTER WALL STIFFNESS	OUTER WALL DAMPING MASS	INNER WALL MASS	BLANKETS TYPE	BLANKETS DENSITY	BLANKETS THICKNESS	SEPTA NO.	SEPTA MASS
A. CONVENTIONAL MATERIALS/HIGH STIFFNESS											
STIFFNESS	18	3	1	2	1	1	OPT	OPT	OPT	OPT	OPT
DAMPING	18	3	1	MAX	2	1					
DOUBLEWALL	18	3	1	MAX	1	2					
B. ADVANCED COMPOSITE MATERIALS/ORTHOGRID											
STIFFNESS	18	3	1	2	1	1					
DAMPING	18	3	1	MAX	2	1					
DOUBLEWALL	18	3	1	MAX	1	2					
	108										

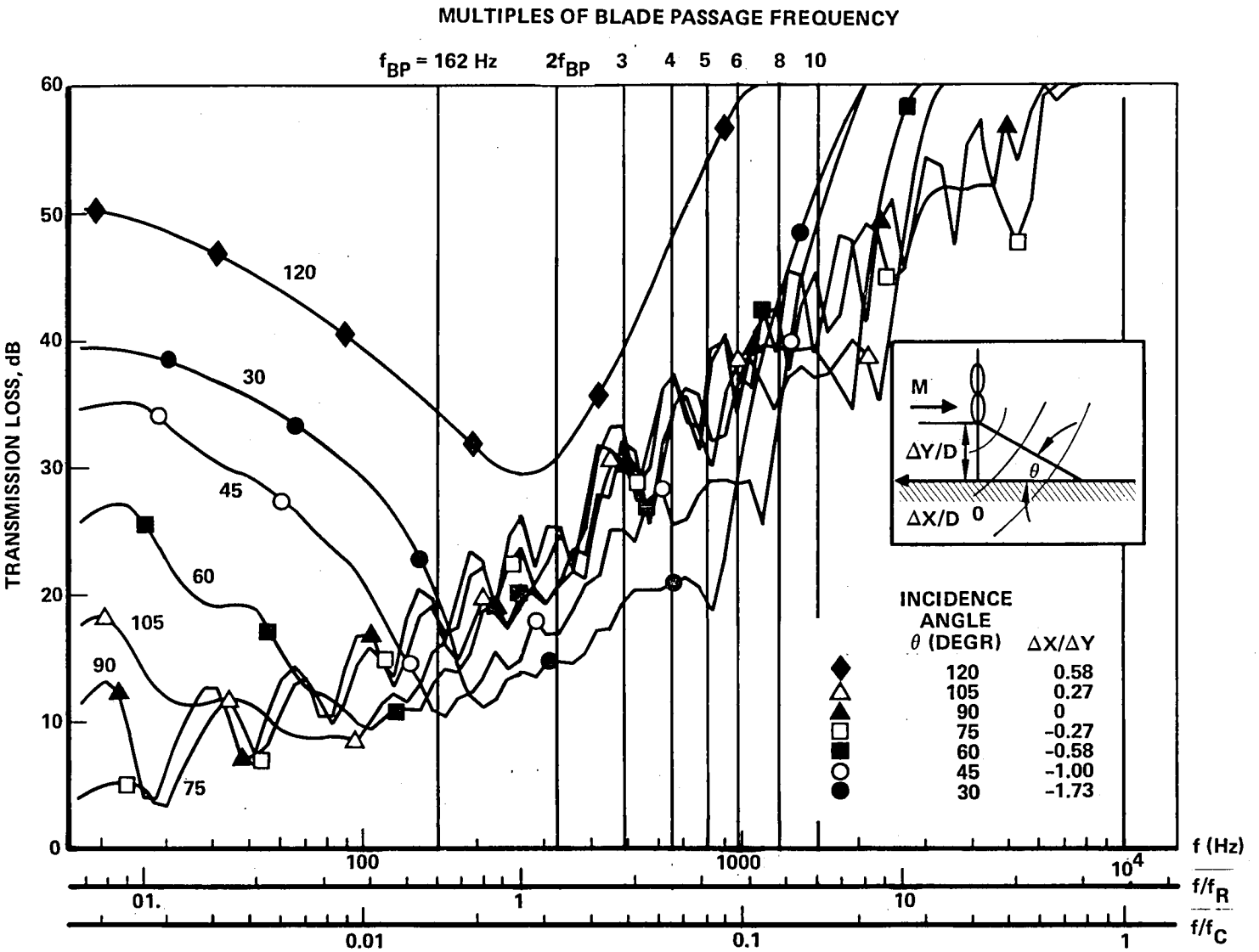

Figure 56. - Baseline fuselage outer wall transmission loss spectra; wide-body aluminum aircraft at M = 0.8, 9144 m (30 000 ft) altitude.

calculations include effects of forward velocity and internal pressure at a flight Mach number of 0.8 and at an altitude of 9144 m (30 000 ft). The cabin is pressurized to an altitude of 2438 m (8000 ft), providing a differential pressure of 45, 197 Pa (6.54 psi) across the cabin wall. A damping loss factor of 6 percent is assumed.

In figure 56 the blade passage frequency of the propfan is noted at 162 Hz along with the next nine harmonics. Notice that the blade passage and second harmonic at $f = 2f_{BP}$ are both near the ring frequency where low values of transmission loss of between 10 and 25 dB are displayed for angles close to normal incidence. Table 7 shows that the peak noise region defined by Segment 4 is exposed to noise from the inboard engine over a range of impingement angles between 0.77 rad (44 deg) at the aft end, and 1.94 rad (111 deg) at the forward end. Since most of the propeller noise is concentrated at the propeller blade passage frequency and its lower harmonics, the low TL calculated for Segment 4 in this frequency region will result in high interior noise levels.

Figure 57 shows calculated interior noise for Segment 4 as a function of fuselage wall surface density for both aluminum and composite wide-body aircraft. All of the configurations retained the baseline stiffness while parametric studies were performed. For each configuration studied a selective outer-wall surface density and loss factor were held constant while the trim panel mass was varied. The baseline surface densities shown for the aluminum aircraft correspond to the data given in table 2. The baseline turbofan sidewall is predicted to yield an interior noise level of 108 dBA if exposed to the propfan exterior noise environment of Spectrum 1 under the assumptions postulated in this study. Figure 13 describes the external noise signature of Spectrum 1 which has an OASPL of 132 dB and an A-weighted level of 123 dBA. It can be seen that the baseline turbofan sidewall construction has provided a noise reduction of about 17 dBA which seems reasonable in comparison to the transmission loss spectra described in Figure 56.

G2.3 Baseline Composite Fuselage Noise Reduction

Figure 57 also shows the noise-reduction performance of a strength-designed, all-composite material outer wall. The baseline surface densities shown correspond to the data given in table 3. The outer-wall structure is approximately 30% lighter than the baseline aluminum structure, and the baseline levels of all outer-wall stiffness properties (the EI and GJ products, etc.) of the skin and all stiffeners are the same as for the aluminum structure. These values are very close approximations to the fuselage designs which resulted when designers were asked to design a composite fuselage design without any special acoustical requirements. The composite fuselage design is summarized in Appendixes B and I.

It is noted that the total surface density required to achieve 80 dBA is about the same for either the aluminum or the composite structure. Therefore, the strength-designed composite structure has an extra penalty for noise

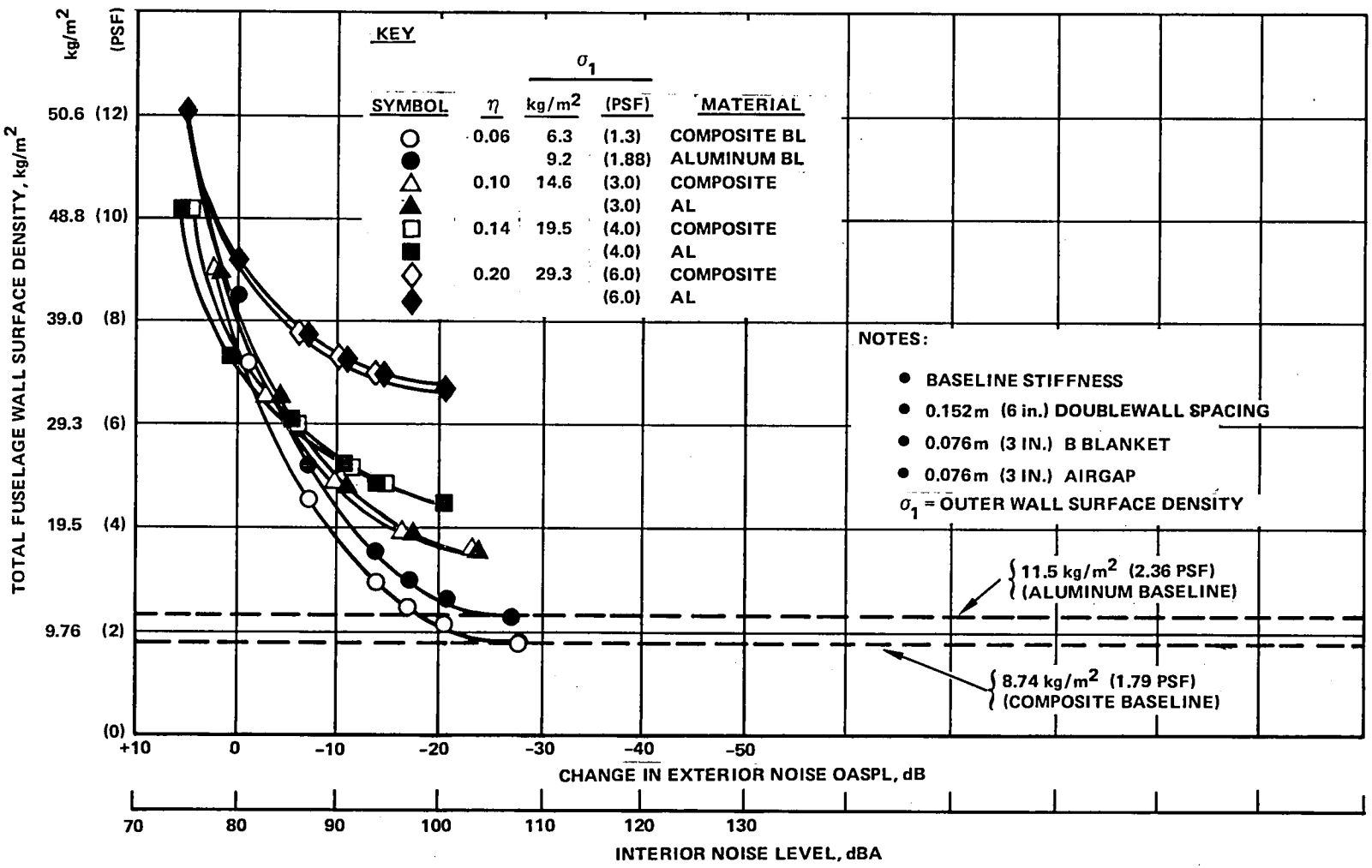

Figure 57. - 4-engine wide-body add-on double-wall study; aluminum and composite structures; segment 4, spectrum 1.

reduction, equal approximately to the difference in baseline structural surface densities. In the data in figure 57, that difference is 30 percent of 9.17 kg/m^2 (1.88 psf) which equals 2.75 kg/m^2 (0.56 psf).

The results suggest that if a composite structure is assumed to have the same outer wall stiffness and damping loss factor as the baseline, then it will require roughly the same total wall surface density and therefore a somewhat greater penalty mass to achieve high noise reductions. Although it is possible that the composite structure might provide inherently higher damping loss factors, the results of figure 57 show that reasonably achievable increases of damping loss factor provided only modest reductions of interior noise.

G2.4 Results for Add-On Noise-Reduction Design

G2.4.1 The behavior of the outer wall with damping treatment.- The next discussion has implications for both aluminum and composite wide-body add-on studies. The outer-wall stiffness is, by definition, unchanged by the outer-wall mass additions. However, the damping loss factor of the outer wall can be increased as a function of the added mass of an appropriately selected viscoelastic damping treatment, according to the schedule shown in Figure 58.

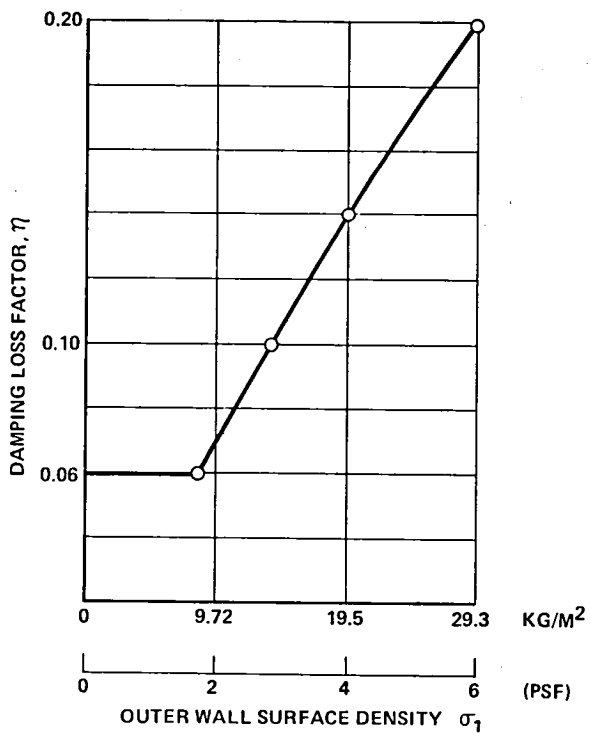

Figure 58. - Damping loss factor vs outer-wall surface density, σ_1

This curve is a conservative envelope of unpublished Lockheed results calculated for various constrained layer damping treatments based on data and procedures described in references 17 and 18 and single unconstrained layer results from reference 17.

The analysis of reference 18 refers to simply supported panels; therefore, to apply the theory to the present case of propeller noise, it is assumed that the equivalent panel bay dimension is equal to one-half of the magnitude of the wavelength in the external acoustic field, as defined by using Koval's theory (see reference 7 or Appendix A). This procedure defines equivalent panel bay dimensions which are much larger than typical aircraft panel bay dimensions. Accordingly, the calculation procedures of reference 17 and 18 yield low damping loss values for the long wavelength shell vibration modes which dominate the low-frequency regime associated with propeller noise transmission. The loss factor data presented in figure 58 are consistent with this result.

G2.4.2 The role of the trim panel.- The surface density of the trim panel is varied to achieve the desired interior noise level for a given outer-wall configuration. Therefore, trim panel surface density, σ_2, is the closing variable in the studies such as figure 57, in which results are expressed as a function of the total surface density of the sidewall.

The trim panel is further assumed to have the following characteristics:

- It maintains its original stiffness, independent of increases of surface density
- The damping loss factor is maintained at 6% independent of surface density
- The trim panel has suitable vibration isolation from the outer-wall structure so that effective double wall behavior is achieved.

G2.4.3 Limp double-wall concept as mathematically modelled. - Appendix E describes the mathematical modelling of both the skin panels and the trim panels. The analysis accounts for stiffness, damping, pressurization and mass in defining the panel impedance. The panel is modelled as a single-degree-of-freedom plate including all the above effects. The impedance expression in Appendix E allows for the coincidence of skin flexural waves with the external acoustic field, including the effects of flow-field convection. The analysis neglects higher order panel bay vibration response since the important propeller excitation harmonics usually occur at frequencies well below the fundamental resonant frequency of the panel. It is therefore unlikely that higher order panel vibration responses will have a significant impact on the results of the present study. Furthermore, the means for increasing trim panel mass without significant stiffening would probably be accomplished by use of "lossy" material such as lead-vinyl. For these reasons, it is believed that

the mathematical model used in this study for panel bay response is quite reasonable.

It is to be noted that neither the skin panel nor the trim panel is entirely limp, because the baseline stiffness is always retained. Since the outer-wall and trim-panel surface density values are considerably increased in the large noise reduction designs, the walls become relatively more limp than the baseline design.

As noted from the discussion in Appendix A, the baseline transmission loss of an untreated cylinder is taken as the lower envelope of either the bare panel response (as described in Appendix E) or the Koval theory smeared-stiffness cylindrical shell response (figure 18). The most common result is that the fundamental panel resonances are important only for add-on designs with very large surface densities. At all other frequencies below the ring frequency, the basic shell transmission loss, as described by Koval's method (reference 7 and Appendix A), generally is lower than that of the individual panel bays.

G2.4.4 Add-on noise reductions for aluminum and composite structures.- The noise-reduction performance of the double wall is shown in figure 57 and summarized in Section 3. To achieve noise reductions which exceed the baseline by less than 25 dBA, it appears desirable to maintain the baseline outer wall surface density and put all of the extra mass into the trim panel. This is illustrated in figure 57, where the baseline outer walls (circular symbols) provide the lowest interior noise levels below a total wall surface density of 32 kg/m^2 (6.5 psf). To achieve noise reductions more than 25 dBA beyond the baseline, the optimum outer wall surface density should be about 19.5 kg/m^2 (4 psf) for both the aluminum and the composite designs (square symbols in figure 57).

The top curve of figure 57 shows a design where the outer-wall surface density has been increased to 29.3 kg/m^2 (6 psf), which is clearly nonoptimum. The least total surface density is obtained when the outer-wall mass is roughly equal to the trim panel in accordance with classical double-wall theory.

In summary, figure 57 displays the characteristic features of a limp double-wall design, though modified by structural dynamics effects as described in the present prediction method. Curves such as figure 57 are shown elsewhere in this Appendix for treatment Segments 3, 5, 6, and 7 away from the propeller disc plane. Figure 57 can be used for variable exterior noise levels by using the scale labelled Change in Exterior Noise OASPL. If Segment 4 were exposed to 10 dB less than the peak design level of 132 dBA, then the -10 ordinate would represent the 80 dBA interior design level. The majority of the penalty mass is contained in Segment 4, therefore, results for Segment 4 are representative of design parameters effects. Data for other segments are used to calculate total aircraft treatment mass penalties.

G2.4.5 The effects of other acoustical treatment design parameters.- The other parameters in the study matrix described in table 14 were investigated and found to have less effect on interior noise than the double-wall optimization study shown in figure 57. Discussion of these other studies will be deferred until the add-on noise-reduction results have been presented for the narrow-body and business aircraft double-wall optimization studies.

There are two reasons for this sequence of results:

- The format of the double-wall, add-on noise-reduction data is similar to figure 57 for all of the aircraft.
- The other parameters investigated (stiffness, outer-wall mass, outer-wall damping, loss factor, stiffener spacing, etc.) were incapable of achieving, by themselves, the requisite large noise reductions without the simultaneous optimal selection of trim panel mass.

G3. 2-ENGINE, NARROW-BODY AIRCRAFT RESULTS

G3.1 Baseline Structure and Interior Noise Level Predictions

The 2-engine narrow-body aircraft has the baseline structural properties defined in Appendix B. The double-wall sidewall construction is similar to that shown in figure 22 except for the stiffener spacing. The exterior noise signature and axial distribution or grazing incidence angle are given in figures 7 and 9, and table 7 of Appendix A. Figure 7 shows that the peak external noise level of 134 dB OASPL for the 2-engine narrow-body, having the standard propeller tip clearance of $\Delta y/D = 0.8$ per reference 5, is 2 dB higher than for the 4-engine, wide-body aircraft with a larger minimum clearance of $\Delta y/D = 1.2$.

The baseline structure of the 2-engine, narrow-body aircraft has 48.3-cm (19-in.) frame spacing, 152-cm (6-in.) stringer spacing and a nominal skin thickness of 0.114 cm (0.045 in.). The wall depth is selected at 15.2 cm (6 in.) with a 7.6-cm (3-in.) B-type fiberglass blanket and air gap adjacent to the skin similar to that shown in figure 22 for the wide-body. The choice of a 15.2-cm (6-in.) wall depth may appear excessive for a narrow-body fuselage in terms of interior space; however, as will be shown in a later section, a significant increase of acoustical treatment penalty mass would be required if the wall space was to be reduced to 7.6 cm (3 in.). The trim panel and blanket properties are the same as given in table 6.

Figure 59 shows the basic untreated transmission loss spectra for various grazing incidence angles, for the baseline narrow-body turbofan-type aluminum aircraft structure under in-flight conditions at an altitude of 9144 m (30 000 ft) and at 0.8 Mach number. These results are governed primarily by the outer wall since the baseline trim panel is too light to provide double-wall benefits for noise reduction.

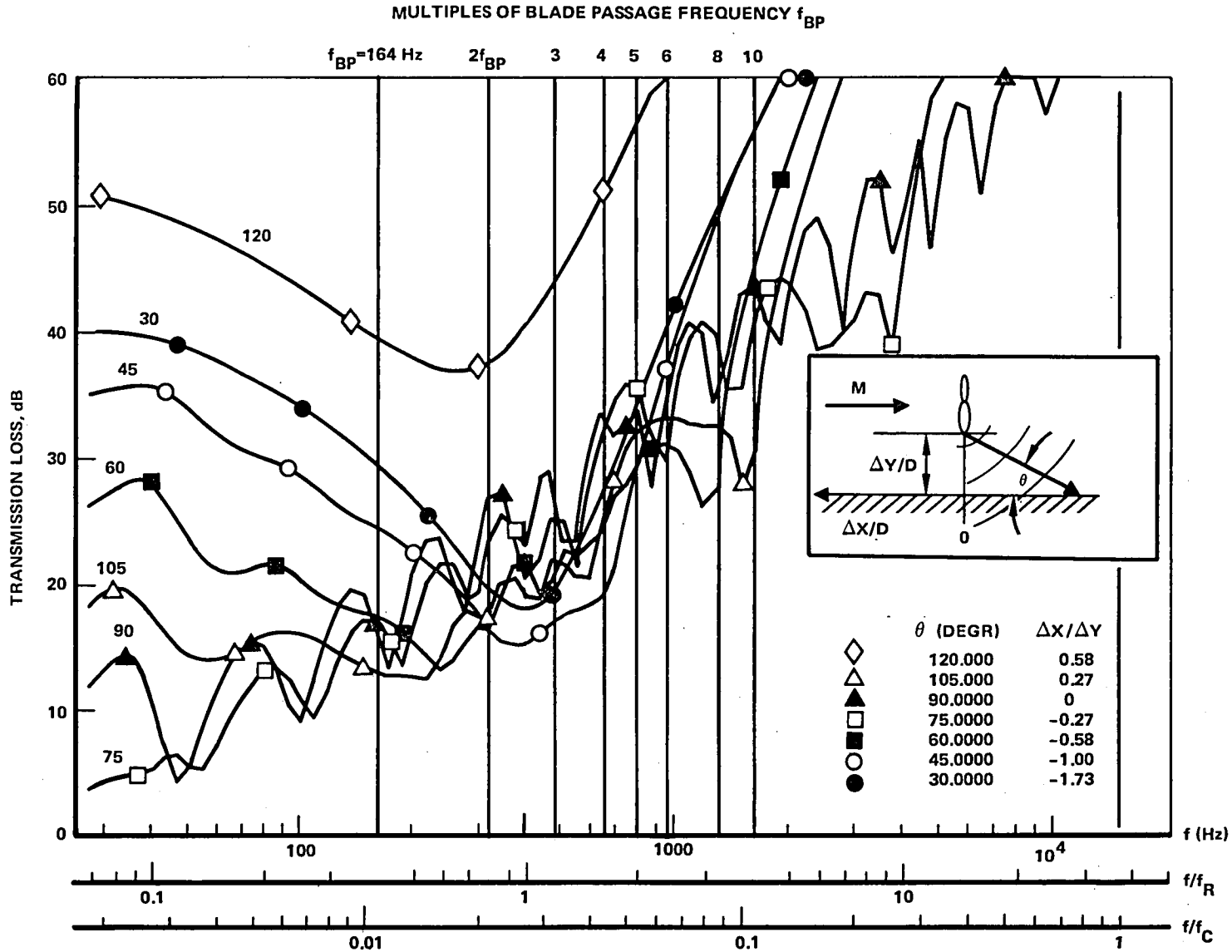

Figure 59. - Baseline fuselage outer-wall transmission-loss spectra, narrow-body aluminum aircraft at M = 0.8, 9144 m (30 000 ft) altitude

From figure 59 it is seen that the transmission loss spectra for the narrow-body fuselage are nearly the same as for the wide-body fuselage, despite the difference in diameter. Since the blade passage frequencies happen to be nearly the same for the wide-body and narrow-body aircraft, then one would expect similar interior noise levels near the peak external noise region defined by Segment 4.

G3.2 Baseline Noise Levels For Aluminum and Composite Structures

Figure 60 shows the double-wall, add-on noise-reduction study results for the 2-engine, narrow-body aircraft. Results are shown for the aluminum structure vs. an all composite material, strength-designed fuselage which is 70% as heavy as the aluminum structure and has equal outer-wall stiffness. At the baseline trim panel mass conditions of 1.61 kg/m^2 (0.33 psf) the aluminum structure yields a peak noise level of 108 dBA, for the baseline outer-wall mass. This result is nearly identical with the baseline wide-body result. The untreated noise levels are about 110 dBA for the lighter baseline composite structures, both for the wide-body and for the narrow-body, as shown in figures 57 and 60.

It is apparent that the strength-designed narrow-body composite structure offers no inherent noise reduction benefits when the outer-wall stiffness and damping loss values are unchanged from the aluminum structure values as is assumed in the present study.

G3.3 Narrow-body, Add-On Noise Reductions for Aluminum and Composite Structures

Figure 60 also summarizes the effects of parametrically varying outer-wall mass and trim panel mass. All of the discussion about the assumptions and mathematical modeling given for the wide-body aircraft also pertains to the results in figure 60. The results show that:

- The optimum configuration for an interior noise design level of 80 dBA (requiring the least penalty mass in the peak noise region of Segment 4) has an outer-wall surface density of 19.5 kg/m^2 (4 psf). The required total surface density of the wall is about 32.2 kg/m^2 (6.75 psf) which includes a B-type fiberglass blanket weighing 0.73 kg/m^2 (0.15 psf) and a trim panel surface density of 12.7 kg/m^2 (2.6 psf). These results hold for both the aluminum and the strength-designed composite aircraft.

- If the external noise is reduced by 10 dB, or if alternatively, the design requirement was 90 dBA interior noise level, then the optimum outer-wall surface densities would be the baseline values of 6.2 kg/m^2 (1.28 psf) for the aluminum aircraft, and 4.3 kg/m^2 (0.89 psf) for the strength-designed all composite material aircraft.

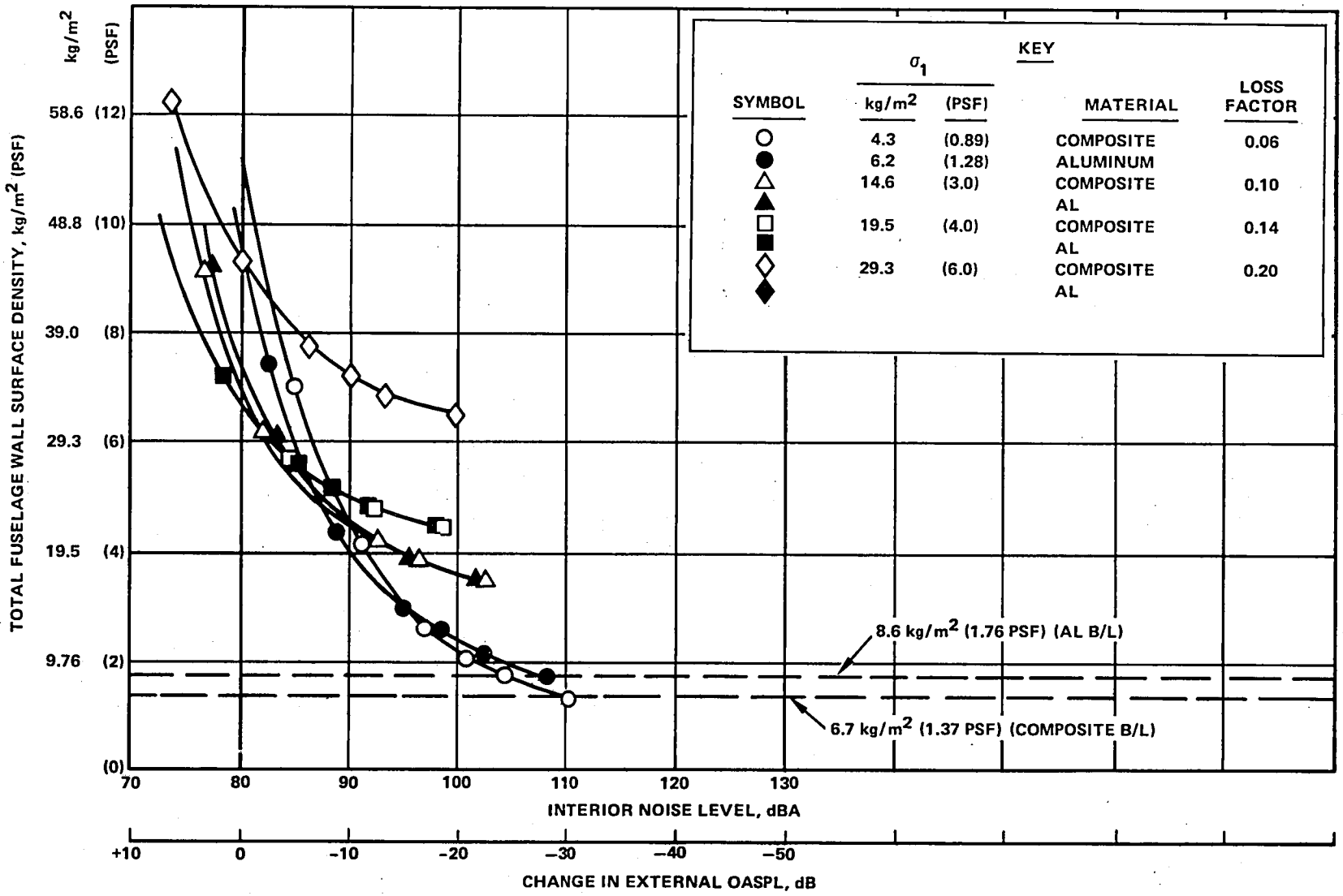

Figure 60. - 2-engine narrow-body double-wall study; aluminum and composite structures; segment 4, spectrum 1.

- In the design range of 82 dBA to 88 dBA, the optimum outer-wall surface density is 14.6 kg/m^2 (3 psf).

- The curve showing results for a 29.3 kg/m^2 (6 psf) outer-wall surface density may provide competitive results if the required interior noise design level was reduced to 70 dBA, or if the external noise level was increased by 10 dB.

In general, wide-body and narrow-body results are quite similar except that the narrow-body requires slightly lower penalties in the peak noise region. The axial distribution of treatment mass differs considerably, however, due to the difference in the external noise signatures, as shown in figures 7 and 8. See also figures 1 and 2.

G4. SMALL BUSINESS AIRCRAFT RESULTS

G4.1 Baseline Structure and Interior Noise Level Predictions

Appendix B describes the baseline structural and sidewall properties of the small business aircraft. This aircraft has a diameter of 2.23 m (7.33 ft.). The structure is assumed to have frame spacing of 50.8 cm (20 in.) with smaller intercostals at axial intervals of 17 cm (6.7 in.). For analysis purposes, the stiffener material for the ring frames and intercostals was redistributed to provide frames of equal total stiffness at intervals of 17 cm (6.7 in.). The longerons or stringers were spaced at intervals of 58.4 cm (23 in.). The effect of the redistribution of frame material at 17 cm intervals was checked by alternative analysis wherein all of the ring frame plus intercostal stiffener material was redistributed at 50.8 cm (20 in.) intervals. The calculated effect upon interior noise results was small; therefore, the mathematical modeling of the frames at 17 cm (6.7 in.) intervals appears to be satisfactory within the context of the present smeared-stiffener theory. The double-wall spacing is chosen to be 10.2 cm (4 in.), anticipating the benefits of a relatively large wall spacing for double-wall noise-reduction performance. The sidewall cross section is similar to figure 22.

G4.2 Baseline Interior Noise Levels For Aluminum and Composite Structures

Figure 61 shows the transmission loss spectra for the baseline aluminum structure at various fixed grazing incidence angles, whose axial positions are noted in the figure caption, expressed as ratios, relative to the propeller

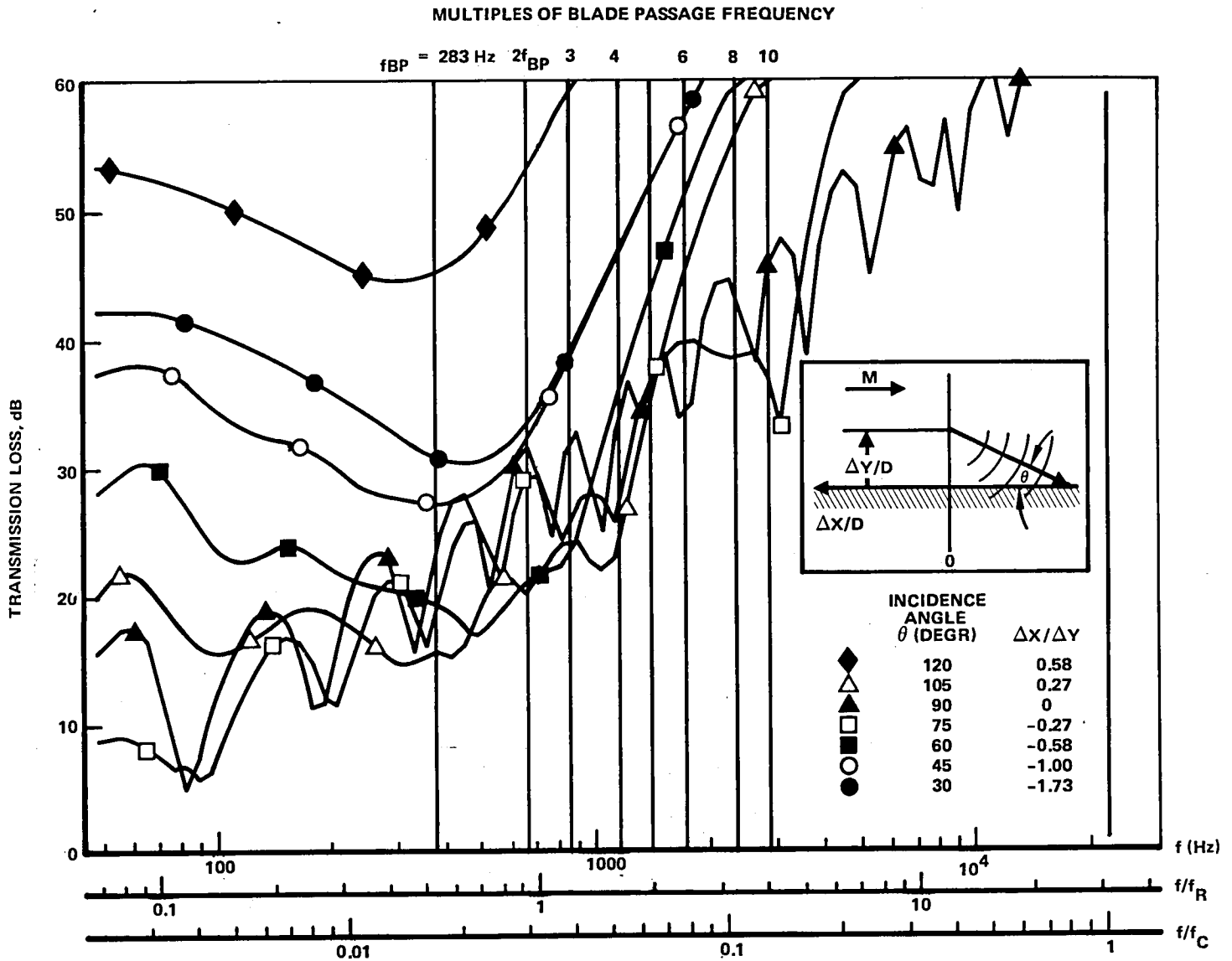

Figure 61. - Baseline fuselage outer-wall transmission-loss spectra; business aluminum aircraft at M = 0.8, 9144 m (30 000 ft) altitude.

tip clearance. The values of $\Delta x/\Delta y$ must be multiplied by 0.8 for this aircraft to obtain the axial position expressed in ratio to the propeller diameter. For this smaller aircraft with a relatively high blade passage frequency of 283 Hz, the calculated transmission-loss values appear to be somewhat higher for lowest propeller harmonics, when compared with the previous wide-body and narrow-body results.

Figure 62 shows the results of the double-wall study. The lowest total surface density values denote the baseline configuration results. The aluminum baseline structure has a total surface density of 6.8 kg/m^2 (1.39 psf), including an outer-wall structural mass of 1.61 kg/m^2 (0.33 psf) and a B-type fiberglass blanket with a thickness of 5.1 cm (2 in.), and a surface density of 0.49 kg/m^2 (0.10 psf). The strength-designed composite structure has a baseline outer-wall structural mass of 3.3 kg/m^2 (0.67 psf) with the same baseline trim panel and fiberglass blanket for a total surface density of 5.37 kg/m^2 (1.10 psf). The baseline structure yields interior noise levels of 111 dBA and 110 dBA for the aluminum and composite structures, respectively. Apparently, the increased A-weighting associated with the higher blade passage frequency tone of this aircraft, compared to the narrow-body and wide-body offsets the benefits of improved transmission loss to yield essentially equal baseline interior noise levels which are 30 dBA higher than the design goal. The ring frequency for this aircraft is 738 Hz and the ratio of blade passage frequency to ring frequency is 0.38 which is very close to the narrow-body ratio of 0.39.

G4.3 Add-On Noise-Reductions For Aluminum and Composite Structures

Figure 62 shows the noise reduction for Segment 4, expressed with outer-wall structural mass as a parameter with four values displayed, including the baseline values for both the aluminum and the composite structures. The trends for the business aircraft are very similar to the wide-body and narrow-body results discussed previously. The following are some of the key features of figure 62:

- For the aluminum structure the optimum outer-wall surface density to achieve 80 dBA is 19.5 kg/m^2 (4 psf). The total surface density is 28.8 kg/m^2 (5.9 psf).

- For the composite structure, the optimum total outer-wall mass to reach 80 dBA is now reduced to 14.6 kg/m^2 (3 psf). The total surface density is 26.4 kg/m^2 (5.4 psf).

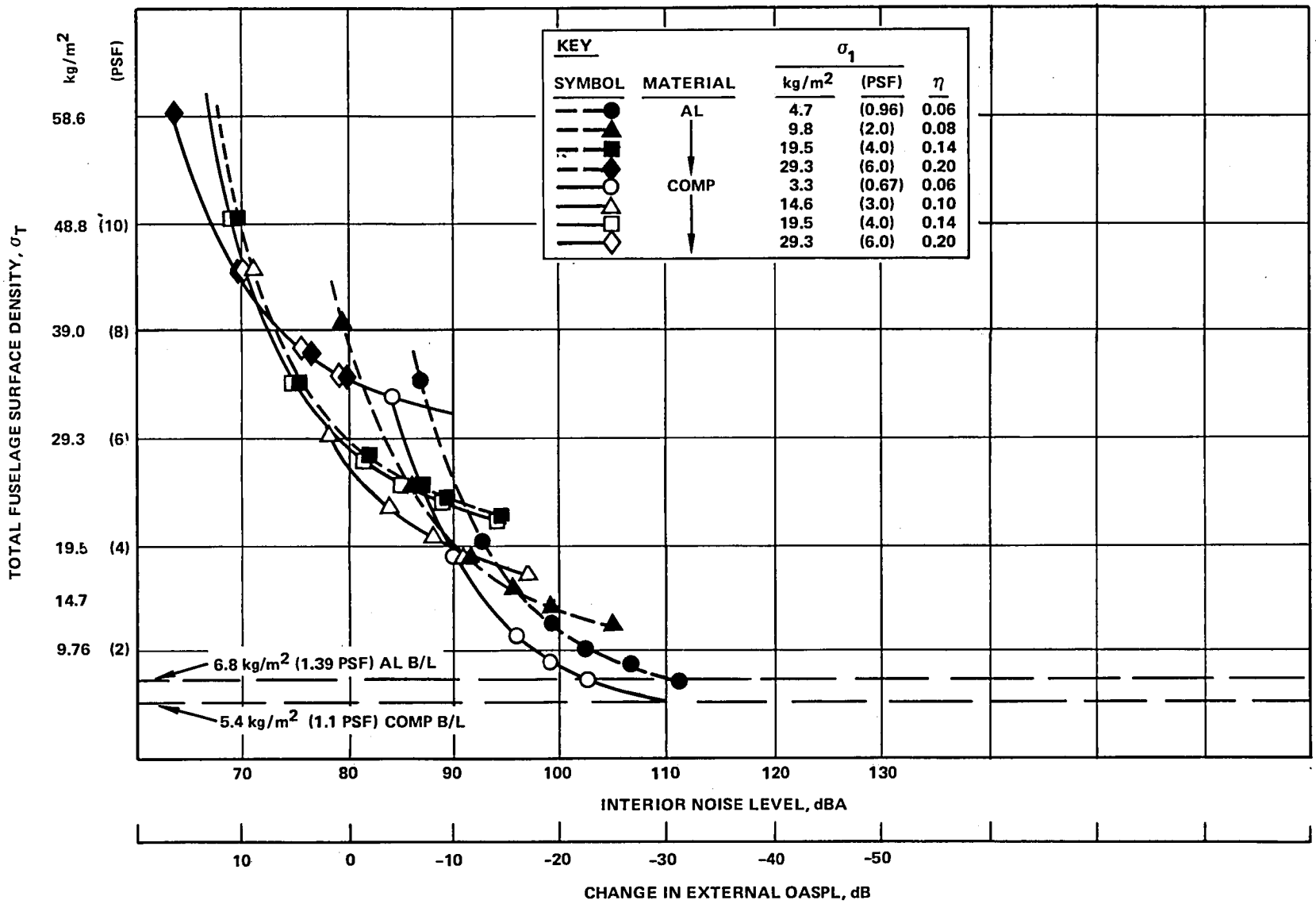

Figure 62. - Business aircraft double-wall study; aluminum and composite structures; segment 4, spectrum 1.

- To achieve a lower interior noise goal of 70 dBA (or to offset a 10 dB increase of exterior noise level) the optimum outer-wall mass is increased to 29.3 kg/m^2 (6 psf). The total surface density is 43.9 kg/m^2 (9 psf).

The reader will note for this smallest aircraft that some difference is beginning to emerge between the composite structure and the aluminum structure. Evidently, a lower value of outer-wall mass of 14.6 kg/m^2 (3 psf) is now the optimum for the composite structure, whereas for the larger aircraft, a 19.5 kg/m^2 (4 psf) outer-wall mass was required.

G5. GENERAL COMMENTS ON DOUBLE WALL PERFORMANCE FOR ALL AIRCRAFT SIZES

In the peak noise region, the optimum division of mass between the outer-wall and the trim panel is nearly equal, which is consistent with the simplified theory of double-wall-mass law behavior, subject to numerous constraints. These constraints included:

- Structural dynamic complexities of the stiffened cylindrical shell as a whole and of the individual trim panels and outer-wall skin bays, as modified by damping treatment.
- Acoustical coupling with the fiberglass blanket and interior air gaps.
- Acoustical coupling to the interior via the P. W. Smith type of radially-inward traveling wave field.
- Strength-design requirements of the outer-wall structure which impose a minimum mass and stiffness level that cannot be reduced, but can only be increased via the addition of damping treatments.
- Trim panel surface density cannot be reduced below its baseline value.

G6. SENSITIVITY OF RESULTS TO CHANGES OF EXTERIOR NOISE LEVEL OR TO CHANGES IN THE DESIGN REQUIREMENTS FOR INTERIOR NOISE

The results shown in figures 57, 60 and 62 display the add-on noise reduction performance of the limp double wall designs for the wide-body, narrow-body and business aircraft, respectively, for the noise region of Segment 4 over a wide range of noise reduction. These curves, therefore, automatically display sensitivities to changes of design criteria, which could be either a) an increase of the local exterior noise level, or b) imposition of a different interior noise design goal.

G7. ADD-ON NOISE REDUCTION PERFORMANCE OF OTHER TREATMENT SEGMENTS AWAY FROM THE PROPELLER DISC REGION, AND THE EFFECTS OF BLADE PASSAGE FREQUENCY VARIATION

G7.1 4-Engine Wide-Body Aircraft

G7.1.1 Segment variation effects.- The results presented thus far have focused upon the comparison of required surface density values in the peak exterior noise region associated with Segment 4. In this discussion, the treatment requirements for the other segments are briefly indicated, as well as some indication of the effects of blade passage frequency variation. The total surface density data for these other segments adjusted locally for changes of external noise within the segment is the basis of penalty mass data presented in Section 3 of this report.

Figures 63 to 65 show the results of the 0.152 m (6 in.) double-wall study for Segments 3 through 7 having the external noise levels as defined nominally in table 7 and showing local variations in figures 7 and 8. Figures 63 to 65 employ a dual abscissa showing the effects of trim panel surface density and also total wall surface density. The latter scale facilitates the direct comparison of mass penalties for designs with differing outer-wall surface densities. These data are used to generate table 15 which summarizes the total wall surface densities required to achieve 80 dBA for each of the segments at three values of outer-wall surface density. Designs with the minimun or baseline value of outer-wall surface density require the least total surface density to achieve 80 dBA for all segments except Segment 4. This result holds true for all aircraft sizes for add-on designs. The curves for Segment 4 in figures 63 and 65 are based on a nominal OASPL of 132 dB which corresponds to a baseline propeller tip clearance of $\Delta y/D = 1.2$ for the inboard engine. The nominal external OASPL design values for all segments are obtained from table 7.

G7.1.2 Blade passage frequency effects.- Figure 66 shows the relationship between blade passage frequency and performance of the limp double wall for the case of an outer-wall surface density of 19.5 kg/m^2 (4 psf) and for a trim-panel surface density of 14.6 kg/m^2 (3 psf). These are nearly optimum parameter selections for the peak noise region, Segment 4. Figure 66 also shows that baseline blade passage frequencies of between 160 Hz, and 200 Hz

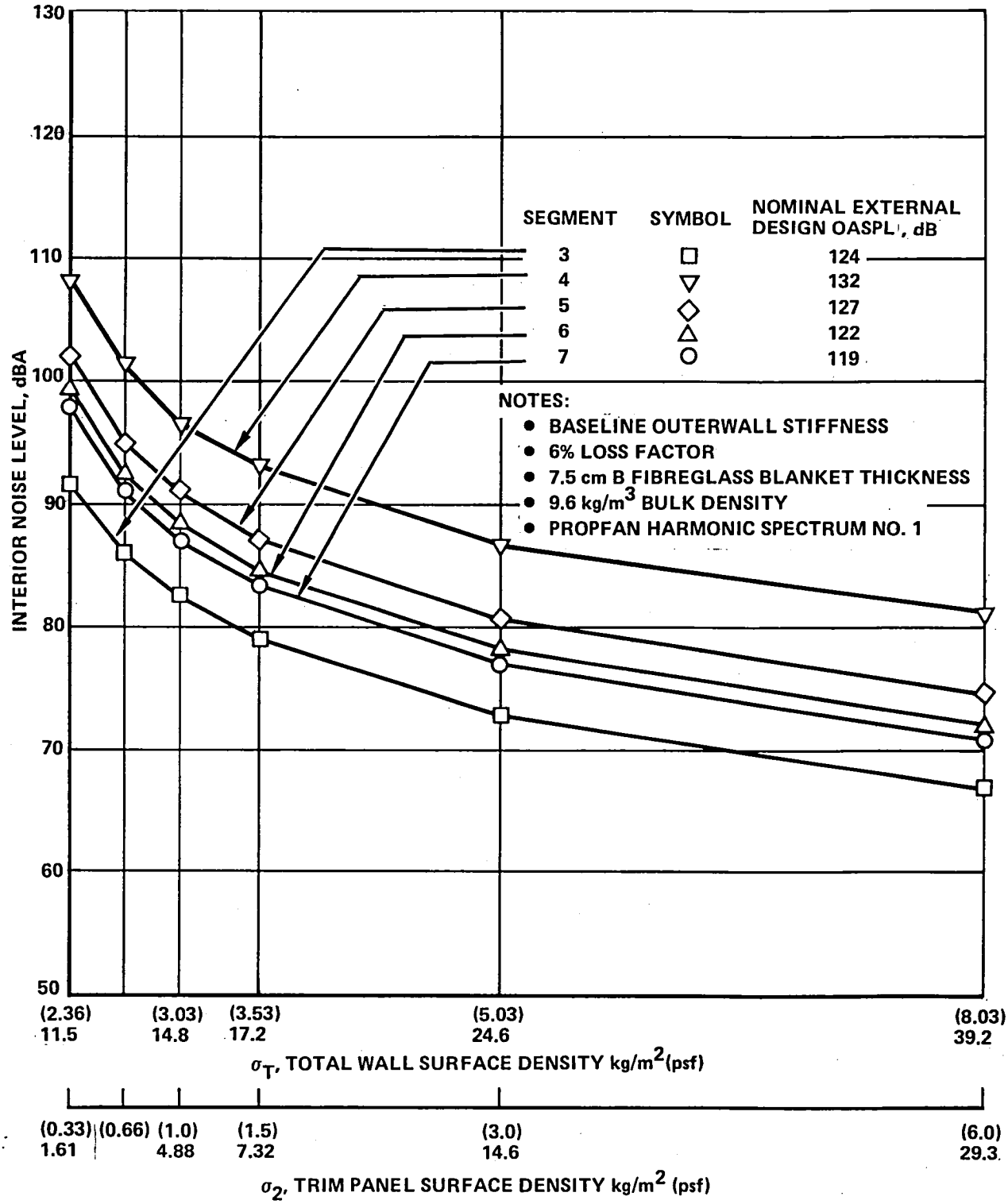

Figure 63. - 4-engine wide-body aluminum aircraft interior noise levels vs total wall surface density for segments 3 to 7; baseline outer-wall surface density 9.17 kg/m^2 (1.88 psf); 0.152 m (6 in.) double-wall study.

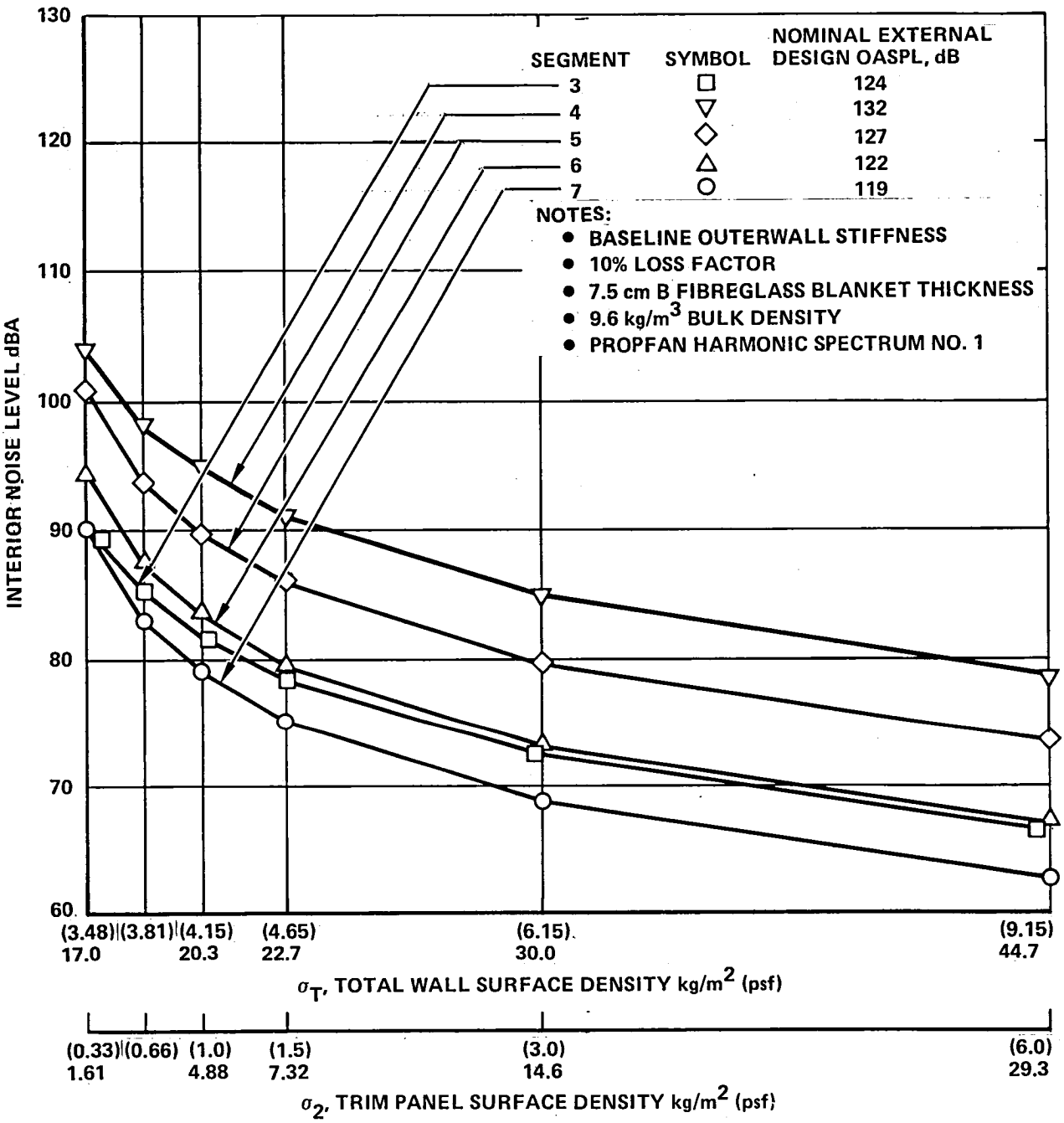

Figure 64. - 4-engine wide-body aluminum aircraft interior noise levels vs total wall surface density for segments 3 to 7; outer-wall surface density 14.6 kg/m^2 (3 psf); 0.152 m (6 in.) double-wall study.

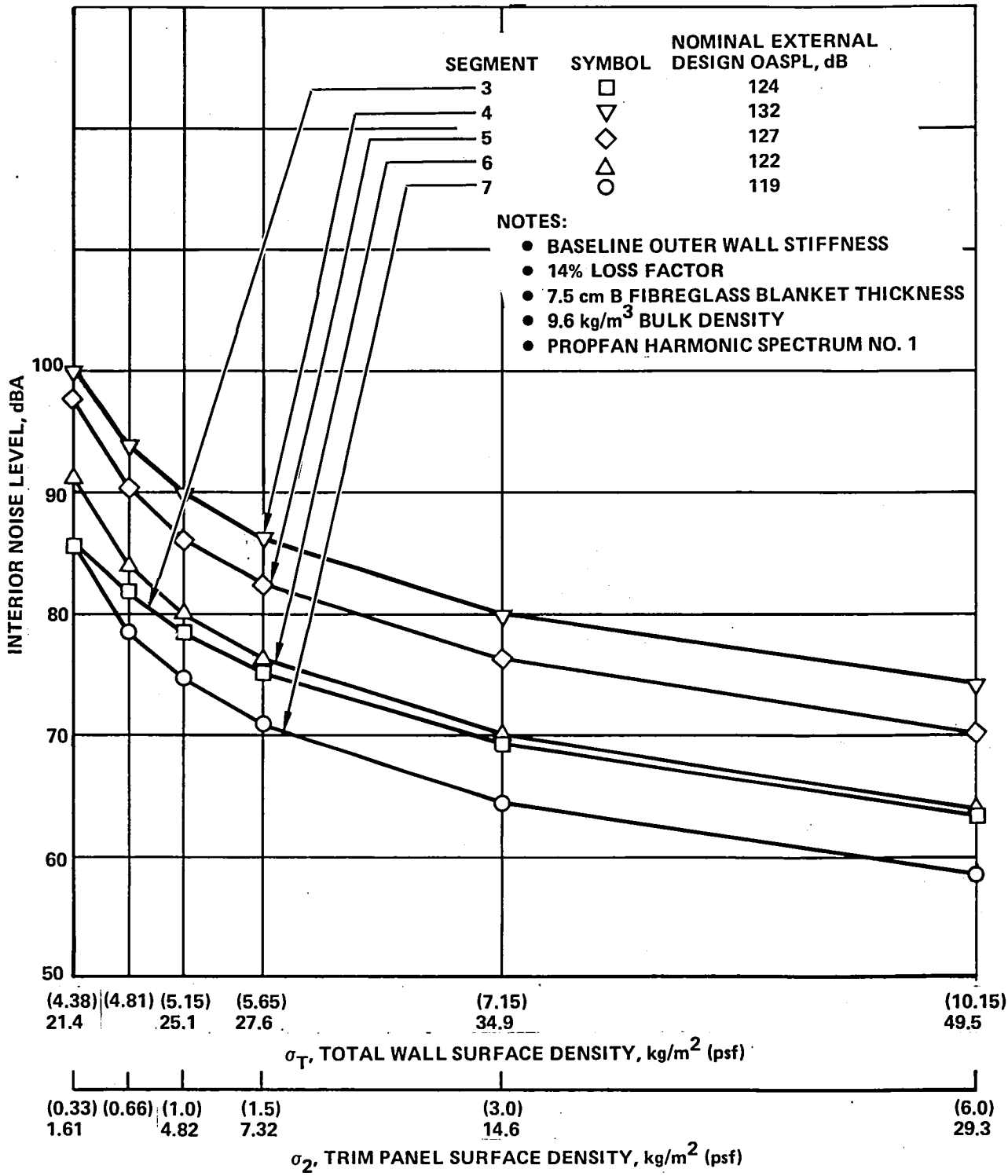

Figure 65. - 4-engine wide-body aluminum aircraft interior noise levels vs total wall surface density for segments 3 to 7; outer-wall surface density 19.5 kg/m^2 (4 psf); 0.152 m (6 in.) double-wall study.

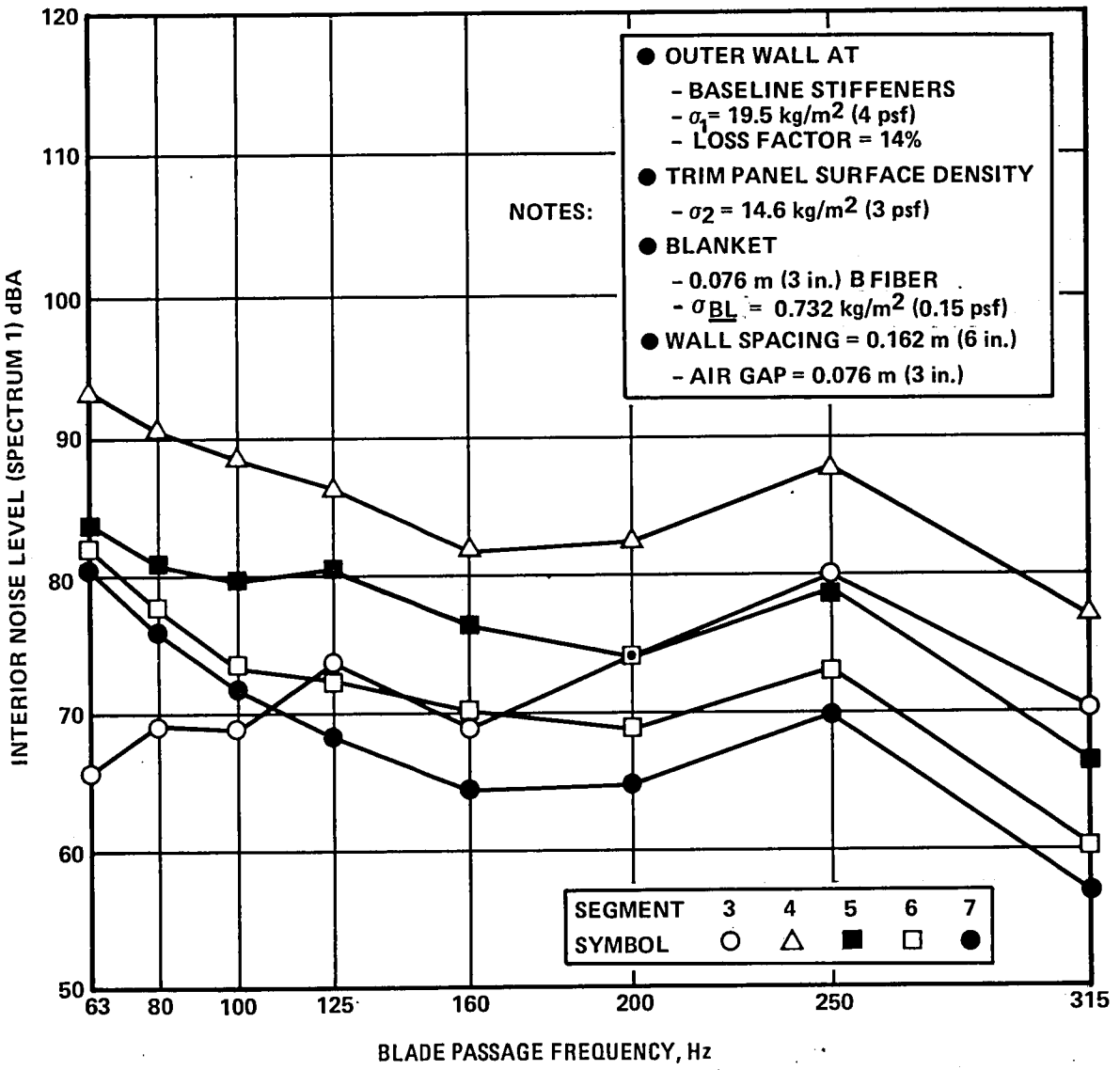

Figure 66. - Blade passage frequency study for aluminum wide-body aircraft; limp double wall add-on noise-control configuration.

TABLE 15. - REQUIRED TOTAL SURFACE DENSITY TO ACHIEVE 80 dBA FOR SEGMENTS 3 TO 7 VS OUTER-WALL SURFACE DENSITY; 4-ENGINE WIDE-BODY AIRCRAFT; 0.152 m (6 IN.) DOUBLE-WALL

		σ_1, Outer Wall Surface Density					
		kg/m^2	(psf)	kg/m^2	(psf)	kg/m^2	(psf)
		9.17	(1.88)	14.6	(3)	19.5	(4)
Segment	Exterior OASPL	σ_T, Total Surface Density					
3	124	16.6	(3.4)	22.0	(4.5)	24.4	(5.0)
4	132	41.5	(8.5)	40.0	(8.2)	35.1	(7.2)
5	127	25.9	(5.3)	30.3	(6.2)	30.3	(6.2)
6	122	22.5	(4.6)	22.5	(4.6)	25.4	(5.2)
7	119	21.0	(4.3)	21.5	(4.4)	22.9	(4.7)

produce the minimum interior noise levels for each segment, except for Segment 3. Segment 3 appears to give slightly better results at low frequency. This result is consistent with the nature of the basic shell transmission loss spectra shown in figure 56 where it is seen that low-frequency transmission loss increases at locations upstream of the propeller disc plane.

The results of figure 66 generally substantiate the benefits claimed in reference 1 of the high blade passage frequency which is a characteristic feature of the propfan. In the present example, the results appear to worsen at 250 Hz; however, this is believed to be due to a skin panel resonance problem which could be eliminated by tuning the selection of stiffener spacing, outer-wall skin thickness, etc., or possibly by an increase of damping. The present configuration is, in fact, optimized for the baseline blade passage frequency of 162 Hz.

G7.2 2-Engine Narrow-Body Aluminum Aircraft

G7.2.1 Segment variation effects.- Figures 67 to 69 show the interior noise levels for Segments 3 to 7 for the narrow-body aluminum aircraft with a 0.152 m (6 in.) double wall. Results are plotted against dual scales of trim panel and total wall surface density. Table 16 shows the total surface

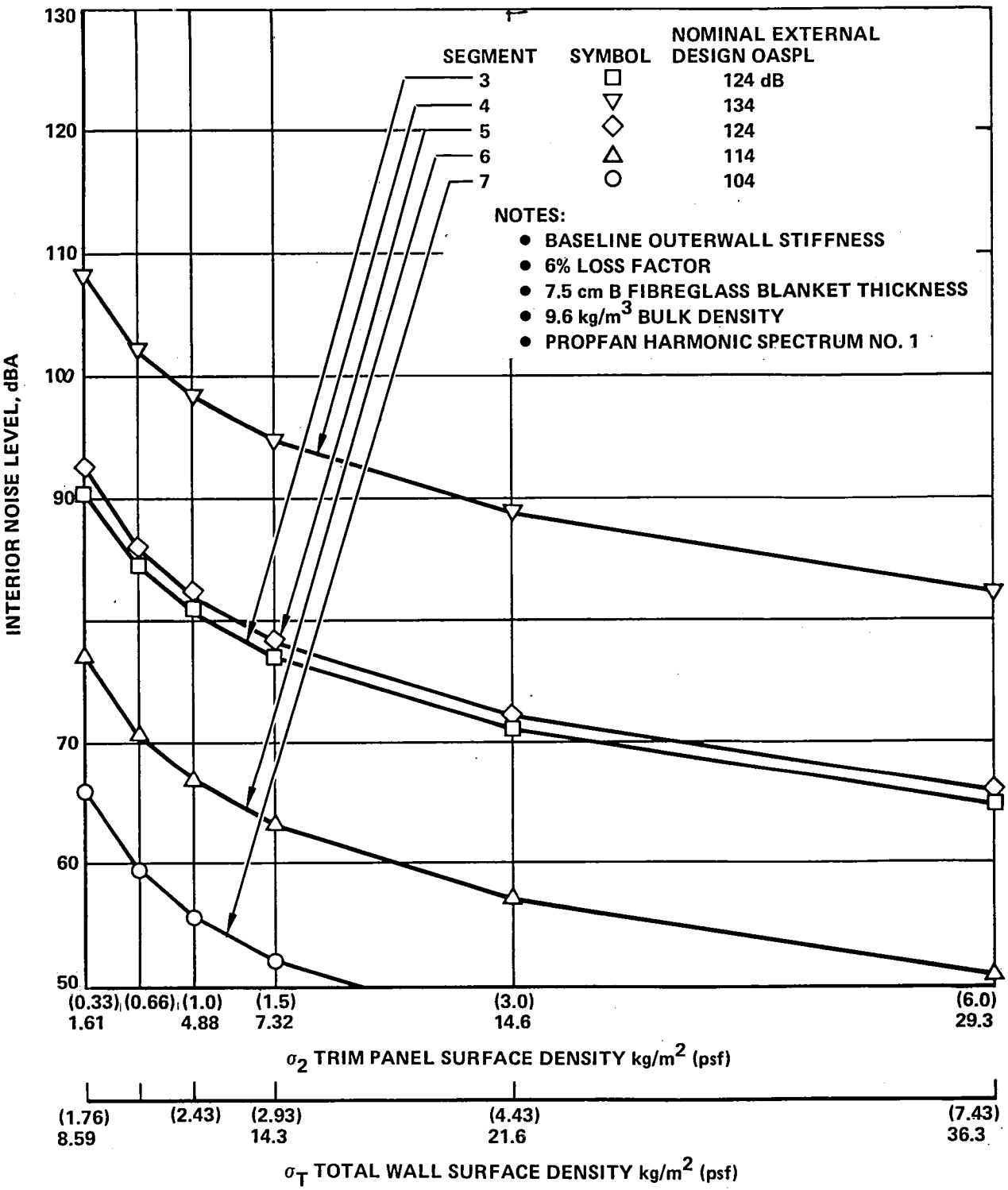

Figure 67. - 2-engine narrow-body aluminum aircraft interior noise levels vs total surface density for segments 3 to 7; baseline outer-wall surface density 6.25 kg/m^2 (1.28 psf), 0.152 m (6 in.) double-wall study.

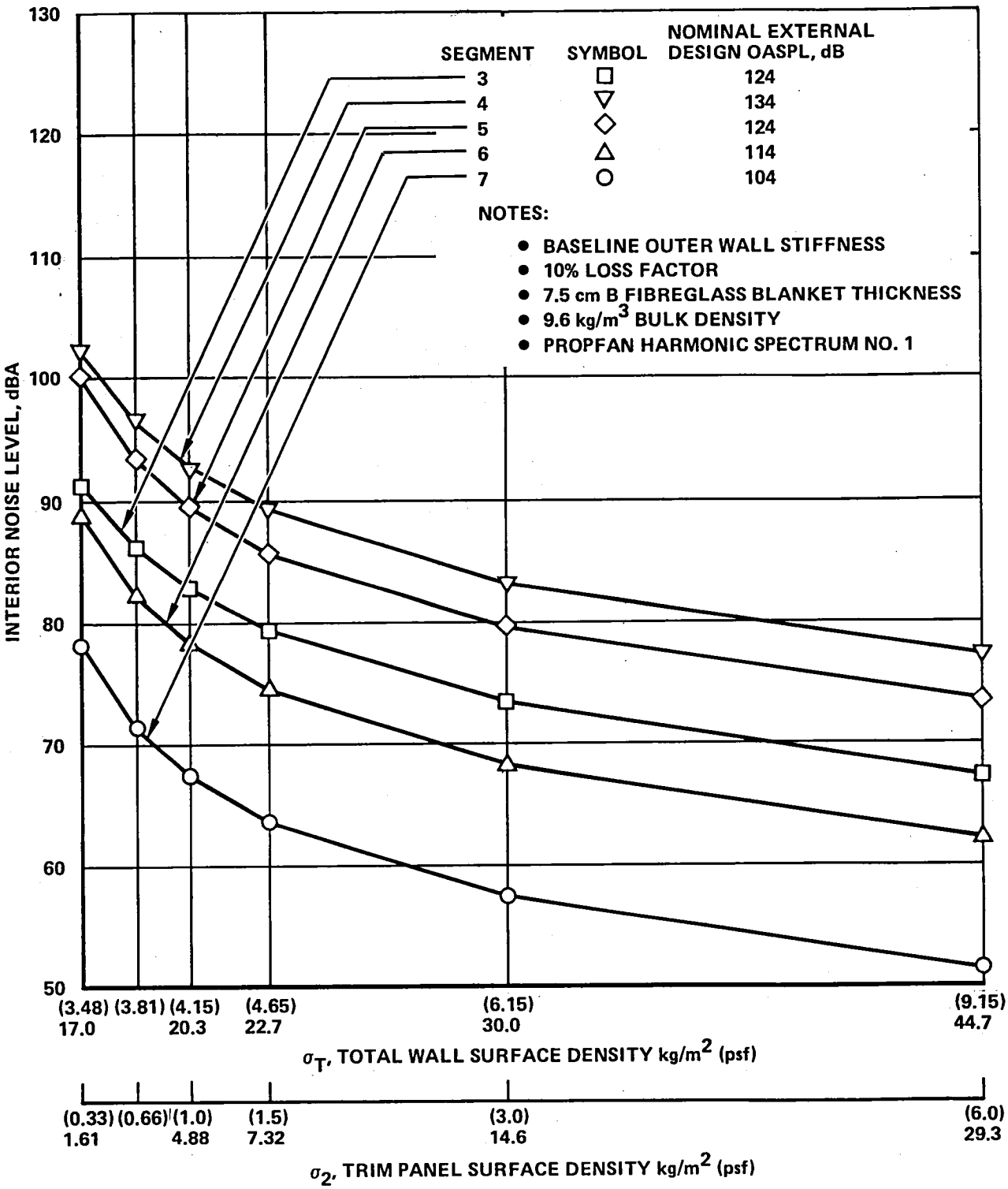

Figure 68. - 2-engine narrow-body aluminum aircraft interior noise levels vs total surface density for segments 3 to 7; outer-wall surface density 14.6 kg/m^2 (3 psf); 0.152 m (6 in.) double-wall study.

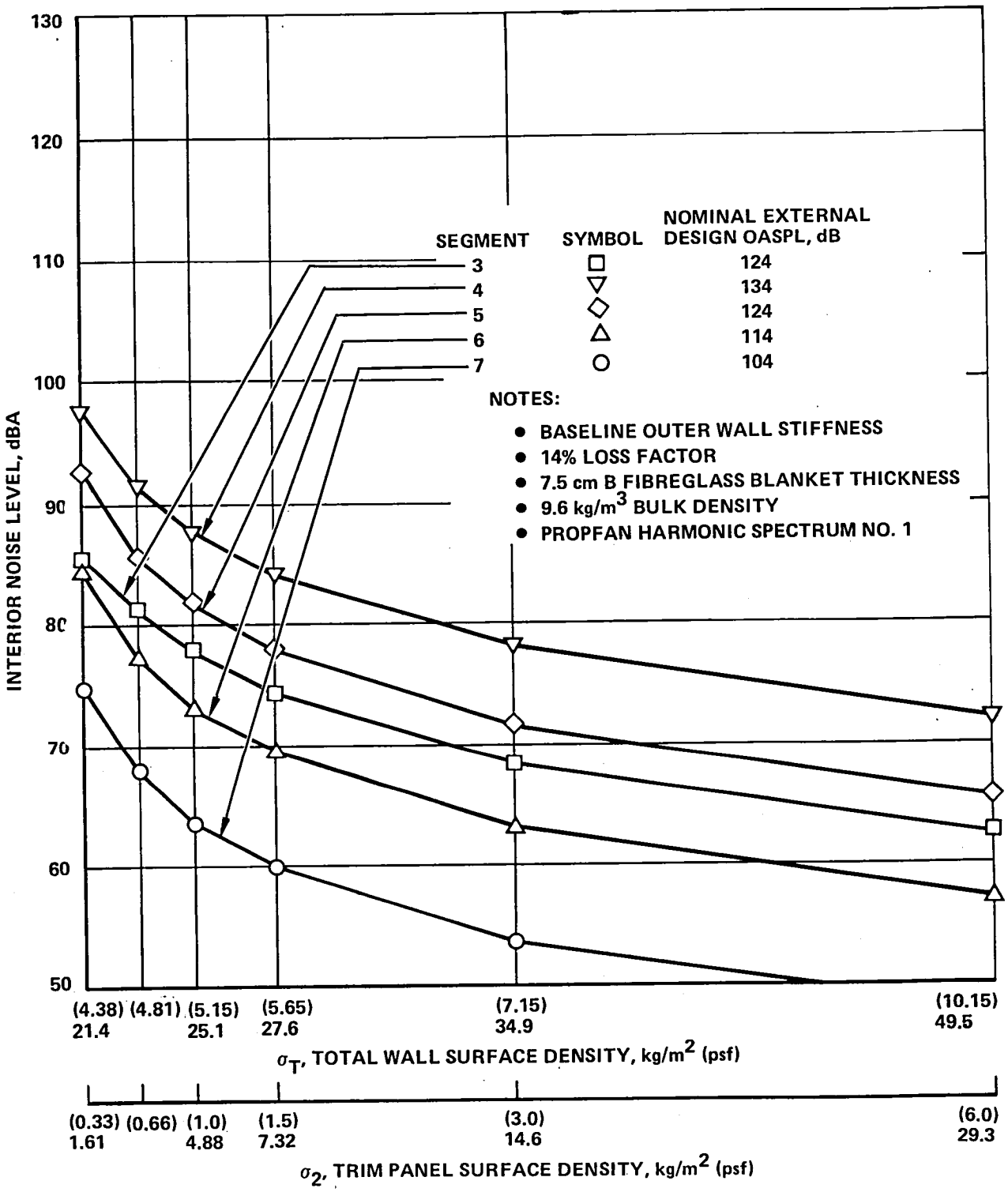

Figure 69. - 2-engine narrow-body aluminum aircraft interior noise levels vs total surface density for segments 3 to 7; outer-wall surface density 19.5 kg/m^2 (4 psf); 0.152 m (6 in.) double-wall study.

density required to achieve 80 dBA for each of the segments, and for each of the three values of outer-wall surface density. The results of table 16 show a behavior similar to that of the wide-body results, namely:

- For Segment 4, the peak noise region, the least treatment penalty mass is obtained with a 19.5 kg/m^2 (4 psf) outer-wall mass surface density
- For Segments 3, 5, 6 and 7 the least treatment penalty mass is obtained by selecting the minimum or baseline value of outer-wall surface density of 6.25 kg/m^2 (1.28 psf)

G7.2.2 Effects of blade passage frequency variation.- Figure 69 shows the effects of varying blade passage frequency for the 2-engine aluminum narrow-body aircraft for a noise control configuration having a 19.5 kg/m^2 (4 psf) outer-wall mass and a 14.6 kg/m^2 (3 psf) trim panel. This is nearly an optimum configuration for the peak noise region 4, Segment 4. The configuration is not optimum, however, for the outer segments away from the propeller disc plane. For these segments it is preferable to retain the baseline outer-wall surface density, as shown in table 16. Figure 70 shows that Segment 4 does achieve best noise reduction performance in the range of blade passage frequencies between 160 to 200 Hz.

TABLE 16. REQUIRED TOTAL WALL SURFACE DENSITY TO ACHIEVE 80 dBA FOR SEGMENTS 3 TO 7 FOR VARIOUS OUTER-WALL SURFACE DENSITY VALUES 2-ENGINE NARROW-BODY ALUMINUM AIRCRAFT, 0.152 m (6 IN.) DOUBLE-WALL

		Outer Wall Surface Density					
Segment	External OASPL dB	kg/m^2 6.25	(psf) (1.28)	kg/m^2 14.6	(psf) (3)	kg/m^2 19.5	(psf) (4)
		Total Wall Surface Density					
3	124	12.2	(2.5)	22.5	(4.6)	23.9	(4.9)
4	134	42.0	(8.6)	37.6	(7.7)	32.7	(6.7)
5	124	14.2	(2.9)	29.3	(6.0)	26.4	(5.4)
6	114	8.6	(1.76)	19.0	(3.9)	22.5	(4.6)
7	104	8.6	(1.76)	17.0	(3.48)	21.4	(4.38)

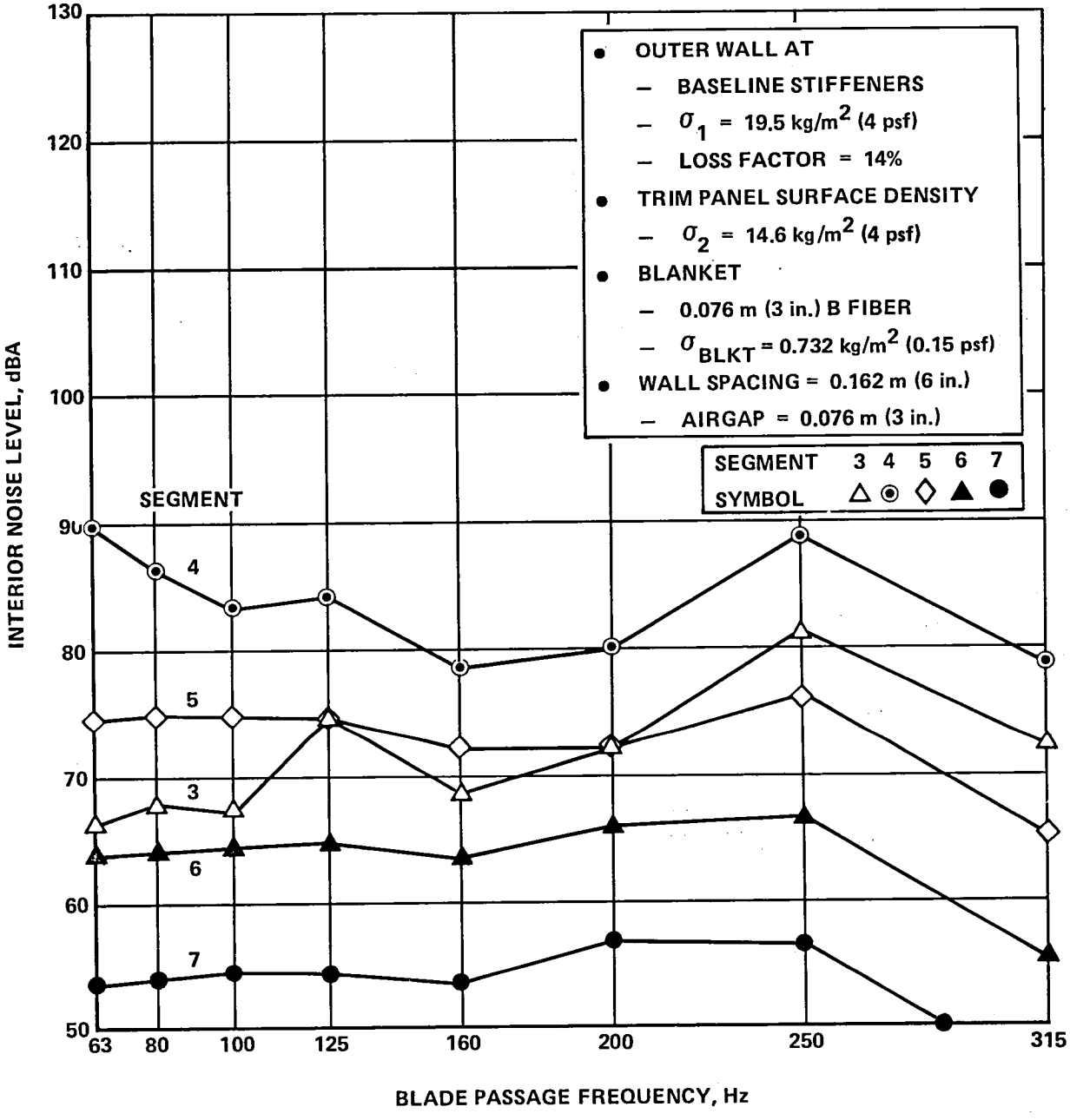

Figure 70. - Blade passage frequency study for narrow-body aluminum aircraft; 19.5 kg/m^2 (4 psf) outer-wall mass, 14.6 kg/m^2 (3 psf) trim-panel mass, 14 percent loss factor.

G7.3 Small Business Aircraft

G7.3.1 Segment variation effects.- Figures 71 to 73 show the required total surface density versus interior noise levels for Segments 3, 4, and 5, respectively. In each figure, the outer-wall surface density is parametrically varied over 4 values from a baseline value of 4.68 kg/m^2 (0.96 psf) to a maximum of 29.3 kg/m^2 (6 psf). These are double-wall studies for a 0.102 m (4 in) wall spacing and a baseline blade passage frequency of 283 Hz.

As in the studies for the larger aircraft, the optimum outer-wall surface density is about 19.6 kg/m^2 (4 psf) for the peak noise region adjacent to Segment 4. For Segments 3 (forward of the disc plane) and 5 (aft of the disc plane), the optimum outer-wall mass appears to be about 9.8 kg/m^2 (2 psf) based on the nominal exterior OASPL value of 124 dB for which these segments were designed. It will shown, later in this report, that if the acoustic treatment penalty mass is adjusted within these segments according to the local external acoustic signature shown in figures 7 and 8, then the optimum outer-wall mass reverts to the baseline value. This will be true for those regions of Segments 3 and 5 where the local exterior noise levels are lower than the nominal values. Results are omitted for Segments 6 and 7 for which also the optimum outer-wall mass is the baseline value.

G7.3.2 Blade passage frequency variation effects.- Figure 74 shows the effect of BPF variations on a nearly optimum noise control configuration for Segment 4. This configuration has a 0.102 m (4 in,) wall depth with a 19.6 kg/m^2 (4 psf) outer-wall mass and a 14.6 kg/m^2 (3 psf) trim panel mass. The total wall surface density used in figure 74 amounts to 34.7 kg/m^2 (7.1 psf) which exceeds the weight requirement to achieve 80 dBA per figure 72, yielding about 75 dBA at the baseline BPF of 283 Hz.

G8 EFFECTS OF OTHER PARAMETERS

G8.1 Introductory Remarks

A large number of parametric studies have been performed during this analytical program. It would not be practical or desirable to include all of the analytical studies in this report. However, an attempt has been made to include all of the results that have been derived from the larger body of data. Selected data are presented in this section to support the conclusions reached during this analytical study program.

G8.2 Effects of Damping Loss Factor

Earlier discussions of the double-wall performance of the outer-wall and trim panel have shown how interior noise was affected when outer-wall loss factor and mass were varied. Structural response is affected by both the mass and damping of the structure. Changing the mass of the structure

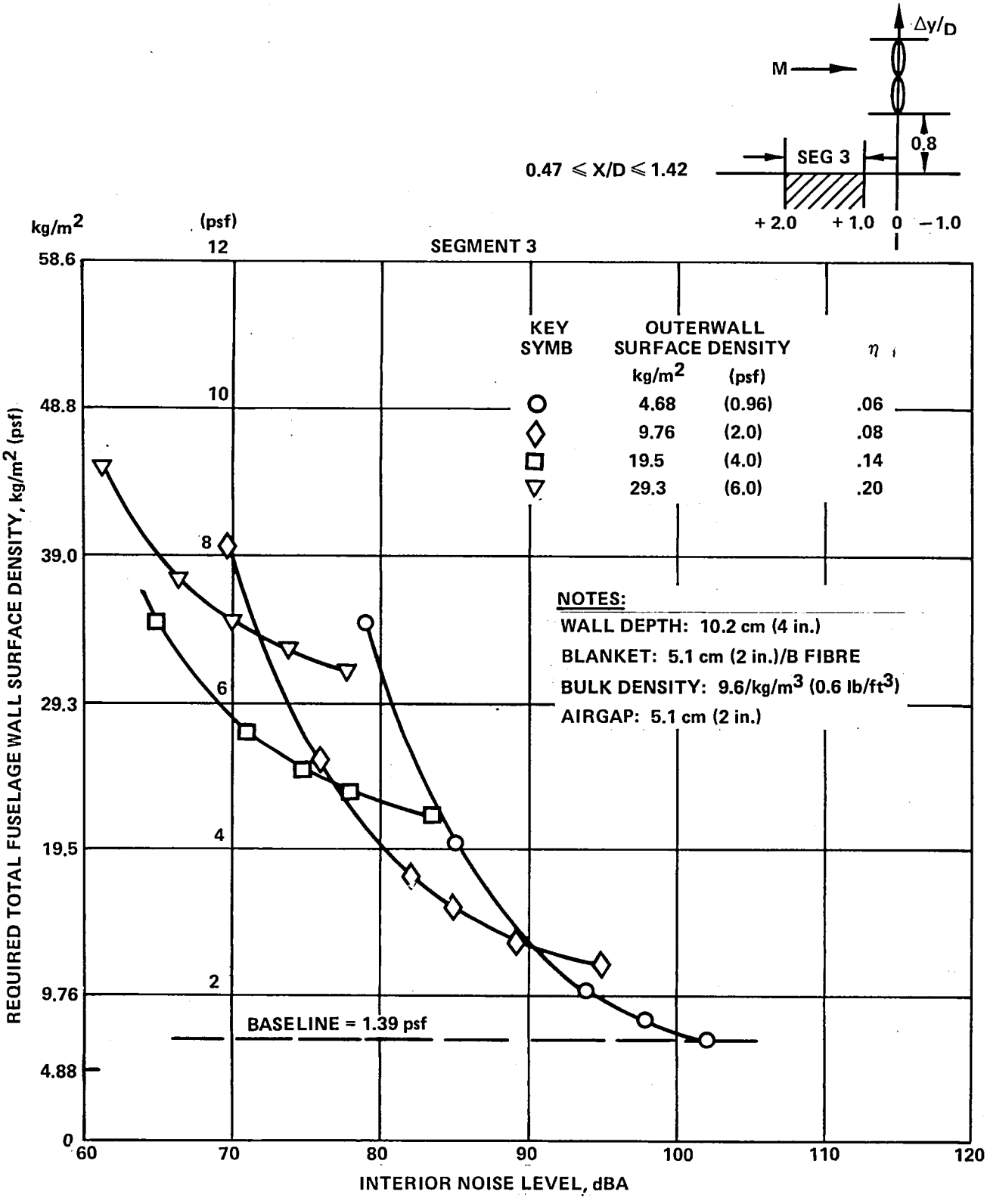

Figure 71. - Double-wall study for business aircraft; segment 3 (upstream of disc plane).

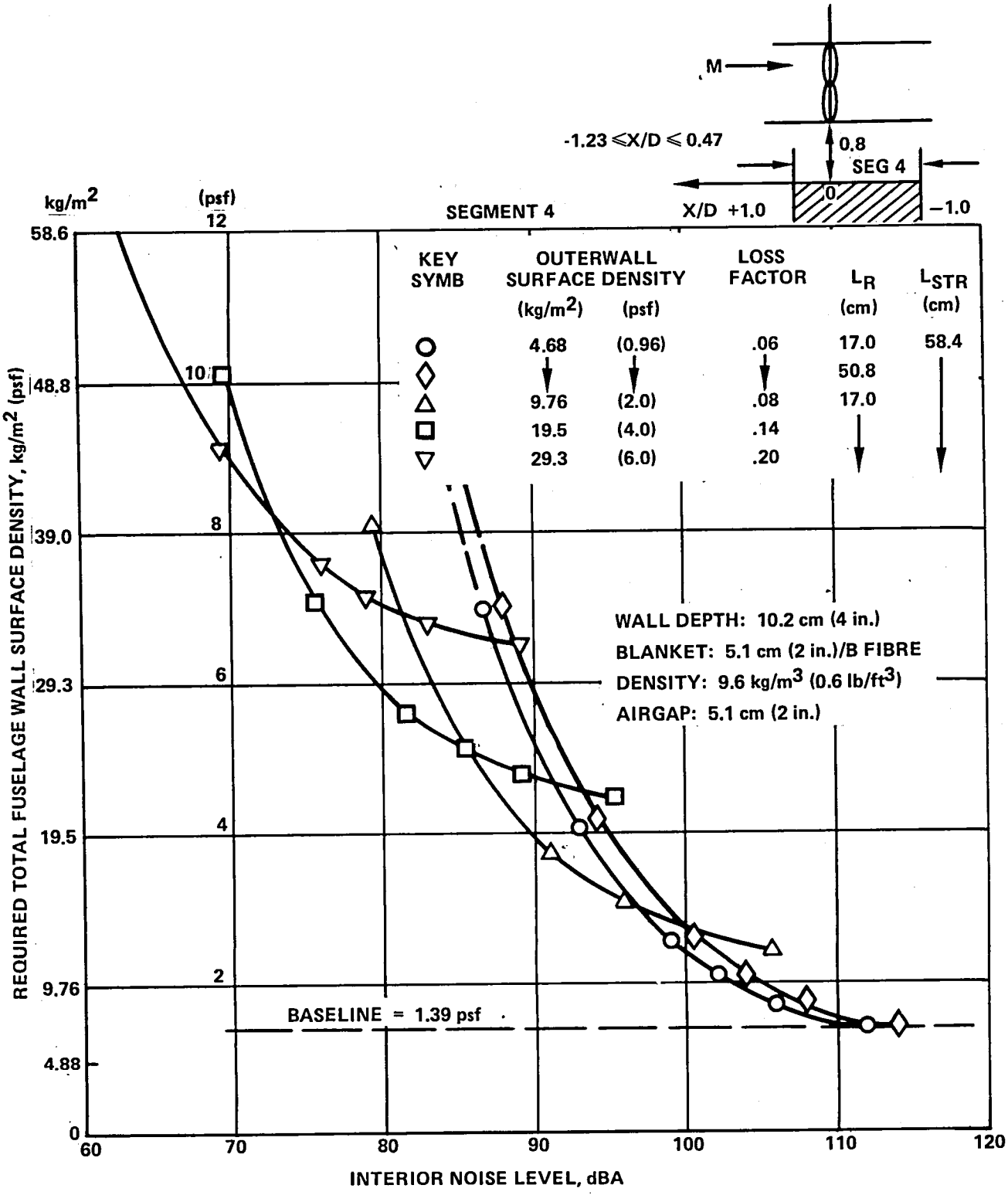

Figure 72. - Double-wall study for business aircraft; segment 4 (peak noise region).

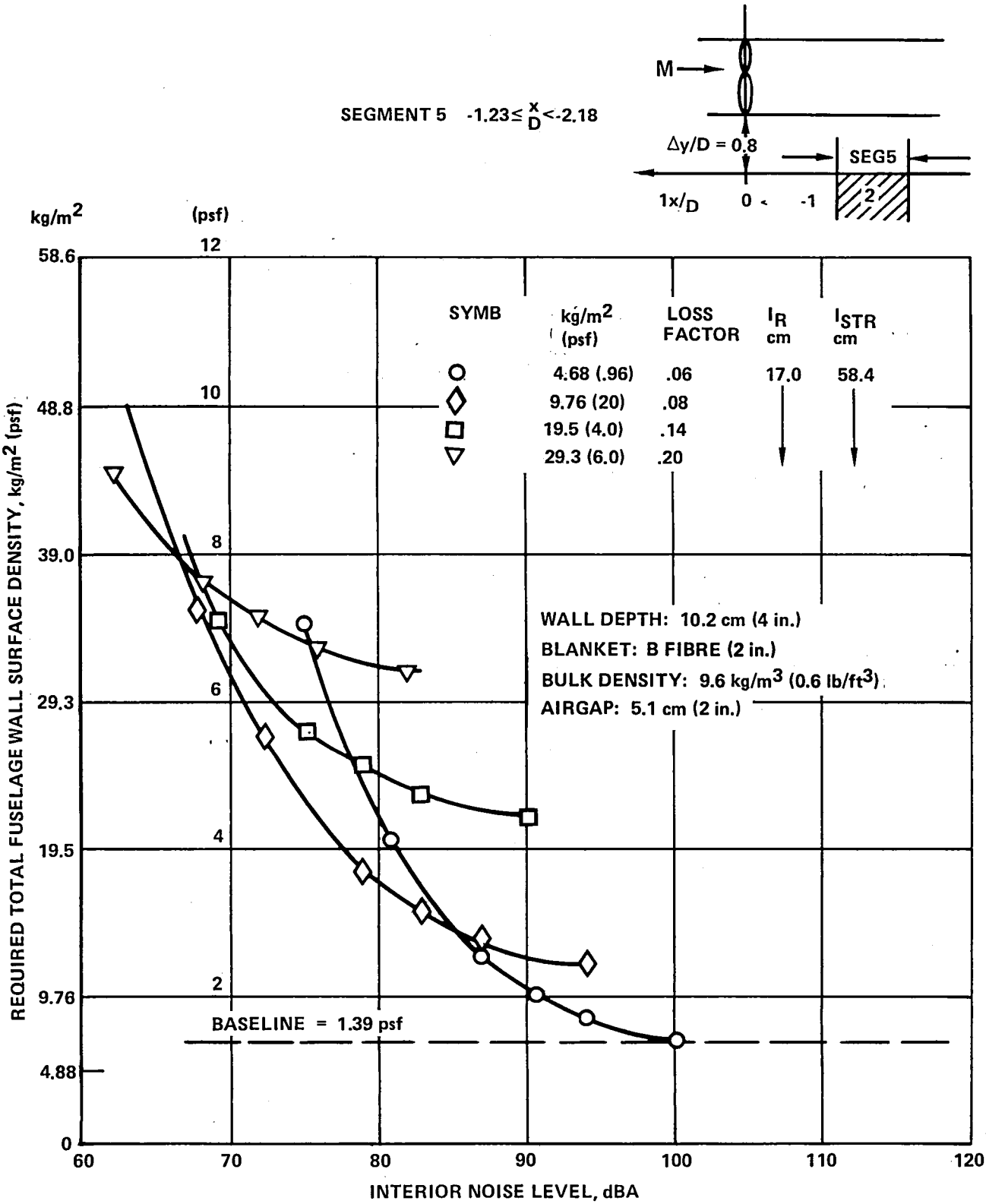

Figure 73. - Double-wall study for business aircraft; segment 5 (downstream of disc plane).

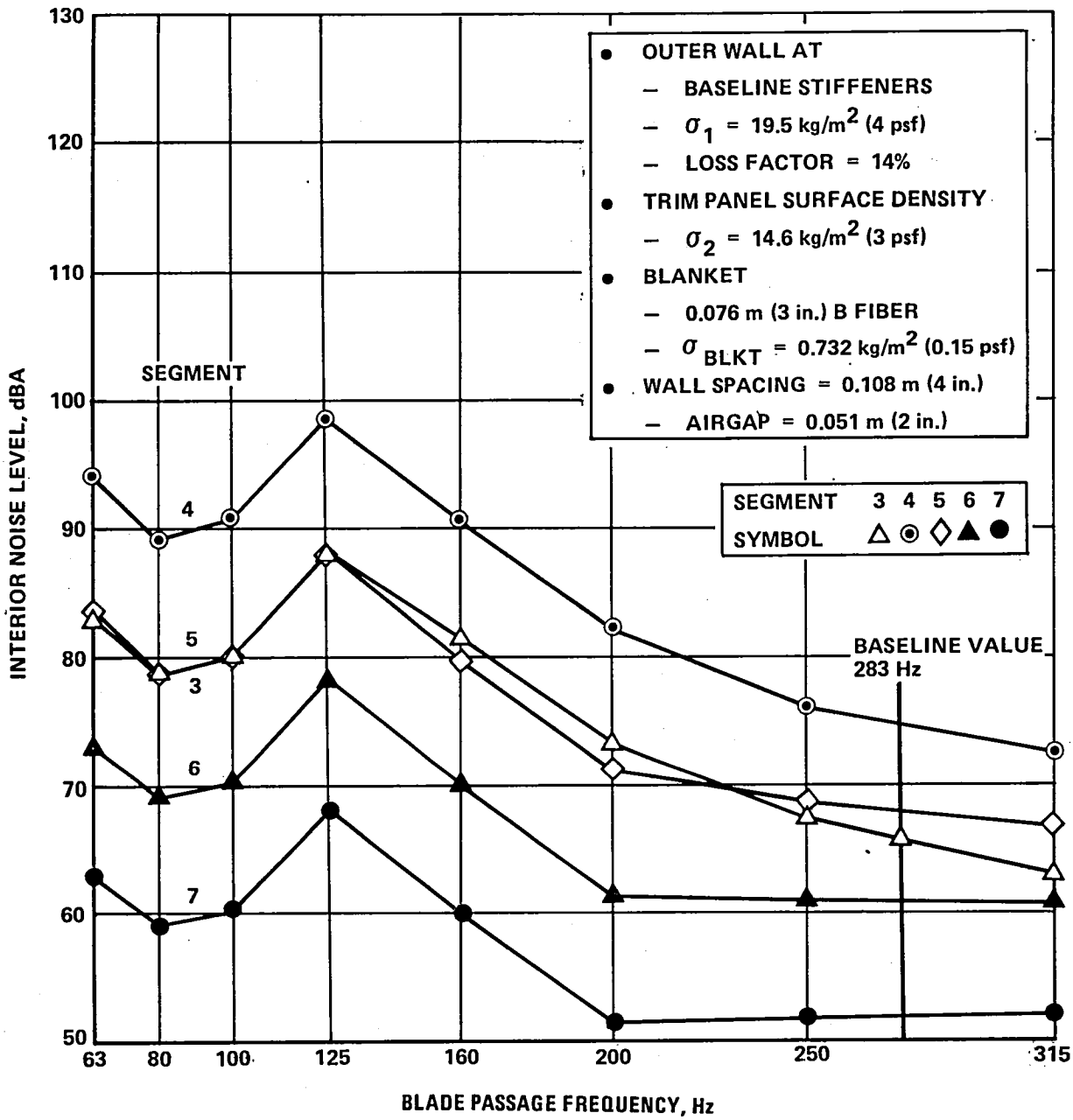

Figure 74. - Blade passage frequency study for small aluminum business aircraft: 19.5 kg/m^2 (4 psf) outer-wall, 14.6 kg/m^2 (3 psf) trim-panel surface density, 14% loss factor; 0.102m (4 in.) double-wall.

affects the dynamic response of the structure and could mask or obscure the effect due to changes in damping loss factor. Therefore, several parametric studies were performed for which the varying parameter was loss factor and all other variables were held constant. The data for Segment 4 and external spectrum number 1 are presented in figure 75. Although the different configurations have interior noise levels which vary over a wide range, the levels for a given configuration are relatively insensitive to significant increases in loss factor. It is therefore concluded that large decreases in interior noise cannot be obtained by increases in damping loss factor alone. However, the mass increases which are associated with increasing outer-wall damping loss factor in an optimum double-wall configuration are seen to be beneficial as discussed earlier. Similar results were obtained for each segment and external spectrum combination.

G8.3 Stiffness Effects

G8.3.1 Effects of skin thickness.- The baseline widebody configuration was used as a vehicle for this parametric study. Skin thickness was increased from its baseline value of 0.15 cm (0.06 in.) up to 0.64 cm (0.25 in.) and the surface density was allowed to increase with skin thickness. This represents one of the more obvious approaches to stiffening a structure. The results for Segment 4 and external spectrum number 1 are shown in figure 76. The aircraft skin surface density is shown as a function of skin thickness on the righthand scale of this figure. Analytical results for the other spectrum numbers and for all combinations of spectrum number and segment number show the same trend. Interior noise is not greatly affected by increases in skin thickness — the largest change occurs when the skin thickness is increased from 0.38 cm (0.15 in.) to 0.51 cm (0.20 in.) for all trim panel surface densities. If the skin thickness is increased to 0.51 cm (0.20 in.) a 3 to 4 dBA reduction is obtained relative to the baseline for an outer-wall surface density increase of 8.8 kg/m^2 (1.8 psf). Since a 28 dBA reduction is required to achieve 80 dBA, simply increasing skin thickness is not a practical means of achieving the desired interior noise goal.

The main problem with increasing skin thickness as a stiffening tool is that the outer-wall panel bay resonant frequencies are controlled by the membrane stresses for a typical pressurized cabin; therefore, the first small increments of skin thickness increase the mass, but do not significantly increase the net stiffness. Hence, the panel bay resonant frequencies are reduced, making them closer to the propeller harmonic excitation frequencies. This problem is compounded because the increased mass of the outer-wall required in a double-wall design tends to further decrease the resonant frequencies of the outer-wall skin panels.

G8.3.2 Outer-wall modulus and moment of inertia.- The stiffness of the outer wall can be changed by varying the moment of inertia or Young's modulus of the structure. In general, the moment of inertia of a structural

SYMBOL	AIRCRAFT TYPE	E/E (BASELINE)	MATERIAL	OUTER WALL SURFACE DENSITY kg/m^2	OUTER WALL SURFACE DENSITY (psf)	TRIM PANEL SURFACE DENSITY kg/m^2	TRIM PANEL SURFACE DENSITY (psf)
●	BUSINESS	1	ALUMINUM	19.6	(4.00)	7.3	(1.50)
▼	BUSINESS	10	ALUMINUM	19.6	(4.00)	1.6	(0.33)
□	BUSINESS	10	COMPOSITE	3.2	(0.67)	1.6	(0.33)
■	NARROW-BODY	10	ALUMINUM	19.6	(4.00)	1.6	(0.33)
○	NARROW-BODY	10	COMPOSITE	4.4	(0.89)	1.6	(0.33)
▲	WIDE-BODY	1	ALUMINUM	19.6	(4.00)	7.3	(1.50)
△	WIDE-BODY	1	COMPOSITE	6.4	(1.30)	7.3	(1.50)
▽	WIDE-BODY	10	COMPOSITE	6.4	(1.30)	1.6	(0.33)
◇	WIDE-BODY	10	ALUMINUM	19.6	(4.00)	1.6	(0.33)

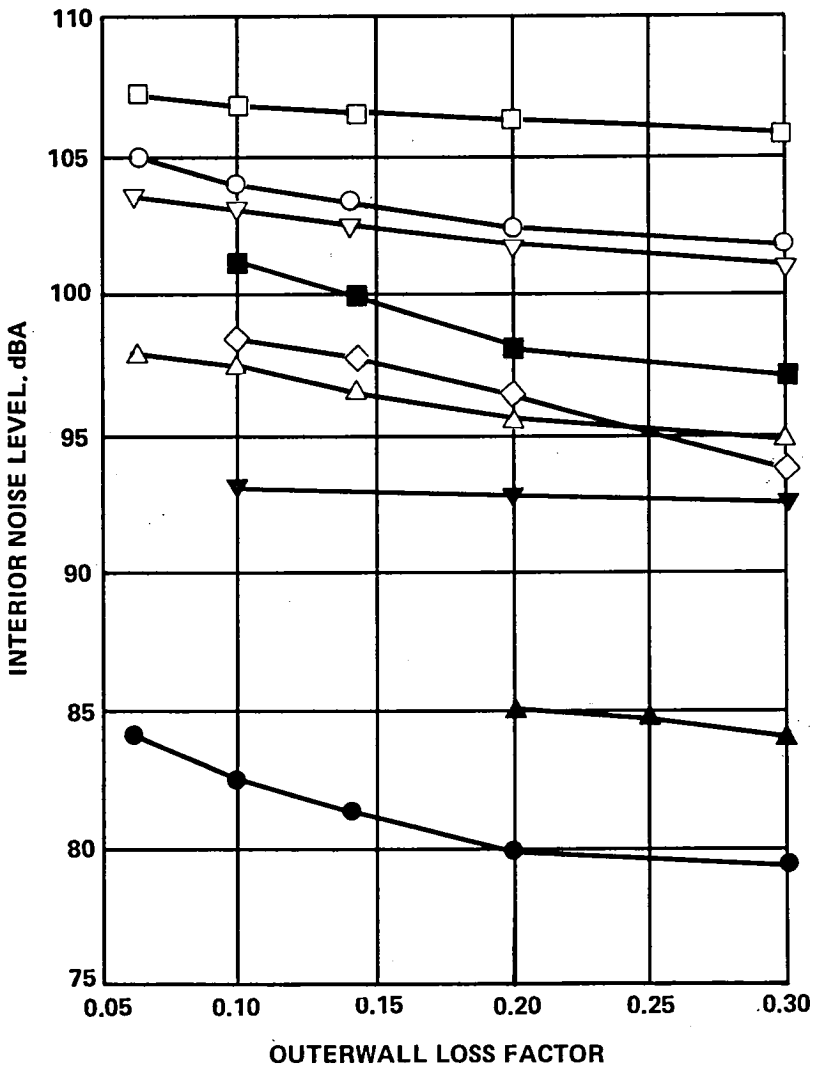

Figure 75. - Damping loss factor parametric studies.

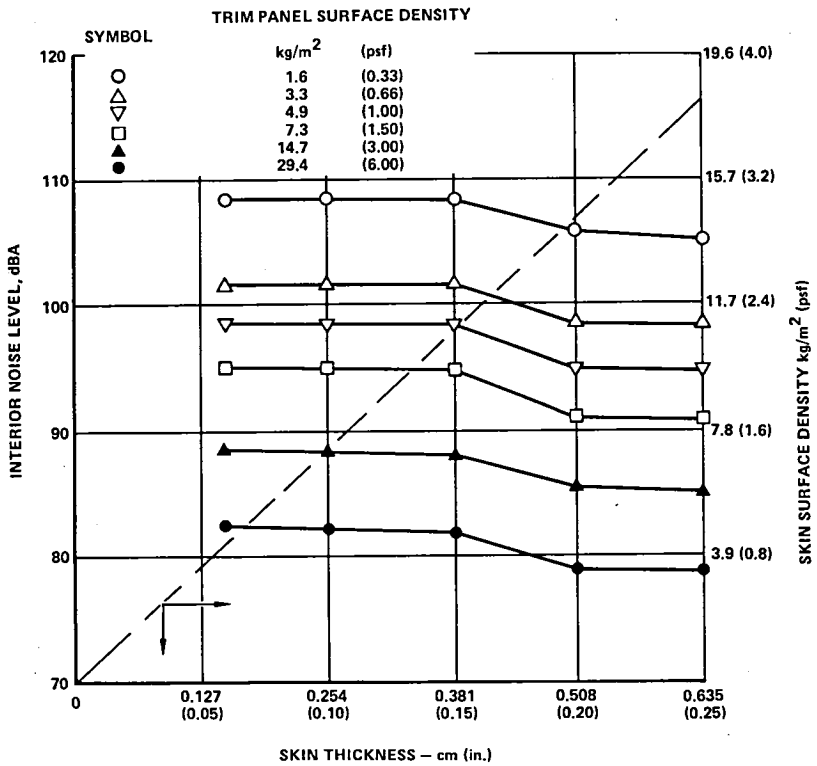

Figure 76. - Wide-body skin thickness parametric studies.

shape can be increased by a redistribution of the mass about the neutral axis. Further increases in stiffness can be achieved without increasing surface density by using a material with a higher Young's modulus. Assuming that a high modulus graphite/epoxy material is suitable and available, then a significant increase in stiffness would be possible with a modest increase outer-wall surface density (see Section 3.2).

It was of interest to investigate the effects of increasing outer-wall moment of inertia without increasing wall surface density. The baseline wide-body aircraft was used for these studies. The moments of inertia of the frames and the stringers were each varied separately without increasing outer-wall surface density and the effect on interior noise is shown in figure 77. Greater interior noise reductions occur when the frame moment of inertia is varied. However, when the I/I (Baseline) ratio exceeds 30, there is little or no effect on interior noise.

Another way of increasing outer-wall stiffness is to increase the modulus of elasticity of the skin and stiffeners. It should be noted that when this is done the speed of sound in the material is changed and the ring frequency shifts according to the relationship.

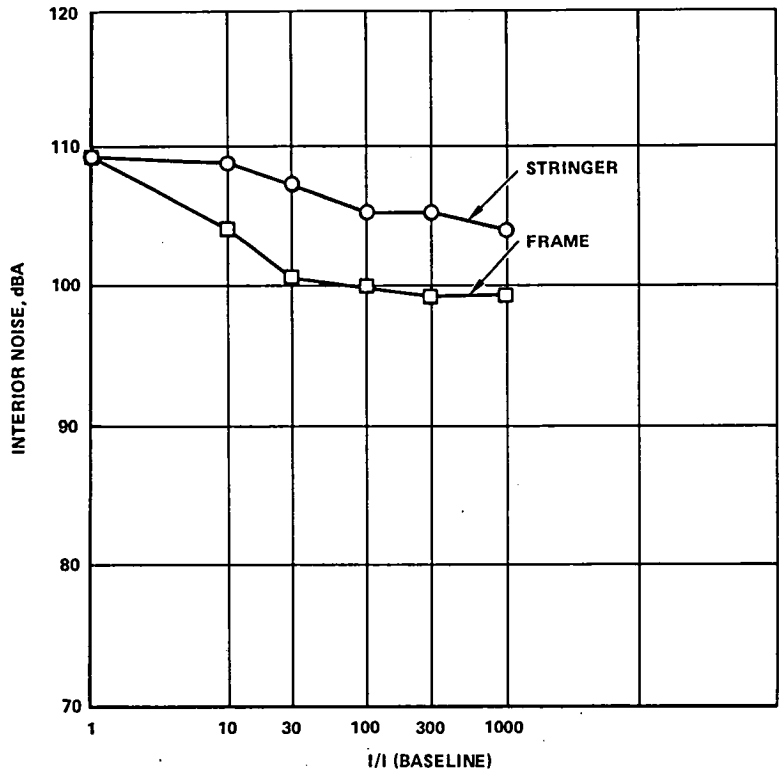

Figure 77. - Baseline aluminum wide-body aircraft frame and stringer stiffness study.

$$f_R = \frac{C_L}{\pi D_f} = \frac{\sqrt{E/\rho}}{\pi D_f}$$

Noise reduction or transmission loss is at or near a minimum in the vicinity of the ring frequency. Therefore, the location of the ring frequency with respect to the propeller fundamental frequency and its harmonics may determine whether the interior noise increases or decreases as modulus of elasticity is increased. Interior noise is shown as a function of modulus of elasticity in figure 78 for the baseline aluminum and baseline composite configurations of each aircraft type. For example, the wide-body configurations benefit from increases in modulus of elasticity within the range of practical values (E/E(BASELINE)) < 30.

These results show that increased stiffness of the stiffeners is somewhat more effective than increases of skin gauge. Appendix H, however, shows a better use of (increased) stiffness in the advanced noise reduction designs, by combining increased stiffness within an optimum double wall design.

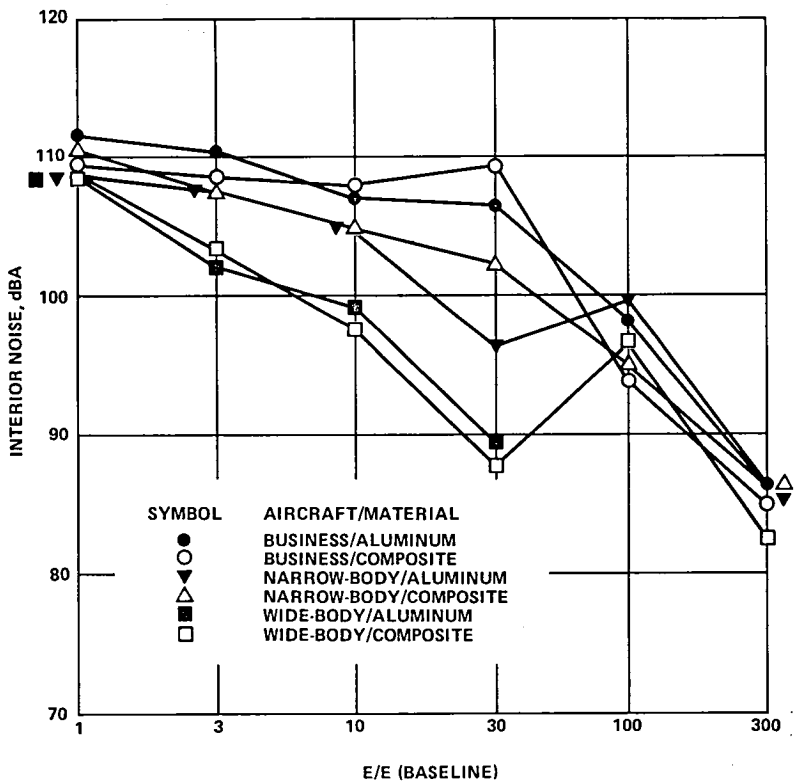

Figure 78. - Baseline aircraft outer-wall modulus parametric study.

G8.3.3 Effect of stiffener spacing.- A convenient means of increasing outer-wall stiffness is to reduce the spacing of the frames and stringers. Analyses of the wide-body aluminum aircraft with outer-wall masses of 19.5 kg/m^3 (4.0 psf) and 29.3 kg/m^3 (6.0 psf) are shown in figure 79 as functions of trim-panel surface density. For this parametric study the loss factor was varied with the outer-wall surface density. The data shown are for Segment 4 and external spectrum number 1. As the stiffener spacing was varied, the density of the skin was changed in order to maintain a constant outer-wall surface density. With baseline stiffener spacings, the 19.5 kg/m^3 (4 psf) and 29.5 kg/m^3 (6 psf) outer-wall results are nearly identical. However, with the reduced frame and stringer spacings the heavier outer-wall results in significantly lower interior noise levels.

Outer-wall stiffness was increased by a factor of three and the stiffener spacing was cut in half for the interior noise predictions shown in figure 80. In contrast to the data shown in figure 79, the wide-body interior noise is essentially unchanged when the stiffener spacing is reduced. However, the narrowbody and business aircraft show significantly lower interior noise when stiffener spacing is reduced with an E/E (baseline) ratio of 3. These results are probably due to the smaller skin panel that results when the stiffener spacing is reduced.

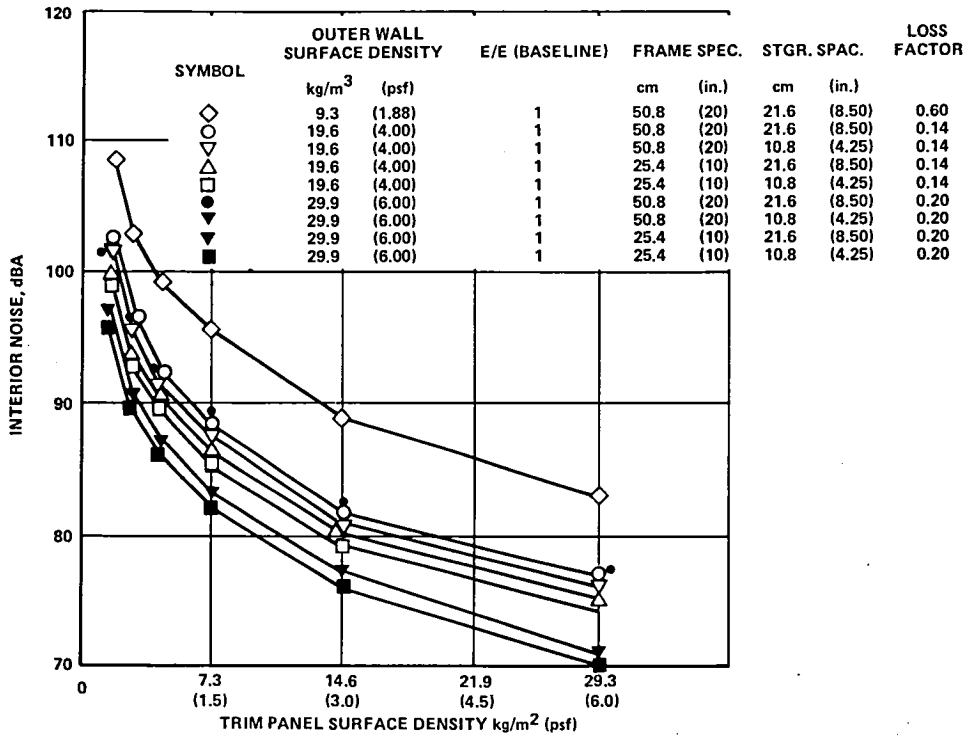

Figure 79. - Stiffener spacing study; segment 4 and external spectrum 1 - wide-body aluminum.

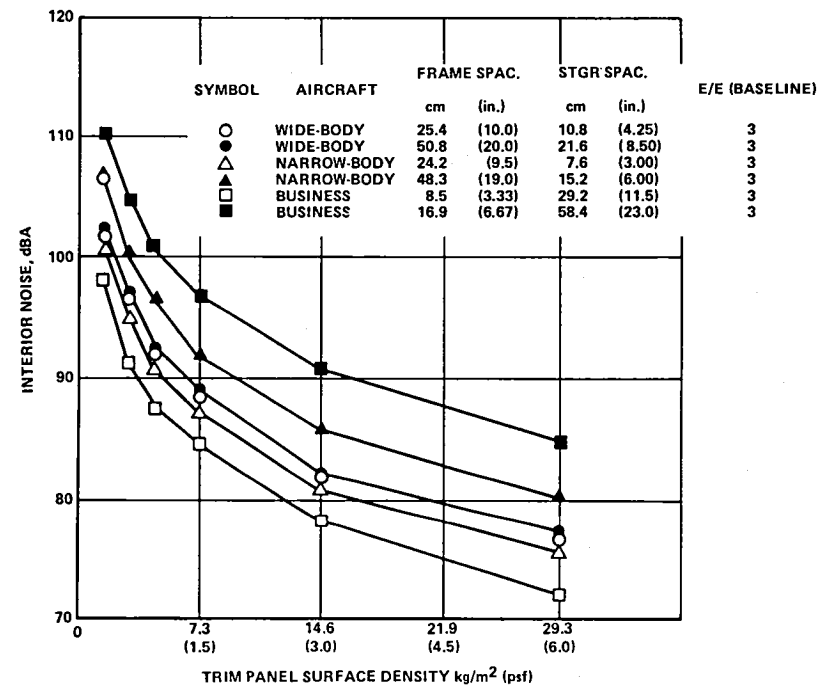

Figure 80. Stiffener spacing study - wide-body, narrow-body and business aircraft; segment 4 and external spectrum 1.

Figures 79 and 80 also illustrate that variations of the trim-panel surface density have a powerful effect in conjunction with outer walls, which have been stiffened by means of reduced spacing between the stiffeners. This effect is further exploited in Appendix H in the study of advanced noise reduction designs.

G8.4 Effects of Fiberglass Blankets

The add-on noise-reduction configurations assumed that an optimized fiberglass blanket would be identified. Three parameters were of particular interest for the optimization study; 1) blanket density, 2) blanket thickness, and 3) fiber diameter. Using the baseline wide-body aluminum aircraft configuration, a parametric study was performed to identify the optimum blanket configuration. The data from this study are shown in figure 81. From these data it was concluded that:

- A density of 9.6 kg/m^3 (0.6 PCF) is optimum for the heavier trim while 38.4 kg/m^3 (2.4 PCF) is optimum for the baseline trim
- A 7.6 cm (3.0 in.) thick blanket is optimum
- A blanket fabricated from "B" fibers is optimum.

The conclusion that filling half the wall space with fiberglass is the optimum thickness was derived from these data and used for all subsequent configuration studies.

As regards the fiber size effect, the nominal diameter of B-type fiber is much larger (3.81 μm (150 μin)) than that of the AA fiber (1.27 μm (50 μin.) diameter)). Viscosity losses therefore begin at a lower frequency for the B-type fiber and yield a net advantage of about 2.5 dBA compared to AA fiber results for most of the configurations analyzed in the present study. Above 600 Hz, the AA-type fiber gives better performance which partly explains its wide use in turbofan aircraft, where boundary layer noise transmission is the dominant source of interior noise.

G8.5 Effects of Wall Space Depth

An important consideration in the acoustical design of an aircraft fuselage is the amount of space provided between the interior trim panel and the exterior skin. In order to provide an increased wall depth for acoustical purposes one can either reduce the interior space or increase the diameter of the fuselage. Neither of these alternatives is desirable unless the acoustical benefit is substantial. Therefore, a study of the relationship between interior noise and wall depth was performed for each aircraft type. Data will be shown for Segment 4 and external spectrum number 1 - similar data exist for other segments and spectra.

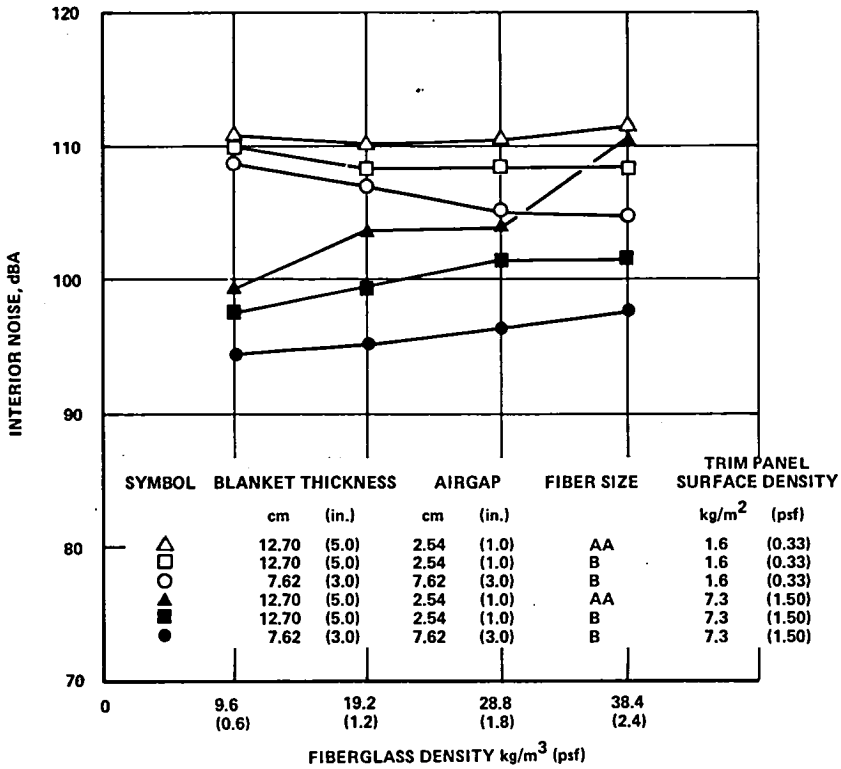

Figure 81. - Fiberglass blanket optimization - wide-body aluminum aircraft.

The baseline wide-body aircraft results are shown in figure 82. There is little benefit derived by increasing wall depth from 15.2 cm (6 in.) to 22.9 cm (9 in.). Figure 83 includes the results for a heavy outer-wall and shows the curious result that increasing wall depth to 30.5 cm (12 in.) is counter-productive. The narrow-body aircraft was analyzed with a 7.6 cm (3 in.) and 15.2 cm (6 in.) wall depth and the business aircraft with a 5.1 cm (2 in.) and 10.2 cm (4 in.) wall depth--the results are shown in figures 84 and 85, respectively. For the narrow-body, reducing the wall depth to a more conventional depth of 7.6 cm (3.0 in.) would entail a significant mass penalty relative to the baseline spacing of 15.2 cm (6 in.). The increased outer-wall diameter to accommodate a 15.2 cm (6 in.) wall depth would result in about a 1.5 percent drag increase and an estimated 68 kg (151 lb) increase of the baseline shell mass. These penalties would more than offset the estimated 1,000 pounds in treatment mass which would be saved by selecting the deeper wall, based on the above approximate calculation.

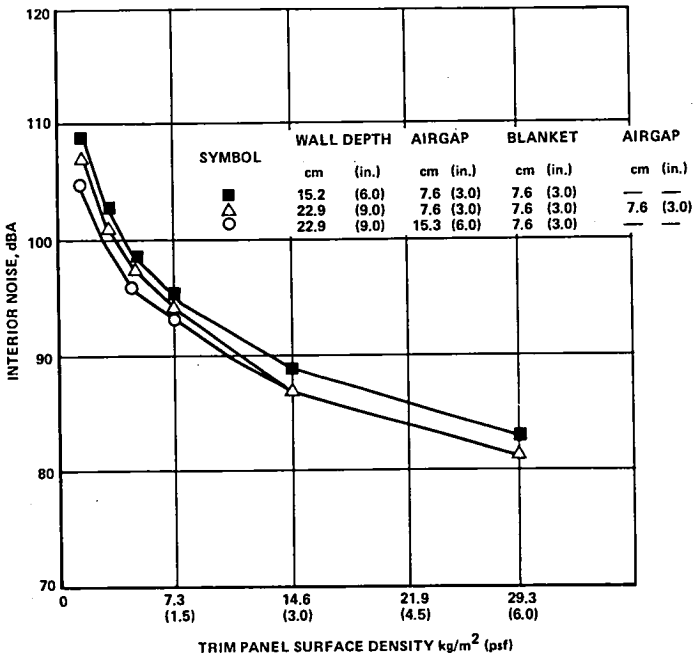

Figure 82. - Wall depth study - baseline wide-body aluminum aircraft.

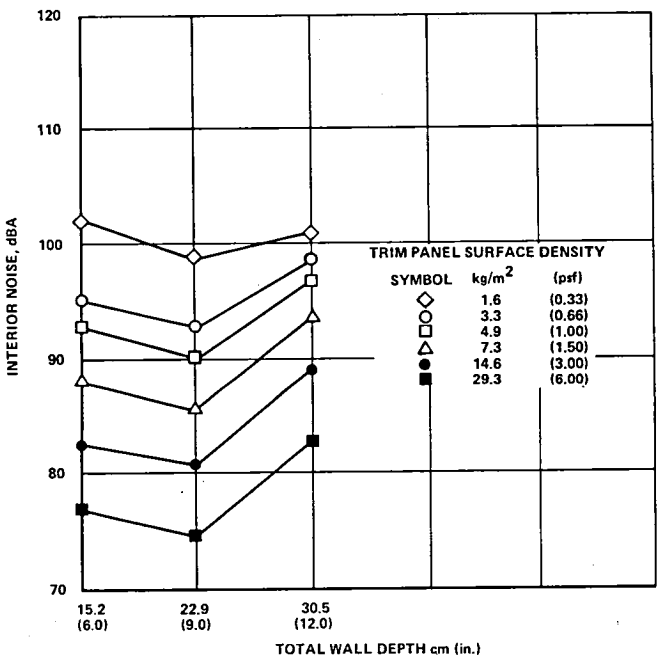

Figure 83. - Wall depth study - wide-body aluminum aircraft with 19.5 kg/m^3 (4.0 psf) outer wall surface density and 0.14 loss factor.

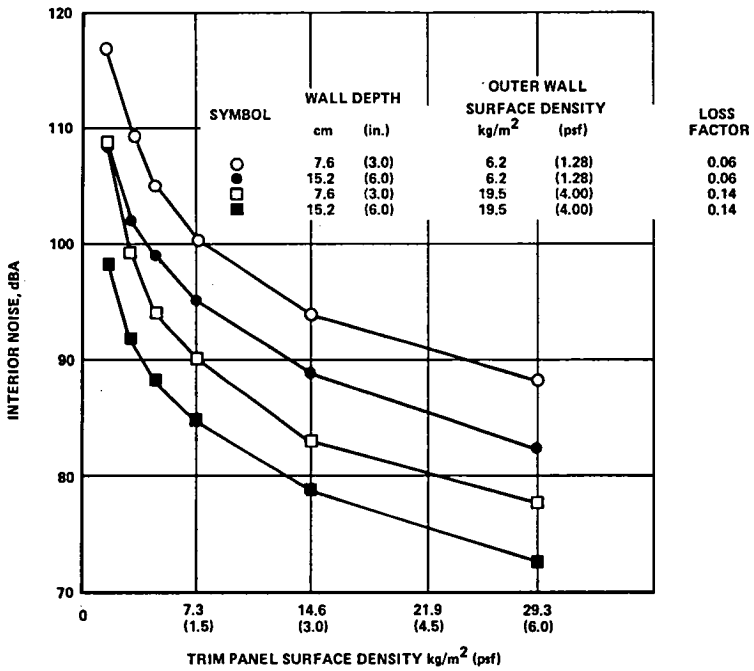

Figure 84. - Wall depth study - narrow-body aluminum aircraft.

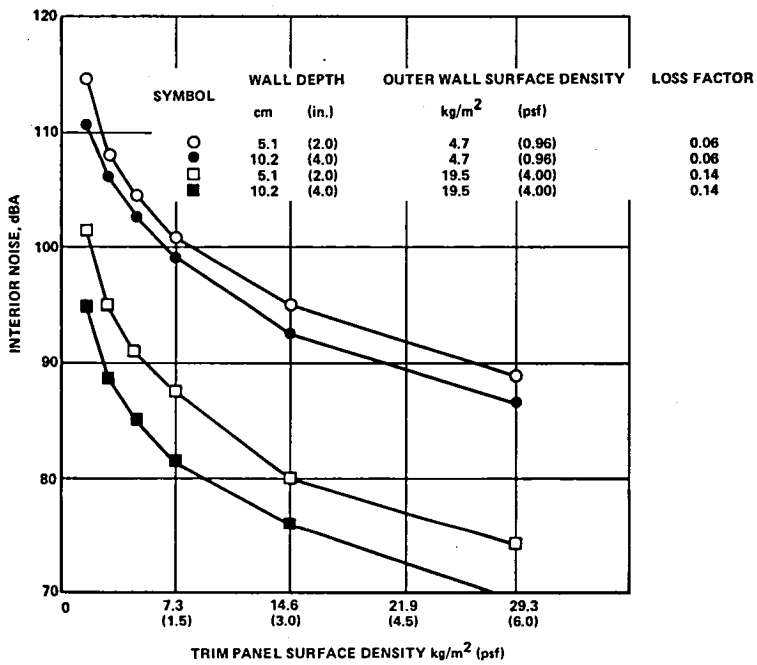

Figure 85. - Wall depth study - aluminum business aircraft.

G8.6 Effects of Midwall Septa

A convenient means of increasing sidewall transmission loss is by the addition of an intermediate limp wall placed between the trim panel and the outer wall. The configuration analyzed for all three aircraft had the septum inboard of the fiberglass blanket, midway between the trim panel and the outer wall. Data are shown in figure 86 for Segment 4 and external spectrum number 1 for the baseline trim panel and a 14.6 kg/m^2 (3 psf) trim panel. Similar data exist for other segments, spectra and trim panel surface densities; however, the data presented are representative of the larger body of data. The dynamics of a multilayered wall configuration are demonstrated as septum surface density is varied. Trends for the wide-body and narrow-body aircraft are nearly identical while the business aircraft data varied considerably. The results generally show that inclusion of a septum is not an efficient tool for propeller noise reduction. The effect of a midwall septum is essentially equivalent to reducing the wall space depth by one-half within a double-wall configuration and is therefore counterproductive. This is illustrated by figure 87 where configurations with a septum at best only approach the performance of an equivalent weight double-wall configuration without a septum.

G8.7 Effect of Propeller Harmonic Content

A peak overall sound pressure level (OASPL) of 134 dB was selected from the Hamilton Standard test data supplied in Reference 5. Three different spectra, all with the same OASPL, were used in the analysis of each aircraft configuration. The harmonic content of each spectrum is shown in figure 13. While spectrum number 1 is the most realistic, the other spectra are of interest in order to determine the sensitivity of interior noise to propfan harmonic content. The relationship between interior noise and propfan harmonic spectrum is shown in figure 88 for a few configurations of each aircraft type. These data were selected as being representative of the analytical study results. The differences between spectra numbers 1 and 2, although substantial, had little effect on interior noise. This can be understood by noting the small difference in the amplitudes at the fundamental frequency and next two harmonics. When spectrum number 3 (flat weighted) was used the interior noise was several dB lower than it was for spectra numbers 1 and 2-approximately the same as the difference in the amplitude at the fundamental frequency.

G8.8 Modal Convergence Study

Interior noise is a function of the number of circumferential cylinder modes that are considered in the analysis. When a sufficient number of modes have been considered, the consideration of additional higher order modes has a negligible effect on interior noise. This effect is shown in figure 89 for Segment 4 of the wide-body aluminum aircraft. The solution has converged

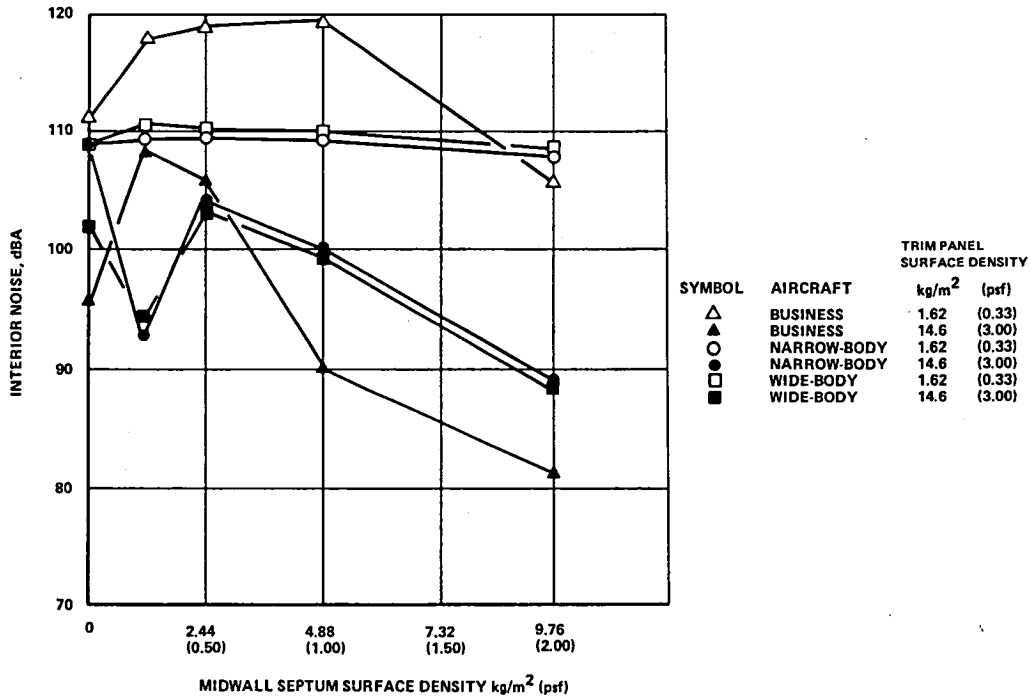

Figure 86. - Midwall septum study - baseline aircraft configurations.

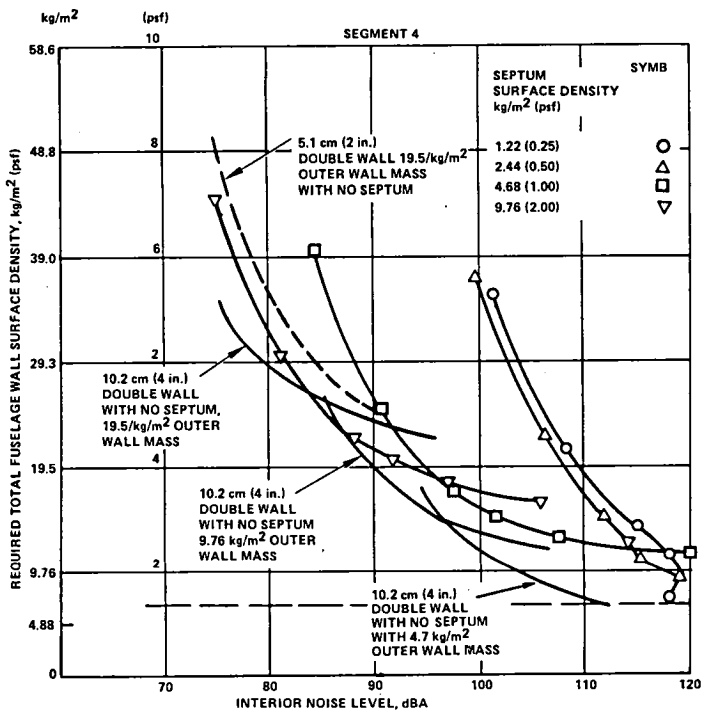

Figure 87. - Double-wall/septum study for business aircraft, segment 4 (peak noise region).

SYMBOL	AIRCRAFT	OUTER WALL SURFACE DENSITY kg/m^2	(psf)	LOSS FACTOR	TRIM PANEL SURFACE DENSITY kg/m^2	(psf)
□	WIDE-BODY BASELINE	9.2	(1.88)	0.06	1.63	(0.33)
■	WIDE-BODY	19.5	(4.00)	0.14	1.63	(0.33)
◇	WIDE-BODY	19.5	(4.00)	0.14	14.6	(3.00)
○	NARROW-BODY BASELINE	6.3	(12.8)	0.06	1.63	(0.33)
●	NARROW-BODY	19.5	(4.00)	0.14	1.63	(0.33)
⌂	NARROW-BODY	19.5	(4.00)	0.14	14.6	(3.00)
△	BUSINESS BASELINE	4.7	(0.96)	0.06	1.63	(0.33)
▲	BUSINESS	19.5	(4.00)	0.14	1.63	(0.33)
◆	BUSINESS	19.5	(4.00)	0.14	14.6	(3.00)

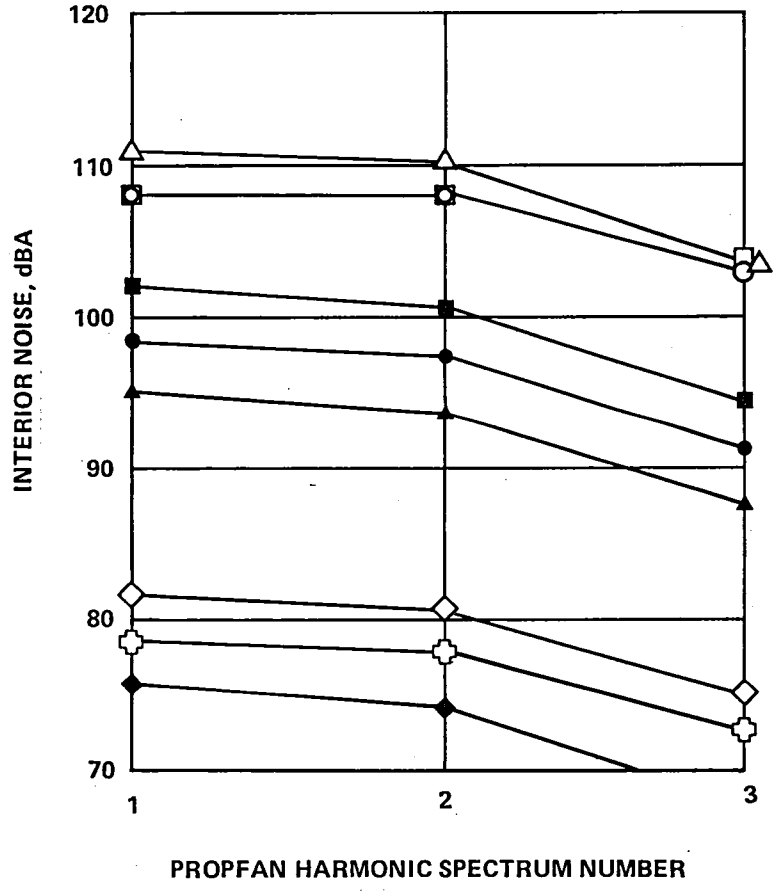

Figure 88. - Effect of propfan harmonics.

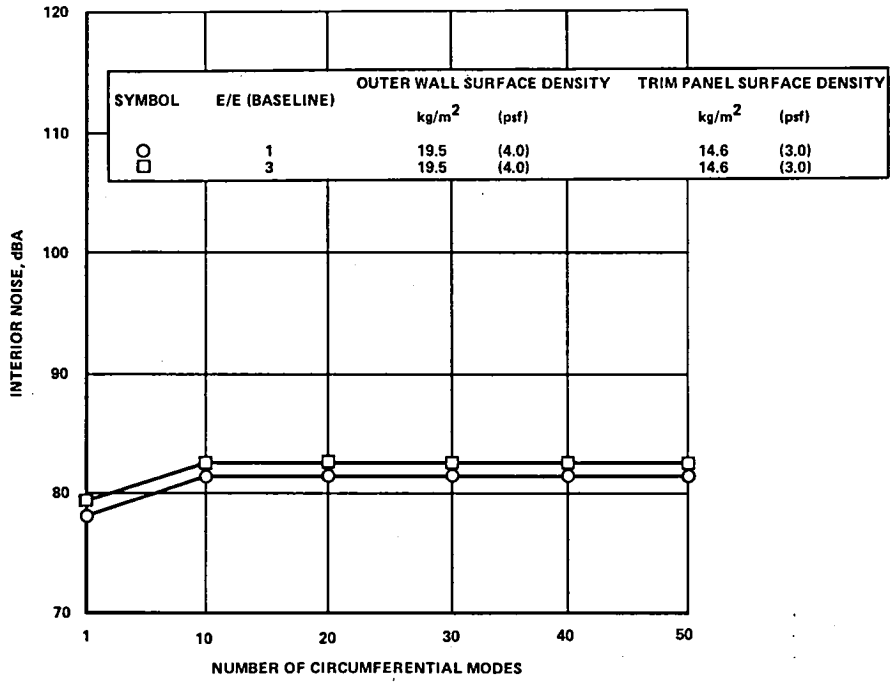

Figure 89. - Convergence of Fourier-Bessel function series solution for wide-body segment 4.

at or before 10 modes — well below the number considered in the Lockheed computer program. The criteria established for the Lockheed analysis was that a sufficient number of modes had been considered when the contribution from a given mode was 100 dB less than that from all the lower order modes.

APPENDIX H
PARAMETRIC STUDY RESULTS FOR ADVANCED NOISE-REDUCTION DESIGNS

H1. DATA PRESENTATION

Figures 4 and 5 of Section 3.2 describe the estimated variation of required outer-wall surface density versus stiffness level when the outer wall is deliberately stiffened. In order to obtain the minimum total wall surface density required to achieve a given interior noise level, it is necessary to vary the trim panel surface density for each combination of outer-wall surface density and outer-wall stiffness level. Results of such calculations are described below.

Figures 90 through 97 show the required total surface density in Segment 4 to achieve a given interior noise level for each of the three aircraft sizes. Figures 90, 92, 94 and 96 show results for advanced aluminum structures at stiffness levels ranging from 3 to 20 times the baseline stiffness. Figures 91, 93, 95 and 97 show results for advanced orthogrid/composite fuselage designs with stiffness levels ranging from 3 to 20 times baseline stiffness. It will be recalled that the baseline composite structure has the same stiffness level as the aluminum baseline structure but is only 70% as heavy.

Figures 90 through 97 also show the effects of varying the relative stiffener spacings, $\bar{\ell}_x = \ell_x/\ell_{x\ \text{Baseline}}$, of the rings and $\bar{\ell}_y = \ell_y/\ell_{y\ \text{Baseline}}$ of the stringers. The data shown are the underlying basis of the optimum advanced noise-reduction designs which are described in Appendix I, and for which acoustical treatment penalty mass data are given in Section 3.2. Each figure also shows results for the add-on noise-reduction design to provide a basis for comparison. In the present studies of high stiffness outer-wall designs, the damping loss factor is maintained at its baseline value of 6 percent, despite the increased outer-wall mass, on grounds that the stiffening material added to the outer wall in this case is not a viscoelastic material. The following is a brief summary of the trends.

H2. DISCUSSION OF RESULTS FOR ADVANCED ALUMINUM DESIGNS

For the wide-body, Figure 90 shows that the optimum configuration when adjusted to the local exterior noise level is one having three to five times the baseline stiffness and retaining the baseline stiffener spacing, $\bar{\ell}_x = 1$. For interior noise levels below 80 dBA, a relative stiffness level of six at one-half stiffener spacing ($\bar{\ell}_x = \bar{\ell}_y = 0.5$) would be competitive. By comparing Figure 90 with Figure 57 of Appendix G, it is apparent that best results are obtained for interior noise levels above 95 dBA by retaining the baseline outer-wall stiffness and mass, but with increased trim-panel mass.

For the narrow-body, figure 92 shows that the lowest total surface density is required when the relative stiffness level $\bar{E}$ is six with one-half

of the baseline stiffener spacing. The narrow-body does not show any benefit of stiffening unless the stiffener spacing is reduced - compare figure 92 with figure 60 of Appendix G. It is seen that for an interior noise design level above 90 dBA, or for a 10-dB reduction of the exterior noise, it is best to retain the baseline outer-wall properties and put all of the treatment mass into the trim panel.

Figures 94 and 96 show results for the advanced aluminum business aircraft. These results illustrate another interesting feature; namely, that both the stringer and ring spacing must be reduced to obtain results better than the add-on design. The curves marked $\bar{\ell}_x = 1$ and $\bar{\ell}_y = 0.5$ denote reduction of stringer spacing but not the ring spacing. Results for the case of one-half stiffener spacing for both the rings ($\bar{\ell}_x = 0.5$) and stringers ($\bar{\ell}_y = 0.5$) at six times stiffness are the only advanced aluminum results which are better than the add-on results. An alternative design retaining the baseline frame spacing but having 0.25 times the baseline stringer spacing has performance slightly worse than the "add-on" design at 80 dBA. By comparing figures 94 and 96 with figure 62 of Appendix G, it is seen that the stiff aluminum design is better than the add-on design in a limited range of 75 to 95 dBA.

One reason for obtaining somewhat poorer results for the stiffened business aircraft can be seen by comparing figures 4 and 5 of Section 5, where it is clear that stiffening the business aircraft with aluminum requires a higher outer-wall mass ratio than is the case for the wide-body and narrow-body designs. It is also noted that the original business aircraft design calls for fewer longerons of greater cross-sectional area for the purpose of reducing the number of parts, and hence to achieve a lower manufacturing cost while maintaining the same axial load carrying capacity. This baseline design concept is not, however, helpful to the present stiffened outer-wall noise-control approach.

H3. DISCUSSION OF RESULTS FOR ADVANCED COMPOSITE/ORTHOGRID DESIGNS

Figure 91 shows results for the wide-body aircraft. The optimun relative stiffness level appears to be $\bar{E} = 6$ with one-half of the baseline stiffener spacing. Comparison with figure 57 of Appendix G shows that the present high stiffness designs are lighter that the strength-designed composite designs when the interior noise levels are required to be below 102 dBA.

For the narrow-body, figure 93 shows that the optimum stiffness level is $\bar{E} = 10$ with one-half of the baseline spacing of the stiffeners. It also appears that $\bar{E} = 20$ with one-half stiffener spacing would be optimum if additional noise reduction was required. The advanced designs are more efficient than the strength-designed composite structures for interior noise design objectives below 102 dBA based on comparison of figure 60 of Appendix G with figure 93.

Figures 95 and 97 show for the business aircraft that the best design is one with one-half of the baseline spacing of both the rings and the stringers, with six to ten times baseline stiffness level, depending on the local external noise level. Results for the configuration having four times the baseline number of stringers are not quite as good, but are still considerably better than the add-on design. Comparison with figure 62 of Appendix G shows that the family of advanced designs is superior to the strength-designed composite structural designs below 102 dBA.

The business aircraft case studies are interesting in the comparison of advanced aluminum and advanced composite results. The use of composite materials allows significant mass penalty savings for almost all of the reduced stiffener spacing cases in figure 97; however, for the advanced aluminum design (figure 96), there is only one clearly advantageous design among those investigated.

H4. GENERAL COMMENT ON ADVANCED ULTRA-STIFF DESIGNS

The results shown herein are promising but display some sensitivity to stiffener spacing and the variation of outer-wall mass versus stiffness; therefore, pending further esperimental verification of the theory and further studies based on discrete stiffener theory, the reader should regard the potential penalty mass savings for such advanced designs with some caution. It appears analytically that the structure can be "tuned" to give either better or worse results by adjusting the outer-wall structural properties and stiffener spacing.

High-stiffness advanced designs appear to be advantageous when the required noise reduction exceeds the noise reduction provided by the baseline structure by more than 10 dBA. For smaller noise reductions, the best investment of the penalty mass is to increase the trim-panel mass while retaining the baseline levels of outer-wall mass and stiffness.

CONCEPT	SYMBOL	$\bar{E}$	$\bar{\ell}_x$	$\bar{\ell}_y$	σ_1 kg/m^2	σ_1 (psf)	η
ADD-ON	○	1	1.0	1.0	19.5	(4.0)	0.14
ADVANCED DESIGN	□	3	1.0	1.0	12.0	(2.45)	0.06
	■	6	0.5	0.5	17.7	(3.63)	
	△	5	1.0	1.0	15.6	(3.20)	
	▲	10	0.5	0.5	23.1	(4.74)	
	◇	10	1.0	1.0	30.4	(6.22)	
	◆	20	0.5	0.5	44.9	(9.21)	

NOTES: ℓ_x = RING SPACING; $\bar{\ell}_x = \ell_x/\ell_x$ BASELINE
ℓ_y = STRINGER SPACING; $\bar{\ell}_y = \ell_y/\ell_y$ BASELINE
$\bar{E}$ = $(EI)/(EI)_{BASELINE}$
σ_1 = OUTER WALL SURFACE DENSITY
η = DAMPING LOSS FACTOR

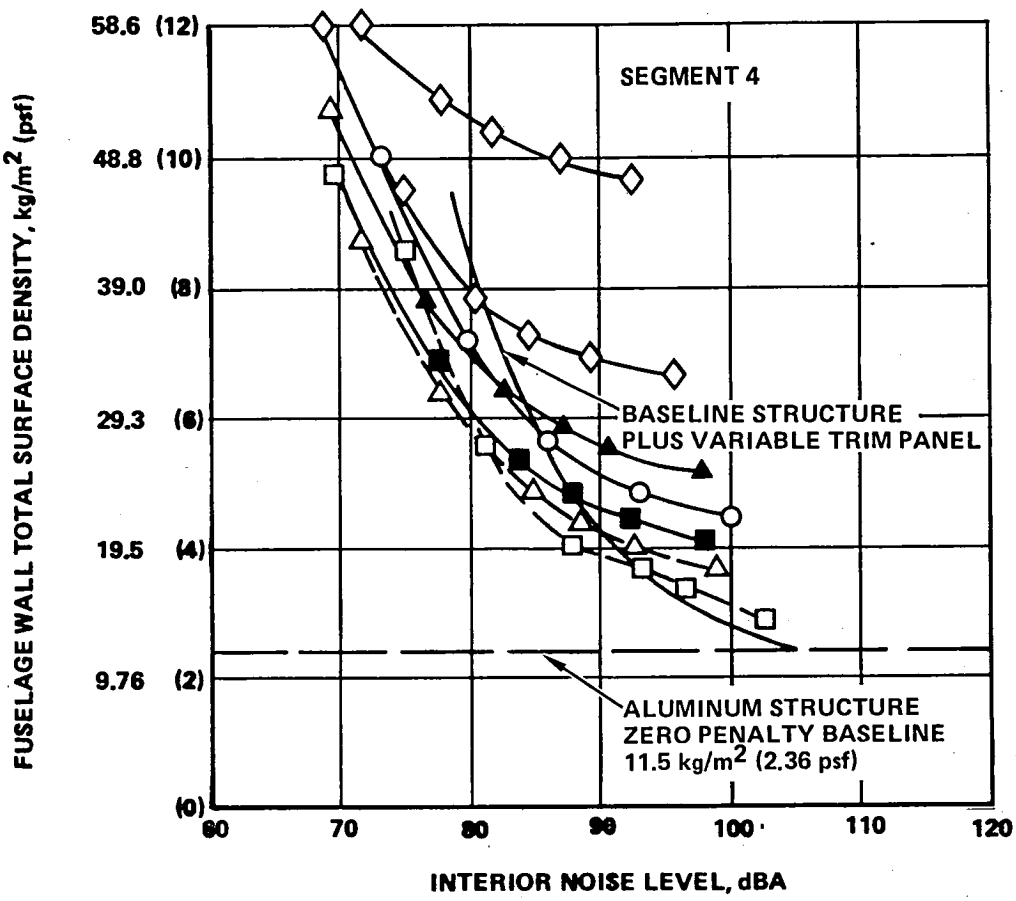

Figure 90. - Comparison of wide-body advanced aluminum vs. add-on noise control; outer-wall mass and stiffness effects.

CONCEPT	SYMBOL	$\bar{E}$	$\bar{\ell}_x$	$\bar{\ell}_y$	σ_1 kg/m^2	σ_1 (psf)	η
ADD-ON	○	1	1.0	1.0	19.5	(4.0)	0.14
ADVANCED DESIGN	□	3	1.0	1.0	7.0	(1.44)	0.06
↓	■	6	0.5	0.5	10.4	(2.13)	↓
	△	5	1.0	1.0	8.0	(1.64)	
	▲	10	0.5	0.5	11.8	(2.42)	
	◇	10	1.0	1.0	11.5	(2.35)	
	◆	20	0.5	0.5	17.0	(3.48)	

NOTES:
- ℓ_x = RING SPACING, $\bar{\ell}_x = \ell_x/\ell_{x\ \text{BASELINE}}$
- ℓ_y = STRINGER SPACING, $\bar{\ell}_y = \ell_y/\ell_{y\ \text{BASELINE}}$
- $\bar{E}$ = $(EI)/(EI)_{\text{BASELINE}}$
- σ_1 = OUTER WALL SURFACE DENSITY
- η = DAMPING LOSS FACTOR

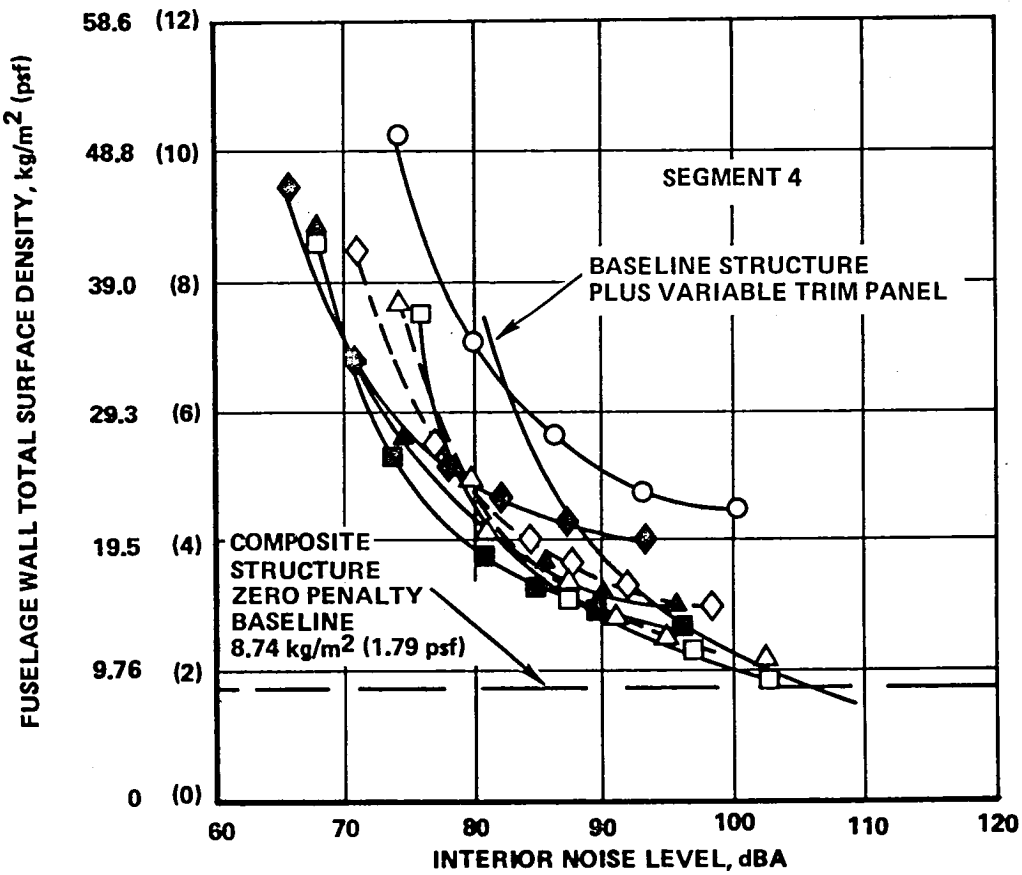

Figure 91. Comparison of wide-body advanced composite vs. add-on noise control; outer-wall mass and stiffness effects.

CONCEPT	SYMBOL	$\bar{E}$	$\bar{\ell}_x$	$\bar{\ell}_y$	σ_1 kg/m^2	(psf)	η
ADD-ON	○	1	1.0	1.0	19.5	(4.0)	0.14
ADVANCED DESIGN	□	3	1.0	1.0	8.4	(1.73)	0.06
	■	6	0.5	0.5	12.6	(2.58)	
	△	5	1.0	1.0	11.1	(2.27)	
	▲	10	0.5	0.5	16.5	(3.38)	
	◇	10	1.0	1.0	17.8	(3.65)	
	◆	20	0.5	0.5	26.6	(5.45)	

NOTES: ℓ_x = RING SPACING $\bar{\ell}_x = \ell_x/\ell_{x\ \text{BASELINE}}$
ℓ_y = STRINGER SPACING $\bar{\ell}_y = \ell_y/\ell_{y\ \text{BASELINE}}$
$\bar{E}$ = $(EI)/(EI)_{\text{BASELINE}}$
σ_1 = OUTER WALL SURFACE DENSITY
η = DAMPING LOSS FACTOR

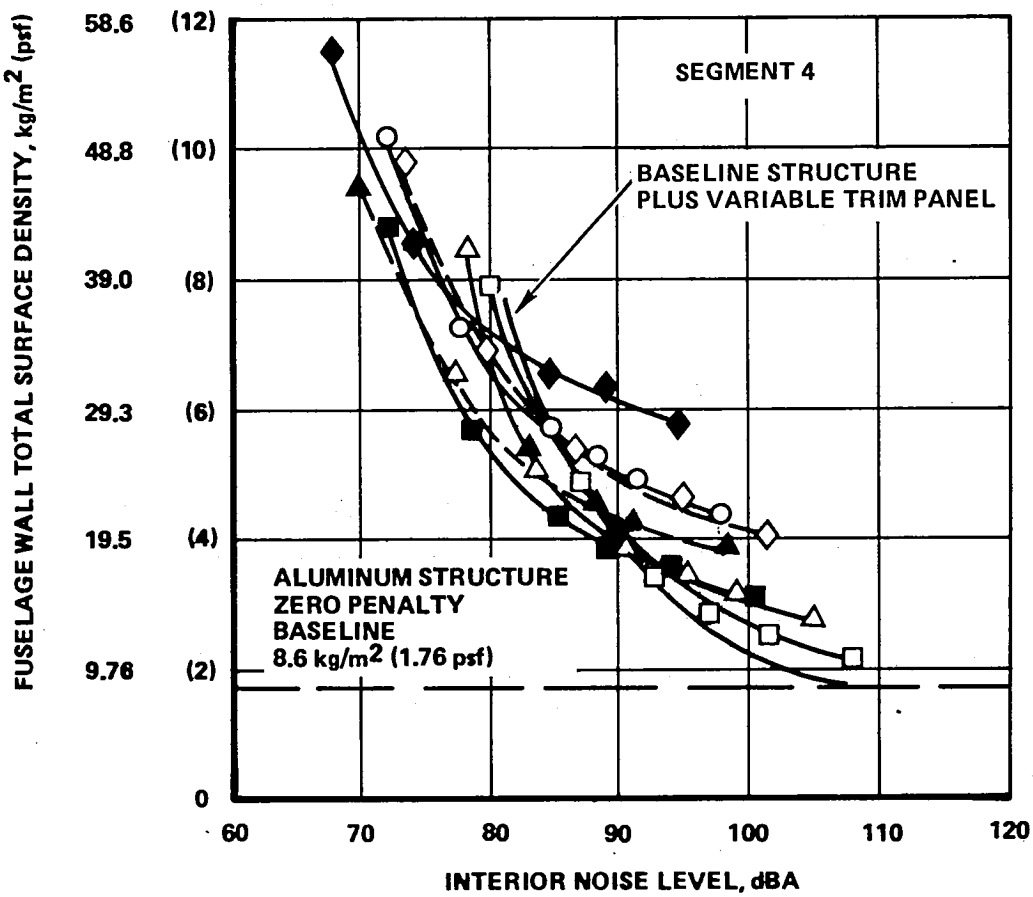

Figure 92. - Comparison of narrow-body advanced aluminum vs. add-on noise control; outer-wall mass, and stiffness effects.

CONCEPT	SYMBOL	$\bar{E}$	$\bar{\ell}_x$	$\bar{\ell}_y$	σ_1 kg/m^2	σ_1 (psf)	η
ADD-ON	○	1	1.0	1.0	19.5	(4.0)	0.14
ADVANCED	□	3	1.0	1.0	5.22	(1.07)	0.06
↓	■	6	0.5	0.5	7.76	(1.59)	↓
	△	5	1.0	1.0	6.00	(1.23)	
	▲	10	0.5	0.5	8.98	(1.84)	
	◇	10	1.0	1.0	8.49	(1.74)	
	◆	20	0.5	0.5	17.8	(3.65)	

NOTES:
- ℓ_x = RING SPACING; $\bar{\ell}_x = \ell_x/\ell_{x\ \text{BASELINE}}$
- ℓ_y = STRINGER SPACING; $\bar{\ell}_y = \ell_y/\ell_{y\ \text{BASELINE}}$
- $\bar{E}$ = $(EI)/(EI)_{\text{BASELINE}}$
- σ_1 = OUTER WALL SURFACE DENSITY
- η = DAMPING LOSS FACTOR

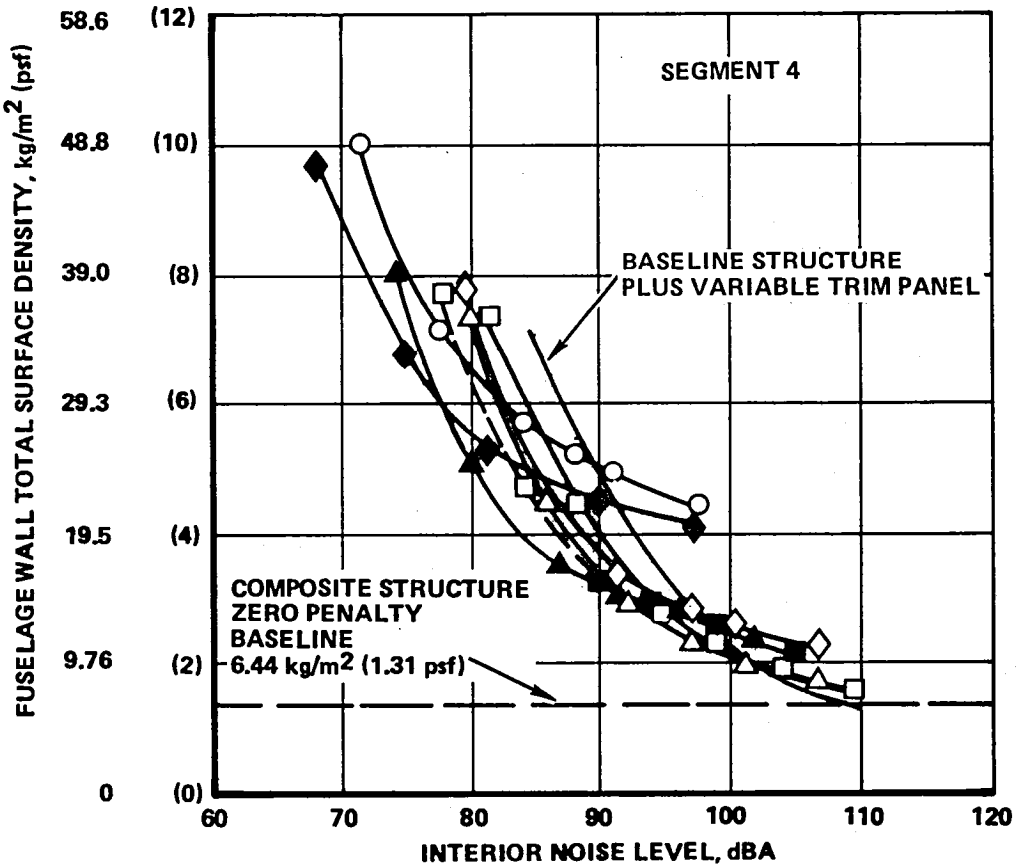

Figure 93. - Comparison of narrow-body advanced composite vs. add-on noise control; outer-wall mass and stiffness effects.

CONCEPT	SYMBOL	$\bar{E}_x, \bar{E}_y$	$\bar{\ell}_x$	$\bar{\ell}_y$	σ_1 kg/m^2	σ_1 (psf)	η
ADD-ON	○	1, 1	1.0	1.0	19.5	(4.0)	0.14
ADVANCED ↓	□	3, 3	1.0	1.0	8.05	(1.65)	0.06
	■	3, 6	1.0	0.5	9.66	(1.98)	↓
	×	6, 6	0.5	0.5	12.3	(2.52)	
	▽	3, 12	1.0	0.25	13.0	(2.66)	
	△	5, 5	1.0	1.0	12.8	(2.62)	
	▲	5, 10	1.0	0.5	14.8	(3.04)	
	◇	10, 10	1.0	1.0	27.0	(5.53)	
	◆	10, 20	1.0	0.5	32.5	(6.65)	

NOTES:
- ℓ_x = RING SPACING $\bar{\ell}_x = \ell_x/\ell_x$ BASELINE
- ℓ_y = STRINGER SPACING $\bar{\ell}_y = \ell_y/\ell_y$ BASELINE
- $\bar{E}_x, \bar{E}_y$ = (EI)/(EI) BASELINE IN x AND y DIRECTIONS
- σ_1 = OUTER WALL SURFACE DENSITY
- η = DAMPING LOSS FACTOR

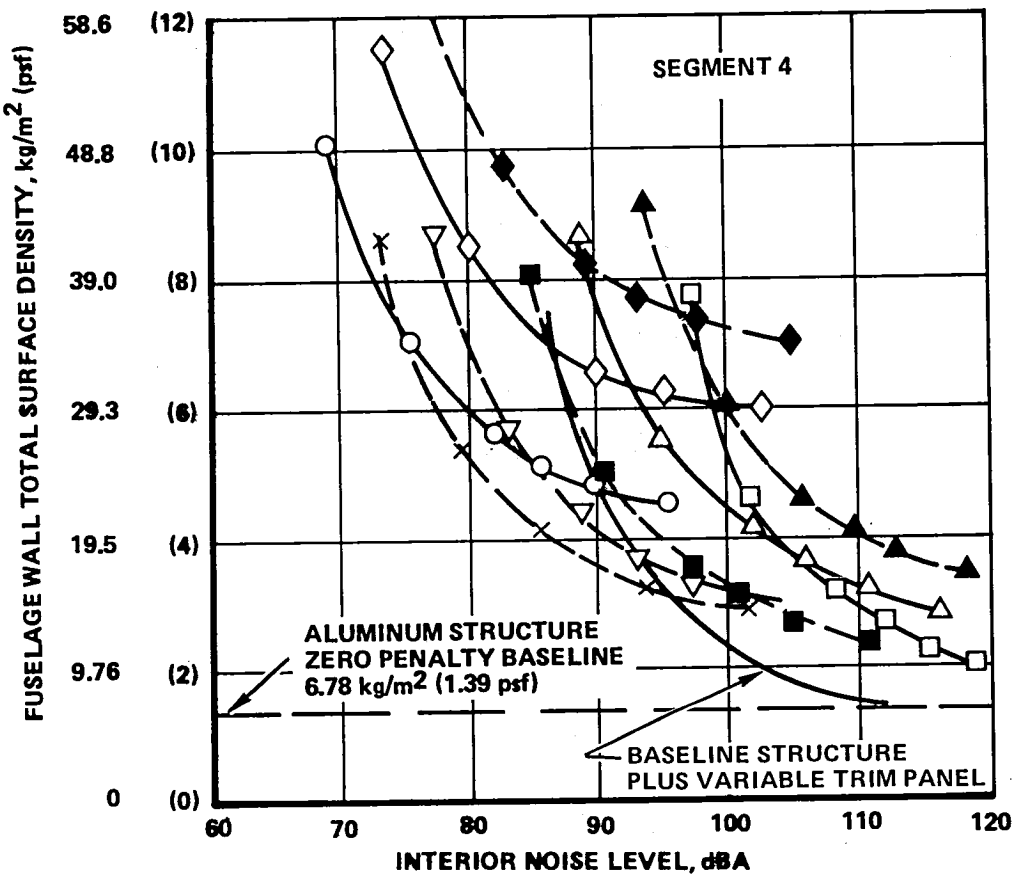

Figure 94.- Comparison of business aircraft advanced aluminum vs. add-on noise control; outer-wall mass and stiffness effects.

CONCEPT	SYMBOL	$\bar{E}_x, \bar{E}_y$	$\bar{\ell}_x$	$\bar{\ell}_y$	σ_1 kg/m^2	σ_1 (psf)	η
ADD-ON	○	1, 1	1.0	1.0	19.5	(4.0)	0.14
ADVANCED	□	3, 3	1.0	1.0	4.29	(0.88)	0.06
↓	▽	3, 12	1.0	0.25	6.88	(1.41)	↓
	■	3, 6	1.0	0.5	5.12	(1.05)	
	×	6, 6	0.5	0.5	6.49	(1.33)	
	△	5, 5	1.0	1.0	5.27	(1.08)	
	▲	5, 10	1.0	0.5	6.34	(1.30)	
	◇	10, 10	1.0	1.0	7.91	(1.62)	
	◆	10, 20	1.0	0.5	9.47	(1.94)	

NOTES:
- ℓ_x = RING SPACING; $\bar{\ell}_x = \ell_x/\ell_{x\ \text{BASELINE}}$
- ℓ_y = STRINGER SPACING; $\bar{\ell}_y = \ell_y/\ell_{y\ \text{BASELINE}}$
- $\bar{E}$ = $(EI)/(EI)_{\text{BASELINE}}$
- σ_1 = OUTER WALL SURFACE DENSITY
- η = DAMPING LOSS FACTOR

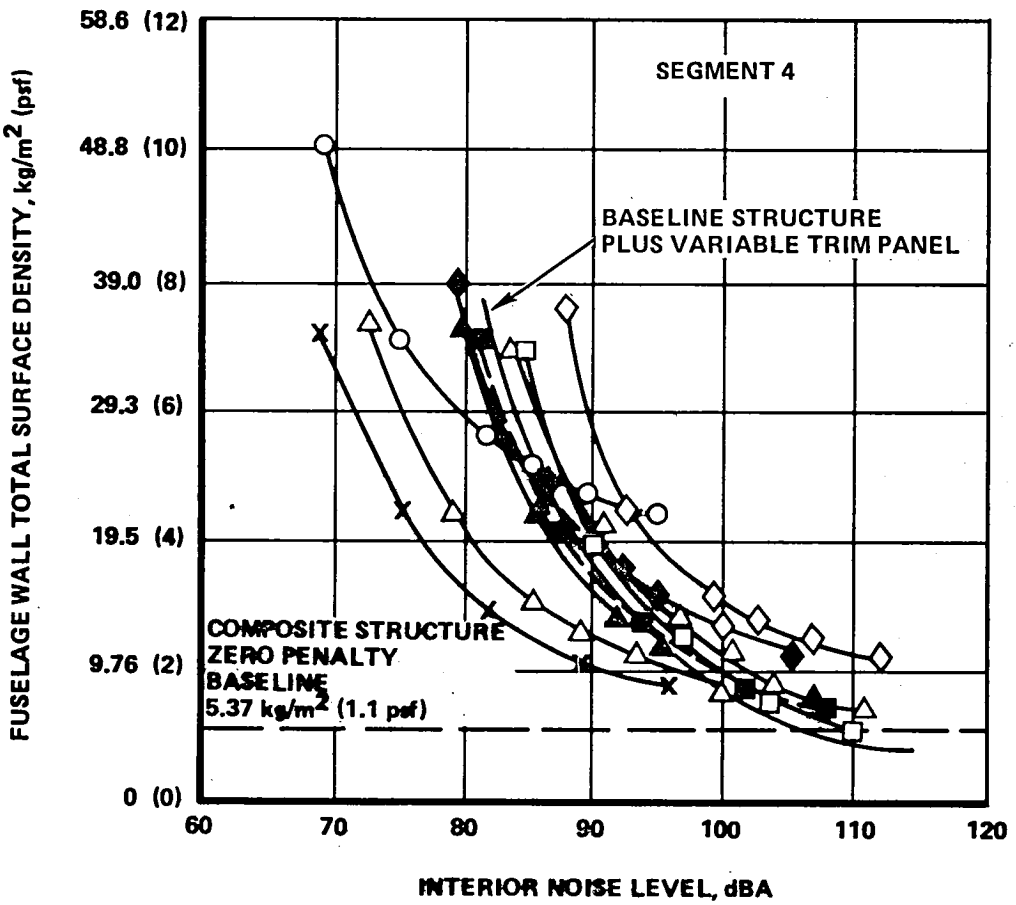

Figure 95.- Comparison of business aircraft advanced composite vs. add-on noise control; outer-wall mass and stiffness effects.

CONCEPT	SYMBOL	$\bar{E}_x, \bar{E}_y$	$\bar{\ell}_x$	$\bar{\ell}_y$	σ_1 kg/m^2	σ_1 (psf)	η
ADD-ON	○	1, 1	1.0	1.0	19.5	(4.0)	0.14
ADVANCED	□	3, 12	1.0	0.25	13.0	(2.66)	0.06
	■	6, 6	0.5	0.5	12.3	(2.52)	
	△	5, 20	1.0	0.25	19.8	(4.06)	
	▲	10, 10	0.5	0.5	18.8	(3.85)	
	◇	10, 40	1.0	0.25	43.5	(8.91)	
	◆	20, 20	0.5	0.5	41.1	(8.43)	

NOTES: ℓ_x = RING SPACING; $\bar{\ell}_x = \ell_x/\ell_{x\ \text{BASELINE}}$
ℓ_y = STRINGER SPACING; $\bar{\ell}_y = \ell_y/\ell_{y\ \text{BASELINE}}$
$\bar{E}$ = $(EI)/(EI)_{\text{BASELINE}}$
σ_1 = OUTER WALL SURFACE DENSITY
η = DAMPING LOSS FACTOR

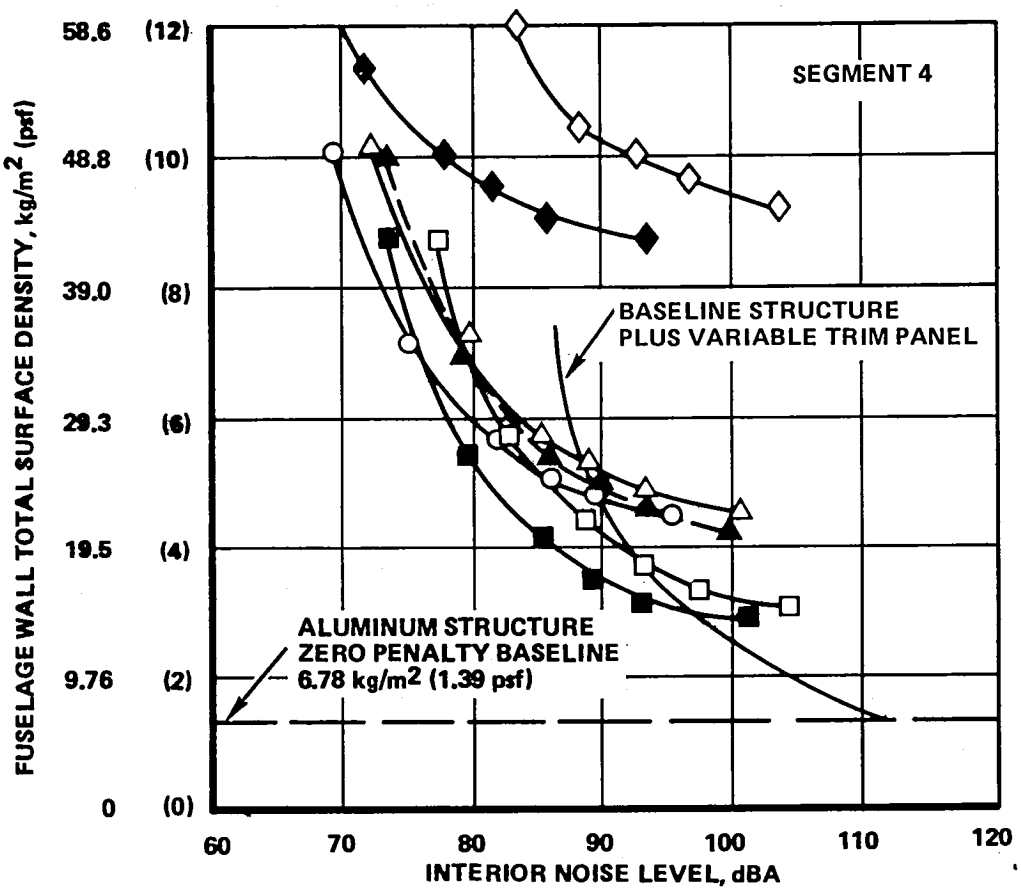

Figure 96.- Comparison of business aircraft advanced aluminum vs. add-on noise control; outer-wall mass and stiffness effects.

CONCEPT	SYMBOL	$\bar{E}_x, \bar{E}_y$	$\bar{\ell}_x$	$\bar{\ell}_y$	σ_1 kg/m^2	σ_1 (psf)	η
ADD-ON	○	1, 1	1.0	1.0	19.5	(4.0)	0.14
ADVANCED	□	3, 12	1.0	0.25	6.88	(1.41)	0.06
	■	6, 6	0.5	0.5	6.49	(1.33)	
	△	10, 20	1.0	0.25	8.44	(1.73)	
	▲	10, 10	0.5	0.5	8.00	(1.64)	
	◇	10, 40	1.0	0.25	12.7	(2.60)	
	◆	20, 20	0.5	0.5	12.0	(2.46)	

NOTES: ℓ_x = RING SPACING; $\bar{\ell}_x = \ell_x/\ell_{x\ \text{BASELINE}}$
ℓ_y = STRINGER SPACING; $\bar{\ell}_y = \ell_y/\ell_{y\ \text{BASELINE}}$
$\bar{E}$ = $(EI)/(EI)_{\text{BASELINE}}$
σ_1 = OUTER WALL SURFACE DENSITY
η = DAMPING LOSS FACTOR

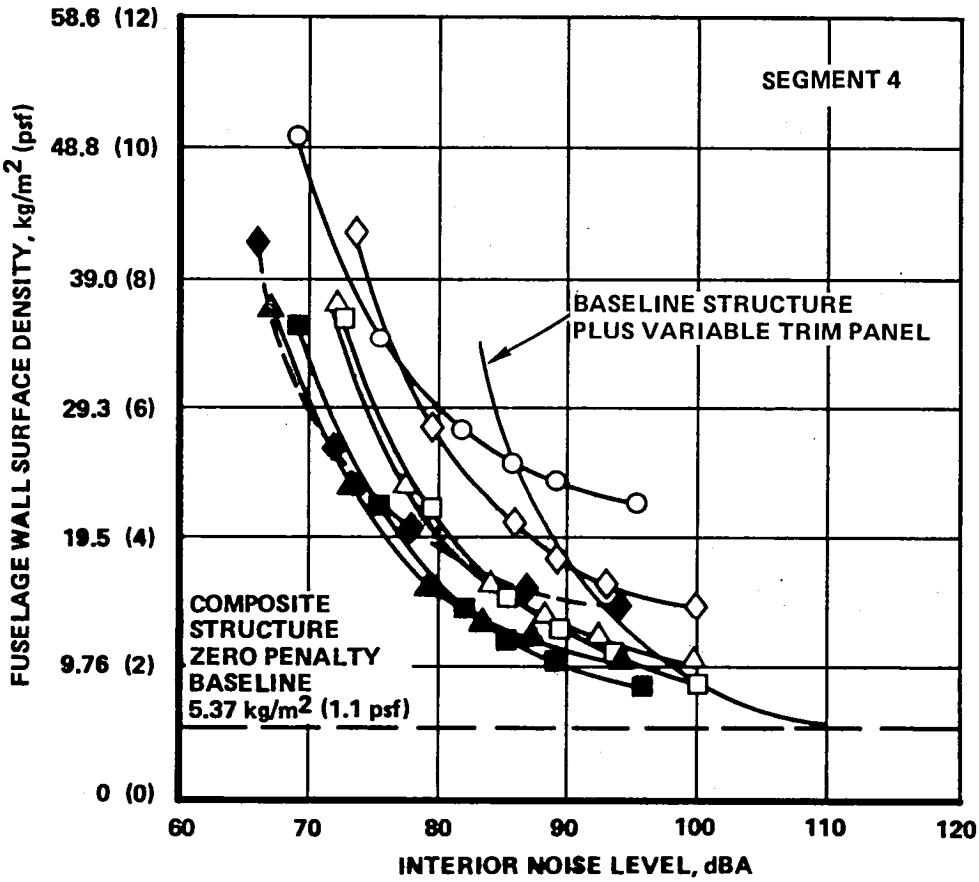

Figure 97.- Comparison of business aircraft advanced composite vs. add-on noise control; outer-wall mass and stiffness effects.

APPENDIX I

DESCRIPTION OF THE AXIAL VARIATION OF THE HIGH NOISE REDUCTION DESIGN CHARACTERISTICS

I1. ADD-ON NOISE REDUCTION DESIGNS

Tables 17 to 22 describe the axial variation of the add-on noise-control elements for the wide-body, narrow-body, and business aircraft, respectively. Three of the designs have aluminum and three have composite outer-wall structure. By definition of these designs, the outer-wall, load-carrying structure is maintained at its baseline strength and stiffness level, so the variable elements include:

- Outer-wall viscoelastic damping layer surface density
- Trim-panel surface density

In principle, the fiberglass blanket properties could have been varied if advantageous; however, earlier studies described in Appendix G indicate that little benefit is derived from such variations within a fixed wall-space depth. The choice of the larger diameter "B" fiber versus the conventional "AA" fiber diameter is the principal result of the studies of fiberglass blanket effects upon low-frequency propeller noise transmission.

I2. ADVANCED NOISE REDUCTION DESIGNS

Tables 23 through 28 describe the six advanced designs for which mass penalty data are given in table 1 of Section 3.2. Three of these designs are described as advanced aluminum, and three are called advanced composite/orthogrid designs. All of these advanced designs are optimized to consider the following features:

- Stiffening of the outer-wall along with the necessary increases of outer surface density as defined by figures 4 and 5 of Section 3
- Use of the correct trim-panel surface density obtained from double wall parametric studies
- Local adjustment of the required noise reduction in proportion to changes in the external noise level as described in Section 3.2.

The data in tables 23 through 28 describe the axial distributions of all of the pertinent noise-control parameters which are required to provide, at minimum total wall surface density, the necessary local noise reduction

(adjusted according to the external noise signatures given in figures 7 and 8 Appendix A). The axial position, X/D, denotes the ratio of distances to propeller diameter forward of the position called zero. This zero position is the position of the propeller disc plane for the 2-engine aircraft having a propeller tip clearance of $\Delta y/D = 0.8$. The optimum local noise-control design is obtained from the envelope of curves such as are shown in Appendix H, where the required total surface is plotted versus required interior noise level. Since the design objective remains at 80 dBA, the increased values of interior noise correspond to reductions of the local exterior noise in accordance with figures 7 and 8, Appendix A.

It is observed in tables 23 through 28 that in the regions of peak noise, the configuration stiffness to baseline stiffness ratios, $\bar{E} = 5$ to 10 are best. For the advanced aluminum wide-body design the baseline stiffener spacing is optimum. For the other designs it appears desirable to use double the number of both stringers and rings (denoted by reduced relative spacings $\bar{\ell}_x = \bar{\ell}_y = 0.5$). For the peakwise region, all of the data for outer-wall section properties, stiffness, ring frame spacing and stringer spacing, are given in Appendix B for each of the three sizes of aircraft in tables 8 through 12.

One other feature which is common to all designs, including the add-on designs, is a uniformity of the optimum configuration for achieving the first 10 to 15 dBA increments of interior noise reduction beyond what is afforded by the baseline turbofan-type structure. For these low noise-reduction increments, all of the treatment mass penalty should be invested in increased trim panel surface density and none in the outer wall.

TABLE 17. - AXIAL DISTRIBUTION OF "ADD-ON" NOISE REDUCTION DESIGN PARAMETERS FOR ALUMINUM 4-ENGINE WIDEBODY AIRCRAFT

Segment	X/D	Surface Density Values						Viscoelastic Layer Thickness	Wall Depth	Blanket Thickness	Airgap Depth
		Outer-Wall Structure	Outer-Wall Viscoelastic	Total Outer-Wall	Trim Panel	Fiberglass Blanket	Total Sidewall				
		σ_1 Struct KG/SQ M (PSF)	σ_{VE} KG/SQ M (PSF)	σ_1 KG/SQ M (PSF)	σ_2 KG/SQ M (PSF)	σ_{BLKT} KG/SQ M (PSF)	σ_T KG/SQ M (PSF)	CM (IN)	CM (IN)	CM (IN)	CM (IN)
3	1.0	9.17 (1.88)	0	9.17 (1.88)	1.61 (.33)	.73 (.15)	11.5 (2.36)	0	15.2 (6)	7.62 (3)	7.62 (3)
↑	.75	↓	↓	↓	↓	↓		↓	↓	↓	↓
	.50	↓	↓	↓	↓	↓		↓	↓	↓	↓
4	.50	↓	↓	↓	5.9 (1.2)	↓	15.8 (3.23)	↓	↓	↓	↓
↓	.25	↓	↓	↓	11.0 (2.25)	↓	20.2 (4.13)	↓	↓	↓	↓
↓	0	↓	10.4 (2.12)	19.5 (4.0)	9.3 (1.9)	↓	29.5 (6.05)	.75 (.29)	↓	↓	↓
↓	-.25	↓	↓	↓	13.2 (2.7)	↓	33.4 (6.85)	↓	↓	↓	↓
↓	-.50	↓	↓	↓	14.6 (3.0)	↓	34.9 (7.15)	↓	↓	↓	↓
↓	-.75	↓	↓	↓	13.2 (2.7)	↓	33.4 (6.85)	↓	↓	↓	↓
↓	-.10	↓	↓	↓	11.0 (2.25)	↓	31.2 (6.40)	↓	↓	↓	↓
↓	-1.25	↓	↓	↓	9.3 (1.9)	↓	29.5 (6.05)	↓	↓	↓	↓
↓	-1.50	↓	0	9.17 (1.88)	16.1 (3.3)	↓	26.0 (5.33)	0	↓	↓	↓
↓	-1.75	↓	↓	↓	13.7 (2.8)	↓	23.6 (4.83)	↓	↓	↓	↓
↓	-2.0	↓	↓	↓		↓		↓	↓	↓	↓
↓	-2.25	↓	↓	↓		↓		↓	↓	↓	↓
6	-2.25	↓	↓	↓		↓		↓	↓	↓	↓
↓	-2.50	↓	↓	↓		↓		↓	↓	↓	↓
7	-2.50	↓	↓	↓	13.2 (2.7)	↓	23.1 (4.73)	↓	↓	↓	↓
↓	-2.75	↓	↓	↓	7.8 (1.6)	↓	17.7 (3.63)	↓	↓	↓	↓
↓	-3.00	↓	↓	↓	3.6 (.74)	↓	13.5 (2.77)	↓	↓	↓	↓
↓	-3.25	↓	↓	↓	2.0 (.41)	↓	10.9 (2.44)	↓	↓	↓	↓
↓	-3.50	↓	↓	↓	1.61 (.33)	↓	11.5 (2.36)	↓	↓	↓	↓

NOTES:
(A) Fiberglass blanket. Bulk density = 9.6 kg/cu m (0.6 lb/cu ft). B-type fiber diameter = 3.81 μm (150 μin)
(B) Viscoelastic layer. Bulk density = 1384.1 kg/cu m (86.4 lb/cu ft). Damping loss factor = .2 at a surface density of 19.5 kg/ sq m
(C) Total treatment mass penalty. = 2283 kg (5033 lb) = 2.31% of TOGW. TOGW = 98640 kg (217 466 lb)
(D) $X/_D$ is positive forward of the propeller disc plane

TABLE 18. - AXIAL DISTRIBUTION OF "ADD-ON" NOISE REDUCTION DESIGN PARAMETERS FOR ALUMINUM 2-ENGINE NARROWBODY AIRCRAFT

Segment	X/D	Surface Density Values: Outer-Wall Structure $\sigma_{1\ Struct}$ KG/SQ M (PSF)	Outer-Wall Viscoelastic σ_{VE} KG/SQ M (PSF)	Total Outer-Wall σ_1 KG/SQ M (PSF)	Trim Panel σ_2 KG/SQ M (PSF)	Fiberglass Blanket σ_{BLKT} KG/SQ M (PSF)	Total Sidewall σ_T KG/SQ M (PSF)	Viscoelastic Layer Thickness CM (IN)	Wall Depth CM (IN)	Blanket Thickness CM (IN)	Airgap Depth CM (IN)
3	.75	6.25 (1.28)	0	6.25 (1.28)	1.61 (.33)	.73 (.15)	8.6 (1.76)	0	15.2 (6)	7.62 (3)	7.62 (3)
	.5				2.5 (.51)		9.5 (1.94)				
4	.5										
	.25				7.3 (1.5)		4.3 (2.93)				
	0		13.3 (2.72)	19.5 (4.0)	8.8 (1.8)		29.0 (5.95)	.960 (.378)			
	-.25				12.7 (2.6)		32.9 (6.75)				
	-.50				11.5 (2.35)		31.7 (6.50)				
	-.75				7.8 (11.6)		28.1 (5.75)				
	-1.0		0	6.25 (1.28)	11.7 (2.4)		18.7 (3.83)	0			
	-1.25				4.6 (.95)		11.6 (2.83)				
5	-1.25										
	-1.50				1.61 (.33)		8.6 (1.76)				

NOTES:

(A) Fiberglass blanket

B-type fiber diameter = 3.81 μm (150 μin)

Bulk density = 9.6 kg/cu m (0.6 lb/cu ft)

(B) Viscoelastic layer

Bulk density = 1384.1 kg/cu m (86.4 lb/cu ft)

(C) Total treatment mass penalty

= 741.4 kg (1634.5 lb) = 1.82% TOGW

(D) TOGW = 40,823 kg (90 000 lb)

(E) $X/_D$ is positive forward of the propeller disc plane

TABLE 19. - AXIAL DISTRIBUTION OF "ADD-ON" NOISE REDUCTION DESIGN PARAMETERS FOR ALUMINUM 2-ENGINE SMALL BUSINESS AIRCRAFT

		Surface Density Values									
		Outer-Wall Structure	Outer-Wall Viscoelastic	Total Outer-Wall	Trim Panel	Fiberglass Blanket	Total Sidewall	Viscoelastic Layer Thickness	Wall Depth	Blanket Thickness	Airgap Depth
Segment	X/D	$\sigma_{1\ Struct}$ KG/SQ M (PSF)	σ_{VE} KG/SQ M (PSF)	σ_1 KG/SQ M (PSF)	σ_2 KG/SQ M (PSF)	σ_{BLKT} KG/SQ M (PSF)	σ_T KG/SQ M (PSF)	CM (IN)	CM (IN)	CM (IN)	CM (IN)
3	.75	4.68 (.96)	0	4.68 (.96)	1.61 (.33)	.49 (.10)	6.78 (1.39)	0	10.2 (4)	5.08 (2)	5.08 (2)
	.50				4.6 (.94)		9.76 (2.0)				
4	.50										
	.25		5.08 (1.04)	9.76 (2.0)	6.6 (1.35)		16.8 (3.45)	.37 (.144)			4.7 (1.86)
	0		14.8 (3.04)	19.5 (4.0)	6.3 (1.30)		26.4 (5.40)	1.072 (.422)			4.0 (1.58)
	-.25				8.8 (1.80)		28.9 (5.90)				
	-.50				7.8 (1.60)		27.8 (5.70)				
	-.75		5.08 (1.04)	9.76 (2.0)	14.2 (2.90)		24.4 (5.00)	.37 (.144)			4.7 (1.86)
	-1.0				6.6 (1.35)		16.8 (3.45)				
	-1.25		0	4.68 (0.96)	6.5 (1.34)		11.7 (2.40)	0			
5	-1.25				2.64 (.54)		7.8 (1.60)				
	-1.50				1.61 (.33)		6.78 (1.39)				

NOTES:
(A) Fiberglass blanket
B-type fiber, diameter = 3.81 μm (150 μin)
Bulk density = 9.6 kg/cu m (0.6 lb/ cu ft)
(B) Viscoelastic layer
Bulk density = 1384.1 kg/cu m (86.4 lb/cu ft)
Damping loss factor = 20% at σ_{VE} = 19.5 kg/sq m
(C) Total treatment penalty = 250 kg (551 lb) = 1.72% TOGW
(D) TOGW = 14 515 kg (32 000 lb)
(E) X/D is positive forward of the propeller disc plane

TABLE 20. - AXIAL DISTRIBUTION OF "ADD-ON" NOISE REDUCTION DESIGN PARAMETERS FOR COMPOSITE WIDEBODY 4-ENGINE AIRCRAFT

Segment	X/D	Surface Density Values: Outer-Wall Structure σ_1 Struct KG SQ M (PSF)	Outer-Wall Viscoelastic σ_{VE} KG SQ M (PSF)	Total Outer-Wall σ_1 KG SQ M (PSF)	Trim Panel σ_2 KG SQ M (PSF)	Fiberglass Blanket σ_{BLKT} KG SQ M (PSF)	Total Sidewall σ_T KG SQ M (PSF)	Viscoelastic Layer Thickness CM (IN)	Wall Depth CM (IN)	Blanket Thickness CM (IN)	Airgap Depth CM (IN)
3	.75	6.4 (1.31)	0	6.4 (1.31)	1.61 (.33)	.73 (.15)	8.74 (1.79)	0	15.2 (6)	7.62 (3)	7.62 (3)
	.50				5.86 (1.2)		13.0 (2.66)				
	.50										
4	.25				9.76 (2.0)		16.8 (3.45)				
	0				21.0 (4.3)		28.1 (5.75)				
	-.25		13.1 (2.69)	(19.5)(4.0)	13.2 (2.7)		33.4 (6.85)	.95 (.374)			
	-.50				14.6 (3.0)		34.9 (7.15)				
	-.75				13.2 (2.7)		33.4 (6.85)				
	-1.00				11.7 (2.4)		32.0 (6.55)				
	-1.25		0	6.4 (1.31)	23.4 (4.8)		30.6 (6.26)	0			
	-1.25										
	-1.50				21.0 (4.3)		28.1 (5.76)				
5	-1.75				18.1 (3.7)		25.2 (5.16)				
	-2.00				15.6 (3.2)		22.7 (4.66)				
	-2.25				12.7 (2.6)		19.8 (4.06)				
6	-2.25										
	-2.50				6.83 (1.4)		14.0 (2.86)				
	-2.50										
7	-2.75				3.51 (.72)		10.6 (2.18)				
	-3.0				2.68 (.55)		9.81 (2.01)				
	-3.25				1.71 (3.5)		8.83 (1.81)				
	-3.50				1.61 (.33)		8.74 (1.79)				

NOTES:

(A) Fiberglass blanket. Bulk density = 9.6 kg/m^3 (0.6 lb/ft^3). B-type fiber diameter = 3.81 μm (150 μin)

(B) Viscoelastic layer. Bulk density 1384 kg/m^3 (86.4 lb/ ft^3). Damping loss factor = .2 at a surface density, σ_1 of 29 kg/m^2 = .06 at σ_1 = 9 kg/m^2 with linear variation

(C) Total treatment mass penalty. = 2441 kg (5381 lb) = 2.47% TOGW. TOGW = 98,641 kg (217,466 lb)

(D) $X/_D$ is positive forward of propeller disc plane

TABLE 21. - AXIAL DISTRIBUTION OF "ADD-ON" NOISE REDUCTION DESIGN PARAMETERS FOR COMPOSITE NARROWBODY 2-ENGINE AIRCRAFT

Segment	X/D	Surface Density Values: Outer-Wall Structure σ_1 Struct KG/SQ M (PSF)	Outer-Wall Viscoelastic σ_{VE} KG/SQ M (PSF)	Total Outer-Wall σ_1 KG/SQ M (PSF)	Trim Panel σ_2 KG/SQ M (PSF)	Fiberglass Blanket σ_{BLKT} KG/SQ M (PSF)	Total Sidewall σ_T KG/SQ M (PSF)	Viscoelastic Layer Thickness CM (IN)	Wall Depth CM (IN)	Blanket Thickness CM (IN)	Airgap Depth CM (IN)
3	.75	4.34 (.89)	0	4.34 (.89)	1.61 (.33)	.73 (.15)	6.7 (1.37)	7.62 (3)	15.2 (6)	7.62 (3)	7.62 (3)
	.50				2.93 (.60)		8.0 (1.64)				
4	.50										
	.25		3.0 (.61)	7.32 (1.5)	6.8 (1.4)		14.9 (3.05)	.215(.085)			
	0		15.2 (3.11)	19.5 (4.0)	8.8 (1.8)		29.0 (5.95)	1.10 (.432)			
	-.25				11.7 (2.4)		32.0 (6.55)				
	-.50				12.2 (2.5)		32.5 (6.65)				
	-.75				7.8 (1.6)		28.1 (5.75)				
	-1.0		3.0 (.61)	7.32 (1.5)	8.5 (1.75)		16.6 (3.40)	.215(.085)			
	-1.25		0	(4.34) (.89)	5.9 (1.20)		10.9 (2.24)				
	-1.25										
5	-1.5				1.61 (.33)		6.7 (1.37)				
	-1.75										
	-2.0										

NOTES:
(A) Fiberglass blanket. Bulk density 9.6 kg/m^3 (0.6 lb/ft^3). B-type fiber diameter = 3.81 μm (150 μin)
(B) Viscoelastic layer. Bulk density 1384 kg/m^3 (86.4 lb/ft^3). Damping loss factor = .2 at a surface density σ_1 = 29 kg/m^2; = .06 at σ_1 = 9 kg/m^2 with linear variation
(C) Total treatment mass penalty = 860 kg (1895 lb) = 2.11% TOGW. TOGW = 40,823 kg (90,000 lb)
(D) X/D is positive forward of the propeller disc plane

TABLE 22. - AXIAL DISTRIBUTION OF "ADD-ON" NOISE REDUCTION DESIGN PARAMETERS FOR COMPOSITE SMALL BUSINESS AIRCRAFT

Segment	X/D	Surface Density Values: Outer-Wall Structure $\sigma_{1\ Struct}$ KG/SQ M (PSF)	Outer-Wall Viscoelastic σ_{VE} KG/SQ M (PSF)	Total Outer-Wall σ_1 KG/SQ M (PSF)	Trim Panel σ_2 KG/SQ M (PSF)	Fiberglass Blanket σ_{BLKT} KG/SQ M (PSF)	Total Sidewall σ_T KG/SQ M (PSF)	Viscoelastic Layer Thickness CM (IN)	Wall Depth CM (IN)	Blanket Thickness CM (IN)	Airgap Depth CM (IN)
3	.75	3.27 (.67)	0	3.27 (.67)	1.61 (.33)	.49 (.10)	5.4 (1.10)	0	10.2 (4)	5.1 (2)	5.1 (2)
	.50				4.6 (.95)		8.4 (1.72)				
4	.50										
	.25				11.0 (2.25)		14.7 (3.02)				
	0		11.4 (2.33)	14.6 (3.0)	7.3 (1.5)		22.5 (4.6)	.82 (.324)			
	-.25				10.7 (2.2)		25.9 (5.3)				
	-.50				11.2 (2.3)		26.4 (5.4)				
	-.75				6.8 (1.4)		22.0 (4.5)				
	-1.0				2.9 (.60)		18.1 (3.70)				
	-1.25		0	3.27 (.67)	5A (1.10)		9.1 (1.87)	0			
5	-1.25										
	-1.5				2.2 (.45)		6.0 (1.22)				
	-1.75				1.61 (.33)		5.4 (1.10)				

NOTES:
(A) Fiberglass blanket. Bulk density 9.6 kg/m^3 (0.6 lb/ft^3). B-type fiber diameter - 3.81 μm (150 μin)
(B) Viscoelastic layer. Bulk density 1384 kg/m^3 (86.4 lb/ft^3). Damping loss factor = .2 at surface density. σ_1 = 29 kg/m^2; .06 at σ_1 = 9 kg/m^2 with linear variation
(C) Total treatment mass penalty = 266 kg (586 lb) = 1.83% TOGW. TOGW = 14515 kg = 32 000 lb
(D) X/D is positive forward of the propeller disc plane

TABLE 23. DESCRIPTION OF "ADVANCED" ALUMINUM NOISE REDUCTION DESIGN FOR 4-ENGINE WIDEBODY AIRCRAFT

SEGMENT	$\frac{X}{D}$	$\bar{E}$	η	$\bar{\ell}_x$	$\bar{\ell}_y$	σ_1		σ_2		σ_{BLKT}		σ_{TOTAL}		UNIFORM PROPERTIES
						$\frac{kg}{m^2}$	(psf)	$\frac{kg}{m^2}$	(psf)	$\frac{kg}{m^2}$	(psf)	$\frac{kg}{m^2}$	(psf)	
3	1.00	1.0	0.06	1.0	1.0	9.17	1.88	1.61	0.33	0.73	0.15	11.5	2.36	(a) Wall Spacing 15.24 cm (6.0 in.)
	0.75													(b) Blanket Properties
	0.50							4.25	0.87			15.8	3.23	• Type: B
4	0.50													• Bulk Density: = 9.6 kg/m³ (0.6 lb/ft³)
↑	0.25	3.0				11.9	2.44	6.39	1.31			19.0	3.90	• Thickness: 7.62 cm (3 in.)
FWD	0.00							10.8	2.21			23.4	4.80	
AFT	−0.25	5.0				15.6	3.20	10.5	2.15			26.8	5.50	(c) Airgap Thickness 7.62 cm (3 in.)
↓	−0.50							12.0	2.45			28.3	5.80	
	−0.75							10.5	2.15			26.8	5.50	
	−1.00	3.0				11.9	2.44	11.8	2.41			24.4	5.00	
	−1.25							10.8	2.21			23.4	4.80	(d) Inboard Propeller Disc Plane at $\frac{X}{D}$ = −0.27
5	−1.25													
	−1.50							9.52	1.95			22.2	4.54	
	−1.75							7.32	1.50			20.0	4.09	
	−2.00							6.34	1.30			19.0	3.89	(e) Outboard Propeller Disc Plane at $\frac{X}{D}$ = 1.012
	−2.25							5.37	1.10			18.0	3.69	
6	−2.25													
	−2.50							2.73	0.56			15.4	3.15	(f) Zero Penalty Total Wall Surface Density $\sigma_{T_{BL}}$ = 11.52 kg/m² (2.36 psf)
7	−2.50													
	−2.75							1.61	0.33			14.3	2.92	
	−3.00	1.0				9.17	1.88	3.61	0.74			13.5	2.77	
	−3.25							1.61	0.33			11.5	2.36	
	−3.50													

Baseline (Zero Penalty) Configuration at Other Locations
Total Treatment Penalty = 1523 kg (3358 lb)
= 1.54% TOGW
TOGW = 98,641 kg (217466 lb)

TABLE 24. DESCRIPTION OF "ADVANCED" ALUMINUM NOISE REDUCTION DESIGN FOR 2-ENGINE NARROWBODY AIRCRAFT

SEGMENT	$\frac{X}{D}$	$\overline{E}$	η	$\overline{\ell_x}$	$\overline{\ell_y}$	σ_1 kg/m²	σ_1 (psf)	σ_2 kg/m²	σ_2 (psf)	σ_{BLKT} kg/m²	σ_{BLKT} (psf)	σ_{TOTAL} kg/m²	σ_{TOTAL} (psf)
3	1.00	1.0	0.06	1.0	1.0	6.25	1.28	1.61	0.33	0.73	0.15	8.59	1.76
	0.75	↓	↓	↓	↓	↓	↓	↓	↓	↓	↓	↓	↓
	0.50	↓	↓	↓	↓	↓	↓	2.49	0.51	↓	↓	9.47	1.94
↑ 4	0.25	1.0	↓	1.0	1.0	↓	↓	7.32	1.50	↓	↓	14.30	2.93
FWD	0.00	6.0	↓	0.5	0.5	12.6	2.58	9.76	2.00	↓	↓	23.10	4.73
AFT	−0.25	↓	↓	↓	↓	↓	↓	13.20	2.70	↓	↓	26.50	5.43
↓	−0.50	↓	↓	↓	↓	↓	↓	12.20	2.50	↓	↓	25.50	5.23
	−0.75	↓	↓	↓	↓	↓	↓	8.78	1.80	↓	↓	22.10	4.53
	−1.00	6.0	↓	0.5	0.5	↓	↓	4.39	0.90	↓	↓	17.70	3.63
	−1.25	1.0	↓	1.0	1.0	6.25	1.28	4.64	0.95	↓	↓	11.60	2.38
5	−1.25	↓	↓	↓	↓	↓	↓	↓	↓	↓	↓	↓	↓
	−1.50	1.0	0.06	1.0	1.0	↓	↓	1.61	0.33	0.73	0.15	8.59	1.76

UNIFORM PROPERTIES

(a) Wall Spacing
15.24 cm (6.0 in.)

(b) Blanket Properties
- Type: B
- Bulk Density
  = 9.6 kg/m³ (0.6 lb/ft³)
- Thickness:
  7.62 cm (3 in.)

(c) Airgap Thickness
7.62 cm (3 in.)

(d) Propeller Disc Plane at
$\frac{X}{D} = 0$

(e) Zero Penalty - Total Wall Surface Density
σ_{TBL} = 8.59 kg/m² (1.76 psf)

Baseline (Zero Penalty) Configuration at Other Locations
Total Treatment Penalty = 616 kg (1357 lb)
= 1.508% TOGW
TOGW= 40,823 kg (90,000 lb)

TABLE 25. DESCRIPTION OF "ADVANCED" ALUMINUM NOISE REDUCTION DESIGN FOR 2-ENGINE BUSINESS AIRCRAFT

SEGMENT	$\frac{X}{D}$	$\bar{E}$	η	$\bar{\ell}_x$	$\bar{\ell}_y$	σ_1		σ_2		σ_{BLKT}		σ_{TOTAL}		UNIFORM PROPERTIES
						$\frac{kg}{m^2}$	(psf)	$\frac{kg}{m^2}$	(psf)	$\frac{kg}{m^2}$	(psf)	$\frac{kg}{m^2}$	(psf)	
3	1.00													(a) Wall Spacing 10.16 cm (4.0 in.)
	0.75	1.0	0.06	1.0	1.0	4.68	0.96	1.61	0.33	0.49	0.10	6.78	1.39	(b) Blanket Properties • Type: B • Bulk Density: = 9.6 kg/m³ (0.6 lb/ft³) • Thickness: 5.08 cm (2.0 in.)
	0.50													
4	0.50							5.56	1.14			10.7	2.20	
↑ FWD	0.25	6.0		0.5	0.5	12.3	2.52	3.32	0.68			16.1	3.30	
	0.00							10.2	2.08			22.9	4.70	
AFT ↓	−0.25							13.1	2.68			25.9	5.30	
	−0.50							11.6	2.38			24.4	5.00	(c) Airgap Thickness 5.08 cm (2.0 in.)
	−0.75							9.17	1.88			22.0	4.50	
	−1.00	6.0		0.5	0.5	12.3	2.52	4.29	0.88			17.1	3.50	
	−1.25	1.0		1.0	1.0	4.68	0.96	7.03	1.44			12.2	2.50	(d) Propeller Disc Plane at $\frac{X}{D} = 0$
5	−1.25													
	−1.50						0.96	1.61	0.33			6.78	1.39	(e) Zero Penalty Total Wall Surface Density $\sigma_{T_{BL}}$ = 6.78 kg/m² (1.39 psf)

Baseline (Zero Penalty) Configuration at Other Locations
Total Treatment Penalty = 225 kg (495 lb)
= 1.55% TOGW
TOGW = 14,515 kg (32,000 lb)

TABLE 26. DESCRIPTION OF "ADVANCED" COMPOSITE NOISE REDUCTION DESIGN FOR 4-ENGINE WIDEBODY AIRCRAFT

SEGMENT	$\frac{X}{D}$	$\bar{E}$	η	$\bar{\ell}_x$	$\bar{\ell}_y$	σ_1 $\frac{kg}{m^2}$	σ_1 (psf)	σ_2 $\frac{kg}{m^2}$	σ_2 (psf)	σ_{BLKT} $\frac{kg}{m^2}$	σ_{BLKT} (psf)	σ_{TOTAL} $\frac{kg}{m^2}$	σ_{TOTAL} (psf)
3	1.00	1.0	0.06	1.0	1.0	6.39	1.31	1.61	0.33	0.73	0.15	8.74	1.79
	0.75	1.0	0.06			↓	↓						↓
	0.50	6.0	↓	0.5	0.5	10.4	2.13	↓	0.33	↓	↓	12.7	2.61
4	0.50	↓	↓	↓	↓	↓	↓	↓	↓	↓	↓	↓	↓
↑	0.25							2.83	0.58				2.86
FWD	0.00							5.27	1.08				3.36
AFT	−0.25							6.73	1.38				3.66
↓	−0.50							7.71	1.58				3.86
	−0.75							6.73	1.38				3.66
	−1.00							5.76	1.18				3.46
	−1.25							↓	↓				↓
5	−1.25							2.15	0.44				2.72
	−1.50							1.85	0.38				2.66
	−1.75							1.61	0.33			12.7	2.61
	−2.00							↓	↓			↓	↓
	−2.25												
6	−2.25												
	−2.50												
7	−2.50	↓	↓	↓	↓	↓	↓	↓	↓	↓	↓	↓	↓
	−2.75												
	−3.00	6.0		0.5	0.5	10.4	2.13	1.61	0.33			12.7	2.61
	−3.25	1.0		1.0	1.0	6.39	1.31	1.76	0.36				1.82
	−3.50	1.0		1.0	1.0	↓	1.31	1.61	0.33				1.79
	−3.75	1.0		↓	↓	↓	↓	↓	0.33	↓	↓	↓	1.79
	−4.00												

UNIFORM PROPERTIES

(a) Wall Spacing
15.24 cm (6.0 in.)

(b) Blanket Properties
- Type: B
- Bulk Density: = 9.6 kg/m^3 (0.6 lb/ft^3)
- Thickness: 7.62 cm (3 in.)

(c) Airgap Thickness
7.62 cm (3 in.)

(d) Inboard Propeller Disc Plane at $\frac{X}{D} = -0.27$

(e) Outboard Propeller Disc Plane at $\frac{X}{D} = -1.012$

(f) Zero Penalty Total Wall Surface Density
$\sigma_{T_{BL}} = 8.74$ kg/m^2 (1.79 psf)

Baseline (Zero Penalty) Configuration at Other Locations
Total Treatment Penalty = 1009 kg (2225 lb)
= 1.023 % TOGW
TOGW = 98,641 kg (217,466 lb)

TABLE 27. DESCRIPTION OF "ADVANCED" COMPOSITE NOISE REDUCTION DESIGN FOR 2-ENGINE NARROWBODY AIRCRAFT

SEGMENT	$\frac{X}{D}$	$\bar{E}$	η	$\bar{\ell}_x$	$\bar{\ell}_y$	σ_1		σ_2		σ_{BLKT}		σ_{TOTAL}		UNIFORM PROPERTIES
						$\frac{kg}{m^2}$	(psf)	$\frac{kg}{m^2}$	(psf)	$\frac{kg}{m^2}$	(psf)	$\frac{kg}{m^2}$	(psf)	
3	1.00	1.0	0.06	1.0	1.0	4.34	0.89	1.61	0.33	0.73	0.15	6.69	1.37	(a) Wall Spacing 15.24 cm (6.0 in.)
	0.75	↓	↓	↓	↓	↓	↓		↓	↓	↓	↓	↓	(b) Blanket Properties
	0.50							3.32	0.68			8.39	1.72	• Type: B
4	0.50	1.0		1.0	1.0	4.34	0.89	↓	↓			↓	↓	• Bulk Density: $= 9.6\ kg/m^3$ ($0.6\ lb/ft^3$)
↑	0.25	6.0		0.5	0.5	8.25	1.69	4.68	0.96			13.7	2.80	• Thickness: 7.62 cm (3.0 in.)
FWD	0.00	10.0		↓	↓	9.52	1.95	10.3	2.10			20.5	4.20	
AFT	−0.25	↓				↓	↓	14.6	3.00			24.9	5.10	(c) Airgap Thickness 7.62 cm (3.0 in.)
↓	−0.50							13.2	2.70			23.4	4.80	
	−0.75	10.0		↓	↓	9.52	1.95	9.27	1.96			19.5	4.00	
	−1.00	6.0		0.5	0.5	8.25	1.69	6.15	1.26			15.1	3.10	
	−1.25	1.0		1.0	1.0	4.34	0.89	5.86	1.20			10.9	2.24	(d) Propeller Disc Plane at $\frac{X}{D} = 0$
5	−1.25	1.0	↓	1.0	1.0	↓	↓	↓	↓	↓	↓		↓	
	−1.50	1.0	0.06	1.0	1.0	4.34	0.89	1.61	0.33	0.73	0.15	6.89	1.37	(e) Zero Penalty Total Wall Surface Density $\sigma_{T_{BL}} = 6.69\ kg/m^2$ (1.37 psf)

Baseline (Zero Penalty) Configuration at Other Locations
Total Treatment Penalty = 573 kg (1264 lb)
= 1.404% TOGW
TOGW = 40,823 kg (90,000 lb)

TABLE 28. DESCRIPTION OF "ADVANCED" COMPOSITE NOISE REDUCTION DESIGN FOR 2-ENGINE BUSINESS AIRCRAFT

SEGMENT	$\frac{X}{D}$	$\bar{E}$	η	$\bar{\ell}_x$	$\bar{\ell}_y$	σ_1 kg/m²	σ_1 (psf)	σ_2 kg/m²	σ_2 (psf)	σ_{BLKT} kg/m²	σ_{BLKT} (psf)	σ_{TOTAL} kg/m²	σ_{TOTAL} (psf)
3	1.00												
	0.75	1.0	0.06	1.0	1.0	3.27	0.67	1.61	0.33	0.49	0.10	5.37	1.10
	0.50	↓	↓	↓	↓	↓	↓	3.22	0.66	↓	↓	6.83	1.43
4	0.50	↓	↓	↓	↓	↓	↓	↓	↓	↓	↓	↓	↓
↑	0.25	6.0	↓	0.5	0.5	6.49	1.33	2.29	0.47	↓	↓	8.78	1.80
FWD	0.00	↓	↓	↓	↓	↓	↓	5.86	1.20	↓	↓	12.8	2.63
AFT	−0.25	10.0	↓	↓	↓	8.00	1.64	6.83	1.40	↓	↓	15.3	3.14
↓	−0.50	↓	↓	↓	↓	↓	↓	6.34	1.30	↓	↓	14.8	3.04
	−0.75	6.0	↓	↓	↓	6.49	1.33	5.37	1.10	↓	↓	12.4	2.53
	−1.00	6.0	↓	0.5	0.5	↓	↓	2.93	0.60	↓	↓	9.91	2.03
	−1.25	1.0	↓	1.0	1.0	3.27	0.67	5.37	1.10	↓	↓	9.13	1.87
5	−1.25	↓	↓	↓	↓	↓	↓	↓	↓	↓	↓	↓	↓
	−1.50	1.0	0.06	1.0	1.0	3.27	0.67	1.61	0.33	↓	↓	5.37	1.10

UNIFORM PROPERTIES

(a) Wall Spacing
10.16 cm (2.0 in.)

(b) Blanket Properties
- Type: B
- Bulk Density:
  = 9.6 kg/m³ (0.6 lb/ft³)
- Thickness:
  5.08 cm (2.0 in.)

(c) Airgap Thickness
5.08 cm (2.0 in.)

(d) Propeller Disc Plane at
$\frac{X}{D} = 0$

(e) Zero Penalty Total Wall Surface Density
$\sigma_{T_{BL}}$ = 5.37 kg/m² (1.1 psf)

Baseline (Zero Penalty) Configuration at Other Locations
Total Treatment Penalty = 107 kg (237 lb)
= 0.740% TOGW
TOGW = 14,515 kg (32,000 lb)

REFERENCES

1. Revell, J. D., and Tullis, R. H., "Fuel Conservation Merits of Advanced Turboprop Transport Aircraft," Lockheed-California Company for NASA/Ames Research Center NASA CR-152096, August 1977.

2. Coykendall, R. E., Curry, J. K., Domke, A. E., and Madsen, S. E., "Study of Cost/Benefit Tradeoffs for Reducing the Energy Consumption of the Commercial Air Transportation System," NASA CR-137891, June 1976.

3. Boeing Commercial Airplane Company Preliminary Design Department, "Energy Consumption Characteristics of Transports Using the Prop-Fan Concept," NASA CR-137937, Nov. 1976.

4. Wilby, J. F., Rennison, D. R., Marsh, A. H., and Wilby, E. G., "Interior Noise Control Prediction Study for High-Speed, Propeller-Driven Aircraft," Bolt Beranek and Newman and Dytec Engineering for NASA Langley, NASA CR-159200, Sept. 1979.

5. Anonymous, "Propfan and Gearbox Near Field Noise Predictions," SP15A77, Hamilton Standard Division United Technologies, 31 October 1977.

6. Smith, P. W., "Sound Transmission Through Thin Cylindrical Shells," JOURNAL OF THE ACOUSTICAL SOCIETY OF AMERICA, Vol. 29, No. 6, pp 721-729, June 1957.

7. Koval, L. R., "On Sound Transmission Into A Thin Cylindrical Shell Under Flight Conditions," JOURNAL OF SOUND AND VIBRATION, Vol. 48, No. 2, pp 265-275, 1976.

8. Cockburn, J. A. and Jolly, A. C., "Structural-Acoustic Response, Noise Transmission Losses and Interior Noise Levels of an Aircraft Fuselage Excited by Random Pressure Fields," USAF, AFFDL-TR-68-2, Wright Patterson Air Force Base, Ohio, August, 1968.

9. Beranek, L. L. and Work, G. A., "Sound Transmission Through Multiple Structures Containing Flexible Blankets," JOURNAL OF THE ACOUSTICAL SOCIETY OF AMERICA, Vol. 21, No. 4, pp 419-428, July 1949.

10. Beranek, L. L., "Acoustical Impedance of Porous Materials," JOURNAL OF THE ACOUSTICAL SOCIETY OF AMERICA, Vol. 13, No. 3, January 1942.

11. Beranek, L. L., "Acoustical Properties of Homogeneous Isotropic Rigid Tiles and Flexible Blankets," JOURNAL OF THE ACOUSTICAL SOCIETY OF AMERICA, Vol. 19, No. 4, July 1947.

12. Mulholland, K. A., Price, A. J. and Parbrook, M. D., "Transmission Loss of Multiple Panels in a Random Incidence Field," JOURNAL OF THE ACOUSTICAL SOCIETY OF AMERICA, Vol. 43, No. 6, June 1968.

13. Cremer, L., "Insulation of Airborne Sound by Rigid Partitions and Insulation of Impact Sound," WADC TR-52-04, Vol. I, Supplement I, Wright Patterson Air Force Base, Ohio, 1955.

14. London, Albert, "Transmission of Reverberant Sound Through Double Walls," JOURNAL OF THE ACOUSTICAL SOCIETY OF AMERICA, Vol. 22, No. 2, March 1950

15. Koval, L. R., "On Sound Transmission into a Stiffened Cylindrical Shell with Rings and Stringers Treated as Discrete Elements," to be published in the JOURNAL OF SOUND AND VIBRATION, 1980.

16. Koval, L. R., "Effect of Longitudinal Stringers on Sound Transmission into a Thin Cylindrical Shell,", JOURNAL OF AIRCRAFT, Vol. 15, No. 12, pp 816-821, December 1978.

17. Ungar, E., "Damping of Panels," NOISE AND VIBRATION CONTROL, Chapter 14, L. Beranek (ed), McGraw Hill, pp 434-474, 1971.

18. Torvik, P. J. and Strickland, D. Z., "Damping Additions for Plates Using Constrained Viscoelastic Layers," JOURNAL OF THE ACOUSTICAL SOCIETY OF AMERICA, Vol. 51, No. 3 (Part 2), pp 985-991, (1972).

19. Koval, L. R., "Effects of Cavity Resonance on Sound Transmission Into a Thin Cylindrical Shell," JOURNAL OF SOUND AND VIBRATION, 59(1), pp 23-33, 1978.

20. Koval, L. R., "On Sound Transmission Into a Stiffened Cylindrical Shell Under Flight Conditions," 3rd AIAA Aero-Acoustics Conference, Palo Alto, Calif., July, 1976, Paper No. 76-549.

21. Peterson, M. R., Boyd, D. E., "Free Vibrations of Circular Cylinders With Longitudinal, Interior Partitions," JOURNAL OF SOUND AND VIBRATION, 60(1), pp 45-62, 8 September 1978.

1. REPORT NO.	2. GOVERNMENT ACCESSION NO.	3. RECIPIENT'S CATALOG NO.
NASA CR 159222		

4. TITLE AND SUBTITLE	5. REPORT DATE
Analytical Study of Interior Noise Control by Fuselage Design Techniques on High-Speed Propeller-Driven Aircraft	4 April 1980
	6. PERFORMING ORG CODE
7. AUTHOR(S)	8. PERFORMING ORG REPORT NO.
Revell, J. D., Balena, F. J., Koval, L. R.*	LR 29382
	10. WORK UNIT NO.
9. PERFORMING ORGANIZATION NAME AND ADDRESS	11. CONTRACT OR GRANT NO.
LOCKHEED-CALIFORNIA COMPANY P.O. BOX 551 BURBANK, CALIFORNIA 91520	NAS1-15427
Consultant 1501 Liberty Drive Rolla, MO 65401	13. TYPE OF REPORT AND PERIOD COVERED FINAL REPORT 7/78 - 12/79
12. SPONSORING AGENCY NAME AND ADDRESS	14. SPONSORING AGENCY CODE
NATIONAL AERONAUTICS AND SPACE ADMINISTRATION LANGLEY RESEARCH CENTER HAMPTON, VA 23665	

15. SUPPLEMENTARY NOTES

This draft submittal supersedes LR 29252, dated 5 October 1979.

16. ABSTRACT

This study determines the acoustical treatment mass penalties required to achieve an interior noise level of 80 dBA for high-speed fuel-efficient propfan-powered aircraft. The prediction method used is based on theory developed by L. R. Koval for the outer shell dynamics, and a modified Cockburn and Jolly approach for "add-on" noise control element performance. The present synthesis of these methods is supported by experimental data.

Three different sized aircraft are studied, including a widebody, a narrow-body, and a business sized aircraft. Noise control penalties are calculated for each aircraft for two kinds of noise control designs, (a) "add-on" designs, where the outer wall structure cannot be changed, and (b) "advanced" designs where the outer wall stiffness level and the materials usage can be altered.

For the "add-on" designs, the mass penalties range from 1.7 to 2.4 percent of the takeoff gross weight (TOGW) of the various aircraft, similar to preliminary estimates reported by Lockheed in the 1977 RECAT study of fuel efficient turboprop aircraft. Results for "advanced" designs now show significant reductions of the mass penalties. For the "advanced" aluminum designs the penalties are 1.5% of TOGW, and for an all-composite aircraft the penalties range from 0.74 to 1.4% of TOGW.

17. KEY WORDS (SUGGESTED BY AUTHOR(S))	18. DISTRIBUTION STATEMENT
Noise reduction, propfan, high-speed propeller, turboprop interior noise, transmission loss, cylindrical shells	

19. SECURITY CLASSIF. (OF THIS REPORT)	20. SECURITY CLASSIF. (OF THIS PAGE)	21. NO. OF PAGES	22. PRICE*

DO NOT REMOVE SLIP FROM MATERIAL

Delete your name from this slip when returning material to the library.

NAME	MS
[illegible]	[illegible]
55	
~~Ray Sung Lin~~	~~370~~

NASA Langley (Rev. May 1988) RIAD N-75